Spectroscopic Constants and Potential Energy Curves of Heavy p-Block Dimers and Trimers

K. BALASUBRAMANIAN†

Department of Chemistry, Arizona State University, Tempe, Arizona 85287-1604

Contents

I. Introduction

The electronic and spectroscopic properties of small clusters of heavy atoms and metal atoms have been the

Krishnan Balasubramanian has been an Associate Professor of Chemistry since 1987 at Arizona State University, Tempe, AZ. He was born in Bangalore, India, in 1956. He received his M.Sc. (Honors) degree from the Birla Institute of Technology and Science, Pilani, India, in 1977 and his M.A. and Ph.D. degrees from The Johns Hopkins University in 1980. He was a postdoctoral associate and visiting lecturer in the Department of Chemistry and Lawrence Berkeley Laboratory, University of California, Berkeley, from 1980 to 1983. From 1983 to 1986 he was an Assistant Professor at Arizona State University. He received the Alfred P. Sloan Fellowship in 1984 and the Camille and Henry Dreyfus Teacher–Scholar Award in 1985. Professor Balasubramanian's research interests include the relativistic quantum chemistry of molecules containing very heavy atoms, chemical applications of group theory, graph theory, and artificial intelligence. He is an author or coauthor of 175 scientific publications.

topics of many experimental[1–40,71–114] and theoretical studies[41–70] in recent years. The intense theoretical and experimental activity in this area has culminated in a wealth of information on the spectroscopic properties and potential energy curves of many heavy dimers and trimers of these species. Investigations of dimers and trimers of such species provide details on the low-lying electronic states, the nature of the heavy atom–atom bond, and periodic trends within various groups. The study of clusters could provide important insights and links to the formation of bulk and solid state from molecular states.

Experimental progress in this area has been phenomenal in recent years[1–40,71–113] due to the advent of laser vaporization and supersonic jet expansion methods.[78–86] Typically, a sample of a foil or sheet of material containing these elements such as a GaAs crystal,[97,100] a Si crystal,[98] or Pt foil[114] is vaporized with a high-energy Nd:YAG laser and passed through a supersonic nozzle. The jet-cooled beam of clusters with varied compositions is then photoionized and investigated by laser spectroscopic methods. A number of other techniques such as sputtering methods,[87–89] rare-gas matrix isolation methods,[32] particle bombardment meth-

†Camille and Henry Dreyfus Teacher–Scholar.

ods[20,115,116] ligand-stripping methods,[90-92] and aggregation within zeolites and molecular sieves[93-96] have been used for cluster generation.

Theoretical ab initio calculations[41-54] on such clusters are on the increase due to advances both in theoretical methods and in supercomputers that utilize powerful software techniques to produce meaningful numbers and to yield information of significance to experimentalists and of great value in enhancing our knowledge of bonding in these systems. Relativistic effective core potentials (RECP)[44,55-67] have become immensely useful and viable alternatives to formidably difficult all-electron calculations for systems as complex as a cluster containing very heavy atoms such as Pb, Sn, Bi, Sb, etc. The RECPs in conjunction with powerful techniques such as the complete active space multiconfiguration self-consistent field (CASSCF) method and configuration interaction calculations (CI)[52,54] have provided reliable results that can be used to either interpret existing experimental information or predict future experiments. Theoretical calculations have also become valuable in designing new experiments.

Clusters of heavy main-group elements comprise a subject themselves, a separate class of unusual compounds whose properties exhibit phenomenal variation as a function of size. Many experimental and theoretical investigations in recent years have demonstrated that the geometries and electronic properties of small clusters containing typically 3-10 atoms have no resemblance at all to the more familiar properties of the bulk. It is this aspect that has made the cluster area perhaps one of the most exciting and challenging areas for both experimental and theoretical activities. Electron affinities and ionization potentials of these species exhibit dramatic alternations as a function of cluster size. The stabilities of these clusters as a function of size exhibit certain numbers, for which clusters are unusually more stable, referred to as magic numbers. The existence of magic numbers is quite intriguing and needs explanation.

Although a considerable amount of information has been accumulated in recent years on such cluster particles, understanding and full rationalization of all the facts are yet to come. The cluster area is thus relatively young compared to the more established traditional area of main-group inorganic chemistry or organometallic chemistry. The objective of the present review is to organize, catalogue, and comrehend the existing information derived from both experimental and theoretical techniques with the intent of promoting further growth in this developing area of research. Although there is a considerable amount of information on larger clusters, we restrict our review to mainly homonuclear dimers, trimers, and some heteronuclear dimers and trimers of such heavy species. A recent review by Mandich et al.[1] has placed special emphasis on larger clusters. For most of the heavy main-group dimers, theoretical calculations are now available. Thus, dimers are reviewed here a bit more exhaustively than possible heteronuclear dimers or trimers. Since the emphasis of this review is more on a comparison of theory and experiment, it is restricted to the heavy p-block dimers Ga_2 to Bi_2 with the exceptions of rare-gas dimers, which mostly form van der Waals complexes in their ground states. The heteronuclear dimers reviewed include GaAs, GaAs$^+$, KrBr$^+$, ICl, and ICl$^+$. The properties of

the heavy trimers Ga_3, Ge_3, Si_3, $GaAs_2$, In_3, and Sn_3 are also reviewed.

Section II briefly outlines both experimental and theoretical techniques employed to investigate small clusters. Section III focuses on spectroscopic properties and potential energy curves of Ga_2 to Bi_2. Section IV reviews the spectroscopic properties and potential energy curves of some heteronuclear dimers. Section V discusses the properties of small trimers, and section VI discusses the combinatorics of clusters. Section VII presents periodic trends among the dimers and trimers reviewed here.

II. Methods of Investigations

A. Experimental Techniques

Mandich et al.[1] have reviewed in depth a number of experimental techniques employed to generate and probe clusters. In this review, we briefly discuss some of these techniques to make it self-contained.

The generation of heavy main-group clusters can be accomplished through a number of methods including evaporation methods,[71-77] jet expansion methods,[78-86] sputtering techniques,[87-89] aggregation methods,[93-96] rare-gas matrix isolation methods,[32] and ligand-stripping methods.[90-92] In recent years, supersonic jet expansion methods have been employed with much success for cluster generation.[78-86,97-101]

Simple evaporation of a source material in an oven can generate small cluster particles of heavy group V elements such as As_2, Sb_2, Bi_2, Bi_4, and Sb_4.[71-77] The oven evaporation method followed by mass spectrometric analysis can unambiguously determine the cluster size. The use of a Knudsen cell containing an effusion orifice is especially suitable for measuring the binding energies and D_0^0 values of small clusters using the second- or third-law thermodynamic methods.[75-77] Many group III-V clusters have been generated by these methods. The main limitation of a simple evaporation method seems to be size; at present, clusters containing at most ten atoms can be generated by this method. Also, this method is not suitable for heteronuclear clusters and alloy clusters.

A popular method for generating clusters of both main-group and transition-metal atoms appears to be the supersonic jet expansion method.[78-86,97-101] In this method, typically a high-energy laser evaporation method is used to form the vapor of the material. This is then expanded into a small nozzle, resulting in the formation of clusters of varied composition. This technique can be used to generate simple clusters and mixed clusters of both refractory and nonrefractory materials. Laser vaporization followed by gas aggregation can yield cold beams of clusters that can be probed further by laser spectroscopic methods. Typically, a pulsed Nd:YAG laser is employed in this method. Smalley and co-workers[78-86] have pioneered this technique for many main-group and transition-metal clusters. Clusters containing up to 55 atoms of the main-group elements and carbon clusters in the range C_1-C_{190} have been generated by these techniques. Mixed main-group clusters such as Ga_xAs_y,[97-99] In_xP_y,[104,106] Sn_xBi_y, Pb_xSb_y,[84,110-112] and Ga_xP_y[117] have also been generated by the evaporation of III-V semiconductor and alloy targets.

Bondybey and co-workers[87-89,140,197] have isolated clusters of heavy main-group elements such as Pb_2, Sn_2, etc. using a sputtering method as well as laser vaporization methods. Clusters of various sizes are sputtered and trapped in rare-gas matrices. The matrix-isolated clusters are then probed by laser-induced fluorescence (LIF) methods. For example, Bondybey and English[87] have investigated Pb_2 using the sputtering method.[87] A disadvantage of this method is that the size of the cluster cannot be determined unambiguously.

Cluster formation can be induced via aggregation of atoms on a support such as molecular sieves or a zeolite.[93-96] This technique involves simple deposition of elemental vapor onto a target in which the atoms are coalesced into small clusters. Other techniques include the ligand-stripping method.[90-92] In this technique, naked clusters are formed by stripping ligands such as CO, H, etc. from a more stable organometallic compound. The stripping is normally induced by high-energy collision with species such as rare-gas atoms, a process that can be called collision-induced dissociation (CID). For example, As_2^+ can be produced from As_2H_4 by this method.[90] The electron-impact method can also be used to produce charged clusters.

Clusters generated by the above-mentioned methods can be probed by a variety of techniques including laser-induced fluorescence, multiphoton ionization and dissociation spectroscopy, especially two-photon and two-color methods, resonance multiphoton methods, time-of-flight and quadrupole mass spectroscopic methods, ion cyclotron resonance mass spectroscopic methods, Raman spectroscopy, visible–UV electronic spectroscopy, and ESR spectroscopy. The mass spectral methods are mainly for the detection of clusters, calibration of cluster sizes, and measurement of relative abundance as a function of size. The other spectroscopic techniques provide valuable information on the low-lying electronic states, geometries, stabilities, ionization potentials, and electron affinities as a function of size and the spin multiplicities of the low-lying electronic states.

The negative-ion photoelectron spectroscopic technique has also provided valuable information on the electronic states of neutral species via ionization of an electron of the anion.[34,36,118-121] The photofragmentation patterns of the cationic[100] and anionic clusters have also provided some fascinating information that is far from understood. For example, the photofragmentation patterns of $Ga_xAs_y^+$ clusters[100] exhibit anomalous patterns that are more reminiscent of metal clusters than of isoelectronic Si_x and Ge_x clusters.[98] Similarly, the photofragmentation patterns of Sb_x and Bi_x clusters are dramatically different. The Si_x^+ and Ge_x^+ clusters fragment into daughters containing 6–11 atoms while metal clusters lose one atom at a time. The photoionization of Ga_xAs_y semiconductor clusters exhibits dramatic even–odd alternations.

B. Theoretical Techniques of Calculations

All the calculations of dimers and trimers reviewed here were done with relativistic effective core potentials.[44,55-62] In the earlier investigations on Pb_2, Sn_2, Tl_2, and Bi_2, these potentials were used in conjunction with

Slater type orbital (STO) basis sets of double-ζ + polarization quality. The calculations that employed STO basis sets were done mostly by using the single-configuration self-consistent field (SCF) method or a generalized valence bond (GVB) method in the case of the ground state of Bi_2 followed by relativistic configuration interaction (RCI) calculations. The RCI calculations included the spin–orbit term derived from RECPs as suggested by Ermler et al.[60] and Hafner and Schwarz.[63] The calculations including the spin–orbit term are called relativistic CI calculations; they included single and double excitations from a multireference list of configurations. In general, the RCI included all low-lying λ–s states of the same Ω symmetry as reference configurations. For example, the RCI calculations of a state of 0_g^+ symmetry could include as reference configurations those configurations that describe $^1\Sigma_g^+(0_g^+)$, $^3\Pi_g(0_g^+)$, $^3\Sigma_g^-(0_g^+)$, etc. and other states of 0_g^+ symmetry. The RCI thus differs from a normal CI in that in the ordinary CI, $^3\Pi_g$ cannot mix with the $^1\Sigma_g^+$ or $^3\Sigma_g^-$ states.

Most of the theoretical calculations made after 1985 were done by using the complete active space MCSCF followed by multireference singles + doubles (CASSCF/MRSDCI/RCI) methods or the first-order CI method employing valence Gaussian basis sets of higher than double-ζ + polarization quality. Recent calculations on In_2, Sb_2, I_2, etc. were done with relatively larger basis sets compared to calculations on Ga_2, Ge_2, As_2, and Se_2.

In the CASSCF method, a set of the most important electrons for chemical bonding (active electrons) are distributed in all possible ways among orbitals referred to as the internal or active orbitals. The active orbitals are normally chosen as the set of orbitals that correlate into valence atomic orbitals at infinite separation of the various atoms in the molecule. The CASSCF method thus provides a zeroth-order starting set of orbitals for inclusion of higher order correlation effects.

The higher order electron correlation effects not included in the CASSCF are taken into account by using the configuration interaction method. The CI calculations are carried out by using the second-order CI method (SOCI), the multireference singles + doubles CI method (MRSDCI), and the first-order CI method (FOCI). The first two methods are more accurate in comparison to the last method. The SOCI calculations included (i) all configurations in the CASSCF, (ii) configurations generated by distributing $n-1$ electrons in the internal space and 1 electron in the external space (n = number of active electrons), and (iii) configurations generated by distributing $n-2$ electrons in the internal space and 2 electrons in the external space in all possible ways. The MRSDCI calculations included a subset of configurations determined by the important configurations in the CASSCF (coefficient ≥ 0.07) as reference configurations. Then single + double excitations were allowed in the MRSDCI. A less accurate method compared to MRSDCI labeled POLCI includes all configurations in the MRSDCI except those generated by distributing 2 electrons in the external space.

We use acronyms such as CASSCF, SOCI, FOCI, MRSDCI, SCF/RCI, POLCI, etc. in this article to describe the nature of the calculations done on various species. Readers are referred to this section and to other reviews[47,52] to comprehend the meanings of these acronyms.

III. Spectroscopic Properties and Potential Energy Curves of Heavy Homonuclear Dimers (Ga_2 to Bi_2)

A. Ga_2

Early investigation of Ga_2 was made by Ginter et al.,[122] who obtained absorption spectra in a furnace in the 19 000–21 000-cm^{-1} region. Later, Douglas et al.[123] reported electronic absorption spectra of Al_2, Ga_2, and In_2. Two absorption bands, one in the range 13 000–15 600 cm^{-1} and the other in the range 24 000–30 000 cm^{-1}, were observed. These authors[123] concluded that the ground state of these dimers was $^1\Sigma_g^+$. Ab initio calculations on Al_2[124] have revealed, however, that the $^3\Pi_u$ state is the lowest state and $^1\Sigma_g^+$ is much higher in energy. Basch et al.[124] reassigned the two electronic bands of Al_2 observed by Douglas et al.[123] to this $^3\Pi_g$ $\leftarrow$ $^3\Pi_u$ and $^3\Pi_g(2) \leftarrow {}^3\Pi_u$ transitions. The vibrational frequency of the ground state of Ga_2 was reported by Froben et al.[192] Related B_2[127,129] and Al_2[124,126,130] molecules have also been studied.

Thermodynamic studies of Ga_2 and related molecules[131,132] revealed that the dissociation energy of Ga_2 is about 1.4 eV. Since the electronic states of Ga_2 have not been well characterized, earlier thermodynamic calculations of D_e assumed an incorrect ground state and partition function.[132] The Ga_2 dimer has also been observed by laser irradiation of a GaAs crystal[125] and in a supersonic jet beam.[97]

Balasubramanian[133] carried out CASSCF/FOCI calculations on Ga_2 that employed RECPs. The RECPs included the outermost $4s^24p^1$ shells in the valence space replacing the rest of the core electrons by relativistic effective core potentials. A (3s3p1d) valence Gaussian basis set was employed for the Ga atom. The d exponent was optimized for the ground state of Ga_2 at the CASSCF level. More recently, Balasubramanian[402] studied many electronic states of Ga_2^+ and Ga_2^-. In the earlier study[133] as noted in an erratum, there was an error in one of the ECP parameters which led to longer bond lengths. However, this was subsequently corrected.

Table 1 shows the possible low-lying states of Ga_2 while Table 2 depicts their dissociation limits and atomic energy separations[134] at the dissociation limits. As seen from these tables, there are at least 20 low-lying states of Ga_2 in the absence of the spin–orbit term.

Table 3 shows the corrected spectroscopic properties of bound states of Ga_2 obtained by Balasubramanian.[133] Among the 18 electronic states investigated by Balasubramanian, the $^3\Delta_u$, $^3\Sigma_u^+$, $^3\Sigma_u^+(II)$, $^3\Pi_g$, and $^1\Pi_g$ curves were found to be repulsive. The calculated potential energy curves of some of many states are shown in Figure 1. As seen from Table 3, the calculated ground state of Ga_2 is $^3\Pi_u$. However, the T_e value of $^3\Sigma_g^-$ is only 410 cm^{-1}. The $^1\Sigma_g^+$ state is 4734 cm^{-1} above the $^3\Pi_u$ state. Evidently, this states does not appear to be the ground state of Ga_2. Consequently, Douglas et al.'s[123] assignment of $^1\Sigma_g^+$ to the ground state of Ga_2 (Al_2) is inconsistent with Balasubramanian's electronic structure calculations.

Table 4 shows the adiabatic and vertical transition energies of allowed electronic dipole transitions for Ga_2. For Ga_2, Douglas et al.[123] reported two absorption bands, one in the 15 590-cm^{-1} region and the other in

TABLE 1. A Few Low-Lying Configurations and the Electronic States Arising from Them for Ga_2

MO configuration	λ-s states
$1\sigma_g^2 1\sigma_u^2 2\sigma_g 1\pi_u$	$^3\Pi_u$, $^1\Pi_u$
$1\sigma_g^2 1\sigma_u^2 1\pi_u^2$	$^3\Sigma_g^-$, $^1\Delta_g$, $^1\Sigma_g^+$
$1\sigma_g^2 1\sigma_u^2 1\pi_u 1\pi_g$	$^3\Delta_u$, $^3\Sigma_u^+$, $^3\Sigma_u^-$, $^1\Delta_u$, $^1\Sigma_u^-$, $^1\Sigma_u^+$
$1\sigma_g^2 1\sigma_u 2\sigma_g 1\pi_u^2$	$^5\Sigma_u^-$, $^3\Sigma_u^-(2)$, $^1\Sigma_u^-$, $^3\Delta_u$, $^3\Sigma_u^+$, $^1\Delta_u$, $^1\Sigma_u^+$
$1\sigma_g^2 1\sigma_u^2 2\sigma_g^2$	$^1\Sigma_g^+$
$1\sigma_g^2 1\sigma_u^2 2\sigma_g 1\pi_g$	$^3\Pi_g$, $^1\Pi_g$
$1\sigma_g^2 1\sigma_u^2 2\pi_u^2$	$^1\Sigma_g^+$
$1\sigma_g^2 1\sigma_u^2 1\pi_g^2$	$^3\Sigma_g^-$, $^1\Delta_g$, $^1\Sigma_g^+$
$1\sigma_g^2 1\sigma_u^2 2\sigma_u^2$	$^1\Sigma_g^+$
$1\sigma_g^2 1\sigma_u^2 2\sigma_g 2\sigma_u$	$^3\Sigma_u^+$, $^1\Sigma_u^+$

TABLE 2. Dissociation Relationships for a Few Low-Lying States of Ga_2

λ-s states	dissociation limit atomic levels	energy Expt[a]
$^3\Sigma_g^-$, $^3\Pi_u$, $^3\Pi_g$, $^3\Delta_u$, $^3\Sigma_u^+(2)$, $^1\Delta_g$, $^1\Pi_u$, $^1\Pi_g$, $^1\Sigma_u^-$, $^1\Sigma_g^+(2)$	$^2P + {}^2P$	0.0
$^3\Pi_g$, $^3\Pi_u$, $^3\Sigma_g^+$, $^3\Sigma_u^+$, $^1\Pi_g$, $^1\Pi_u$, $^1\Sigma_g^+$, $^1\Sigma_u^+$	$^2P + {}^2S(4s^25s)$	24 789

[a] From ref 134.

the 29 934-cm^{-1} region. These bands were assigned by those authors to $A^1\Pi_u \leftarrow X^1\Sigma_g^+$ and $B^1\Sigma_u^+ \leftarrow X^1\Sigma_g^+$, respectively. However, as seen from Table 4, the $^1\Pi_u$ state is below the $^1\Sigma_g^+$ state. Further, the most probable candidate for the ground state is $^3\Pi_u$. Balasubramanian[133] argued that the most consistent allowed electric dipole transition for the 15 590-cm^{-1} is the $A^3\Pi_g \leftarrow X^3\Pi_u$ transition. The absorption bands in the 29 000-cm^{-1} region could be assigned to the $^3\Pi_g(II) \leftarrow X^3\Pi_u$ transition. The theoretical T_{vert} (29 102 cm^{-1}) is most consistent with the observed bands in this region.

Ginter et al.[122] reported emission bands in the 19 500–22 000-cm^{-1} region for Ga_2. It can be inferred from Tables 3 and 4 that the most probable transition for these bands is the $^3\Sigma_u^-(I) \rightarrow {}^3\Sigma_g^-(I)$ transition. The theoretical transition energy for this transition (21 191 cm^{-1}) was found to be in very good agreement with the observed bands in this region (19 000–21 000 cm^{-1}).

The theoretical dissociation energy of the ground state of Ga_2 obtained by Balasubramanian[133] was found

TABLE 3. FOCI Spectroscopic Properties of Ga_2[a]

state	R_e (Å)	T_e (cm^{-1})	ω_e (cm^{-1})	O_e (eV)
$X^3\Pi_u$	2.762	0	158	1.18
$^3\Sigma_g^-$	2.506	446	197	1.13
$^1\Pi_u$	2.802	4037	145	0.68
$^1\Sigma_g^+$	2.954	4129	129	0.67
$^1\Delta_g$	2.584	4274	168	0.65
$^1\Sigma_g^+(II)$	2.912	8267	125	-
$^3\Sigma_u^-$	2.681	20 978	166	-
$^1\Delta_u$	2.702	28 772	210	-
$^3\Pi_g(II)$	3.495	29 877	86	-
$^3\Delta_u(II)$	2.407	30 325	292	-
$^1\Sigma_u^+$	2.757	35 706	210	-
$^4\Pi_g(II)$	3.261	36 722	58	
$^3\Pi_g(III)$	2.471	37 865	315	
$^3\Sigma_g^-(III)$	2.773	40 125	164	
$^3\Delta_g$	3.063	43 383	84	
$^1\Pi_g(III)$	2.389	45 318	153	
$^3\Pi_u(III)$	2.831	45 875	125	
$^1\Sigma_u^+(II)$	3.444	44 687	84	
$^1\Pi_u(III)$	2.743	54 052	353	

[a] From ref 133. The A state observed in the A ← X broad band was system assigned to the $^3\pi_g \leftarrow ^3\pi_u$ transition.[133]

to be 1.2 eV. This was in reasonable agreement with the thermodynamic value of 1.4 eV.[131,132] However, the thermodynamic value needs to be recalculated by using the correct partition function for Ga_2. Balasubramanian's calculations on Ga_2 should be useful in calculating the partition function.

A number of low-lying allowed electric dipole transitions exist for Ga_2, many of which have not yet been observed (Table 4). Specifically, $^3\Sigma_g^- \rightarrow ^3\Sigma_u^-(II)$ is an allowed dipole transition, which falls in the region of 41000 cm^{-1}. The theoretical transition energy should be slightly higher than the true energy. The $^3\Sigma_g^-(II) \leftarrow$ $X^3\Pi_u$ and $^3\Sigma_g^-(I) \leftarrow X^3\Pi_u$ transitions are allowed in the perpendicular direction. The former transition energy is in the 28000-cm^{-1} region. Transitions originating from the $^1\Pi_u$ electronic state to the $^1\Pi_g$ as well as $^1\Pi_g(II)$ states should also be investigated.

Table 5 depicts the contribution of various electronic configurations to the electronic states of Ga_2. As seen from Table 5, the ground state ($^3\Pi_u$) as well as $^1\Pi_u$ is dominantly $1\sigma_g^2 1\sigma_u^2 2\sigma_g 1\pi_u$. The $^3\Sigma_g^-$ and $^1\Delta_g$ states arise from the $1\sigma_g^2 1\sigma_u^2 1\pi_u^2$ configuration. The $^1\Sigma_g^+$ state exhibits an interesting behavior as a function of internuclear distance. At short and near-equilibrium distances this state is a mixture of $1\sigma_g^2 1\sigma_u^2 1\pi_u^2$ and $1\sigma_g^2 1\sigma_u^2 2\sigma_g^2$ configurations. Consequently, the R_e value of the $^1\Sigma_g^+$ state is quite different from the R_e values of the $^3\Sigma_g^-$ and $^1\Delta_g$ states, which are predominantly $1\sigma_g^2 1\sigma_u^2 1\pi_u^2$. At longer distances, $^1\Sigma_g^+(II)$ exhibits approximately the opposite behavior in that $1\sigma_g^2 1\sigma_u^2 1\pi_u^2$ makes a significant contribution at long distances.
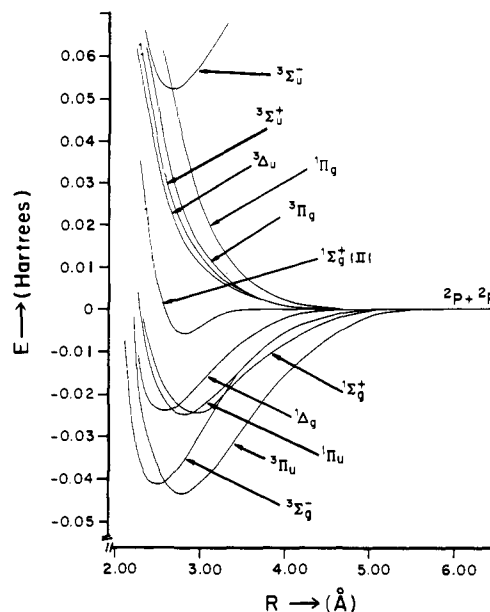

Figure 1. Potential energy curves for the electronic states of Ga_2 (reprinted from ref 133; copyright 1986 American Chemical Society). See Table 3 for spectroscopic labels of experimentally known states.

TABLE 4. Vertical and Adiabatic Excitation Energies for Dipole-Allowed Transitions[a]

Electronic Transitions	T_{vert} (cm^{-1})	T_e (cm^{-1})
$A^3\Pi_g \leftarrow X^3\Pi_u$	14 147	b
$^3\Sigma_g^- \leftarrow ^3\Sigma_u^-$	22 052	21 191
$^3\Sigma_g^- \leftarrow ^3\Sigma_u^-(II)$	41 570	41 307
$^3\Pi_u \leftarrow ^3\Sigma_g^-$	1 288	410
$^3\Pi_u \leftarrow ^3\Sigma_g^-(II)$	32 419	27 954
$B^3\Pi_g(II) \leftarrow X^3\Pi_u$	29 102	27 565
$^1\Pi_u \leftarrow ^1\Sigma_g^+$	1 029	1 026
$^1\Pi_u \leftarrow ^1\Pi_g$	12 248	b
$^1\Pi_u \leftarrow ^1\Pi_g(II)$	31 172	29 493

[a] From ref 133. [b] Final electronic state is not bound.

The Rydberg configurations make substantial contributions to the $^3\Sigma_u^+(III)$, $^3\Sigma_u^+(II)$, and $^3\Delta_u$ states at short distance. For the first two states, the contributions from Rydberg configurations are 23% and 16%, respectively. The theoretical T_e value for the $^3\Sigma_u^+(III)$ state should therefore not be regarded as accurate since the valence basis set needs to be extended further for proper description of Rydberg orbitals. For the $^3\Sigma_u^-$ and $^3\Sigma_u^-(II)$ states of spectroscopic interest, the contribution of the Rydberg configurations at the equilibrium geometry is small. The total contribution of Rydberg configurations for the $^3\Sigma_u^-(II)$ state at 2.50 Å is 4%. The total contribution of Rydberg states for the $^3\Sigma_u^-$ state at 3.00 Å (equilibrium geometry) is 9%. At long distances, however, these states eventually become Rydberg states, as their dissociation limits include Rydberg atoms. More recently, Shim and Gingerich[304] completed all-electron calculations on Ga_2 and Ga_3. Their results are in good agreement with Balasubramanian's results on Ga_2 shown in Table 3.

TABLE 5. Contributions (%) of Various Configurations to the Electronic States of Ga_2

state	distance	$1\sigma_g^2 1\sigma_u^2 2\sigma_g \pi_u$	$1\sigma_g^2 1\sigma_u^2 \pi_u^2$	$1\sigma_g^2 1\sigma_u^2 \sigma_u \pi_g$	$1\sigma_g^2 1\sigma_u^2 2\sigma_u \pi_u$	$1\sigma_g^2 1\sigma_u^2 2\sigma_g \pi_g$	$1\sigma_g^2 1\sigma_u^2 2\sigma_g^2$	$1\sigma_g^2 1\sigma_u^2 \pi_u^2$	$1\sigma_g^2 1\sigma_u^2 2\sigma_u \pi_g$
$^3\Pi_u$	3.00	89							1.57
	5.00	70							22
$^3\Sigma_g^-$	2.70		88					2	
	4.00		72					19.3	
$^1\Pi_u$	3.00	88							2.5
	5.00	64							27
$^1\Delta_g$	2.85		85					5.6	
	3.00		54					37	
$^1\Sigma_g'$	3.00		48				32	4.2	
	3.25		38				38	4.2	
	3.75		52				18	15	
	5.00		53					38	
$^1\Sigma_g'(II)$	3.00		31				40	8.3	
	3.25		37				32.5	12	
	3.75		15				48	10	
$^3\Delta_u$	2.80								
$^3\Pi_g$	3.00			91	8	73.3			
	5.00				31	60			

state	distance	$1\sigma_g^2 1\pi_u^2 \pi_u^2$	$1\sigma_g^2 1\sigma_u^2 \pi_u \pi_g$	$1\pi_g^2 1\sigma_u^2 2\sigma_u \pi_u$	$1\sigma_g^2 1\sigma_u^2 2\sigma_g \pi_g$	$1\sigma_g^2 1\sigma_u^2 \pi_u^2$	$1\sigma_g^2 1\sigma_u 2\sigma_g \pi_u$	$1\sigma_g^2 1\sigma_u 2\sigma_g \pi_u^2$	$1\sigma_g^2 1\sigma_u 2\sigma_g \pi_g^2$	$1\sigma_g^2 1\sigma_u^2 2\sigma_g 2\sigma_u$
$^3\Sigma_u^-$	2.70		68					8.6		
	3.00		66					12	1	
	4.00		84						2	
$^1\Pi_g$	3.00			18	64					
	5.00			34	58					
$^3\Pi_g(II)$	3.00			54	5		13.7			
	5.00			56	29					
$^3\Sigma_g^-(II)$	4.00	17				66				
$^3\Sigma_u^-(II)$	2.50		4					76		
	2.70		3					74		
	3.00		2					70		
$^1\Pi_g(II)$	3.00			47.5	16		16			
	5.00			50	29					
$^3\Sigma_u^+$	2.55		90							
	2.80		91							
$^3\Sigma_u'(II)$	2.25							79	3.3	2
	2.55							43		21
	2.80							3		49
$^3\Sigma_u'(III)$	2.55							33		24
	2.80							69	7.4	1
$^3\Delta_u(II)$	2.80							76	4	

B. Ge_2

The only spectroscopic study of Ge_2 appears to be the Raman and fluorescence spectroscopic investigation of Froben and Schulze.[135] The other experimental study on Ge_2 is that of Gingerich and co-workers[136] which deals with the dissociation energy of Ge_2. Shim et al.[137] as well as Pacchioni[138] have studied the lowest lying states of Ge_2 using the Hartree–Fock (HF)/CI method. The molecular orbitals for CI calculations were obtained by a single-configuration SCF treatment. As Shim et al.[137] noted, starting with MOs obtained by different states led to different results in this method. Thus, a single-configuration SCF treatment does not seem to be very reliable for obtaining the spectroscopic properties of excited states. Also, the splitting between the $^3\Sigma_g^-$ and $^3\Pi_u$ states is small for Ge_2, analogous to Ga_2.

Balasubramanian[139] made CASSCF/FOCI calculations on Ge_2 employing RECPs that retained the $4s^2 4p^2$ outer shells in the valence space. A (3s3p1d) valence Gaussian basis set of the same quality employed for Ga_2 was used for Ge_2. Table 6 shows a few low-lying MO

configurations and a list of possible λ–s states for Ge_2. Table 7 shows the dissociation limits for the low-lying states of Ge_2. As seen from these tables, there are many low-lying states for Ge_2.

Table 8 shows the theoretical spectroscopic properties (R_e, T_e, ω_e) of 14 low-lying electronic states of Ge_2 obtained by Balasubramanian.[139] Figure 2 shows the potential energy curves of some of these states. As one can see from Table 8, the ground state of Ge_2 is $X^3\Sigma_g^-$; however the $^3\Pi_u$ state is only 767 cm^{-1} above the $^3\Sigma_g^-$ state. Since this splitting is small, the possibility of $^3\Pi_u$ being the ground state cannot be ruled out since higher order correlation corrections not included in Balasubramanian's calculations[139] may reverse the ordering.

Table 9 shows the adiabatic transition energies of some allowed electric dipole transitions. The most important transition originating from the ground state ($^3\Sigma_g^-$) is the $^3\Sigma_u^- \leftrightarrow X^3\Sigma_g^-$ transition. The theoretical energy separation for this transition is 20 979 cm^{-1}. The corresponding transition was observed for Sn_2 at 18 222 cm^{-1}.[140] It seems that to date this transition has not been observed for Ge_2. The spectroscopic bands in this

TABLE 6. A Few Low-Lying Electronic Configurations of Ge₂ and the λ-s States Arising from Them[a]

MO configuration	λ-s states
$2\sigma_g^2 1\pi_u^2$	$^3\Sigma_g^-$, $^1\Delta_g$, $^1\Sigma_g^+$
$2\sigma_g 1\pi_u^3$	$^3\Pi_u$, $^1\Pi_u$
$1\pi_u^4$	$^1\Sigma_g^+$
$2\sigma_g 2\sigma_u 1\pi_u^2$	$^5\Sigma_u^-$, $^3\Sigma_u^-(2)$, $^1\Sigma_u^-$, $^3\Delta_u$, $^3\Sigma_u^+$, $^1\Delta_u$, $^1\Sigma_u^+$
$2\sigma_g^2 2\sigma_u 1\pi_u$	$^3\Pi_g$, $^1\Pi_g$
$2\sigma_g^2 1\pi_u 1\pi_g$	$^3\Delta_u$, $^3\Sigma_u^-$, $^3\Sigma_u^+$, $^1\Delta_u$, $^1\Sigma_u^+$, $^1\Sigma_u^-$

[a] The $1\sigma_g^2 1\sigma_u^2$ shell is not shown.

TABLE 7. Dissociation Relationships for a Few Molecular States of Ge₂

Molecular States	Atomic States	Energy of the separated atoms[a]
$^1\Sigma_g^+(2)$, $^1\Sigma_u^-$, $^1\Pi_g$, $^1\Pi_u$, $^1\Delta_g$, $^3\Sigma_u^+(2)$, $^3\Sigma_g^-$, $^3\Pi_g$, $^3\Pi_u$, $^3\Delta_u$, $^5\Sigma_g^+(2)$, $^5\Sigma_u^-$, $^5\Pi_g$, $^5\Pi_u$, $^5\Delta_g$	$^3P + {}^3P$	0.0
$^3\Sigma_g^+$, $^3\Sigma_u^+$, $^3\Sigma_g^-(2)$, $^3\Sigma_u^-(2)$, $^3\Pi_g(3)$, $^3\Pi_u(3)$, $^3\Delta_g(2)$, $^3\Delta_u(2)$, $^3\Phi_g$, $^3\Phi_u$	$^3P + {}^1D$	7126

[a] From ref 134.

TABLE 8. Theoretical Spectroscopic Constants of Ge₂[a]

State	R_e (Å)	T_e (cm^{-1})	ω_e (cm^{-1})
$^3\Sigma_g^-$	2.44	0	259
$^3\Pi_u$	2.34	767	251
$^1\Delta_g$	2.50	3982	255
$^1\Sigma_g^+$	2.44	5521	192
$^1\Pi_u$	2.35	5794	269
$^1\Sigma_g^+$(II)	2.41	10 840	258
$^3\Delta_u$	2.88	13 534	162
$^3\Pi_g$	2.67	13 995	167
$^3\Pi_g$(II)	2.69	17 373	165
$^1\Pi_g$	2.95	17 465	99
$^3\Sigma_u^-$	2.93	20 979	152
$^3\Sigma_u^-$(II)	3.68	24 634	100
$^1\Delta_u$	2.86	29 078	156
$^1\Pi_u$(II)	3.25	32 663	125

[a] The experimental $D_0{}^0$ = 2.65 eV (Kingcade et al.[136]) compared to CASSCF/FOCI D_e(Ge₂) = 2.3 eV. All spectroscopic constants are from ref 139.
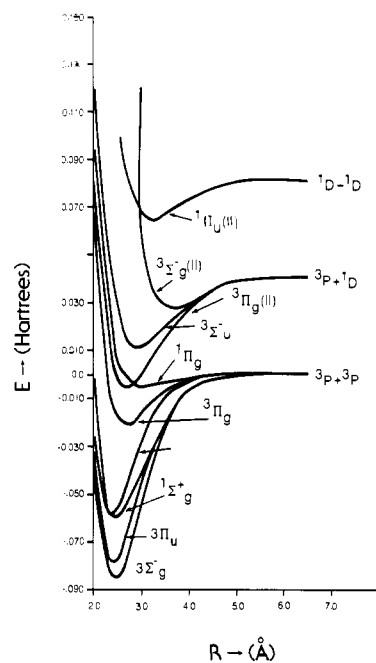
Figure 2. Potential energy curves for the low-lying electronic states of Ge₂ (reprinted from ref 139; copyright 1987 Academic Press, Inc.).

region should be intense and well resolved. The $^3\Pi_g$ ↔ $^3\Pi_u$ transition is also important. Balasubramanian's calculations predicted this transition to be in the 13000-cm^{-1} region. The $^3\Pi_u$ ↔ $^3\Sigma_g^-$ transition energy for Ge₂ is much lower than the corresponding 0_u^+ ↔ 0_g^+ transition for Sn₂ or Pb₂.

The $^1\Sigma_g^+$ state may be observable with small probability in the $^3\Sigma_u^-(0_u^+)$ → $^1\Sigma_g^+(0_g^+)$ emission, since Ge₂ is a reasonably heavy molecule. The theoretical energy for this transition is 15 460 cm^{-1}.[139] If the $^3\Sigma_u^-$ state can be populated, then this transition should be observable in emission. In the same way, the $^3\Sigma_u^-(0_u^+)$ → $1\Sigma_g^+$(II) transition should be observable in the 10 140-cm^{-1} region. The $^3\Pi_g$(II) ↔ $^3\Pi_u$ transition is also an important allowed electric dipole transition. As seen from Table 9 this transition occurs at 16 503 cm^{-1}. The electronic spectra that correspond to the $^1\Pi_g$ ↔ $^1\Pi_u$ and $^1\Pi_u$(II) ↔ $^1\Pi_g$ transitions should be in the regions of 12 204 and 15 198 cm^{-1}, respectively.

The theoretical CASSCF/FOCI[139] D_e value for the ground state (X$^3\Sigma_g^-$) of Ge₂ is 2.29 eV. This is in reasonable agreement with the experimental value of 2.65 eV reported by Gingerich and co-workers.[136] The small discrepancy between the calculated and observed values

could be attributed to higher order correlation corrections as well as the use of effective core potentials. Balasubramanian's D_e[139] was found to be close to the HF/CI calculation of Pacchioni,[138] which yielded a D_e value of 2.34 eV. Balasubramanian's vibrational frequencies of the $^3\Sigma_g^-$ and $^3\Pi_u$ states were in reasonable agreement with those of Shim et al.[137] The value reported by Pacchioni[138] for the $^3\Pi_u$ state (195 cm^{-1}), however, is different from Balasubramanian's and that of Shim et al.[137] For both Sn₂ and Pb₂ the vibrational frequencies of $^3\Sigma_g^-$ and $^3\Pi_u$ differ by at most 10%.

TABLE 9. Adiabatic Transition Energies of Allowed Electric Dipole Transitions of Ge_2^a

Transition	Energy (cm⁻¹)	Transition	Energy (cm⁻¹)
$^3\Pi_u \rightarrow {}^3\Sigma_g^-$	767	$^3\Pi_g(II) \rightarrow {}^3\Pi_u$	16 503
$^3\Sigma_g^-(II) \rightarrow {}^3\Sigma_u^-$	3655	$^3\Sigma_u^- \rightarrow {}^3\Sigma_g^-$	20 979
$^3\Pi_g(II) \rightarrow {}^3\Delta_u$	3839	$^1\Pi_u(II) \rightarrow {}^1\Sigma_g^+(II)$	21 623
$^1\Sigma_g^+(II) \rightarrow {}^1\Pi_u$	5579	$^3\Pi_u(II) \rightarrow {}^3\Sigma_g^-$	24 357
$^1\Pi_g \rightarrow {}^1\Pi_u$	12 204	$^1\Delta_u \rightarrow {}^1\Delta_g$	25 096
$^3\Pi_g \rightarrow {}^3\Pi_u$	13 125	$^1\Pi_u(II) \rightarrow {}^1\Sigma_g^-$	27 142
$^1\Pi_u(II) \rightarrow {}^1\Pi_g$	16 198	$^1\Pi_u(II) \rightarrow {}^1\Delta_g$	28 681

^{a}From ref 139.

TABLE 10. Contributions of Various Configurations to the Electronic States of Ge_2 at Their Equilibrium Geometries^a

State	Configurations
$^3\Sigma_g^-$	$2\sigma_g^2 1\pi_u^2$ (85%), $2\sigma_g^2 1\pi_g^2$ (2%)
$^3\Pi_u$	$2\sigma_g 1\pi_u^3$ (80%), $2\sigma_g 1\pi_u 1\pi_g^2$ (7%)
$^1\Delta_g$	$2\sigma_g^2 1\pi_u^2$ (83%), $2\sigma_g^2 1\pi_g^2$ (5%)
$^1\Pi_u$	$2\sigma_g 1\pi_u^3$ (80%), $2\sigma_g 1\pi_u 1\pi_g^2$ (8%)
$^1\Sigma_g^+$	$2\sigma_g^2 1\pi_u^2$ (63%), $1\pi_u^4$ (17%), $2\sigma_g^2 1\pi_g^2$ (6%)
$^1\Sigma_g^+(II)$	$1\pi_u^4$ (52%), $2\sigma_g^2 1\pi_u^2$ (17%), $1\pi_u^2 1\pi_g^2$ (14%)
$^3\Delta_u$	$2\sigma_g^2 1\pi_u 1\pi_g$ (82%), $1\pi_u^3 1\pi_g$ (3%)
$^3\Sigma_g^-$	$2\sigma_g 1\pi_u^2 1\pi_g$ (83%), $2\sigma_g 1\pi_u^3$ (2%)
$^3\Pi_g(II)$	$2\sigma_g 1\pi_u^2 1\pi_g$ (83%), $2\sigma_u 1\pi_u 1\pi_g^2$ (2%)
$^3\Sigma_u^-$	$2\sigma_g^2 1\pi_u 1\pi_g$ (57%), $2\sigma_g 2\sigma_u 1\pi_u^2$ (17%), $1\pi_u^3 1\pi_g$ (8%), $2\sigma_g 2\sigma_u 1\pi_g^2$ (4%)
$^3\Sigma_g^-(II)$	$2\sigma_g 2\sigma_u 1\pi_u 1\pi_g$ (47%), $2\sigma_g^2 1\pi_g^2$ (16%), $2\sigma_g^2 1\pi_u^2$ (15%), $1\pi_u^2 1\pi_g^2$ (10%)
$^1\Delta_u$	$2\sigma_g^2 1\pi_u 1\pi_g$ (54%), $2\sigma_g 2\sigma_u 1\pi_u^2$ (17%), $1\pi_u^3 1\pi_g$ (14%), $2\sigma_g 2\sigma_u 1\pi_g^2$ (3%)
$^1\Pi_u(II)$	$2\sigma_g 1\pi_u 1\pi_g^2$ (57%), $2\sigma_g 1\pi_u^3$ (15%), $2\sigma_u 1\pi_u^2 1\pi_g$ (11%)

^{a}From ref 139.

However, Pacchioni's ω_e for $^3\Pi$ is 17% smaller.

Table 10 shows the contributions of various MO configurations to the FOCI wave function of the electronic states of Ge_2. As seen from Table 10, the $^3\Sigma_g^-$ and $^1\Delta_g$ states are predominantly $2\sigma_g^2 1\pi_u^2$. The $^3\Pi_u$ and $^1\Pi_u$ states are composed predominantly of the $2\sigma_g 1\pi_u^3$ configuration. Like Ga_2, the $^1\Sigma_g^+$ state of Ge_2 exhibits an interesting behavior as a function of internuclear distance. At short distances, it was found to be predominantly made of the $1\pi_u^4$ configuration. At near-equilibrium geometries this state was found to be a mixture of $2\sigma_g^2 1\pi_u^2$ and $1\pi_u^4$ configurations. The $^1\Sigma_g^+(II)$ state is also a mixture of these two configurations, with the latter configuration making a greater contribution at its near-equilibrium geometry. Thus, these states exhibit avoided crossings. As seen from Table 10, corre-

TABLE 11. Dissociation Relationships for a Few Low-Lying States of As_2

Molecular States	Atomic States	Energy (cm⁻¹)^a
$^1\Sigma_g^+, {}^3\Sigma_u^+, {}^5\Sigma_g^+, {}^7\Sigma_u^+$	$^4S + {}^4S$	0.0
$^3\Sigma_g^+, {}^3\Sigma_u^+, {}^3\Pi_g, {}^3\Pi_u, {}^3\Delta_g, {}^3\Delta_u,$ $^5\Sigma_g^+, {}^5\Sigma_u^+, {}^5\Pi_g, {}^5\Pi_u, {}^5\Delta_g, {}^5\Delta_u$	$^4S + {}^2D$	10,790
$^3\Sigma_g^-, {}^3\Sigma_u^-, {}^3\Pi_g, {}^3\Pi_u,$ $^5\Sigma_g^-, {}^5\Sigma_u^-, {}^5\Pi_g, {}^5\Pi_u$	$^4S + {}^2P$	13,530
$^1\Sigma_g^+(3), {}^1\Sigma_u^-(2), {}^1\Pi_g(2), {}^1\Pi_u(2),$ $^1\Delta_g(2), {}^1\Delta_u, {}^1\Phi_g, {}^1\Phi_u, {}^1\Gamma_g,$ $^3\Sigma_u^+(3), {}^3\Sigma_g^-(2), {}^3\Pi_u(2), {}^3\Pi_g(2),$ $^3\Delta_u(2), {}^3\Delta_g, {}^3\Phi_u, {}^3\Phi_g, {}^3\Gamma_u$	$^2D + {}^2D$	21,580

^{a}Experimental atomic energy separations from ref 134.

lation seems to be a bit more important for the $^3\Pi_u$ state than the $^3\Sigma_g^-$ state. Consequently, higher order correlation effects may lower the $^3\Pi_u$ state a bit more compared to the $^3\Sigma_g^-$ state. The $^3\Sigma_u^-$ state is a mixture of the $2\sigma_g^2 1\pi_u 1\pi_g$, $2\sigma_g 2\sigma_u 1\pi_u^2$, and $1\pi_u^3 1\pi_g$ configurations, suggesting the existence of another $^3\Sigma_u^-$ state that would also be a mixture of these and other configurations. Although Balasubramanian[139] did not calculate the energies of this state at all distances, on the basis of the splitting of this state at 2.75 Å from the equilibrium geometry of the ground state it was predicted that the T_e value of this state should be below 29 000 cm⁻¹.

C. As_2

Electronic spectra of As_2 were first observed by Gibson and MacFarlane[71] in 1934. These authors[71] studied the absorption spectrum of As_2 in the 40 500-cm⁻¹ region. The vibrational levels of the excited state participating in these bands were highly perturbed and predissociated, which led to the prediction of crossing of another potential energy curve with this curve. Later, a number of authors studied the As_2 molecule experimentally.[141–154,158] These studies included both absorption and emission spectra of As_2 in the visible and vacuum-UV regions. Particular systems that have been observed include A ↔ X, C → X, C ← A, a → X, B → X, d → X, and D → c. Among these, the A ↔ X system has been extensively studied. Vibrational and rotational analyses of a number of observed systems have been carried out.[146,150] Heimbrook et al.[156] studied the As_2 dimer generated by evaporating gallium arsenide which was then trapped in solid neon. These authors[156] studied vibronic bands of three systems of As_2 designated as the c ↔ X, e → X, and a ↔ X systems. Both the ionization potential[147] and the electron affinity[148] of As_2 have been measured.

Theoretical calculations on As_2 include those of Kok and Hall,[155] Watanabe et al.,[157] and Balasubramanian.[159] The first two works were restricted only to the ground state of As_2.[155,157] Balasubramanian[159] carried out CASSCF/FOCI calculations on 18 electronic states of As_2 using RECPs (4s²4p³ shell of As included explicitly

TABLE 12. Spectroscopic Properties of As$_2$^{a}

State	R_e (Å)		T_e (cm^{-1})		ω_e (cm^{-1})	
	Theory	Expt.	Theory	Expt.	Theory	Expt.
$X^1\Sigma_g^+$	2.164	2.103	0	0	394	430
$c^3\Sigma_u^+$	2.418	2.304	11 860	14 500	235	314
$e^3\Delta_u$	2.357	--	19 976	19 915	324	330
$^3\Pi_g$	2.58	--	26 053	--	316	--
$a^3\Sigma_u^-$ 0_u^+	2.345	2.279	26 406	24 641	341	337
$^3\Delta_g$	2.756	--	30 676	--	179	--
$^1\Delta_u$	2.313	--	30 743	--	341	--
$^1\Sigma_g^+$(II)	2.561	--	32 722	--	274	--
$^1\Pi_g$	2.298	--	33 262	--	317	--
$^1\Sigma_g^+$(III)	2.654	--	41 228	--	221	--
$A^1\Sigma_u^+$	2.466	[2.50]	43 207	[40 349]	253	[260]
$b^3\Pi_u$(II)	2.561	--	44 669	--	200	--
$^1\Pi_u$	2.535	--	45 327	--	216	--
$^1\Delta_g$	2.747	--	47 668	--	174	--
$^1\Pi_u$(II)	2.74	--	51 294	--	108	--

^{a} Theoretical spectroscopic constants are from ref 159. Experimental values are from ref 37.

Figure 3. Potential energy curves for the low-lying singlet electronic states of As$_2$ (reprinted from ref 159; copyright 1987 Academic Press, Inc.). See Table 12 for spectroscopic labels of known states.

Figure 4. Potential energy curves for the low-lying triplet states of As$_2$ (reprinted from ref 159; copyright 1987 Academic Press, Inc.). See Table 12 for spectroscopic labels of known states.

in valence) and a valence (3s3p1d) Gaussian basis set. The CASSCF active space included four a$_1$, two b$_2$, and two b$_1$ orbitals in the C_{2v} group. The FOCI calculations included up to 27 000 configurations while the CASSCF calculations included up to 384 configurations.

Table 11 shows the possible low-lying electronic states of As$_2$ and their dissociation limits. As seen in Table 11, due to the 4s^{2}4p^3 open-shell ground state of the As atom, As$_2$ has the largest number of possible valence electronic states of all the dimers in that row. The ground state of As$_2$ is a $^1\Sigma_g^+$ state arising from $1\sigma_g^2 1\sigma_u^2 2\sigma_g^2 1\pi_u^4$, which represents a triple bond between As atoms.

Table 12 shows the spectroscopic properties of a number of low-lying states of As$_2$. Also indicated in that table are the assignments of the states that have been observed experimentally. Figure 3 shows the potential energy curves of low-lying singlet states, and Figure 4 shows the potential energy curves of the triplet states. As seen from Table 12, the theoretical bond length of the ground state is ~0.06 Å longer than the experimental value. The slightly longer bond was attributed by Balasubramanian[159] to higher order correlation effects that were not included in the FOCI calculations and the use of RECPs.

The strongest electric dipole transition from the ground state is the $A^1\Sigma_u^+ \leftrightarrow X^1\Sigma_g^+$ transition. The first $^1\Sigma_u^+$ state is calculated 43 207 cm^{-1} above the ground state (Table 12). This has been characterized experimentally as the A $\leftrightarrow$ X system in the 40 350-cm^{-1} region. The calculated ω_e and R_e values of the A state are in very good agreement with the experimental values. The $^1\Sigma_u^+$ state is a mixture of the $1\sigma_g^2 1\sigma_u^2 2\sigma_g^2 1\pi_u^3 1\pi_g$,
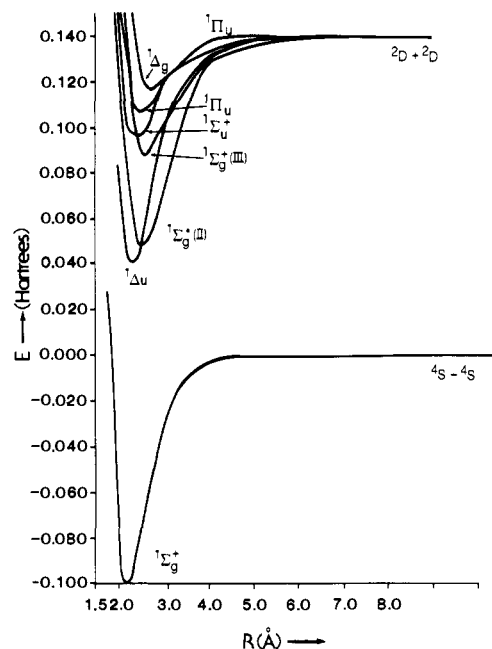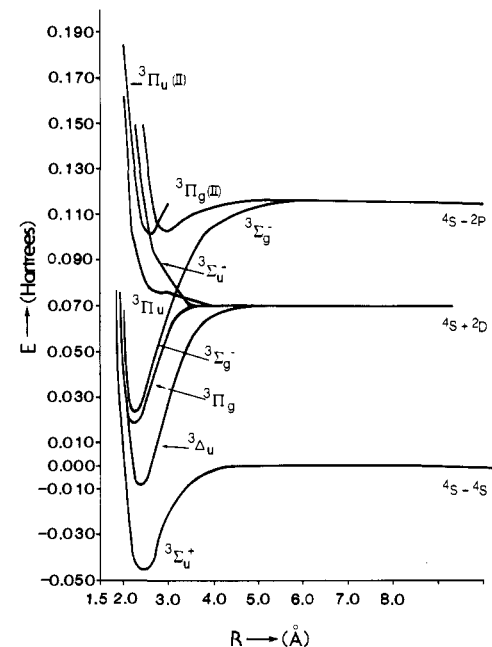
$1\sigma_g^2 1\sigma_u^2 2\sigma_g 2\sigma_u 1\pi_u^4$, and $1\sigma_g^2 1\sigma_u^2 1\pi_u 1\pi_g^3$ configurations.

As already mentioned, the A $\leftrightarrow$ X bands are predissociated and have been studied by many authors. Balasubramanian's[159] theoretical calculations supported the existence of a B state near the A state, which had the same symmetry, since the A state is a mixture of several configurations. The exact nature of the state predissociating the A $\leftrightarrow$ X bands has not yet been established.

Heimbrook et al.[156] observed vibronic bands of As$_2$ in the red, yellow, and blue–near-UV regions. These transitions were labeled c $\leftrightarrow$ X$^1\Sigma_g^+$, e $\leftrightarrow$ X, and a $\leftrightarrow$ X. These authors[156] also tentatively assigned the a, c, and

TABLE 13. Leading Configurations of the Various Electronic States of As₂ at Their Equilibrium Geometries[a]

State	Configuration
$^1\Sigma_g^+$	$1\sigma_g^2 1\sigma_u^2 2\sigma_g^2 1\pi_u^4$ (82%), $1\sigma_g^2 1\sigma_u^2 2\sigma_g^2 1\pi_u^2 1\pi_g^2$ (9%)
$^3\Sigma_u^-$	$1\sigma_g^2 1\sigma_u^2 2\sigma_g^2 1\pi_u^3 1\pi_g$ (75%), $1\sigma_g^2 1\sigma_u^2 2\sigma_g^2 1\pi_u 1\pi_g^3$ (11%)
$^3\Delta_u$	$1\sigma_g^2 1\sigma_u^2 2\sigma_g^2 1\pi_u^3 1\pi_g$ (92%), $1\sigma_g^2 1\sigma_u^2 2\sigma_g^2 1\pi_u 1\pi_g^3$ (7%)
$^3\Pi_g$	$1\sigma_g^2 1\sigma_u^2 2\sigma_g 1\pi_u^4 1\pi_g$ (76%), $1\sigma_g^2 1\sigma_u^2 2\sigma_g 1\pi_u^2 1\pi_g^3$ (10%)
$^3\Sigma_u^-$	$1\sigma_g^2 1\sigma_u^2 2\sigma_g^2 1\pi_u^3 1\pi_g^2$ (87%)
$^3\Delta_g$	$1\sigma_g^2 1\sigma_u^2 2\sigma_g^2 1\pi_u^2 1\pi_g^2$ (86%), $1\sigma_g^2 1\sigma_u^2 2\sigma_g^2 1\pi_u^2 1\pi_g^2$ (4%)
$^1\Delta_u$	$1\sigma_g^2 1\sigma_u^2 2\sigma_g^2 1\pi_u^3 1\pi_g$ (86%), $1\sigma_g^2 1\sigma_u^2 2\sigma_g 2\sigma_u 1\pi_u^3 1\pi_g^2$ (3%)
$^1\Sigma_g^+(II)$	$1\sigma_g^2 1\sigma_u^2 2\sigma_g^2 1\pi_u^2 1\pi_g^2$ (57%), $1\sigma_g^2 1\sigma_u^2 2\sigma_g^2 1\pi_u^4$ (15%)
$^1\Pi_g$	$1\sigma_g^2 1\sigma_u^2 2\sigma_g 1\pi_u^4 1\pi_g$ (82%), $1\sigma_g^2 1\sigma_u^2 2\sigma_g^2 1\pi_u^2 1\pi_g^3$ (5%)
$^1\Sigma_g^-(III)$	$1\sigma_g^2 1\sigma_u^2 2\sigma_g^2 1\pi_u^2 1\pi_g^2$ (89%)
$^1\Sigma_u^-$	$1\sigma_g^2 1\sigma_u^2 2\sigma_g^2 1\pi_u^3 1\pi_g$ (47%), $1\sigma_g^2 1\sigma_u^2 2\sigma_g 2\sigma_u 1\pi_u^4$ (22%), $1\sigma_g^2 1\sigma_u^2 2\sigma_g^2 1\pi_u 1\pi_g^3$ (17%)
$^3\Pi_u(II)$	$1\sigma_g^2 1\sigma_u^2 2\sigma_g 1\pi_u^3 1\pi_g^2$ (85%), $1\sigma_g^2 1\sigma_u^2 2\sigma_g 1\pi_u^3 1\pi_g^2$ (1.5%)
$^1\Pi_u$	$1\sigma_g^2 1\sigma_u^2 2\sigma_g 1\pi_u^4 1\pi_g^2$ (81%), $1\sigma_g^2 1\sigma_u^2 2\sigma_g 1\pi_u 1\pi_g^4$ (2%)
$^1\Delta_g$	$1\sigma_g^2 1\sigma_u^2 2\sigma_g 1\pi_u^2 1\pi_g^2$ (61%), $1\sigma_g^2 1\sigma_u^2 2\sigma_g 2\sigma_u 1\pi_u^3 1\pi_g$ (12%), $1\sigma_g^2 1\sigma_u^2 1\pi_u^4 1\pi_g^2$ (11%)
$^1\Sigma_u^-(II)$	$1\sigma_g^2 1\sigma_u^2 2\sigma_g 1\pi_u^3 1\pi_g^2$ (53%), $1\sigma_g^2 1\sigma_u^2 2\sigma_g 1\pi_u 1\pi_g^4$ (22.4%)

[a] Numbers in parentheses are contributions in percentage; from ref 159.

e states to the $^1\Sigma_g^+$, $^3\Sigma_u^+$, and $^3\Delta_u$ states. As seen from Table 12, theoretical calculations support the assignment of the a, c, and e states to the $^3\Sigma_u^-$, $^3\Sigma_u^+$, and $^3\Delta_u$ states. The calculated ω_e values of these states are in reasonable agreement with the experimental results.

The b → X system was observed by Almy and co-workers,[141-143] although no spectroscopic properties have been reported for the b state, since the b → X system appears to be weak. A possible candidate for the b state is a $^3\Pi_u$ state. Balasubramanian's calculations[159] supported the existence of a $^3\Pi_u$ state whose T_e value is 44 669 cm⁻¹ and was designated as $^3\Pi_u(II)$. The experimentally observed bands for the b → X systems are consistent with the theoretical T_e value. Although the $^3\Pi_u \rightarrow ^1\Sigma_g^+$ transition is not allowed in the absence of spin-orbit interaction, the spin-orbit effects seem to be large enough to give rise to the weak $0_u^+ \rightarrow ^1\Sigma_g^+$ transition, where 0_u^+ arises from $^3\Pi_u$. Alternatively, the $^3\Pi_u(1_u) \rightarrow ^1\Sigma_g^+$ transition should also have been observable in the perpendicular direction via spin-orbit mixing of $^3\Pi_u$ with $^1\Pi_u$.

Many electronic states are reported in Table 12 that have not yet been observed. Specifically, the $^1\Pi_u \leftrightarrow ^1\Sigma_g^+$ transition is an allowed electric dipole transition. The calculated T_e value of the $^1\Pi_u$ state is 45 327 cm⁻¹. Thus, this system should be observable in both absorption and emission. Sibai et al.[150] have observed bands in the 42 400-44 500-cm⁻¹ region. The theoretical T_e value of the $^1\Pi_u$ state seems to support the assignment of these bands to the $^1\Pi_u \leftarrow$ X transition, although this assignment is not yet confirmed. The $^1\Pi_u(II) \leftrightarrow X^1\Sigma_g^+$ transition is also an allowed electric dipole transition. From the calculated properties of the $^1\Pi_u(II)$ state (Table 12),

this transition lies at 51 300 cm⁻¹. The theoretical ω_e value of the $^1\Pi_u(II)$ state is 108 cm⁻¹, indicating the broad nature of the potential surface of the $^1\Pi_u(II)$ state. A number of unclassified bands have been observed[158] in the 47 000-55 000-cm⁻¹ region. Thus, the absorption bands in this region could tentatively be assigned to the $^1\Pi_u(II) \leftarrow X^1\Sigma_g^+$ transition.

There are many allowed electronic transitions originating from excited electronic states that appear not to have been observed. The $^3\Pi_u \leftrightarrow ^3\Pi_g$ transition is a strong allowed transition and could be observed as the $^3\Pi_u \rightarrow ^3\Pi_g$ emission system. The approximate energy for this transition is 18 616 cm⁻¹. The $^3\Delta_g \rightarrow ^3\Delta_u$ transition occurs at 10 728 cm⁻¹, and the $^1\Delta_u \rightarrow ^1\Delta_g$ transition could be observed in the region of 17 000 cm⁻¹. None of the bound excited $^1\Sigma_g^+$ states (Table 12) have been characterized experimentally. Emission from the $A^1\Sigma_u^+$ state to all lower $^1\Sigma_g^+$ states is allowed. The $A^1\Sigma_u^+ \rightarrow ^1\Sigma_g^+(II)$ emission could be observed at 10 485 cm⁻¹. The $^1\Sigma_g^+(III)$ and $^1\Sigma_g^+(II)$ states would be accessible in emission from the $B^1\Sigma_u^+$ state. The $^+\Pi_g \rightarrow ^1\Pi_u$ and $^1\Pi_g \rightarrow ^1\Pi_u(II)$ transitions could be observed at 12 065 and 18 032 cm⁻¹, respectively. None of these transitions have been observed.

The theoretical D_e of the ground state of As₂ obtained by using the CASSCF/FOCI method[159] was found to be 21 860 cm⁻¹ or 2.71 eV. The spectroscopic D_e value was obtained by extrapolating the predissociated A-X bands into the $^4S + ^2D$ atomic states.[142,143] The D_e value obtained this way (3.96 eV)[142] should not be regarded as accurate, and usually such extrapolations provide only an upper limit. Nevertheless, second-order correlation corrections could increase the D_e value of the ground state. The D_e of As₂ should, however, be closer to 3.8 eV, and thus CASSCF/FOCI calculations underestimate the D_e of As₂.

Table 13 shows the important configurations contributing to the electronic states near the equilibrium geometries of the various states.[159] As seen from Table 13, the ground state of As₂ was found to be predominantly the triple-bond configuration $1\sigma_g^2 1\sigma_u^2 2\sigma_g^2 1\pi_u^4$, although the $1\sigma_g^2 1\sigma_u^2 2\sigma_g^2 1\pi_u^2 1\pi_g^2$ configurations also make an appreciable contribution, thereby lowering the bond order to 2.64. In Table 13 the sums of the squares of the various configuration spin functions compatible with the electronic distribution are shown. The $A^1\Sigma_u^+$ state participating in the strong A ↔ X system is a mixture of $1\sigma_g^2 1\sigma_u^2 2\sigma_g^2 1\pi_u^3 1\pi_g$, $1\sigma_g^2 1\sigma_u^2 2\sigma_g 2\sigma_u 1\pi_u^4$, and other configurations. The $c^3\Sigma_u^+$ state is predominantly $1\sigma_g^2 1\sigma_u^2 2\sigma_g^2 1\pi_u^3 1\pi_g$. The $a^3\Sigma_u^-$ state is composed of the $1\sigma_g^2 1\sigma_u^2 2\sigma_g^2 1\pi_u^3 1\pi_g$ configuration. From the contributions of the $A^1\Sigma_u^+$ state, it can be deduced that the orthogonal $B^1\Sigma_u^+$ state should be a mixture of the $1\sigma_g^2 1\sigma_u^2 2\sigma_g 2\sigma_u 1\pi_u^4$, $1\sigma_g^2 1\sigma_g^2 2\sigma_g^2 1\pi_u 1\pi_g^3$, and $1\sigma_g^2 1\sigma_u^2 2\sigma_g^2 1\pi_u^3 1\pi_g$ configurations; the first configuration would probably make the highest contribution to the B state.

D. Se₂

The Se₂ dimer has been studied by a number of investigators.[160-172] The earlier works on the spectroscopy of Se₂ are summarized in ref 37. The O₂ analogues of the Schumann-Runge bands that are attributed to the B-X system are observed for Se₂ in the 26 000-cm⁻¹ region. These bands for Se₂ were found to be perturbed by an A state.[165] The B-X, A-X, and a-x systems have

TABLE 14. A Few Low-Lying Electronic Configurations of Se_2 and the λ-s and ω-ω States Arising from Them[a]

Electronic configuration	λ-s states	ω-ω states
$2\sigma_g^2 1\pi_u^4 1\pi_g^2$	$^3\Sigma_g^-$	0_g^+, 1_g
	$^1\Delta_g$	2_g
	$^1\Sigma_g^+$	0_g^+
$2\sigma_g^2 1\pi_u^3 1\pi_g^3$	$^3\Delta_u$	3_u, 2_u, 1_u
	$^3\Sigma_u^-$	0_u^+, 1_u
	$^3\Sigma_u^+$	0_u^-, 1_u
	$^1\Delta_u$	2_u
	$^1\Sigma_u^+$	0_u^+
	$^1\Sigma_u^-$	0_u^-
$2\sigma_g^2 2\sigma_u^1 1\pi_u^4 1\pi_g$	$^3\Pi_u$	0_u^+, 0_u^-, 1_u, 2_u
	$^1\Pi_u$	1_u
$2\sigma_g 2\sigma_u 1\pi_u^4 1\pi_g^2$	$^5\Sigma_u^-$	0_u^-, 1_u, 2_u
	$^3\Sigma_u^-(2)$	$0_u^+(2)$, $1_u(2)$
	$^1\Sigma_u^-$	0_u^-
	$^3\Delta_u$	1_u, 2_u, 3_u
	$^3\Sigma_u^+$	0_u^-, 1_u
	$^1\Delta_u$	2_u
	$^1\Sigma_u^+$	0_u^+

[a] The $1\sigma_g^2 1\sigma_u^2$ shell arising from the valence s is not shown.

TABLE 15. Dissociation Relationships for a Few Low-Lying States of Se_2

Molecular states	Atomic states	Energy of the atoms (cm^{-1})[a]
$^1\Sigma_g^+(2)$, $^1\Sigma_u^-$, $^1\Pi_g$, $^1\Pi_u$, $^1\Delta_g$,	$^3P + ^3P$	0.0
$^3\Sigma_u^+$, $^3\Sigma_g^-$, $^3\Pi_g$, $^3\Pi_u$, $^3\Delta_u$,		
$^5\Sigma_g^+(2)$, $^5\Sigma_u^-$, $^5\Pi_g$, $^5\Pi_u$, $^5\Delta_g$		
$^3\Sigma_g^+$, $^3\Sigma_u^+$, $^3\Sigma_g^-(2)$, $^3\Sigma_u^-(2)$,	$^3P + ^1D$	9576
$^3\Pi_g(3)$, $^3\Pi_u(3)$, $^3\Delta_g(2)$,		
$^3\Delta_u(2)$, $^3\Phi_g$, $^3\Phi_u$		

[a] From ref 134.

TABLE 16. Spectroscopic Properties of Se_2[a]

State	R_e (Å) Calcd.	R_e (Å) Expt.	T_e (cm^{-1}) Calcd.	T_e (cm^{-1}) Expt.	ω_e (cm^{-1}) Calcd.	ω_e (cm^{-1}) Expt.
X $^3\Sigma_g^-$ 0_g^+ X_1	2.244	2.166	0.0	0.0	357	385
1_g X_2	2.240	--	664	512	360	387
a $^1\Delta_g(2_g)$	2.27	--	4652	-4000	341	320
b $^1\Sigma_g^+$ $0_g^+(II)$	2.30		8557	7958	323	355
a $^3\Delta_u$	2.51	--	15241	16321	246	258
$^3\Sigma_u^+$	2.52	--	15651	--	244	--
A $^3\Pi_u$ (0_u^+)	(2.71)	2.51	21277	24111	197	195
A$^3\Pi_u(1_u)$	(2.72)	2.54	21961	24940	194	187
$^3\Pi_u(2_u)$	(2.73)	--	22837	--	189	--
B $^3\Sigma_u^-$	2.54	2.44	24822	25980	232	246
$^3\Sigma_g^-(II)$	3.12	--	30567	--	133	--
$^3\Pi_g(II)$	3.01	--	31582	--	122	--
$^3\Pi_u(II)$	3.32	--	33325	--	--	--
$^3\Delta_u(II)$	3.40	--	33712	--	--	--
$^1\Delta_u$	2.53	--	36814	--	233	--
$^1\Pi_g(II)$	2.58	--	39173	--	325	--
$^1\Delta_u(II)$	2.92	--	41270	--	141	--
$^1\Pi_g(III)$	2.90	--	42556	--	159	--

[a] Experimental values for the X_1, X_2, and B states quoted here are from Huber and Herzberg's book.[37] Experimental values for the $^1\Delta_g$, $^1\Sigma_g^+(0_g^+)$, $^3\Pi_u(0_u^+)$, and $^3\Pi_u(1_u)$ states are from ref 168, 164, 165, and 162, respectively. Theoretical values are from ref 172.

also been observed in a matrix by Bondybey and English.[163] Prosser et al.[164] have observed a $B0_u^+ - b^1\Sigma_g^+$ system by populating the B and A electronic states with a 4131-Å krypton ion laser. In addition, a C–X system was also observed in the 53000-cm^{-1} region. Below 26000 cm^{-1}, five λ-s states of Se_2 and some of their spin–orbit components have been observed. These states were given the labels B, A, a, b, and X, among which B, A, b, and X have been tentatively assigned.

The nature of the state perturbing the $B^3\Sigma_u^-$ state is not well-known. This has been the subject of many investigations.[165,169,170] Further, unlike O_2, the nature of the electronic states below the B state is not clearly understood. Theoretical study of the low-lying electronic states of Se_2 was made by Balasubramanian with the objective of comprehending the nature of the low-lying electronic states of Se_2.[172] He assigned the experimental spectra by a comparison of calculated and observed values. Saxon and Liu[173] have shown that such theoretical calculations yield reasonable spectroscopic constants for O_2 even if errors in D_e may be appreciable. Experimental study of other related group VI and group IV dimers is also quite intense.[174–177]

Balasubramanian[172] carried out CASSCF/FOCI calculations on 20 low-lying electronic states of Se_2 em-

ploying (3s3p1d) valence Gaussian basis sets and RECPs that included the outer $4s^2 4p^4$ shells explicitly in the valence space. The internal space consisted of four a_1 orbitals, two b_2 orbitals, and two b_1 orbitals for Se_2. The FOCI calculations of Se_2 included up to 10750 configurations.
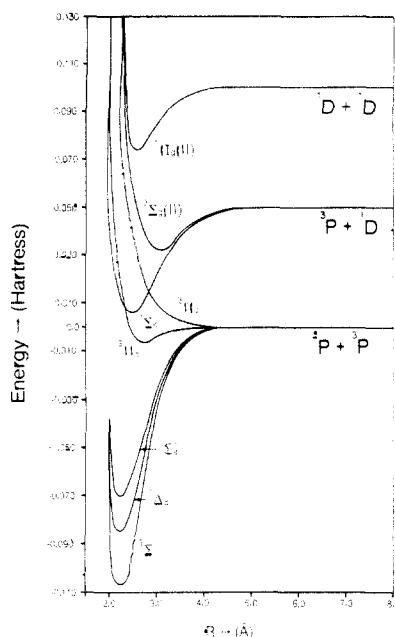
Figure 5. Potential energy curves for the low-lying states of Se_2 (reprinted from ref 172; copyright 1987 American Chemical Society). See Table 16 for spectroscopic labels of known states.

Table 14 depicts the possible low-lying electronic states of Se_2 in both λ-s and ω-ω coupling. Table 15 shows the dissociation relationships for the low-lying electronic states of Se_2. The ground state of Se_2 is evidently an $X^3\Sigma_g^-$ state arising from the $1\sigma_g^2 1\sigma_u^2 2\sigma_g^2 1\pi_u^4 1\pi_g^2$ configuration analogous to O_2. Many of the low-lying electronic states enumerated in these tables were studied by Balasubramanian.

Spin–orbit interaction was also introduced by Balasubramanian[172] to some of the electronic states of Se_2 ($^3\Sigma_g^-$, $^1\Sigma_g^+$, $^3\Pi_u(0_u^+)$, $^3\Pi_u(1_u)$) with the objective of estimating the effect of spin–orbit interaction. This was accomplished through the RCI scheme. A double-ζ STO basis set optimized for the ^3P ground state of the Se atom was employed in SCF/RCI calculations. The ω-ω states arising from the $^3\Sigma_g^-$, $^1\Delta_g$, and $^1\Sigma_g^+$ states were obtained by using the orbitals generated from SCF calculations of the $^3\Sigma_g^-$ state. The ω-ω states arising from the $^3\Pi_u$ and $^1\Pi_u$ states were calculated by using the $^3\Pi_u$ SCF orbitals since $^3\Sigma_g^-$ SCF did not produce a good $2\sigma_u$ orbital as this is unoccupied in the $^3\Sigma_g^-$ state.

The RCI calculations of the 0_g^+ state of Se_2 included single and double excitations from Cartesian reference configurations arising from $1\sigma_g^2 1\sigma_u^2 2\sigma_g^2 1\pi_u^4 1\pi_g^2(^3\Sigma_g^-, ^1\Sigma_g^+)$ and $1\sigma_g^2 1\sigma_u^2 2\sigma_g 1\pi_u^4 1\pi_g^3(^3\Pi_g)$. The 1_g state included five reference configurations arising from $^3\Sigma_g^-(1_g)$, $^3\Pi_g(1_g)$, and $^1\Pi_g(1_g)$. The 2_g state included eight reference configurations arising from $^1\Delta_g$ and $^3\Pi_g$. Balasubramanian[172] also carried out RCI calculations of the 0_u^+, 1_u, and 2_u components of the $^3\Pi_u$ state. The 0_u^+ state included limited single and double excitations from 24 reference configurations arising from a number of $^3\Pi_u$ references and $^3\Sigma_u^-$ references. The 1_u state calculations included $^3\Pi_u$, $^1\Pi_u$, and $^3\Sigma_u^+$ references, while the 2_u calculations included only $^3\Pi_u$ references.

Table 16 shows theoretical and experimental spectroscopic properties (R_e, T_e, and ω_e) of the low-lying electronic states of Se_2. The potential energy curves of some of these states are shown in Figure 5. As seen from Table 16, the ground state (X) is the $^3\Sigma_g^-$ state

arising from the $1\sigma_g^2 1\sigma_u^2 2\sigma_g^2 1\pi_u^4 1\pi_g^2$ configuration. The discrepancies in theoretical R_e and ω_e values of the ground state are within 3–6% of the experimental values. The ω_es of the various states in Table 16 were calculated by using a cubic polynomial fit of energies at near-equilibrium geometries. The small discrepancy between calculated and observed values arises partly from the errors in fits (usually within ± 15 cm^{-1}) and partly from higher order correlation corrections and basis set effects that influence the ω_e values.

The strongest electronic transition originating from the ground state is the $B^3\Sigma_u^- - X^3\Sigma_g^-$ system. The theoretical properties of the $^3\Sigma_u^-$ state are in very good agreement with the spectroscopic values, confirming the earlier assignment of this system. There have been a few experimental investigations on electronic states below the B state. Specifically, the A state in the A–X system was identified by Heaven et al.[169] The T_e value of the A state reported by these authors is about 24 111 cm^{-1}. Balasubramanian's[172] theoretical calculations confirmed the existence of a $^3\Pi_u(0_u^+)$ state with a theoretical T_e of 21 277 cm^{-1} in this region. Thus, the A state was found to be most consistent with $^3\Pi_u(0_u^+)$. The $^3\Pi_u(0_u^+)$ spin–orbit state could mix with $^3\Sigma_u^-(0_u^+)$, although Balasubramanian's RCI calculations revealed that this contamination is negligible for $^3\Pi_u(0_u^+)$ at its equilibrium geometry. Similarly, the mixing of the $^3\Pi_u(1_u)$, $^3\Sigma_u^-(1_u)$, and $^1\Pi_u(1_u)$ state was found to be relatively small for the selenium dimer. Balasubramanian's[172] theoretical R_e value for the A state did not agree well with the value calculated from the experimental spectroscopic data. A similar deficiency was found in the $^3\Pi_u$ states of Br_2 and I_2. The $^3\Pi_u$ state is weakly bound and its surface is shallow. The basis set that was used in conjunction with effective core potentials does not appear to be of sufficient quality to compute the spectroscopic properties of weakly bound excited states. Diffuse basis functions and polarization functions could be important for the $^3\Pi_u$ and $^1\Pi_u$ excited states.

Bondybey and English[163] have observed spectroscopic bands with a T_e value of 16 321 cm^{-1}, which they attributed to a weak electronic transition. These authors call this an a–X system, although this designation could also be used for the 4000-cm^{-1} system. To differentiate the two systems, the state with T_e = 4000 cm^{-1} was denoted by Balasubramanian as a'. Theoretical calculations suggested the existence of a $^3\Delta_u$ state in the neighborhood of the observed electronic bands. The theoretical and experimental ω_e values were also found to be in very good agreement. Further, the $^3\Delta_u \leftrightarrow {}^3\Sigma_g^-$ transition is dipole forbidden, supporting the experimental observation of weak electronic bands in this system. The above reasonings led Balasubramanian to suggest the assignment of this system to the $a^3\Delta_u - X^3\Sigma_g^-$ forbidden transition.

Prosser et al.[164] and Winter et al.[168] characterized an electronic state (b) with a T_e value of 7958 cm^{-1}. The b state was tentatively assigned to the $^1\Sigma_g^+$ electronic state. As seen from Table 16, the results of theoretical calculations support this assignment. The fact that the theoretical and the experimental T_e values of this state are in excellent agreement and that there is no other electronic state with this T_e value led Balasubramanian[172] to confirm unambiguous assignment of the b state to the $^1\Sigma_g^+$ state arising from the $1\sigma_g^2 1\sigma_u^2 2\sigma_g^2 1\pi_u^4 1\pi_g^2$ configuration.

Yee and Barrow[170] studied the absorption and fluorescence spectra of gaseous Se_2 in the 5145–4880-Å region. These authors assigned these bands to an n ↔ a transition where the upper state is believed by these authors[170] to be a relatively weakly bound 1_u state which perturbs the $B^3\Sigma_u^-(0_u^+)$ state. The a state is predicted to be approximately 4000 cm^{-1} above the $X^3\Sigma_g^-(0_g^+)$ ground state and was tentatively assigned to $^1\Delta_g$ based on the lower vibrational frequency of this state compared to that of the ground state ω_e. The theoretical spectroscopic properties for the $^1\Delta_g(2_g)$ state (Table 16) certainly support this assignment. The experimental ω_e value (320 cm^{-1}) does not follow the theoretical trend in Table 16, which implies that the ω_e value of the $^1\Delta_g(2_g)$ state should be 20 cm^{-1} less than the ω_e value of the $^3\Sigma_g^-(0_g^+,1_g)$ states. While the spin–orbit coupling lowers the T_e value of the $^1\Delta_g$ state by 95 cm^{-1}, it does not change the R_e and ω_e values at all. This is primarily a consequence of the fact that the $^1\Delta_g$ state was not found to be contaminated with other λ–s states that give rise to a 2_g ω–ω state such as $^3\Pi_g$. While it is possible that small errors could be introduced by the procedure used by Balasubramanian[172] to calculate ω_es by fitting energies using a cubic polynomial in the near vicinity of the equilibrium geometry, this was ruled out by Balasubramanian based on the fact that identical distances were used for all four states, namely, 0_g^+, 1_g, 2_g, and 0_g^+(II). Consequently, it appears that the experimental ω_e of the $a^1\Delta_g$ state (320 cm^{-1}) is somewhat low and should be about 368 cm^{-1}; this was arrived at by decreasing the experimental ω_e value of the $^3\Sigma_g^-(1_g)$ state by 19 cm^{-1} as implied by the theoretical calculations.

The small difference in the ω_e values of the $X_1 0_g^+$ and $X_2 1_g$ states is mainly due to the spin–orbit mixing of $^3\Sigma_g^-(0_g^+)$ with $^1\Sigma_g^+(0_g^+)$. The 0_g^+ state was found to be a mixture of $^3\Sigma_g^-$ (81%) and $^1\Sigma_g^+$ (8%) λ–s states in the vicinity of the equilibrium geometry. The R_e of $^1\Sigma_g^+$ was found to be larger than the corresponding value for $^3\Sigma_g^-$, and the ω_e value is smaller than that of the $^3\Sigma_g^-$ state. The R_e and ω_e values of the $^3\Sigma_g^-$ and $^1\Sigma_g^+$ states when weighted with appropriate spin–orbit contaminations (81%, 8%) were found to be in accord with the theoretical R_e and ω_e values for the $X_1 0_g^+$ state in Table 16.

Jenouvrier[165] has studied the perturbations of the bands in the $B(^3\Sigma_u^-(0_u^+))$–X system. There is some confusion introduced by using the label A to designate the state that perturbs the B state and the $A^3\Pi_u(0_u^+)$ state. The A state that was found to perturb the B state was assigned to $A^3\Pi_u(1_u)$ by Jenouvrier.[165] It is best to refer to these two states with their Ω quantum number in parentheses. The $A^3\Pi_u(1_u)$ state is 1000 cm^{-1} below the $B0_u^+$ state. There is also another state designated A′ assigned to $A(^1\Pi_u(1_u))$ by Jenouvrier[165] which was also assigned as the state perturbing the B state. The A′ state was found to be only 110 cm^{-1} below the B state.[165] From Table 16 it can be seen that the theoretical 1_u state (predominantly $^3\Pi_u$) is 685 cm^{-1} above the $^3\Pi_u(0_u^+)$ state. The corresponding experimental splitting reported by Jenouvrier[165] is 829 cm^{-1} and is thus in reasonable agreement with the predicted spin–orbit splitting for this state. However, the larger theoretical R_e value was attributed by Balasubramanian to the basis set and suggested further extension of basis sets with more diffuse functions and polarization functions since they appeared to play a significant role

especially for the weakly bound excited states.

As seen from Table 16, the theoretical bond length for the $B^3\Sigma_u^-$ state is 0.1 Å longer than the experimental value primarily due to the limitations of the basis set. The worst case is the $^1\Pi_u$ state, which actually comes out to be repulsive theoretically, while the experimental A′ state, which is tentatively assigned to $^1\Pi_u(1_u)$,[165] is bound, although somewhat less than the A states. More extensive calculations that include diffuse basis functions and polarization functions are needed to calculate the properties of the states perturbing the B states.

Table 16 shows a number of electronic states of Se_2 that are yet to be observed. Specifically, the $^3\Sigma_g^-$(II) state, which has the same symmetry as the ground state, can be observed in the $^3\Sigma_u^- \rightarrow {}^3\Sigma_g^-$(II) emission system if the C state can be populated. The $^3\Pi_u$(II) state has a minimum at a long distance. The dipole-allowed $^3\Pi_u$(II) ← $X^3\Sigma_g^-$ transition should be observable in the 33 000-cm^{-1} region.

The theoretical CASSCF/FOCI D_e of the ground state of Se_2 was found to be 2.91 eV.[172] A number of experimental D_e values were obtained from the predissociation of $B0_u^+$ bands (3.41, 3.16, and 3.10 eV).[37]

TABLE 17. Leading Configuration(s) Contributing to the Low-Lying States of Se_2 at Their Equilibrium Geometries[a]

State	Configuration
$^3\Sigma_g^-$	$2\sigma_g^2 1\pi_u^4 1\pi_g^2$ (89%)
$^1\Delta_g$	$2\sigma_g^2 1\pi_u^4 1\pi_g^2$ (89%), $2\sigma_g^2 1\pi_u^2 1\pi_g^4$ (6%)
$^1\Sigma_g^+$	$2\sigma_g^2 1\pi_u^4 1\pi_g^2$ (82%), $2\sigma_g^2 1\pi_u^2 1\pi_g^4$ (9%)
$^3\Delta_u$	$2\sigma_g^2 1\pi_u^3 1\pi_g^3$ (90%), $2\sigma_u^2 1\pi_u^3 1\pi_g^3$ (3%)
$^3\Sigma_u^+$	$2\sigma_g^2 1\pi_u^3 1\pi_g^3$ (90%), $2\sigma_u^2 1\pi_u^3 1\pi_g^3$ (3%)
$^3\Pi_u$	$2\sigma_g^2 2\sigma_u 1\pi_u^4 1\pi_g$ (66%), $2\sigma_g^2 2\sigma_u 1\pi_u^2 1\pi_g^3$ (22%)
$^3\Sigma_u^-$	$2\sigma_g^2 1\pi_u^3 1\pi_g^3$ (73%), $2\sigma_g 2\sigma_u 1\pi_u^4 1\pi_g^2$ (14%), $2\sigma_g 2\sigma_u 1\pi_u^2 1\pi_g^4$ (4%)
$^3\Sigma_g^-$(II)	$2\sigma_g 2\sigma_u 1\pi_u^3 1\pi_g^3$ (42%), $2\sigma_g^2 1\pi_u^2 1\pi_g^4$ (38%), $2\sigma_g^2 1\pi_u^4 1\pi_g^2$ (8%)
$^3\Pi_g$(II)	$2\sigma_g^2 2\sigma_u 1\pi_u^3 1\pi_g^2$ (78%), $2\sigma_u^2 2\sigma_g 1\pi_u^2 1\pi_g^3$ (7.3%)
$^3\Pi_u$(II)	$2\sigma_g^2 2\sigma_u 1\pi_u^2 1\pi_g^3$ (48%), $2\sigma_g^2 2\sigma_u 1\pi_u^4 1\pi_g$ (23%), $2\sigma_g 2\sigma_u^2 1\pi_u^3 1\pi_g^2$ (20%)
$^3\Delta_u$(II)	$2\sigma_g 2\sigma_u 1\pi_u^4 1\pi_g^2$ (38%), $2\sigma_g 2\sigma_u 1\pi_u^2 1\pi_g^4$ (27%), $2\sigma_g^2 1\pi_u^3 1\pi_g^3$ (24%), $2\sigma_u^2 1\pi_u^3 1\pi_g^3$ (5%)
$^1\Delta_u$	$2\sigma_g^2 1\pi_u^3 1\pi_g^3$ (73%), $2\sigma_g 2\sigma_u 1\pi_u^4 1\pi_g^2$ (14%), $2\sigma_g 2\sigma_u 1\pi_u^2 1\pi_g^4$ (3%)
$^1\Pi_g$(II)	$2\sigma_g 1\pi_u^4 1\pi_g^3$ (84%), $2\sigma_g 2\sigma_u^2 1\pi_u^4 1\pi_g$ (2%)
$^1\Pi_g$(III)	$2\sigma_g^2 2\sigma_u 1\pi_u^3 1\pi_g^2$ (87%)

[a] From ref 172. The $1\sigma_g^2 1\sigma_u^2$ shell is not shown.

Photoionization and thermochemical studies seem to favor the higher value.[171] Yee and Barrow[170] obtained an upper bound for D_e as $27\,096 + 2\lambda''$, where $2\lambda''$ is the $0_g^+-1_g$ splitting. They used a somewhat smaller value of 367 cm⁻¹ for this splitting compared to the theoretical splitting and the observed splitting (Table 16). Balasubramanian corrected this by taking the $0_g^+-1_g$ splitting as 512 cm⁻¹. Balasubramanian thus obtained an upper value for D_e as $27\,608$ cm⁻¹, still eliminating the highest of the three possible D_e values considered by these authors ($27\,700$, $25\,710$, or $25\,166$ cm⁻¹). Thus, the D_e value should be about 3.19 eV. The theoretical value of 2.91 eV seems to favor this more than the 3.41-eV value. A more accurate CASSCF/second-order CI followed by Davidson's correction for unlinked cluster correction may yield a D_e value in closer agreement with the experimental results.

Table 17 shows the weights of the leading configurations in the FOCI wave functions of the electronic states of Se₂. As seen from Table 17, the $^3\Sigma_g^-$, $^1\Delta_g$, and $^1\Sigma_g^+$ states are dominated by the $2\sigma_g^2 1\pi_u^4 1\pi_g^2$ configuration. The $^3\Delta_u$ state observed in the $^3\Delta_u-X^3\Sigma_g^-$ system arises from the $2\sigma_g^2 1\pi_u^3 1\pi_g^3$ configuration. The $A^3\Pi_u$ state was found to be a mixture of the $2\sigma_g^2 2\sigma_u 1\pi_u^4 1\pi_g$ and $2\sigma_g^2 2\sigma_u 1\pi_u^2 1\pi_g^3$ configurations. The $B^3\Sigma_u^-$ state was found to be a mixture of the $2\sigma_g^2 1\pi_u^3 1\pi_g^3$, $2\sigma_g 2\sigma_u 1\pi_u^4 1\pi_g^2$, and $2\sigma_g 2\sigma_u 1\pi_u^2 1\pi_g^4$ configurations. This seems to suggest that the C state observed in the $C^3\Sigma_u^-$ system should be dominated by the $2\sigma_g 2\sigma_u 1\pi_u^4 1\pi_g^2$ configuration, although since this state is observed in the 53 000-cm⁻¹ region, contributions from Rydberg configurations could become significant.

The spin–orbit contamination of the 0_g^+ ground state of Se₂ was found to be 81% $^3\Sigma_g^-$ and 8% $^1\Sigma_g^+$. The $0_g^+(II)$ state is 74% $^1\Sigma_g^+$ and 8% $^3\Sigma_g^-$. The 1_u component of $^3\Pi_u$ was found to be actually 73% $^3\Pi_u$ ($1\sigma_g^2 1\sigma_u^2 2\sigma_g^2 2\sigma_u 1\pi_u^4 1\pi_g$), 2% $^1\Pi_u$ ($1\sigma_g^2 1\sigma_u^2 2\sigma_g^2 2\sigma_u 1\pi_u^4 1\pi_g$), 18% $^3\Pi_u$ ($1\sigma_g^2 1\sigma_u^2 2\sigma_g^2 2\sigma_u 1\pi_u^2 1\pi_g^3$), and 0.2% $^1\Pi_u$ ($1\sigma_g^2 1\sigma_u^2 2\sigma_g^2 2\sigma_u 1\pi_u^2 1\pi_g^3$).

E. Br₂ and Br₂⁺

There are numerous spectroscopic investigations on Br₂. A summary of spectroscopic investigations up to 1977 can be found in the book by Huber and Herzberg.[37] Brand and Hoy[38] have published a more recent review on the experimental spectra of halogens. The electronic spectra of Br₂ in the region below 60 000 cm⁻¹ [37,38] reveal the existence of X, A, B, C, D, E, F, G, and H states. Among these, the A, B, C, F, and G states are observed in either absorption from the ground state or emission to the ground state. The D, E, and H states are observed in D → B, E ↔ B, and H → B transitions. The ground state X is assigned unambiguously to the $^1\Sigma_g^+$ state. The A and B states are the 1_u and 0_u^+ spin–orbit components of a $^3\Pi_u$ state. The C state was assigned to the $^1\Pi_u$ state. The exact nature of these states (electronic configurations contributing to these states) and the other upper states was not clearly established from experiment alone, although the symmetry of the upper states is known in many cases from the intensities of these transitions.

The B–X system has been studied by a number of workers. Rotational analysis, Franck–Condon factors, and the long-range potentials have been obtained for the B state by Barrow et al.[178] Ishiwata, Ohtoshi, and

TABLE 18. Spectroscopic Properties of Br₂[a]

Assignment	State	R_e (Å) Theory	R_e (Å) Expt.	T_e (cm⁻¹) Theory	T_e (cm⁻¹) Expt.	ω_e (cm⁻¹) Theory	ω_e (cm⁻¹) Expt.
X 0_g^-	$^1\Sigma_g^+$	2.33	2.28	0	0	321	325
A' 2_u	$^3\Pi_u(2_u)$	2.81	2.68	10360	[13220]	152	[165]
A 1_u	$^3\Pi_u(1_u)$	2.83	2.70	10620	13905	154	153
B 0_u^+	$^3\Pi_u(0_u^+)$	2.81	2.68	11931	15903	155	168
C' 2_g	$^3\Pi_g(II)$	3.21	3.17	48227	48930	157	151
E 0_g^-	$^3\Pi_g(II)\ 0_g^+$		3.19		49778		151
F 0_u^-	$^3\Sigma_u^-\ 0_u^+$	3.14	3.28	49530	53900	155	156
	$^3\Sigma_u^-(1_u)$	3.14		49630		165	
D 0_u^-	$^2\Pi_u(II)\ 0_u^-$	3.38	3.17	49965	49929	152	134
f 0_g^+	$^3\Sigma_g^-(II)\ 0_g^-$	3.23	3.17	50277	53102	157	153
G 0_u^-	$^1\Sigma_u^+(II)\ 0_u^+$	3.00		57578	56337	159	[250]
	$^3\Pi_g(II)$	3.15		60674		170	
	$^3\Pi_u(II)$	3.32		62210		162	

[a] Theoretical spectroscopic constants for X(0_g^+) were obtained with the CASSCF/SOCI (4s4p2d basis) method. The theoretical D_e(Br₂) including spin–orbit effects = 1.87 eV compared to experimental D_e(Br₂) = 1.97 eV. All theoretical constants are from ref 181. Experimental constants and assignments are from ref 38.

TABLE 19. Spectroscopic Properties of Br₂⁺ [a]

State	r_e (Å) Theory	T_e (cm⁻¹) Theory	T_e (cm⁻¹) Expt.	ω_e (cm⁻¹) Theory	ω_e (cm⁻¹) Expt.
X₁ $^2\Pi_g$ (3/2)	2.30	0	0	343	376
X₂ $^2\Pi_g$ (1/2)	2.30	3043	2820	342	
A₁ $^2\Pi_u$ (3/2)	2.62	11 017		194	190
A₂ $^2\Pi_u$ (1/2)	2.60	14 117	16 414	137	132
$^2\Delta_g$	3.04	20 312		128	
B $^2\Sigma_g^+$	3.05	20 584		127	
$^2\Pi_u$ (II)	3.58	20 718		89	
$^2\Sigma_g^+$ (1/2)	2.79	25 033		199	

[a] Theoretical constants are from ref 181.

Tanaka[179] identified an ion-pair state which they designated as an f state by a two-photon excitation technique. A transition from the ground state X to B followed by B to f was induced by using a two-photon technique. Subsequently, the fluorescence from the f to B state was detected. As these authors[179] pointed out, there was some controversy on the nature of some of the ion-pair states of Br₂.

Mulliken[180] derived the expressions for the energy levels related to the $^3\Pi$ and $^1\Pi$ states which enabled interpretation and assignment of the A–X, B–X, and C–X systems.

Theoretical investigations before Balasubramanian's calculations[181] were limited to the ground state of Br_2.[182,183] Schwerdtfeger et al.[182] employed a SCF/CI method with semiempirical pseudopotentials for the ground state of Br_2. The calculation by Andzelm et al.[183] employed a single-configuration SCF treatment which tended to give a poor D_e. Balasubramanian carried out the first theoretical calculations on the excited states of Br_2. Boerrighter et al.[184] made HF/limited CI calculations on the electronic states of Br_2^+.

Balasubramanian[181] carried out CASSCF/FOCI calculations on 16 electronic states of Br_2 and 6 low-lying electronic states of Br_2^+. Spin–orbit effects were taken into account by using the relativistic configuration interaction method which employed a double-ζ STO + polarization basis set for the bromine atom. The CASSCF/FOCI calculations were made by using a valence Gaussian basis set of (3s3p1d) and (4s4p2d) quality. For the ground state, Balasubramanian also carried out full second-order CI calculations which included up to 210880 configurations and tested the effect of spin–orbit interaction on the dissociation energies.

The theoretical spectroscopic properties (R_e, T_e, ω_e) of the bound states of Br_2 calculated by Balasubramanian are shown in Table 18, and those of Br_2^+ are shown in Table 19. The potential energy curves of some of the electronic states dissociating to the ground-state atoms in the absence of spin–orbit interaction are shown in Figure 6. The corresponding curves for Br_2^+ obtained with the FOCI method of calculation are shown in Figure 7.

As seen from Table 18, the $X0_g^+$ ground state of Br_2 has a theoretical FOCI R_e value (3s3p1d basis) 0.1 Å longer than the experimental value of 2.28 Å. The larger basis set at the SOCI level of calculation yielded better results. The calculated FOCI ω_e was found to be 10% lower than the experimental value of 325 cm^{-1}, although the SOCI method improves this.

Spectroscopic bands of Br_2 observed below 60000 cm^{-1} were assigned to the A $\leftrightarrow$ X, B $\leftrightarrow$ X, and C $\leftarrow$ X transitions. The A and B states are now well characterized as $^3\Pi_u(1_u)$ and $^3\Pi_u(0_u^+)$ states, respectively. The A and B states observed in the A $\leftrightarrow$ X and B $\leftrightarrow$ X transitions can thus be assigned unambiguously since the 0_u^+ state should be well above $^3\Pi_u(1_u)$. The experimental T_e values for the B and A states (15900, 13900 cm^{-1}) are consistent with the trend suggested by theoretical calculations. The experimental ω_e values (153, 167 cm^{-1}) were found to be in very good agreement with the theoretical ω_e value for the $^3\Pi_u$ state (155 cm^{-1}). The C state was observed in the C $\leftarrow$ X absorption system. It is also considered to be responsible for the predissociation of the B state. Although at the FOCI level of approximation the $^1\Pi_u$ state appeared to be repulsive, higher order correlation effects and a larger basis set could lead to a bound $^1\Pi_u$ state. Nevertheless, the C state must be relatively weakly bound since the absorption spectra that corresponded to the C $\leftarrow$ X system are continuous.[37,38]

The D state observed in the D $\rightarrow$ B system is most probably due to the $^3\Pi_g \rightarrow {}^3\Pi_u$ transition. Since the B state is a 0_u^+ state, it was suggested by Balasubrama-
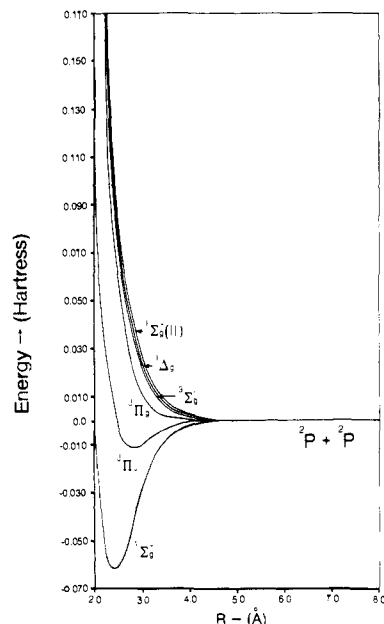

Figure 6. Potential energy curves for the low-lying states of Br_2 (reprinted from ref 181; copyright 1988 Elsevier Science Publishers B.V.). See Table 18 for spectroscopic labels of known states.
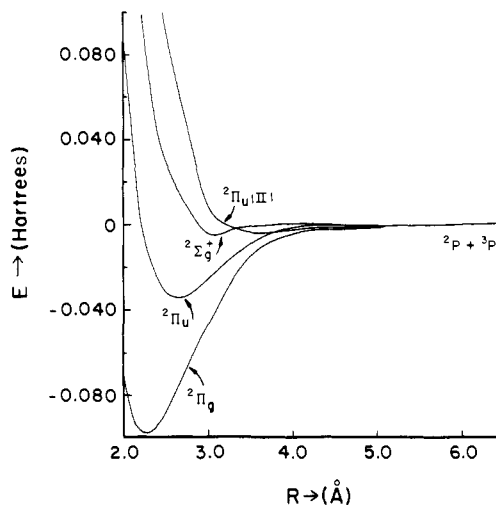

Figure 7. Potential energy curves for the low-lying states of Br_2^+ (reprinted from ref 181; copyright 1988 Elsevier Science Publishers B.V.). See Table 19 for spectroscopic labels of known states.

nian[181] that the 0_g^+ and 1_g components of the $^3\Pi_g(II)$ state are the most probable candidates for this transition. Since the $^3\Pi_g(II)$ state arises from more than a half-filled π shell, the 2_g and 1_g states are lower than the 0_g^+ and 0_g^- states, and consequently, the D state was assigned to 1_g. The E state observed in the E $\leftrightarrow$ B transition was assigned to the $^3\Pi_g(II)(0_g^+)$ state.

The F state observed in the F $\rightarrow$ X system could be due to the $^3\Sigma_u^-(0_u^+) \rightarrow {}^1\Sigma_g^+(0_g^+)$ or $^3\Pi_u(II)(0_u^+) \rightarrow {}^1\Sigma_g^+(0_g^+)$ transition. The theoretical spin–spin effects reported in Table 18 for the $^3\Sigma_u^-$ as well as the $^1\Sigma_u^+$ state were obtained with a calculation that included only the $^3\Sigma_u^-$ and $^1\Sigma_u^+$ reference configurations and are thus crude.

Ishiwata et al.[179] have studied the f $\rightarrow$ B transition using the X $\rightarrow$ B $\rightarrow$ f two-photon transition. These authors call the f state an ion-pair state since the calculated R_e value of the f state (3.17 Å) is much longer than the R_e value of the ground state. The f state was tentatively assigned to a $^3\Sigma_g^-(0_g^+)$ state. It can be seen from Table 18 that the theoretical R_e and ω_e values of

the $^3\Sigma_g^-$(II) state are in excellent agreement with the experimental values obtained by Ishiwata et al.[179] The observed T_e value of this state is lower than the value reported in Table 18 since the $^3\Sigma_g^-$(II) state is split by spin–orbit interaction. The 0_g^+ component is lower than the unsplit $^3\Sigma_g^-$ state. Thus, the f state participating in the f → B system was found to be most consistent with the 0_g^+ component of the $^3\Sigma_g^-$(II) state. The first $^3\Sigma_g^-$ state was found to be repulsive.

The G → X system observed in the 56 337-cm^{-1} region should be due to the $G^1\Sigma_u^1(0_u^+) \to X^1\Sigma_g^+(0_g^+)$ transition. The calculated T_e values of 57 576 cm^{-1} in the absence of spin–orbit interaction was found to be most consistent with this assignment. The rotational analysis of this system should be carried out to confirm this assignment.

The spectroscopic constants of Br_2^+ are shown in Table 19. Ionization of the highest occupied orbital of the $^1\Sigma_g^+$ ground state of Br_2, namely, the $1\pi_g$ orbital, yields the lowest state of Br_2^+ as the $^2\Pi_g$ state arising from the $1\sigma_g^2 1\sigma_u^2 2\sigma_g^2 1\pi_u^4 1\pi_g^3$ configuration. There is another possible low-lying state arising from the $1\sigma_g^2 1\sigma_u^2 2\sigma_g 1\pi_u^4 1\pi_g^4$ configuration ($^2\Sigma_g^+$). Balasubramanian[181] carried out CASSCF/FOCI calculations that employed the (3s3p1d) basis set on the $^2\Pi_g$, $^2\Pi_u$, $^2\Delta_g$, $^2\Sigma_g^+$, and $^2\Pi_u$(II) electronic states of Br_2^+ which dissociated into $Br^+(^3P) + Br(^2P)$.

The ground state of Br_2^+ is the $^2\Pi_g(3/2)$ electronic state arising primarily from the $1\sigma_g^2 1\sigma_u^2 2\sigma_g^2 1\pi_u^4 1\pi_g^3$ configuration (see Table 19). The R_e value of the ground state of Br_2^+ is about 0.08 Å shorter than the R_e of the ground state of Br_2. The vibrational frequency is correspondingly larger (about 40 cm^{-1}). There are no experimental R_e values known for the electronic states of Br_2^+. Since the (3s3p1d) basis set tended to yield R_e values 0.1 Å larger than the true values, Balasubramanian[181] predicted that the true R_e values of the $^2\Pi_g$-(3/2,1/2) states should be 2.22 Å.

The experimental photoelectron spectra of Br_2 yielded substantially different ω_e values for the two components of the $^2\Pi_u$ excited state.[185] The reliability of these analyses was questioned in the literature. The ω_e value deduced from the photoelectron spectra[185] for $^2\Pi_u(3/2)$ is 190 cm^{-1}, while for the $^2\Pi_u(1/2)$ state it is 152 cm^{-1}. Usually, the vibrational frequencies of the spin–orbit components of a λ–s state cannot differ that much unless there is considerable contamination of one of the components with another λ–s state due to spin–orbit coupling. As seen from Table 19, the theoretical vibrational frequencies of the two components of the first excited $^2\Pi_u$ state are 194 and 137 cm^{-1}, supporting the experimental values deduced from the photoelectron spectra.[185] The substantial difference in the two vibrational frequencies was puzzling. This difference arises from the interaction of the $^2\Pi_u(1/2)$ state with the $^4\Sigma_u^-(1/2)$ and $^2\Sigma_u^+(1/2)$ λ–s states in the vicinity of its equilibrium geometry. These two states undergo avoided crossing, influencing the R_e and ω_e values of the $^2\Pi_u(1/2)$ state. Note that the R_e is about 0.02 Å shorter than that of the $^2\Pi_u(3/2)$ state. The $^2\Pi_u(3/2)$ component, however, is less contaminated, and thus its vibrational frequency is not substantially different from that of the $^2\Pi_u$ state obtained without the spin–orbit term.

The vertical ionization potential of Br_2 at the FOCI level of theory was calculated to be about 9.55 eV, while

the adiabatic ionization energy was calculated as 9.47 eV. The ionization potential of the bromine atom calculated from the long-distance splitting of $Br_2(^1\Sigma_g^+)$–$Br_2^+(^2\Pi_g)$ was 10.45 eV compared to an experimental value of 11.8 eV. Thus, the FOCI ionization potentials are 10% smaller compared to the experimental values mainly due to basis set and higher order correlation errors. When these values were corrected for the vertical and adiabatic ionization potentials of Br_2, Balasubramanian obtained 10.51 and 10.42 eV, respectively. The vertical ionization potential calculated this way was identical with the photoelectron spectroscopic and photoionization value of 10.52 eV obtained by several authors.[185–187]

The dissociation energy (D_e) of Br_2^+ obtained for the $^2\Pi_g$ state was calculated as 2.7 eV using FOCI calculations. Such calculations are typically 10–15% in error compared to true values due to higher order correlation corrections and basis set limitations. If this value is corrected for these errors, a value of 3.04 eV is obtained, which was found to be in reasonable agreement with a D_0^0 value of Br_2^+ estimated through the following relationship:

$$D_0^0(Br_2^+) = D_0^0(Br_2) + IP(Br) - IP(Br_2)$$

The value obtained from this formula and experimental data is 3.26 eV.

The photoelectron spectra of Br_2 were recorded by Cornford et al.[185] as well as Potts and Price.[186] The photoelectron spectra exhibited two states in the 19 000–21 600-cm^{-1} region and a third state in the 30 000-cm^{-1} region. Since photoelectron spectra typically involve ionization of a neutral molecule, these bands must arise from vertical rather than adiabatic transitions. The theoretical vertical transition energies and the splittings of the photoelectron spectral peaks are compared in Table 20. The agreement between these two values is remarkable, which led Balasubramanian to reinterpret the photoelectron spectral bands as due to vertical rather than adiabatic transitions. As seen from Table 19, the T_e values of these states are much lower than their T_{vert} since the R_e values of the excited states are much longer. Consequently, the earlier listing of these separations as (T_e) (for example, see ref 37) must be corrected to T_{vert}.

There is a discrepancy in the $^2\Pi_g(3/2)$–$^2\Pi_g(1/2)$ splitting obtained from photoelectron spectroscopy[185,186] and the convergence of the Rydberg series. Venkateswarlu[188] fit these series designated as R_1 and R_2 into the following formulas:

$$R_1(\nu_1) = 85165 - R/(n-s)^2$$

$$R_2(\nu_2) = 88306 - R/(n-s)^2$$

$$n = 5, 6, ...,$$

where the R_1 series converged into the Br_2^+ $^2\Pi_g(3/2)$ state while the R_2 series converged into the $^2\Pi_g(1/2)$ state. The $^2\Pi_g(3/2)$–$^2\Pi_g(1/2)$ splitting calculated from the above formulas (3141 cm^{-1}) is a bit high compared to the splitting obtained from the photoelectron spectra and Balasubramanian's theoretical calculations.[181] Balasubramanian's calculated splitting of 3043 cm^{-1} is between this value and the value of 2820 cm^{-1} obtained from the photoelectron spectra.[185] Nonetheless, the theoretical spin–orbit splitting was found to be within

TABLE 20. Vertical Transition Energies for Br$_2^+$ [a]

Transition	T_{vert} (cm^{-1})	
	theory	experimental
$^2\Pi_g(3/2) \rightarrow {}^2\Pi_g(1/2)$	3030	2820
$^2\Pi_g(3/2) \rightarrow {}^2\Pi_u(3/2)$	18 170	19 290
$^2\Pi_g(3/2) \rightarrow {}^2\Pi_u(1/2)$	21 478	21 602
$^2\Pi_g(3/2) \rightarrow {}^2\Sigma_g^+(1/2)$	34 600	(30 700) [b]
$^2\Pi_g(3/2) \rightarrow {}^2\Pi_u(II)$	56 752	

[a] Theoretical values are from ref 181. [b] The value is not certain.

TABLE 21. Spectroscopic Properties of the Ground State of Br$_2$ at Various Levels of Theory [a]

Method	Basis Set	R_e (Å)	ω_e (cm^{-1})	D_e (eV) Uncorrected [b]	Corrected [c]
FOCI	(3s3p1d)	2.37	303	1.73	1.79
FOCI	(4s4p2d)	2.34	319	1.82	1.88
SOCI	(4s4p2d)	2.33	321	1.77	1.87

[a] From ref 181. [b] Without spin–orbit and Davidson's corrections. [c] With spin–orbit and Davidson's corrections.

the calculational error bars of both values.

Table 20 shows the spectroscopic constants of the X ground state of Br$_2$ obtained by Balasubramanian using various theoretical methods. The simplest calculation employed the FOCI method with a (3s3p1d) basis set, while the most sophisticated calculation used the SOCI method with a (4s4p2d) basis set (210 880 CSF's). The uncorrected D_e is the value obtained from the appropriate calculations without the Davidson correction for unliked clusters and spin–orbit correction. The Davidson correction was estimated from the calculation by Schwerdtfeger et al.,[182] which yielded a D_e of 1.33 eV without the Davidson correction using a CISD method and 1.73 eV after the correction. The spin–orbit interaction decreased the D_e by 0.3 eV. Both these corrections were applied by Balasubramanian (Table 21). As seen from Table 21, the (4s4p2d) basis set yielded better D_e, R_e, and ω_e values compared to the (3s3p1d) basis set. The improvement in D_e obtained by the SOCI method is marginal, although there are improvements in the R_e and ω_e values. The best D_e (1.88 eV) obtained by Balasubramanian[181] compared quite favorably with an experimental value of 1.97 eV. The same calculation gave an ω_e value of 321 cm^{-1} compared to the experimental values of ω_e = 325 cm^{-1} and R_e = 2.28 Å.[37]

The theoretical spin–orbit splitting of the bromine atom[181] ($^2P_{3/2}$–$^2P_{1/2}$ splitting) from asymptotic splittings of molecular states of Br$_2$ was found to be 3915 cm^{-1} compared to an experimental value[134] of 3685 cm^{-1}. The curves in Figure 6, which do not include spin–orbit splittings, are actually split apart at long distances. The spin–orbit contamination of various λ–s states became significant in this region in the RCI wave functions. For the ground state $^1\Sigma_g^+$ the curve was found to be almost identical with the one reported in Figure 6 at near-equilibrium distances in the absence of spin–orbit in-

TABLE 22. Contributions of Various Configurations to the Low-Lying Electronic States of Br$_2$ at Their Near-Equilibrium Geometries [a]

State	Configuration(s)
$^1\Sigma_g^+$	$2\sigma_g^2 1\pi_u^4 1\pi_g^4$ (94%), $2\sigma_u^2 1\pi_u^4 1\pi_g^4$ (3%)
$^3\Pi_u$	$2\sigma_g^2 2\sigma_u 1\pi_u^4 1\pi_g^3$ (89%), $2\sigma_g 2\sigma_u^2 1\pi_u^3 1\pi_g^4$ (8%)
$^1\Pi_u$	$2\sigma_g^2 2\sigma_u 1\pi_u^4 1\pi_g^3$ (90%), $2\sigma_g 2\sigma_u^2 1\pi_u^3 1\pi_g^4$ (7%)
$^3\Pi_g(II)$	$2\sigma_u^2 2\sigma_g 1\pi_u^4 1\pi_g^3$ (64%), $2\sigma_g^2 2\sigma_u 1\pi_u^3 1\pi_g^4$ (26%)
$^3\Sigma_u^-$	$2\sigma_g^2 2\sigma_u^2 1\pi_u^3 1\pi_g^3$ (90%)
$^3\Pi_u(II)$	$2\sigma_g 2\sigma_u^2 1\pi_u^3 1\pi_g^4$ (64%), $2\sigma_g^2 2\sigma_u 1\pi_u^4 1\pi_g^3$ (26%)
$^3\Sigma_g^-(II)$	$2\sigma_g^2 2\sigma_u^2 1\pi_u^2 1\pi_g^4$ (56%), $2\sigma_g^2 2\sigma_u^2 1\pi_u^4 1\pi_g^2$ (34%)
$^1\Sigma_u^+$	$2\sigma_g 2\sigma_u 1\pi_u^4 1\pi_g^4$ (74%), $2\sigma_g^2 2\sigma_u^2 1\pi_u^3 1\pi_g^3$ (15%) Rydberg configurations (3%)
$^1\Pi_g(II)$	$2\sigma_g 2\sigma_u^2 1\pi_u^4 1\pi_g^3$ (58%), $2\sigma_g^2 2\sigma_u 1\pi_u^3 1\pi_g^4$ (33%)
$^1\Pi_u(II)$	$2\sigma_g 2\sigma_u^2 1\pi_u^3 1\pi_g^4$ (64%), $2\sigma_g^2 2\sigma_u 1\pi_u^4 1\pi_g^3$ (25%)

[a] From ref 181. The $1\sigma_g^2 1\sigma_u^2$ shell is omitted. For the $^1\Pi_u$ state the contribution is at 2.50 Å.

teraction. At long distances the curve shifted downward to dissociate the $^2P_{3/2} + {}^2P_{3/2}$ atoms. The ground-state atoms were found to be more stabilized by the spin–orbit interaction than the ground-state molecule.

The potential curves in Figure 7 for Br$_2^+$ also did not include spin–orbit effects and were actually split apart by spin–orbit interaction. At the equilibrium the RCI spin–orbit splitting was found to be 3030 cm^{-1}. The spin–orbit splitting of the Br$^+$ ion ^3P state into $^3P_2$, $^3P_1$, and $^3P_0$ components was obtained by Balasubramanian et al.[189] using the RCI method in an investigation on the collision of Br$^+$ with Kr. The $^3P_2$–$^3P_1$ and $^3P_2$–$^3P_0$ splittings of Br$^+$ were calculated as 3182 and 4675 cm^{-1}.

Table 22 depicts the contributions of the leading configurations in the FOCI wave function of the various electronic states in the absence of spin–orbit interaction. As seen from Table 22, with the exceptions of $^3\Pi_g(II)$, $^3\Pi_u(II)$, $^3\Sigma_g^-(II)$, $^1\Sigma_u^+$, $^1\Pi_g(II)$, and $^1\Pi_u(II)$, other states have leading contributions with weights $\geq 85\%$.

The 0_g^+ ground state of Br$_2$ was found to be 93% $^1\Sigma_g^+(2\sigma_g^2 1\pi_u^4 1\pi_g^4)$ and 0.2% $^3\Pi_g(2\sigma_u 1\pi_u^3 1\pi_g^4)$. The $^3\Pi_u(0_u^+)$ state was also found to be pure $^3\Pi_u(0_u^+)$ at near-equilibrium geometries. The $^3\Pi_u(1_u)$ state is 49% $^3\Pi_u$-$(2\sigma_g^2 2\sigma_u 1\pi_u^4 1\pi_g^3)$, 12% $^1\Pi_u(2\sigma_g^2 2\sigma_u 1\pi_u^4 1\pi_g^3)$, and 7% $^3\Sigma_u^+(2\sigma_g^2 2\sigma_u^2 1\pi_u^3 1\pi_g^3)$ at 6.50 bohr. The $^3\Pi_u(2_u)$ state is 62% $^3\Pi_u(2\sigma_g^2 2\sigma_u 1\pi_u^4 1\pi_g^3)$, 30% $^3\Pi_u(2\sigma_g 2\sigma_u^2 1\pi_u^3 1\pi_g^4)$, and 9% $^3\Delta_u(2\sigma_g^2 2\sigma_u^2 1\pi_u^3 1\pi_g^3)$. The $0_u^+(II)$ state is predominantly $^3\Sigma_u^-(0_u^+)$ (91%); $^1\Sigma_u^+(0_u^+)$ states arising from $2\sigma_g 2\sigma_u 1\pi_u^4 1\pi_g^4$ and $2\sigma_g^2 2\sigma_u^2 1\pi_u^3 1\pi_g^3$ make nonnegligible

TABLE 23. Contributions of Various λ–s Configurations to the Low-Lying States of Br_2^+ [a]

State	R (a.u.)	Contribution	State	R (a.u.)	Contribution
$^2\Pi_g(3/2)$	4.75	$2\sigma_g^2 1\pi_u^4 1\pi_g^3:^2\Pi_g$ (90), $2\sigma_u^2 1\pi_u^4 1\pi_g^3:^2\Pi_g$ (3), $2\sigma_g 2\sigma_u 1\pi_u^3 1\pi_g^4:^4\Pi_g$ (2)	$3/2_u$	5.25	$2\sigma_g^2 1\pi_u^3 1\pi_g^4:^2\Pi_u$ (59), $2\sigma_g 2\sigma_u 1\pi_u^4 1\pi_g^3:^2\Pi_u$ (7); $^4\Pi_u$ (2.3), $2\sigma_u^2 1\pi_u^3 1\pi_g^4:^2\Pi_u$ (2.4); $2\sigma_g^2 2\sigma_u 1\pi_u^4 1\pi_g^2:^4\Sigma_u^-$ (16); $^2\Delta_u$ (1.3)
$^2\Pi_g(3/2)$	5.00	$2\sigma_g^2 1\pi_u^4 1\pi_g^3:^2\Pi_g$ (75), $2\sigma_u^2 1\pi_u^4 1\pi_g^3:^2\Pi_g$ (6), $2\sigma_g 2\sigma_u 1\pi_u^3 1\pi_g^4:^4\Pi_g$ (6)	$1/2_u$	4.25	$2\sigma_g^2 1\pi_u^3 1\pi_g^4:^2\Pi_u$ (87), $2\sigma_g 2\sigma_u 1\pi_u^4 1\pi_g^3:^2\Pi_u$ (6.7); $^4\Pi_u$ (0.4), $2\sigma_u^2 1\pi_u^3 1\pi_g^4:^2\Pi_u$ (1.2), $2\sigma_g^2 2\sigma_u 1\pi_u^4 1\pi_g^2:^4\Sigma_u^-$ (1.4), $^2\Sigma_u^-$ (0.1)
$^2\Pi_g(1/2)$	4.75	$2\sigma_g^2 1\pi_u^4 1\pi_g^3:^2\Pi_g$ (89), $2\sigma_u^2 1\pi_u^4 1\pi_g^3:^2\Pi_g$ (3), $2\sigma_g 2\sigma_u 1\pi_u^4 1\pi_g^3:^2\Pi_g$ (5), $2\sigma_g 2\sigma_u 1\pi_u^4 1\pi_g^3:^4\Pi_g$ (0.2), $2\sigma_g 1\pi_u^4 1\pi_g^4:^2\Sigma_g^+$ (0.9)			
$^2\Pi_g(1/2)$	5.00	$2\sigma_g^2 1\pi_u^4 1\pi_g^3:^2\Pi_g$ (74), $2\sigma_u^2 1\pi_u^4 1\pi_g^3$ (5), $2\sigma_g 2\sigma_u 1\pi_u^4 1\pi_g^3:^2\Pi_g$ (11); $^4\Pi_g$ (7)	$1/2_u$	4.50	$2\sigma_g^2 1\pi_u^3 1\pi_g^4:^2\Pi_u$ (81); $2\sigma_g 2\sigma_u 1\pi_u^4 1\pi_g^2:^2\Pi_u$ (7.2); $^4\Pi_u$ (0.6), $2\sigma_u^2 1\pi_u^3 1\pi_g^4:^2\Pi_u$ (1.5); $2\sigma_g^2 2\sigma_u 1\pi_u^4 1\pi_g^2:^4\Sigma_u^-$ (6)
$3/2_u$	4.50	$2\sigma_g^2 1\pi_u^3 1\pi_g^4:^2\Pi_u$ (82), $2\sigma_g 2\sigma_u 1\pi_u^4 1\pi_g^3:^2\Pi_u$ (7); $^4\Pi_u$ (1.3), $2\sigma_u^2 1\pi_u^3 1\pi_g^4:^2\Pi_u$ (0.8), $2\sigma_g^2 2\sigma_u 1\pi_u^4 1\pi_g^2:^4\Sigma_u^-$ (1.3), $^2\Delta_u$ (0.7)	$1/2_u$	4.75	$2\sigma_g^2 1\pi_u^3 1\pi_g^4:^2\Pi_u$ (26), $2\sigma_g 2\sigma_u 1\pi_u^4 1\pi_g^3:^2\Pi_u$ (3); $^4\Pi_u$ (0.2), $2\sigma_u^2 1\pi_u^3 1\pi_g^4:^2\Pi_u$ (0.6), $2\sigma_g^2 2\sigma_u 1\pi_u^4 1\pi_g^2:^4\Sigma_u^-$ (50); $^2\Sigma_u^+$ (3.4)
$3/2_u$	4.75	$2\sigma_g^2 1\pi_u^3 1\pi_g^4:^2\Pi_u$ (76), $2\sigma_g 2\sigma_u 1\pi_u^4 1\pi_g^3:^2\Pi_u$ (8); $^4\Pi_u$ (1.5), $2\sigma_u^2 1\pi_u^3 1\pi_g^4:^2\Pi_u$ (1.9), $2\sigma_g^2 2\sigma_u 1\pi_u^4 1\pi_g^2:^4\Sigma_u^-$ (6), $^2\Delta_u$ (1)	$1/2_u$	5.00	$2\sigma_g^2 1\pi_u^3 1\pi_g^4:^2\Pi_u$ (3), $2\sigma_g^2 2\sigma_u 1\pi_u^4 1\pi_g^2:^4\Sigma_u^-$ (61); $^2\Sigma_u^+$ (7.3)
$3/2_u$	5.00	$2\sigma_g^2 1\pi_u^3 1\pi_g^4:^2\Pi_u$ (68), $2\sigma_g 2\sigma_u 1\pi_u^4 1\pi_g^3:^2\Pi_u$ (7.6); $^4\Pi_u$ (2), $2\sigma_u^2 1\pi_u^3 1\pi_g^4:^2\Pi_u$ (2.2), $2\sigma_g^2 2\sigma_u 1\pi_u^4 1\pi_g^2:^4\Sigma_u^-$ (11); $^2\Delta_u$ (1.3)	$1/2_u$	5.25	$2\sigma_g^2 1\pi_u^3 1\pi_g^4:^2\Pi_u$ (1.1), $2\sigma_g^2 2\sigma_u 1\pi_u^4 1\pi_g^2:^4\Sigma_u^-$ (58); $^2\Sigma_u^+$ (9)
			$1/2_u$	5.50	$2\sigma_g^2 1\pi_u^3 1\pi_g^4:^2\Pi_u$ (84), $2\sigma_g 2\sigma_u 1\pi_u^4 1\pi_g^3:^2\Pi_u$ (8); $^4\Pi_u$ (1), $2\sigma_u^2 1\pi_u^3 1\pi_g^4:^2\Pi_u$ (5)

[a] From ref 181. Note that the $^2\Pi_u(1/2)$ state exhibits an avoided crossing. The $1\sigma_g^2 1\sigma_u^2$ shell is omitted. Numbers in parentheses are contributions in percentage.

contributions (3%). The $^3\Pi_g(1_g)$ state was found to be $^3\Pi_g$ (34%) and $^1\Pi_g$ (30%), $^3\Pi_g$ (20%) and $^1\Pi_g$ (15%) arising from $2\sigma_g 2\sigma_u^2 1\pi_u^4 1\pi_g^3$ at 6.00 bohr. Consequently, spin–orbit contamination is more significant in excited states than the ground state.

The leading configuration contributing to the FOCI of the $^2\Pi_g$ ground state of Br_2^+ was found to be $(1\sigma_g^2 1\sigma_u^2) 2\sigma_g^2 1\pi_u^4 1\pi_g^3$ (0.950) at 2.25 Å. The $^2\Pi_u$ state was predominantly $(1\sigma_g^2 1\sigma_u^2) 2\sigma_g^2 1\pi_u^3 1\pi_g^4$ (0.925), while the $^2\Pi_u$(II) state was found to be predominantly $(1\sigma_g^2 1\sigma_u^2) 1\pi_u^4 2\sigma_g 1\pi_g^3 2\sigma_u$ (0.902). The $^2\Sigma_g^+$ and $^2\Delta_g$ states arise from the $(1\sigma_g^2 1\sigma_u^2) 2\sigma_g^2 2\sigma_u 1\pi_u^3 1\pi_g^3$ configuration (85%) at 3.0 Å. The $^3\Sigma_g^+$(II) state was found to be predominantly $1\sigma_g^2 1\sigma_u^2 2\sigma_g 1\pi_u^4 1\pi_g^4$.

Table 23 displays the contributions of various λ–s configurations to the low-lying states of Br_2^+. As seen from Table 23, the $^2\Pi_g(3/2)$ state is predominantly composed of the $2\sigma_g^2 1\pi_u^4 1\pi_g^3$ configuration. At long distances, the $^4\Pi_g$ state arising from the $2\sigma_g 2\sigma_u 1\pi_u^3 1\pi_g^4$ configurations makes a substantial contribution. The $^3\Pi_g(1/2)$ component also exhibits a parallel behavior. The compositions of the two spin–orbit components of $^2\Pi_u$ are interesting as a function of internuclear distance. The 3/2 component of $^2\Pi_u$ was found to be predominantly $2\sigma_g^2 1\pi_u^3 1\pi_g^4(^2\Pi_u)$ up to 4.75 bohr. At 5.00 bohr, the $^4\Sigma_u^-(3/2)$ state arising from the $2\sigma_g 2\sigma_u 1\pi_u^4 1\pi_g^2$ configuration makes a substantial contribution. Although this contribution is significant (~11–16%), it is not large enough to induce an avoided crossing. The $1/2_u$ component, to the contrary, exhibited a different composition. Up to $R = 4.50$ bohr, this state was found to be predominantly the $^2\Pi_u$ state arising from the

TABLE 24. Dissociation Relationships for the Low-Lying States of In_2

	dissociation limits		
		energies (cm^{-1})	
λ-s states	atomic states	expt.[a]	theory[b]
$^3\Pi_u$, $^3\Sigma_g^-$, $^1\Pi_u$, $^1\Delta_g$ $^1\Sigma_g^+(2)$, $^1\Sigma_u^-$, $^3\Delta_u$ $^3\Sigma_u^+(2)$, $^3\Pi_g$, $^1\Pi_g$	$^2p + {}^2p$	0.0	0.0
$^3\Sigma_g^+$, $^3\Sigma_u^+$, $^3\Pi_g$, $^3\Pi_u$, $^1\Sigma_g^+$, $^1\Sigma_u^+$, $^1\Pi_g$, $^1\Pi_u$	$^2p + {}^2s$ $(5s^26s)$	24 373	26 579
$^3\Sigma_g^+(2)$, $^3\Sigma_u^+(2)$, $^3\Sigma_g^-$, $^3\Sigma_u^-$, $^3\Pi_g(2)$, $^3\Pi_u(2)$, $^3\Delta_g$, $^3\Delta_u$ $^1\Sigma_g^+(2)$, $^1\Sigma_u^+(2)$, $^1\Sigma_g^-$, $^1\Sigma_u^-$, $^1\Pi_g(2)$, $^1\Pi_u(2)$, $^1\Delta_g$, $^1\Delta_u$	$^2p + {}^2p$ $(5s^26p)$	31 816	32 746

	dissociation limits		
		energies (cm^{-1})	
ω-ω states	atomic states	expt.	theory
0_g^+, 0_u^-, 1_u	$^2P_{1/2} + {}^2P_{1/2}$	0.0	0.0
2_u, 2_g, $1_u(2)$, $1_g(2)$ 0_g^+, 0_u^+, 0_g^-, 0_u^-	$^2P_{1/2} + {}^2P_{3/2}$	2213	2195
3_u, 2_u, 2_g, $1_u(2)$ 1_g, $0_g^+(2)$, $0_u^-(2)$	$^2P_{3/2} + {}^2P_{3/2}$	4426	4399

[a] From ref 134. [b] From ref 194.

$2\sigma_g^2 1\pi_u^3 1\pi_g^4$ configuration. However, at 4.75 bohr, it became predominantly $^4\Sigma_u^-(1/2)$ (50%) while $^2\Pi_u(1/2)$ makes a 26% contribution. At 5.00 bohr, the contribution of $^2\Pi_u(1/2)$ drops to 3% while $^4\Sigma_u^-(1/2)$ increases to 61% accompanied by an increased $^2\Sigma_u^+(1/2)$ contribution (7%), whereas at 5.50 bohr, the $^2\Pi_u(1/2)$ dominates once again. This avoided crossing of $^4\Sigma_u^-(1/2)$ and $^2\Pi_u(1/2)$ explains the large difference in the vibrational frequencies (ω_es) in the photoelectron spectra of these two states.

After the author's manuscript[181] on Br_2 and Br_2^+ went to press, he became aware of two investigations on Br_2^+.[184,190] The laser spectroscopic investigation of the A–X system by Hamilton[190] yielded a T_e value of 16 414 cm^{-1} for the A state. If the A state is assigned to $^2\Pi_u$-(1/2), the agreement between the calculated T_e and this value is good. Boerrighter et al.[184] carried out HF/limited CI calculation that included spin–orbit matrix elements in an empirical manner for Br_2^+. The author's RCI[181] calculations, which included single and double excitations from many λ–s configurations, were in overall agreement with Boerrighter's[184] findings that the vibrational frequencies of the two components of the $^2\Pi_u$ state differ due to avoided crossings. However, the author differed from Boerrighter et al.[184] in the states that induce avoided crossings in that the author's calculations revealed it to be the $^4\Sigma_u^-(1/2)$ state which undergoes avoided crossing with $^2\Pi_u(1/2)$. The $^2\Pi_u$-(3/2) state mixes heavily with $^4\Sigma_u^-(3/2)$ instead of $^2\Delta_u$-

(3/2) as suggested by Boerrighter et al.[184] but does not undergo avoided crossing. The bond lengths calculated by Boerrighter et al.[184] for the $^2\Pi_u$ components are also much too long.

F. In_2

The emission spectra of In_2 were studied in a King furnace by Ginter et al.[122] and also earlier by Wajnkrac.[191] The investigation of Ginter et al.[122] on In_2 revealed emission bands in the 16 800–20 000-cm^{-1} region centered at 18 000 cm^{-1}. Douglas et al.[123] studied the electronic absorption spectra of Al_2, Ga_2, and In_2 in cryogenic matrices. These authors found two systems, one at 13 000 cm^{-1} and the other centered near 27 690 cm^{-1}, for In_2. Douglas et al.[123] assigned the ground state of Al_2, Ga_2, and In_2 to a $^1\Sigma_g^+$ state and the absorption bands to $A^1\Pi_u \leftarrow {}^1\Sigma_g^+$ and $B^1\Sigma_u^+ \leftarrow X^1\Sigma_g^+$ transitions, respectively. The theoretical investigation of Balasubramanian[133] on Ga_2 revealed these assignments to be incorrect and showed that the most consistent assignments of the bands observed by Douglas et al.[123] for Ga_2 are $A^3\Pi_g \leftarrow X^3\Pi_u$ and $B^3\Pi_g \leftarrow X^3\Pi_u$ (see section III.A). The dissociation energy of In_2 was calculated as $D_e \sim$ 1 eV using mass spectrometric techniques.[193]

Froben et al.[192] recorded the Raman spectra of matrix-isolated Ga_2, In_2, and Tl_2. They deduced approximate spectroscopic constants for the ground state of In_2 and Tl_2 using the Guggenheimer method assuming

TABLE 25. Spectroscopic Properties of In₂ Calculated with the FOCI/RCI Method[a]

State	r_e (Å)	T_e (cm⁻¹)	ω_e (cm⁻¹)	D_e (eV)
$X^3\Pi_u(0_u^-)$	3.14	0	111	0.83
$^3\Pi_u(0_u^+)$	3.12	231	114	1.07
$^3\Pi_u(1_u)$	3.13	625	113	0.75
$^3\Pi_u(2_u)$	3.14	1397	113	0.93
$^3\Pi_u$	3.13	963	114	1.02
$^3\Sigma_g^-(0_g^-)$	2.89	1444	132	0.61
$^3\Sigma_g^-(1_g)$	2.88	1947	141	0.82
$^3\Sigma_g^-$	2.87	2006	142	0.90
$^1\Pi_u(1_u(II))$	3.20	4701	98	0.58
$^1\Pi_u$	3.20	4629	98	0.57
$^1\Sigma_g^+(0_g^+(II))$	3.29	5112	91	0.51
$^1\Delta_g(2_g)$	2.98	5158	109	0.41
$^1\Delta_g$	2.97	5274	110	0.49
$^1\Sigma_g^+(1_u)(0_g^+(III))$	3.29	8334	89	--
$^3\Sigma_u^-(0_u^-(II))$	3.04	19 600	119	2.76
$^3\Sigma_u^-$	3.04	19 635	120	2.77
$B^3\Pi_g(II)(0_g^-(II))$	3.49	26 104	70	1.14
$^3\Pi_g(1_g)$	3.49	26.631	70	1.14
$^1\Sigma_u^-$	3.08	27 149	120	1.54
$^3\Delta_u(1_u)$	2.77	28 582	131	1.66
$^3\Pi_u(1_u)$	4.67	30 952	47	0.60
$^3\Sigma_u^-(1_u)$	2.73	31 797	--	--
$^1\Delta_g(II)$	3.36	33 589	64	1.03

[a] From ref 194.

a ground state of $^3\Sigma^-$ for In₂. This estimate was subsequently found to be incorrect by Balasubramanian and Li.[194]

Balasubramanian and Li[194] carried out CASSCF/FOCI/RCI calculations employing RECPs for the indium atom which retained the outer $4d^{10}5s^25p^1$ shells explicitly in the molecular calculations. A (3s3p3d) valence Gaussian basis set was employed. The $4d^{10}$ shells of the In atoms were allowed to relax at the CASSCF level but no excitations from these shells were allowed. The CASSCF active space consisted of four a_1, two b_2, and two b_1 orbitals in the C_{2v} group.

RCI calculations[194] were carried out to estimate the spin–orbit corrections for the spectroscopic properties, dissociation energies, and potential energy curves. RCI calculations were carried out by using the orbitals generated by a SCF calculation of the $^3\Pi_u$ ground state of In₂ employing a double-ζ STO basis set. Identical RCI calculations were also carried out omitting the spin–orbit term. The differences in spectroscopic properties and energies obtained with and without the spin–orbit term were then applied as corrections to the corresponding CASSCF/FOCI properties.

Table 24 shows the dissociation relationships for the low-lying states of In₂ with and without spin–orbit
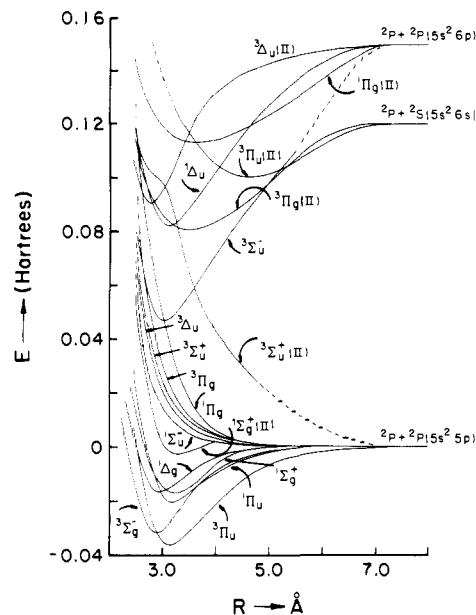

Figure 8. Potential energy curves of In₂ obtained without the spin–orbit term using the CASSCF/FOCI method (reprinted from ref 194; copyright 1988 American Institute of Physics). See Table 25 for spectroscopic labels of known states.
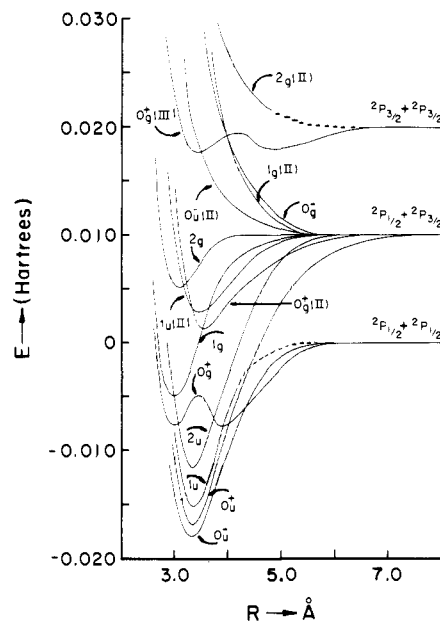

Figure 9. Potential energy curves of In₂ including spin–orbit effects (reprinted from ref 194; copyright 1988 American Institute of Physics). See Table 25 for spectroscopic labels of known states.

terms. Also shown in that table are the theoretical and experimental asymptotic splittings[134] of molecular states. As seen from Table 24, the agreement between the theoretical and experimental In atom splittings is very good.

The spectroscopic properties of 23 electronic states of In₂ are shown in Table 25.[194] The spectroscopic properties listed in that table for states without ω–ω components were obtained without the spin–orbit integral. The ground state of In₂ is a $^3\Pi_u(0_u^-)$ state as seen from Table 25.

Figures 8 and 9 show the potential energy curves of electronic states of In₂ without and with spin–orbit terms, respectively. The curves in Figure 8 were obtained by using the CASSCF/FOCI calculations. The

TABLE 26. Some Allowed Electric Dipole Transitions and the Transition Energies for In_2[a]

Transition	T (cm^{-1})	Transition	T (cm^{-1})
$^3\Sigma^-_{1g} \leftarrow ^3\Pi_{0^-_u}$	1947	$^3\Delta_u(11) \leftarrow ^3\Pi_g(11)$	1951
$^3\Pi_{0^-_g} \leftarrow ^3\Pi_{0^-_u}$	12423	$^3\Pi_u(11) \leftarrow ^3\Pi_g(11)$	4321
$^3\Pi_g(1_g(11)) \leftarrow ^3\Pi_{0^-_u}$	12889	$^3\Pi_g(11) \leftarrow ^3\Pi_{0^+_u}$	26400
$^3\Pi_g(2_g(11)) \leftarrow ^3\Pi_{1_u}$	13220	$^3\Sigma^-_{0^+_g} \leftarrow ^3\Pi_{1_u}$	819
$^3\Pi_g(11)(0^-_g(11)) \leftarrow ^3\Pi_{0^-_u}$	26104	$^3\Sigma^-_{1g} \leftarrow ^3\Pi_{1_u}$	322
$^3\Pi_g(11) \leftarrow ^3\Pi_{0^-_u}$	26631	$^3\Sigma^-_u(0^+_u(11)) \leftarrow ^3\Sigma^-_{0^+_g}$	18156
$^3\Pi_g(1_g(11)) \leftarrow ^3\Pi_{1_u}$	12264	$^3\Sigma^-_{1g} \leftarrow ^3\Pi_{2_u}$	550
$^3\Pi_g(1_g(11)) \leftarrow ^3\Pi_{0^-_u}$	12658	$^3\Pi_g(11) \leftarrow ^3\Pi_{2_u}$	25234
$^3\Pi_g(1_g(11)) \leftarrow ^3\Pi_{2_u}$	11492	$^3\Sigma^-_u(11) \leftarrow ^3\Sigma^-_{0^+_g}$	30323
$^3\Pi_{0^-_g} \leftarrow ^3\Pi_{1_u}$	11803	$^3\Pi_u(11) \leftarrow ^3\Sigma^-_{0^+_g}$	29508
$^3\Pi_g(2g(11)) \leftarrow ^3\Pi_{2_u}$	12448	$^3\Sigma^-_u(0^-_u(11)) \leftarrow ^3\Sigma^-_g$	17653
$^3\Pi_g(11)(0^-_g(11)) \leftarrow ^3\Pi_{1_u}$	25006	$^3\Sigma^-_u(11) \leftarrow ^3\Sigma^-_{1g}$	29820
$^3\Sigma^-_{0^+_g} \leftarrow ^3\Sigma^-_{0^+_u}$	1213	$^3\Pi_u(11) \leftarrow ^3\Sigma^-_{1g}$	29005
$^3\Sigma^-_{1g} \leftarrow ^3\Sigma^-_{0^-_u}$	1115	$^1\Sigma^-_g(0^-_g(11)) \leftarrow ^1\Pi_u(1_u(11))$	411
$^1\Pi_g(11) \leftarrow ^1\Pi_u(1_u(11))$	28988	$^1\Delta_{2g} \leftarrow ^1\Pi_u(1_u(11))$	457
$^1\Delta_u \leftarrow ^1\Delta_{2g}$	21991	$^1\Sigma^-_g(11)(0^-_g(11)) \leftarrow$	3533
$^1\Pi_g(11) \leftarrow ^1\Delta_u$	6540	$^1\Pi_u(1_u(11))$	

[a] From ref 194. A two-way arrow indicates both states are bound. A one-way arrow indicates that the originating state is bound. The transition energies are adiabatic if both states are bound and vertical if one state is bound.

curves in Figure 9 were obtained by using RCI calculations that included the spin–orbit coupling accurately, but correlations were included to a lesser degree compared to the CASSCF/FOCI method.

As seen from Table 25, the calculated R_e, ω_e, and D_e for the ground state ($^3\Pi_u(0^-_u)$) of In_2 are 3.14 Å, 111 cm^{-1}, and 0.83 eV, respectively. The In–In bond strength in the 0^-_u state is reduced by 19% due to spin–orbit interaction. The R_e value is correspondingly increasing while ω_e is decreased. The theoretical spectroscopic properties of the ground state of In_2 are in conflict with the values reported by Froben et al.[192] using an approximate Guggenheimer method which resulted in an R_e value of 2.8 Å, which is too short for In_2. The ω_e value calculated by this method (115 cm^{-1}) is, however, in reasonable agreement with the theoretical results of Balasubramanian and Li.[194] The dissociation energy of 0.87 eV deduced by Froben et al.[192] agreed with the Balasubramanian–Li theoretical value of 0.83 eV. The mass spectrometric methods yield a slightly higher D_e of 1 eV. A similar discrepancy in the R_e value of Tl_2 was noted before. Pitzer and co-work-

ers[195,196] obtained a bond length of 3.54 Å for the ground state of Tl_2, disagreeing with the 3-Å value reported by Froben et al.[192] using the same technique.

The experimental bands of the A $\leftarrow$ X, B $\leftarrow$ X, and the emission systems were centered at 13 000, 27 690, and 18 000 cm^{-1}, respectively.[122,123,130] Table 26 shows both vertical and adiabatic transition energies of allowed dipole transitions of In_2. As seen from Table 26, the most consistent transition for the 13 000-cm^{-1} absorption band is the $A(^3\Pi_g(0^-_g)) \leftarrow X(^3\Pi_u(0^-_u))$ transition. The theoretical vertical transition energy of 12 423 cm^{-1} is in very good agreement with the experimental band center (13 000 cm^{-1}). Since the $^3\Pi_g$ curve is repulsive, it is seen only in absorption. The B $\leftarrow$ X system was assigned by Balasubramanian and Li[194] to the $B(^3\Pi_g(0^-_g)) \leftarrow X(0^-_u)$ transition. The theoretical transition energy of 26 400 cm^{-1} was found to be in excellent agreement with the experimental value of 27 690 cm^{-1}.

The emission spectra observed by Ginter et al.[122] (18 000-cm^{-1} region) are most consistent with the $^3\Sigma^-_u(0^+_u) \leftrightarrow ^3\Sigma^-_g(0^+_g)$ transition. The theoretical T_e of 18 156 cm^{-1} found by Balasubramanian and Li was in remarkable agreement with this value; thus, Balasubramanian and Li assigned this to the $^3\Sigma^-_u(0^+_u) \leftrightarrow ^3\Sigma^-_g(0^+_g)$ system.

Many transitions listed in Table 26 have not yet been observed. Among the transitions in Table 26, only the above-mentioned three transitions have been observed. Thus, there is considerable room for further study in the electronic spectra of In_2. There are no vibrational or rotational analyses done on the observed spectra. Specifically, the vibrational/rotational analysis of the bands in ($^3\Sigma^-_u$–$^3\Sigma^-_g$) should be done for a comparison of theoretical R_e and ω_e values of these states.

Spin–orbit effects were found to be significant for In_2 since the atomic splitting of the indium atom is 2213 cm^{-1}. The $^3\Pi_u(0^-_u)$–$^3\Pi_u(2_u)$ splitting of 1400 cm^{-1} was about 64% of the indium $^2P_{1/2}$–$^2P_{3/2}$ atomic splitting. The spin–orbit splitting stabilizes the $^3\Pi_u(0^+_u)$ state with respect to the separated atoms while it destabilizes the $^3\Pi_u(0^-_u)$ ground state of In_2 since the $^3\Pi_u(0^+_u)$ state dissociates into $In(^2P_{1/2})$ + $In(^2P_{3/2})$ atoms while the ground state (0^-_u) dissociates into $In(^2P_{1/2})$ + $In(^2P_{1/2})$. The influence of spin–orbit coupling on the bond lengths and the vibrational frequencies is subtle. The spin–spin splitting of the $^3\Sigma^-_g$ state is much smaller (503 cm^{-1}) compared to that of the $^3\Pi_u$ state. Spin–orbit coupling also changes the shapes of the potential energy curves of some of the excited states of In_2. For example, the double minima in the 0^+_g and $0^+_g(III)$ surfaces are attributed to avoided crossings induced by spin–orbit coupling.

Table 27 shows the contributions of various important configurations to the FOCI wave functions of the electronic states of In_2. As seen from Table 27, the $^3\Pi_u$ ground state and the $^3\Sigma^-_g$ state are dominated by a single electronic configuration. The $^1\Sigma^+_g$ and $^1\Sigma^+_g(II)$ states are mixtures of several electronic configurations. For the $^1\Sigma^+_g$ state, both the $2\sigma^2_g$ and $1\pi^2_u$ configurations make substantial contributions. Thus, correlation effects are somewhat significant for the $^1\Sigma^+_g$ states. The shoulder in the $^3\Sigma^+_u(II)$ curve (see Figure 8) is due to an avoided crossing as seen from Table 27. At long distances this state was found by Balasubramanian and Li[194] to be

TABLE 27. Contributions of Important Configurations to the FOCI Wave Functions of In_2[a]

State	Percentage of Contributions	State	Percentage of Contributions
$^3\Pi_u$	$2\sigma_g 1\pi_u$ (87)	R = 2.5 Å	$1\sigma_u 2\sigma_g 1\pi_u^2$ (76), $1\pi_u 1\pi_g$ (8),
$^3\Sigma_g^-$	$1\pi_u^2$ (85), $1\pi_g^2$ (2)		$1\sigma_u 2\sigma_g 1\pi_g^2$ (4)
$^1\Pi_u$	$2\sigma_g 1\pi_u$ (86), $1\pi_g 2\sigma_u$ (3)	$^3\Pi_g$(II)	$1\pi_u 2\sigma_u$ (47), $1\sigma_u 1\pi_u$ (28),
$^1\Delta_g$	$1\pi_u^2$ (82), $1\pi_g^2$ (6)		$1\pi_u 3\sigma_u$ (3), $1\sigma_g 1\pi_g$ (2)
$^1\Sigma_g^+$	$2\sigma_g^2$ (51), $1\pi_u^2$ (28), Rydberg (4),		$1\pi_u 4\sigma_u$ (3), $2\sigma_g 1\pi_g$ (2),
	$1\pi_g^2$ (2)		$1\sigma_u 2\sigma_g 5\sigma_u 1\pi_g$ (1)
$^1\Sigma_g^+$(II)	$1\pi_u^2$ (53), $2\sigma_g^2$ (17), $1\pi_g^2$ (15)	$^1\Delta_u$	$1\pi_u 1\pi_g$ (68), $1\sigma_u 2\sigma_g 1\pi_u^2$ (14),
$^1\Sigma_u^-$	$1\pi_u 1\pi_g$ (87)		$1\pi_u 2\pi_g$ (3), $1\pi_u 3\pi_g$ (2)
$^3\Delta_u$	$1\pi_u 1\pi_g$ (89)	$^3\Delta_u$(II)	$1\sigma_u 2\sigma_g 1\pi_u^2$ (79), $1\pi_u 1\pi_g$ (4),
$^3\Sigma_u^+$	$1\pi_u 1\pi_g$ (89)		$1\sigma_u 2\sigma_g 1\pi_g^2$ (4), $1\sigma_g 2\sigma_g 1\pi_u 1\pi_g$ (1)
$^3\Pi_g$	$2\sigma_g 1\pi_g$ (77), $1\pi_u 2\sigma_u$ (4), $1\sigma_u 1\pi_u$ (3)	$^3\Pi_u$(II)	$2\sigma_u 1\pi_g$ (61), $2\sigma_g 1\pi_u$ (9),
$^1\Pi_g$	$2\sigma_g 1\pi_g$ (69), $1\pi_u 2\sigma_u$ (13),		$1\sigma_u 1\pi_g$ (7), $1\sigma_u 2\sigma_g 1\pi_u 2\sigma_u$ (3),
	$2\sigma_g 2\pi_g$ (3)		$4\sigma_u 1\pi_g$ (1), $1\sigma_g 2\sigma_g 2\sigma_u 1\pi_g$ (1),
$^3\Sigma_u^-$	$1\pi_u 1\pi_g$ (61), $1\sigma_u 2\sigma_g 1\pi_u^2$ (19),		$3\sigma_u 1\pi_g$ (1),
	$1\sigma_u 2\sigma_g 1\pi_g^2$ (2), $1\pi_u 2\pi_g$ (3),		$1\sigma_g 1\pi_u$ (2), $1\sigma_g 1\sigma_u 2\sigma_u 1\pi_u 1\pi_g^2$ (1)
	$1\pi_u 3\pi_g$ (2)	$^1\Pi_g$(II)	$2\sigma_u 1\pi_u$ (50), $2\sigma_g 1\pi_g$ (15),
R = 3.4 Å	$2\sigma_g 2\sigma_u$ (64), $2\sigma_g 3\sigma_u$ (10),		$1\sigma_u 1\pi_u$ (10)
	$2\sigma_g 4\sigma_u$ (8), $2\sigma_u 4\sigma_g$ (2)		$3\sigma_u 1\pi_u$ (4), $4\sigma_u 1\pi_u$ (4)
$^3\Sigma_u^-$(II) R = 3.2 Å	$2\sigma_g 2\sigma_u$ (56), $2\sigma_g 3\sigma_u$ (11),	$^3\Sigma_u^-$(II)	$1\sigma_u 2\sigma_g 1\pi_u^2$ (71), $1\pi_u 1\pi_g$ (10),
	$2\sigma_g 4\sigma_u$ (10), $1\sigma_u 2\sigma_g 1\pi_u^2$ (5)		$1\sigma_u 2\sigma_g 1\pi_g^2 1\pi_g^2$ (1)
R = 3.0 Å	$1\sigma_u 2\sigma_g 1\pi_u^2$ (45), $2\sigma_g 2\sigma_u$ (22),		
	$2\sigma_g 3\sigma_u$ (6), $2\sigma_g 4\sigma_u$ (4)		

[a] From ref 194.

predominantly composed of the $2\sigma_g 2\sigma_u$ configuration. At short distances, the contribution from the $1\sigma_u 2\sigma_g 1\pi_u^2$ configurations became important, resulting in an avoided crossing of these two states. The $^3\Sigma_u^-$ state was found to be a mixture of $1\pi_u 1\pi_g$, $1\sigma_u 2\sigma_g 1\pi_u^2$, and other configurations.

Table 28 shows the contributions of various λ–s states in the RCI wave functions of In_2. The 0_u^-, 0_u^+, and 2_u states are relatively pure ($^3\Pi_u$) while the 1_u state exhibited 2% triplet–singlet mixing. The most significant effect of spin–orbit contamination was found to be on the 0_g^+ states. The 0_g^+ curves exhibited avoided crossings. At short distances, the 0_g^+(I) state was found to be predominantly $1\pi_u^2(^3\Sigma_g^-)$ while at intermediate distances, contributions from $1\pi_u^2(^3\Sigma_g^-)$ and $2\sigma_g^2(^1\Sigma_g^+)$ became significant. At longer distances, the two states undergo an avoided crossing leading to a second minimum in the 0_g^+ surface. This avoided crossing is transferred to the 0_g^+(II) and 0_g^+(III) roots, as seen from

the weights of the various λ–s states as a function of internuclear distance (Table 28).

Table 29 shows the Mulliken populations of various electronic states of In_2 obtained from FOCI natural orbitals. As seen from Table 29, the $5s^2$ shell is not an inert shell since Mulliken populations of In are between 1.79 and 1.84. The participation of the $5s^2$ shell in bonding is certainly of interest since for Tl_2 the corresponding $6s^2$ shell was found to be inert.[195,196] The $5s^2$ shell is not that inert for In_2 since some of the 5s electrons are promoted to the 5p shell. The In–In bond is thus expected to be stronger than the Tl–Tl bond, which is consistent with their calculated dissociation energies. Some of the excited states, especially the $^3\Sigma_u^-$, $^3\Pi_g$(II), $^3\Delta_u$(II), and $^3\Sigma_u^-$(II) states, arise from excitation of the 5s electron into the 5p shell as seen from their Mulliken s populations. The s populations for these states are 1.38–1.70. The In–In overlap populations are larger for the $^3\Sigma_g^-$, $^3\Pi_u$, and $^1\Delta_g$ states.

TABLE 28. Weights of Various λ–s Configurations in the ω–ω States of In₂[a]

States	R (Bohr)	Percentage of Contributions	States	R (Bohr)	Percentage of Contributions
0_u^-	6.0	$2\sigma_g 1\pi_u(^3\Pi_u)$ (93)	2_g	6.0	$1\pi_u^2(^1\Delta_g)$ (84), $1\pi_g^2(^1\Delta_g)$ (11)
0_u^+	6.0	$2\sigma_g 1\pi_u(^3\Pi_u)$ (95)		5.5	$1\pi_u^2(^3\Sigma_g^-)$ (68), $1\sigma_u 2\sigma_g 1\pi_u^2(^3\Sigma_g^-)$ (19)
1_u	6.0	$2\sigma_g 1\pi_u(^3\Pi_u)$ (93), $2\sigma_g 1\pi_u(^1\Pi_u)$ (2)	$0_g^+(III)$	6.5	$1\pi_u^2(^1\Sigma_g^+)$ (59), $2\sigma_g^2(^1\Sigma_g^+)$ (9), $1\pi_g^2(^1\Sigma_g^+)$ (16), $1\pi_u^2(^3\Sigma_g^-)$ (10)
2_u	6.0	$2\sigma_g 1\pi_u(^3\Pi_u)$ (95)		7.5	$1\pi_u^2(^1\Sigma_g^+)$ (44), $1\pi_u^2(^3\Sigma_g^-)$ (21), $1\pi_g^2(^1\Sigma_g^+)$ (20), $1\pi_g^2(^3\Sigma_g^-)$ (5)
0_g^+	5.5	$1\pi_u^2(^3\Sigma_g^-)$ (89), $1\pi_g^2(^3\Sigma_g^-)$ (4)			
	6.5	$1\pi_u^2(^3\Sigma_g^-)$ (42), $2\sigma_g^2(^1\Sigma_g^+)$ (25), $1\pi_u^2(^1\Sigma_g^+)$ (16)	0_g^-	6.0	$2\sigma_g 1\pi_g(^3\Pi_g)$ (92)
	7.5	$2\sigma_g^2(^1\Sigma_g^+)$ (70), $2\sigma_u^2(^1\Sigma_g^+)$ (5), $1\pi_u^2(^1\Sigma_g^+)$ (8)	$1_g(II)$	6.0	$2\sigma_g 1\pi_g(^3\Pi_g)$ (87), $2\sigma_g 1\pi_g(^1\Pi_g)$ (4)
1_g	5.5	$1\pi_u^2(^3\Sigma_g^-)$ (91), $1\pi_g^2(^3\Sigma_g^-)$ (5)	$0_u^-(II)$	6.0	$1\pi_u 1\pi_g(^1\Sigma_u^-)$ (65), $1\pi_u 1\pi_g(^3\Sigma_u^+)$ (23)
$0_g^+(II)$	5.5	$1\pi_u^2(^1\Sigma_g^+)$ (71), $2\sigma_g^2(^1\Sigma_g^+)$ (8), $1\pi_u^2(^3\Sigma_g^-)$ (8), $1\pi_g^2(^3\Sigma_g^-)$ (18)	$2_g(II)$	6.0	$2\sigma_g 1\pi_g(^3\Pi_g)$ (92)
	6.5	$2\sigma_g^2(^1\Sigma_g^+)$ (57), $1\pi_u^2(^3\Sigma_g^-)$ (33)	$0_u^+(II)$	5.5	$1\pi_u 1\pi_g(^3\Sigma_u^-)$ (97)
	7.5	$1\pi_u^2(^3\Sigma_g^-)$ (51), $2\sigma_g^2(^1\Sigma_g^+)$ (14), $1\pi_g^2(^3\Sigma_g^-)$ (15), $1\pi_u^2(^1\Sigma_g^+)$ (9), $1\pi_g^2(^1\Sigma_g^+)$ (5)	$0_g^-(II)$	6.5	$2\sigma_u 1\pi_u(^3\Pi_g)$ (55), $1\sigma_u 1\pi_u(^3\Pi_g)$ (40)
$1_u(II)$	6.0	$2\sigma_g 1\pi_u(^1\Pi_u)$ (92), $2\sigma_g 1\pi_u(^3\Pi_u)$ (2)			

[a] From ref 194.

G. Sn₂

The electronic spectra of Sn₂ have been obtained by Bondybey and co-workers[87,140,177,197] as well as Nixon and co-workers.[198,200] Bondybey and co-workers have studied Sn₂ using laser-induced fluorescence of matrix-isolated Sn₂. The spectroscopic constants of the $X0_g^+$ ground state of Sn₂ have been obtained. The strongest absorption for Sn₂ is the 0_u^+–$X0_g^+$ system at 18 223 cm⁻¹. An emission system in the 12 000–14 000-cm⁻¹ region was assigned as terminating in a state 3000–5000 cm⁻¹ above the ground state. The spectroscopic properties of some of these states have been calculated from the electronic spectra.

Balasubramanian and Pitzer[201] carried out SCF/RCI calculations including spin–orbit coupling on ten low-lying electronic states of Sn₂ employing a double-ζ STO basis set. The partition function of Sn₂ was also calculated with the objective of correcting the thermodynamic D_0^0 value of Sn₂. Unfortunately, in the final correction term, these authors had wrong sign, which was subsequently corrected in an erratum. After the paper by Balasubramanian and Pitzer[201] appeared, Pacchioni[202] calculated the low-lying electronic states of Sn₂ and Pb₂. He used semiempirical pseudopotentials and the MRDCI method.

Table 30 shows the dissociation limits for low-lying molecular states of Sn₂ and the energies of separated atoms. The tin dimer has many more low-lying electronic states compared to Ge₂, mainly due to larger spin–orbit coupling.

TABLE 29. Mulliken Population Analysis of In₂ᵃ

State	GROSS In	In(s)	In(p)	In(d)	Overlap In-In
$^3\Pi_u$	13.000	1.835	1.133	10.031	0.335
$^3\Sigma_g^-$	13.000	1.786	1.193	10.030	0.544
$^1\Sigma_u^-$	13.000	1.838	1.128	10.033	0.290
$^1\Delta_g$	13.000	1.794	1.179	10.027	0.477
$^1\Sigma_g^+$	13.000	1.859	1.114	10.027	0.256
$^1\Sigma_g^+(II)$	13.000	1.855	1.127	10.018	0.212
$^1\Sigma_u^-$	13.000	1.834	1.143	10.023	-0.120
$^3\Delta_u$	13.000	1.842	1.136	10.022	-0.156
$^3\Sigma_u^+$	13.000	1.842	1.136	10.022	-0.161
$^3\Pi_g$	13.000	1.824	1.146	10.031	-0.341
$^1\Pi_g$	13.000	1.872	1.100	10.028	-0.740
$^3\Sigma_u^-$	13.000	1.645	1.322	10.033	0.146
$^3\Sigma_u^+(II)$	13.000	1.845	1.151	10.003	-2.650
$^3\Pi_g(II)$	13.000	1.649	1.321	10.030	-1.017
$^1\Delta_u$	13.000	1.697	1.266	10.037	0.067
$^3\Delta_u(II)$	13.000	1.369	1.612	10.019	0.755
$^3\Pi_u(II)$	13.000	1.824	1.170	10.005	-0.399
$^1\Pi_g(II)$	13.000	1.772	1.200	10.027	-1.012
$^3\Sigma_u^-(II)$	13.000	1.373	1.590	10.032	0.756

ᵃThe population analyses were carried out at R_e if the state is bound; otherwise they were carried out at the R_e of the ground state. From ref 194.

TABLE 30. Dissociation Limits of Some Molecular States of Sn₂

Molecular states	Dissociated atoms	Energies of dissociated atoms in cm⁻¹ Sn₂ᵃ
0_g^+	$^3P_0 + ^3P_0$	0.0
0_g^-, 0_u^-, 1_g, 1_u	$^3P_0 + ^3P_1$	1 691.8
0_g^+, 0_u^+, 1_g, 1_u, 2_g, 2_u	$^3P_0 + ^3P_2$	3 427.7
$0_g^+(2)$, 0_u^-, 1_g, 1_u, 2_g	$^3P_1 + ^3P_1$	3 383.6
0_g^+, 0_u^+, $0_g^-(2)$, $0_u^-(2)$, $1_g(3)$, $1_u(3)$, $2_g(2)$, $2_u(2)$, 3_g, 3_u	$^3P_1 + ^3P_2$	5 119.5
$0_g^+(3)$, $0_u^-(2)$, $1_g(2)$, $1_u(2)$, $2_g(2)$, 2_u, 3_g, 3_u, 4_g	$^3P_2 + ^3P_2$	6 855.4
0_g^+, 0_u^-, 1_g, 1_u, 2_g, 2_u	$^3P_2 + ^1D_2$	10 304.9

ᵃAtomic energies from ref 134.

TABLE 31. Spectroscopic Constants of Several Low-Lying States of Sn₂ and the Corresponding Values Obtained without the Spin–Orbit Termᵃ

	State	T_e (cm⁻¹)	R_e (Å)	ω_e (cm⁻¹)
X	0_g^+	0	2.76	197
	1_g	342	2.75	205
	2_u	1 477	2.62	218
	1_u	2 509	2.62	220
	2_g	7 159	2.81	178
	0_u^-	4 084	2.63	219
	0_u^+	4 192	2.63	221
	$1_u(II)$	7 260	2.62	232
	$1_g(II)$	9 964	2.95	88
	$0_g^+(II)$	8 002	2.78	116
C	$0_u^+(II)$	18 223		
	$^3\Sigma_g^-$	1 694	2.75	204
	$^3\Pi_u$	3 218	2.62	219
	$^1\Sigma_g^-$	7 901	2.81	140

ᵃFrom ref 201. The T_e value of the $0_u^+(II)$ is an experimental value from ref 140.

Table 31 shows the theoretical spectroscopic constants for Sn₂ calculated by Balasubramanian and Pitzer.[201] Figure 10 shows the potential energy curves of the g states of Sn₂, while Figure 11 shows the corresponding curves for the u states of Sn₂.

The vibrational frequency of the ground state of Sn₂ is well-known as 188 cm⁻¹ in rare-gas matrices[199,200] and 190 cm⁻¹ in the gas phase.[197] The theoretical value 197 cm⁻¹ agrees well within the estimated uncertainty of 10 cm⁻¹.

Most of the excited electronic states that have been observed in Sn₂ lie above the 10 000-cm⁻¹ level of the highest state among those calculated theoretically. The first 0_u^+ state of Sn₂ is at 4192 cm⁻¹, which appears not to have been studied experimentally.

The strongest absorption in Sn₂ is to a second 0_u^+ state at 18 223 cm⁻¹ from the ground state. An emission in the 12 000–14 000-cm⁻¹ range for Sn₂ was interpreted[198] as leading to a state about 3000–5000 cm⁻¹ above the ground state with a harmonic vibration frequency about 195 cm⁻¹. Both the 0_u^+ and 0_u^- states near 4100 cm⁻¹ fit the first criterion, and the 1_u state at 2500 cm⁻¹ is probably close enough to be considered. These are all components of the $^3\Pi_u$ term in Λ–S coupling. Their theoretical ω_es are a bit too high, near 220 cm⁻¹. Since these bands are relatively broad and both the vibrational assignment and the anharmonicity are uncertain, it is not clear if the experimental ω_es are definitive. Balasubramanian and Pitzer[201] suggested the possibility that this array of bands contains contributions from more than one transition involving the 0_u^+, 0_u^-, or 1_u states.

The thermodynamic "third-law" method[204,205] of calculation of D_e of Sn₂ from mass spectrometric data requires knowledge of the partition function of the molecule and the dissociated atoms. The molecular
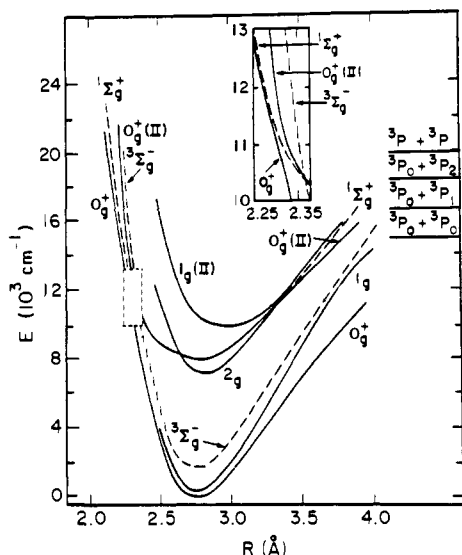
Figure 10. Potential energy curves for the g electronic states of Sn_2 (reprinted from ref 201; copyright 1983 American Institute of Physics). See Table 31 for spectroscopic labels of known states.

Figure 11. Potential energy curves for the u electronic states of Sn_2 (reprinted from ref 201; copyright 1983 American Institute of Physics). See Table 31 for spectroscopic labels of known states.
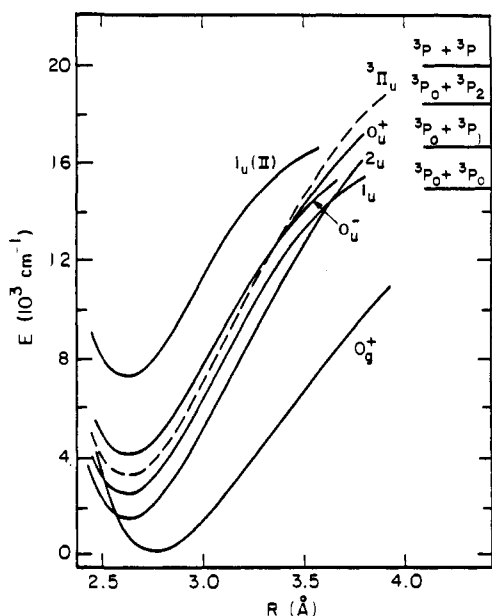
parameters of Sn_2 were estimated in this calculation. Spectroscopic measurements[87,140,199,200] have provided vibrational frequencies in good agreement with the Balasubramanian–Pitzer theoretical calculations. Balasubramanian and Pitzer[201] corrected the D_e obtained from mass spectrometry using the correct partition function. This method is described below. A similar correction to the D_e of Pb_2 was made by Pitzer.[203]

In general, the partition of a diatomic molecule can be separated into translational, rotational, vibrational, and electronic factors. While the translational factors are the same for all electronic states, the rotational factor depends on R_e (or B_e) and the vibrational factor on ω_e. Hence these factors should be considered separately for each electronic state. Consequently, the complete partition function for a diatomic molecule can be expressed as

$$q = q_{tr}(T,P)\sum_i q_{rot}(T,R_{e,i})q_{vibr}(T,\omega_{e,i})g_i e^{-\Delta\epsilon_i/kT}$$

where $\Delta\epsilon_i$ is the excitation energy above the ground state ($\Delta\epsilon = T_e$), g_i is the electronic degeneracy, q_{rot} and q_{vibr} are the rotational and vibrational partition functions, and the sum is over all electronic states that make an appreciable contribution.

The lowest electronic state usually makes the predominant contribution to the partition function denoted by q_0, which can be factored out. Thus, the above expression for q can be rewritten for a diatomic molecule as

$$q = q_0\sum_i \left(\frac{R_{e,i}}{R_{e,0}}\right)^2 \frac{1 - \exp(-hc\omega_{e,0}/kT)}{1 - \exp(-hc\omega_{e,i}/kT)}\left(\frac{g_i}{g_0}\right)e^{-\Delta\epsilon_i/kT}$$

In the above expression, the vibrational factor is approximated by that for a harmonic oscillator.

Balasubramanian and Pitzer[201] calculated q for Sn_2 using $\omega_{e,0} = 189$ cm^{-1} and the theoretical spectroscopic constants in Table 31 for other states. At 1600 K the sum in q above was found to be 2.93, which was only a bit smaller than the value 3 assumed before on the basis of a $^3\Sigma_g^-$ ground state. A much greater change arises, however, from the reduction of $\omega_{e,0}$ from the value of 300 cm^{-1} assumed before[204,205] to 189 cm^{-1}. The change in R_e is smaller but also significant.

The mass spectral data[204] were presented in the form of D_0^0 values for a many temperatures from 1472 to 1769 K calculated on the basis of a partition function with defined parameters. The correction to each D_0^0 value can be shown to be

$$\delta D_0^0 = RT \ln (q'/q'')$$

where q' was the originally assumed partition function and q'' is the corrected value. At 1600 K, the ratio q''/q' is 1.43, which yields a δD_0^0 of −1.15 kcal mol^{-1}. The corrected D_0^0 is 1.94 eV, in excellent agreement with a theoretical value of 1.86 eV.

H. Sb₂

Electronic spectra of the antimony dimer (Sb_2) have been studied by many investigators. In summary, Genard[206] first studied the fluorescence spectrum of antimony vapor, which revealed four bands in the 2968–3132-Å region. Naudé[207] observed two bands, which were assigned to the D ← X$^1\Sigma_g^+$ and F ← X$^1\Sigma_g^+$ systems. Nakamura and Shidei[208] showed the existence of another system. Almy and Schultz[209] found two other systems, assigned to A ↔ X$^1\Sigma_g^+$ and B ↔ X$^1\Sigma_g^+$. Mrozowski and Santaram[210] studied the D → X$^1\Sigma_g^+$ system in emission. Sfeila et al.[211] carried out the vibrational and rotational analyses of the B → X bands observed in emission, which provided the spectroscopic constants for the B and X states. Topouzkhanian et al.[212,213] carried out the vibrational and rotational analysis of the D ↔ X systems.

Laser-induced fluorescence spectra in rare-gas matrices have been recorded by Gerber and Kuscher[214] as well as Bondybey and co-workers.[215] Sontag and Weber[216,217] have also investigated the laser-induced fluorescence and Raman spectra of Sb_2 and Sb_4 in rare-gas matrices. All these investigations have resulted in accurate determination of the spectroscopic constants of the X, A, and B states.

Bondybey, Schwarz, and Griffiths[215] observed fluorescence bands in the 15 000-cm^{-1} region, tentatively

assigned to a $^3\Sigma_u^+$–$X^1\Sigma_g^+$ based on the similarity of these bands to the Vegard–Kaplan system of N_2. Balasubramanian and Li[219] have shown that this assignment is not consistent with the theoretical separation of the $^3\Sigma_u^+$ state from the ground state and reassigned these bands to the $^3\Delta_u(1_u)$–$X^1\Sigma_g^+$ system.

Mass spectroscopic investigations of antimony clusters also have been carried out by Kordis and Gingerich.[218] The vacuum-UV spectra of Sb_2 have been recorded.[147]

Balasubramanian and Li[219] carried out relativistic complete active space MCSCF (CASSCF) calculations followed by large-scale configuration interaction and RCI calculations on 33 electronic states of Sb_2 lying below 44000 cm^{-1}. An extended (4s4p3d) basis set that included polarization functions was employed. The outer $4d^{10}5s^25p^3$ shells (15 electrons) were explicitly retained in these calculations. The rest of the core electrons were replaced by the relativistic effective core potentials.

CASSCF and CI calculations of all the electronic states were done in the C_{2v} group, and a few states were also calculated in the D_{2h} group to compute the effect of higher order correlations. The D_{2h} symmetry was chosen to facilitate the inclusion of higher order excitations since in the D_{2h} group the configuration counts are much smaller compared to the same calculations in the C_{2v} group. Following CASSCF, CI calculations were carried out with the first-order CI (FOCI) approximation.

The CASSCF/FOCI calculations, although they appeared to be satisfactory for calculating the R_e and ω_e values of various electronic states, were found to be somewhat less accurate for energy separations of electronic states of Sb_2. These calculations yielded only 70% or less of the experimental dissociation energies, especially for group V dimers, for which correlation effects were found to be quite severe. Hence, the effects of higher order excitations not included in the CASSCF/FOCI calculations were studied by the CASSCF/MRSDCI methodology for a few low-lying electronic states of interest. MRSDCI calculations of Sb_2 included single and double excitations from a set of chosen reference configurations that had a coefficient ≥ 0.07 in the CASSCF. The CASSCF calculations included up to 400 configurations, while the MRSDCI calculations included between 60000 and 300000 configurations.

Balasubramanian and Li[219] also carried out RCI calculations to estimate the spin–orbit effects. The RCI calculations were carried out by using the recently developed RCI method for polyatomics which employs natural orbitals obtained from a CASSCF/CI calculation and Gaussian basis sets. The RCI calculations included possible low-lying λ–s states that had the same Ω symmetry and potentially mix in the RCI.

Table 32 shows the spectroscopic constants of 33 electronic states of Sb_2 including spin–orbit effects obtained with the CASSCF/FOCI/RCI methodology. The calculated FOCI potential energy curves are shown in Figures 12 and 13 for the singlet and triplet states, respectively. Figure 14 shows the potential energy curves of Sb_2 which included spin–orbit effects. As seen from Table 32, the spin–orbit components of a given λ–s state came out in a group. That is, the spin–orbit contamination for Sb_2 is not so large as to cause a

TABLE 32. Spectroscopic Properties of Sb_2 Calculated with the FOCI/RCI Method[a]

state	R_e (Å) Theor.	R_e (Å) Expt.	T_e (cm^{-1}) Theor.	T_e (cm^{-1}) Expt.	ω_e (cm^{-1}) Theor.	ω_e (cm^{-1}) Expt.	D_e (eV) Theor.
X $^1\Sigma_g^+$ (0_g^+)	2.59	2.34	0	0	246	270	1.86
$^1\Sigma_g^-$	2.59		836		245		1.85
$^3\Sigma_u^+$ (1_u)	2.82		7923		177		0.93
$^3\Sigma_u^-$ (0_u^-)	2.83		7910		173		0.92
$^3\Sigma_u^+$	2.83		8409		176		0.91
$^3\Delta_u$ (2_u)	2.78		16036		198		1.63
a $^3\Delta_u$ (1_u)	2.78		16388	14991	197	217	1.42
$^3\Delta_u$ (3_u)	2.78		16412		199		1.53
$^3\Delta_u$	2.78		16505		197		1.58
$^3\Pi_g$ (0_g^-)	2.67		19887		217		1.11
$^3\Pi_g$ (0_g^+)	2.69		20439		198		1.07
$^3\Pi_g$ (1_g)	2.67		21052		213		0.80
$^3\Pi_g$ (2_g)	2.67		21423		211		0.70
$^3\Pi_g$	2.67		22418		214		0.95
B $^3\Sigma_u^-$ (0_u^-)	2.76	2.48	22176	19055	205	219	1.59
$^1\Sigma_u^-$ (1_u)	2.76		22435		205		1.59
$^3\Sigma_u^-$	2.76		22260		205		1.58
$^1\Delta_u$ (2_u)	2.77		21370		204		2.44
$^1\Delta_u$	2.76		22976		206		2.46
$^3\Sigma_g^+$	3.07		23472		140		0.72
$^3\Delta_g$	3.07		23496		140		0.72
$^1\Sigma_g^+$(II)	2.93		26158		193		2.06
$^1\Sigma_u^-$	2.73		26614		211		2.57
$^1\Pi_g$	2.67		27570		218		1.89
$^3\Sigma_g^-$	3.05		31319		143		1.42
$^1\Sigma_g^+$(III)	3.05		33525		151		1.15
$^1\Delta_g$	3.05		33583		148		1.14
K,L $^3\Pi_u$ (1_u)	2.95		36154	31400	141		0.85
D $^1\Sigma_u^-$	2.89		36243	32087	159	209	1.79
$^1\Pi_u$	2.91		37156		152		0.70
$^1\Sigma_g^-$	3.16		39048		116		0.47
$^1\Pi_g$ (1_g)	3.14		42100		86		0.65
$^1\Sigma_g^-$	3.21		42567		120		0.55

[a] Theoretical constants are from ref 219. Most of the experimental values are from ref 137 (see text).

Figure 12. Potential energy curves of the singlet electronic states of Sb_2 (reprinted from ref 219; copyright 1989 Academic Press, Inc.). See Table 32 for spectroscopic labels of known states.
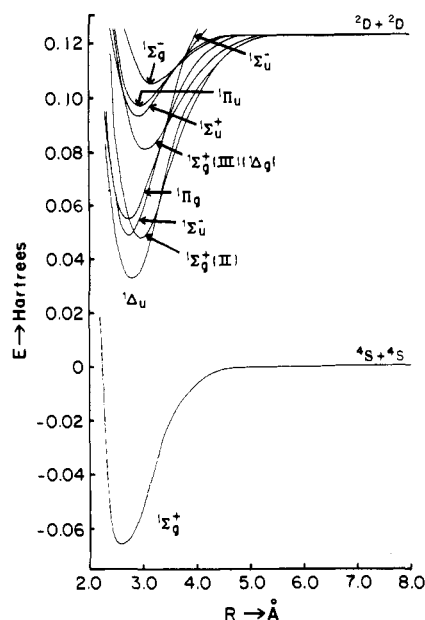

Figure 13. Potential energy curves of the triplet electronic states of Sb_2 (reprinted from ref 219; copyright 1989 Academic Press, Inc.). See Table 32 for spectroscopic labels of known states.
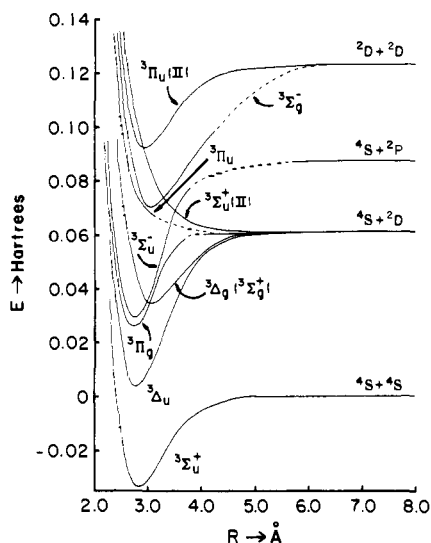
change in the relative ordering of the electronic states. The ordering of the spin–orbit components of most of the low-lying states of Sb_2 followed Hund's rule with the exception of the $^3\Delta_u(1_u)$ state. The contamination of $^3\Sigma_u^+(1_u)$ with $^3\Delta_u(1_u)$ lowered $^3\Sigma_u^+(1_u)$ and raised $^3\Delta_u$-(1_u) relative to the $^3\Delta_u$ state. The spin–spin and spin–orbit splittings of the $^3\Sigma_u^+$ and $^3\Sigma_u^-$ states were found to be smaller compared to the $^3\Delta_u$ and $^3\Sigma_u^-$ states. Similarly, spin–orbit mixing of $^3\Delta_u(2_u)$ with $^1\Delta_u(2_u)$ lowered the $^3\Delta_u(2_u)$ state.

Table 33 shows the spectroscopic constants of nine low-lying electronic states of Sb_2 obtained with more accurate CASSCF/MRSDCI/RCI calculations.[219] In comparing the results of Tables 32 and 33, one can see that R_e shrinks by 0.01 Å due to higher order correlations. The vibrational frequency improved by 4.5% for the ground state. The main effect of higher order correlations not included in the FOCI was found to be
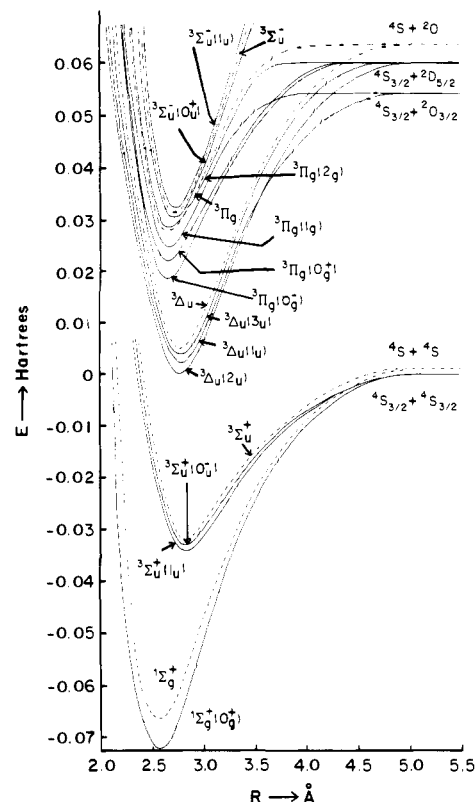

Figure 14. Potential energy curves of the low-lying electronic states of Sb_2 (reprinted from ref 219; copyright 1989 Academic Press, Inc.). See Table 32 for spectroscopic labels of known states.

on the dissociation energies. The calculated D_es increased by 17% due to the higher order correlations. The refined theoretical D_e (2.17 eV)[219] was still about 30% smaller than an experimental (thermodynamic) value of 3.09 eV obtained by the Knudsen effusion mass spectrometric method.[218]

The R_e and ω_e values of the X ground state deduced from laser-induced fluorescence experiments are 2.48 ± 0.02 Å and 269 cm^{-1}. The best levels of calculations (MRSDCI) of Balasubramanian and Li[219] yielded 2.58 Å and 259 cm^{-1}. The slightly longer bond length is attributable to the effective core potential approximations by Balasubramanian and Li.[219] The longer bond lengths and slightly lower vibrational frequencies appear to be the general trend in the effective core potential calculations and are consistent with other calculations on comparable systems.

Table 34 shows the dipole-allowed transitions for Sb_2 and their adiabatic transition energies. As seen from Table 34, there are 31 allowed electronic transitions. Among the transitions listed in Table 34, only four to five transitions appear to have been observed, all from the ground state, and only two of them were experimentally well characterized.

Two experimental systems labeled B–X and A–X, where X is the $^1\Sigma_g^+(0_g^+)$ ground state, have been studied to a considerable extent. The T_e value of the B state deduced from the experimental spectra is 19000–19070 cm^{-1}. Balasubramanian and Li[219] calculated the CASSCF/MRSDCI/RCI separation of $^3\Sigma_u^-(0_u^+)$ from the $X(0_g^+)$ ground state to be 20255 cm^{-1}, in reasonable agreement with the experimental results. The ω_e value of the B state deduced from experiments was found to be 218 cm^{-1}. The small discrepancy between the theoretical value and the experimental result is about the

TABLE 33. Spectroscopic Constants of Various Low-Lying Electronic States of Sb₂ Calculated with the MRSDCI/RCI Method[a]

State	R_e (Å)		T_e (cm^{-1})		ω_e (cm^{-1})		D_e (eV)	
	Theor.	Expt.	Theor.	Expt.	Theor.	Expt.	Theor.	Expt.
X $^1\Sigma_g^+(0_g^+)$	2.58	2.34	0	0	259	270	2.17	3.09
$^1\Sigma_g^+$	2.58		836		258		2.16	
$^3\Sigma_u^+(1_u)$	2.78		8760		199		1.04	
$^3\Sigma_u^+(0_u^-)$	2.79		8847		198		1.03	
$^3\Sigma_u^+$	2.79		9346		198		1.02	
$^3\Delta_u(2_u)$	2.77		15284		199		1.80	
A $^3\Delta_u(1_u)$	2.77	2.64	15636	14991	198	217	1.59	
$^3\Delta_u(3_u)$	2.77		15660		200		1.73	
$^3\Delta_u$	2.77		15753		198		1.71	
B $^3\Sigma_u^-(0_u^+)$	2.75	2.48	20235	19068	205	219	2.03	
$^3\Sigma_u^-(1_u)$	2.75		20314		205		2.03	
$^3\Sigma_u^-$	2.75		20339		205		2.02	
$^1\Delta_u(2_u)$	2.73		23509		234		--	
$^1\Delta_u$	2.72		25115		232		--	
D $^1\Sigma_u^+$	2.86		33945	32087	180	209	--	
$^3\Pi_u(II)$	2.94		36296		161		--	

[a] From ref 219.

same for both the ground state and the excited states. The predicted difference in the ω_e values between the X and B states (54 cm^{-1}) was found to be in excellent agreement with the experimental difference of the ω_e values of the X and B states. Likewise the theoretical difference in the R_e values of the X and B states (0.17 Å) was found to be in full agreement with the experimental difference of 0.17 Å. This appeared to substantiate the assumption that the small discrepancy between the theoretical and experimental results is mainly due to the effective core potential approximation. The calculations of Balasubramanian and Li[219] confirmed the earlier assignment of the B state to the 0_u^+ component of $^3\Sigma_u^-$ Bondybey et al.[215].

Bondybey et al.[215] as well as Sontag and Weber[216] studied the A–X system both in the gas phase and in a rare-gas matrix. The T_e and ω_e values of the A state deduced from these experiments are 14990 and 217 cm^{-1}, respectively. The R_e value of the A state has not yet been obtained from the gas-phase experiments, but in the Ar matrix a value of 2.64 Å has been suggested. As seen from Table 33, the most consistent electronic transition for the A–X system with the theoretical calculations of Li and Balasubramanian is the $^3\Delta_u$-

(1_u)–$^1\Sigma_g^+(0_g^+)$ transition. The theoretical adiabatic transition energy of 15636 cm^{-1} is in very good agreement with the observed value of 14995 cm^{-1}. Further, the theoretical R_e and ω_e values when corrected for the ECP approximation and electron correlation (ΔR_e = -0.17 Å, $\Delta\omega_e$ = +18 cm^{-1}) yield 2.60 Å and 216 cm^{-1}. These values are in remarkable agreement with the experimental values of 2.64 Å and 217 cm^{-1}. Further, there is no other allowed electric dipole transition in this region. Bondybey and co-workers[215] noted that the fluorescence in the 15000-cm^{-1} region exhibited an intensity ratio of $I_\parallel/I_\perp$ = 1.32. This ratio is close to a $\Delta\Omega$ = +1 intensity ratio of $^4/_3$ = 1.33, suggesting the A state to be a 1_u state. However, they assigned the A state to $^3\Sigma_u^+(1_u)$ based on the Vegard–Kaplan system of N_2 and As₂. But the separations of the electronic states of N_2 are quite different from those of Sb₂, and thus it seemed that it is not entirely correct to assign the observed transitions of Sb₂ based on N_2 or even As₂. The $^3\Sigma_u^+(1_u)$ state of Sb₂ is much lower ($T_e \sim$ 8760 cm^{-1}) in energy and thus did not appear to be a probable candidate for the A state seen in the region of 15000 cm^{-1} (see Table 33). Moreover, the $^3\Sigma_u^+$ state has a slightly longer bond length (2.79 Å) and much lower ω_e value (177 cm^{-1}). Even if these values are corrected for the ECP approximations, the theoretical R_e and ω_e values of the $^3\Sigma_u^+(1_u)$ state are 2.65 and 195 cm^{-1}. The experimentally observed A state had a higher ω_e value of 217 cm^{-1}. All these reasonings together with the energy separation of $^3\Delta_u(1_u)$ led Balasubramanian and Li[219] to speculate that the A state observed in the A–X system is most probably the 1_u component of the $^3\Delta_u$ state.

The experimental T_e and ω_e values are uncertain for the D–X system observed in the 32087-cm^{-1} region. Theoretical calculations of Balasubramanian and Li[219] suggested (see Table 34) three candidates for the D state ($^3\Pi_u(II)$, $^1\Sigma_u^+$, and $^1\Pi_u$). The vibrational frequencies of the $^3\Pi_u$ and $^1\Pi_u$ states are somewhat smaller compared to an uncertain experimental ω_e of the D state (209 cm^{-1}).[37] The most probable candidate for the D state was believed to be the $^1\Sigma_u^+$ state since its ω_e value should increase by at least 15 cm^{-1} due to higher order correlations (184 cm^{-1}). The predicted theoretical ω_e value of the D state after correction for the ECP approximation (202 cm^{-1}) was found to be in remarkable agreement with an uncertain experimental value of 209 cm^{-1}. Balasubramanian and Li assigned the observed D–X system tentatively to the $D^1\Sigma_u^+$–$X^1\Sigma_g^+$ transition.

Sontag and Weber[216] identified a new electronic system, which they called K–X, in the 32000-cm^{-1} region below the D state. The vibrational and rotational constants of the K state have also been determined. The R_e and ω_e values deduced from laser-induced fluorescence experiments are 2.841 Å and 127 cm^{-1}, respectively. From Tables 33 and 34, the most consistent candidate for the K state is $^3\Pi_u(0_u^+)$, arising from the second root of the $^3\Pi_u$ state. The theoretical R_e and ω_e values (2.96 Å and 141 cm^{-1}) are in reasonable agreement with the experimental values, although the experimental values themselves are not very definitive due to perturbations with nearby electronic states.

Sibai et al.[213] carried out the rotational analysis of the D ← X system. They found that the vibrational levels of the D state were quite perturbed by another electronic state in this region designated as the L state. As seen from Tables 32 and 33, there are many probable

TABLE 34. Some Allowed Electric Dipole Transitions of Sb_2 and Their Transition Energies[a]

Transitions	T (cm⁻¹)			Transitions	T (cm⁻¹)		
	FOCI/RCI	MRSDCI/RCI	Observed		FOCI/RCI	MRSOCI/RCI	Observed
$^3\Sigma_u^+(1_u) \to {}^1\Sigma_g^+(0_g^+)$	7823	8760		$^1\Sigma_g^+(II) \to {}^3\Sigma_u^+(1_u)$	18335		
$^3\Delta_u(1_u) \to {}^1\Sigma_g^+(0_g^+)$	16388	15636	A 14965	$^1\Pi_g \to {}^3\Sigma_u^+(1_u)$	19747		
$^3\Sigma_u^-(0_u^+) \to {}^1\Sigma_g^+(0_g^+)$	22176	20255	B 19070	$^3\Sigma_g^- \to {}^3\Sigma_u^+(1_u)$	23496		
$^3\Sigma_u^-(1_u) \to {}^1\Sigma_g^+(0_g^+)$	22435	20514		$^1\Sigma_g^+(III) \to {}^3\Sigma_u^+(1_u)$	25702		
$^3\Pi_u(II) \to {}^1\Sigma_g^+(0_g^+)$	36154	36296	K L 31400	$^1\Delta_g \to {}^3\Sigma_u^+(1_u)$	25760		
$^1\Sigma_u^+ \to {}^1\Sigma_g^+(0_g^+)$	36243	33945	O 32087	$^1\Sigma_g^- \to {}^3\Sigma_u^+(1_u)$	31225		
$^1\Pi_u \to {}^1\Sigma_g^+(0_g^+)$	37156			$^1\Pi_g(II) \to {}^3\Sigma_u^+(1_u)$	34824		
$^3\Pi_u(1_u) \to {}^1\Sigma_g^+(0_g^+)$	41024		F 44433 ?	$^3\Pi_g(0_g^-) \to {}^3\Sigma_u^+(0_u^-)$	11977		
$^3\Sigma_u^+(II) \to {}^1\Sigma_g^+(0_g^+)$	44492		H 44780 ?	$^3\Pi_g(1_g) \to {}^3\Sigma_u^+(0_u^-)$	13142		
$^1\Pi_u(II) \to {}^1\Sigma_g^+(0_g^+)$	42100			$^3\Sigma_g^+ \to {}^3\Sigma_u^+(0_u^-)$	15562		
$^3\Pi_g(0_g^-) \to {}^3\Sigma_u^+(1_u)$	12064			$^3\Delta_g \to {}^3\Sigma_u^+(0_u^-)$	15586		
$^3\Pi_g(0_g^+) \to {}^3\Sigma_u^+(1_u)$	12616			$^1\Pi_g \to {}^3\Sigma_u^+(0_u^-)$	19660		
$^3\Pi_g(1_g) \to {}^3\Sigma_u^-(1_u)$	13229			$^3\Sigma_g^- \to {}^3\Sigma_u^+(0_u^-)$	23409		
$^3\Pi_g(2_g) \to {}^3\Sigma_u^+(1_u)$	13602			$^1\Sigma_g^- \to {}^3\Sigma_u^+(0_u^-)$	31138		
$^3\Sigma_g^+ \to {}^3\Sigma_u^+(1_u)$	15649			$^1\Pi_g(II) \to {}^3\Sigma_u^+(0_u^-)$	34737		
$^3\Delta_g \to {}^3\Sigma_u^+(1_u)$	15673						

[a] From ref 219.

candidates for the L state. Since the K and L states are close in energy and are both below the $D(^1\Sigma_u^+)$ state, Balasubramanian and Li[219] tentatively assigned the L state to $^3\Pi_u(1_u)$.

A series of absorption bands labeled as the H ← X and F ← X systems were observed at 44 400 and 44 760 cm⁻¹, respectively, by Topouzkhanian and co-workers.[212] Balasubramanian and Li's calculations are consistent with these observations in that there are at least three allowed electric dipole transitions in the 44 000-cm⁻¹ region. The $^3\Pi_u$ and $^3\Sigma_u^+(II)$ states are repulsive while the $^1\Pi_u(II)$ state is bound. It was not evident which one of the three possible candidates corresponded to the H and F states. Balasubramanian and Li[219] argued that the experimental (uncertain) ω_e value of the H state (479 cm⁻¹) is unreasonable for a heavy species such as Sb_2.

As seen from Table 34, there are 22 electronic transitions predicted by theoretical calculations that appear to have not yet been observed. With the exception of the $^3\Sigma_u^+(1_u) \leftrightarrow X^1\Sigma_g^+$ transition, all other transitions involve excited electronic states and thus would depend upon the lifetimes of these states. The

$^3\Sigma_u^+(1_u)$–$X^1\Sigma_g^+(0_g^+)$ transition is allowed in the perpendicular direction ($\Delta\Omega = 1$), and this should certainly be observable in the 8000-cm⁻¹ region. If this state is detected, the assignment of the A state to $^3\Delta_u(1_u)$ by Balasubramanian and Li[219] will be confirmed. The 2_u component of the $^3\Delta_u$ state could also be observed with multiphoton methods.

Table 35 depicts the weights of various electronic configurations in the FOCI and RCI wave functions of the electronic states of Sb_2. As seen from Table 35, electron correlation effects are quite important even for the ground state of Sb_2. The weights of the leading configurations are >80% for the $^3\Delta_u$, $^3\Sigma_u^-$, $^1\Delta_u$, $^3\Sigma_g^+$, $^3\Delta_g$, $^1\Sigma_u^-$, $^1\Pi_g$, $^3\Sigma_g^-$, $^1\Sigma_g^+(III)$, $^1\Delta_g$, $^3\Pi_u(II)$, $^1\Pi_u$, and $^3\Pi_u$ states. The $^1\Sigma_u^+$ state is the most complex mixture in that three spatial configurations contribute to a great extent for this state.

Table 35 also shows the spin–orbit contaminations in the RCI wave functions of the electronic states of Sb_2. The mixing of the $^1\Sigma_g^+$ state with the $^3\Pi_g(0_g^+)$ state was found to be only 2% for the ground state at its equilibrium geometry. This is also reflected in the relatively small lowering of the D_e of Sb_2 by the spin–orbit term

TABLE 35. Contributions of Important Configurations to the FOCI Wave Functions and the λ-s Contributions to the $\omega-\omega$ States of Sb_2 [a]

$^1\Sigma_g^+(0_g^+)$	$2\sigma_g^2 1\pi_u^4(^1\Sigma_g^+)$ (82), $2\sigma_g^2 1\pi_u^2 1\pi_g^2(^1\Sigma_g^+)$ (12), $2\sigma_g^1 1\pi_u^4 1\pi_g^1(^3\Pi_g)$ (2)
$^1\Sigma_g^+$	$2\sigma_g^2 1\pi_u^4$ (79), $2\sigma_g^2 1\pi_u^2 1\pi_g^2$ (10)
$^3\Sigma_u^+(1_u)$	$2\sigma_g^2 1\pi_u^3 1\pi_g^1(^3\Sigma_u^+)$ (83), $2\sigma_g^2 1\pi_u^1 1\pi_g^3(^3\Sigma_u^+)$ (12), $2\sigma_g^2 1\pi_u^3 1\pi_g^1(^3\Delta_u)$ (3)
$^3\Sigma_u^+(0_u^-)$	$2\sigma_g^2 1\pi_u^3 1\pi_g^1(^3\Sigma_u^+)$ (85), $2\sigma_g^2 1\pi_u^1 1\pi_g^3(^3\Sigma_u^+)$ (12)
$^3\Sigma_u^-$	$2\sigma_g^2 1\pi_u^3 1\pi_g^1$ (78), $2\sigma_g^2 1\pi_u^1 1\pi_g^3$ (11), $2\sigma_g^1 1\pi_u^4 2\sigma_u^1$ (1)
$^3\Delta_u(2_u)$	$2\sigma_g^2 1\pi_u^3 1\pi_g^1(^3\Delta_u)$ (84), $2\sigma_g^2 1\pi_u^1 1\pi_g^3(^3\Delta_u)$ (8), $2\sigma_g^2 1\pi_u^3 1\pi_g^1(^1\Delta_u)$ (5)
$^3\Delta_u(1_u)$	$2\sigma_g^2 1\pi_u^3 1\pi_g^1(^3\Delta_u)$ (87), $2\sigma_g^2 1\pi_u^1 1\pi_g^3(^3\Delta_u)$ (8), $2\sigma_g^2 1\pi_u^3 1\pi_g^1(^3\Sigma_u^+)$ (1)
$^3\Delta_u(3_u)$	$2\sigma_g^2 1\pi_u^3 1\pi_g^1(^3\Delta_u)$ (87), $2\sigma_g^2 1\pi_u^1 1\pi_g^3(^3\Delta_u)$ (3)
$^3\Delta_u$	$2\sigma_g^2 1\pi_u^3 1\pi_g^1$ (84), $2\sigma_g^2 1\pi_u^1 1\pi_g^3$ (7)
$^3\Pi_g(0_g^-)$	$2\sigma_g^1 1\pi_u^4 1\pi_g^1(^3\Pi_g)$ (86), $2\sigma_g^1 1\pi_u^2 1\pi_g^3(^3\Pi_g)$ (10)
$^3\Pi_g(0_g^+)$	$2\sigma_g^1 1\pi_u^4 1\pi_g^1(^3\Pi_g)$ (82), $2\sigma_g^1 1\pi_u^2 1\pi_g^3(^3\Pi_g)$ (10), $2\sigma_g^2 1\pi_u^4(^1\Sigma_g^+)$ (3)
$^3\Pi_g(1_g)$	$2\sigma_g^1 1\pi_u^4 1\pi_g^1(^3\Pi_g)$ (85), $2\sigma_g^1 1\pi_u^2 1\pi_g^3(^3\Pi_g)$ (10)
$^3\Pi_g(2_g)$	$2\sigma_g^1 1\pi_u^4 1\pi_g^1(^3\Pi_g)$ (85), $2\sigma_g^1 1\pi_u^2 1\pi_g^3(^3\Pi_g)$ (11)
$^3\Pi_g$	$2\sigma_g^1 1\pi_u^4 1\pi_g^1$ (79), $2\sigma_g^1 1\pi_u^2 1\pi_g^3$ (9)
$^3\Sigma_u^-(0_u^+)$	$2\sigma_g^2 1\pi_u^3 1\pi_g^1(^3\Sigma_u^-)$ (96)
$^3\Sigma_u^-(1_u)$	$2\sigma_g^2 1\pi_u^3 1\pi_g^1(^3\Sigma_u^-)$ (96)

$^3\Sigma_u^-$	$2\sigma_g^2 1\pi_u^3 1\pi_g^1$ (86), $2\sigma_g^2 1\pi_u^1 1\pi_g^3$ (3)
$^1\Delta_u(2_u)$	$2\sigma_g^2 1\pi_u^3 1\pi_g^1(^1\Delta_u)$ (95)
$^1\Delta_u$	$2\sigma_g^2 1\pi_u^3 1\pi_g^1$ (88)
$^3\Sigma_g^+$	$2\sigma_g^2 1\pi_u^2 1\pi_g^2$ (89), $1\pi_u^2 1\pi_g^2 2\sigma_u^2$ (3)
$^3\Delta_g$	$2\sigma_g^2 1\pi_u^2 1\pi_g^2$ (89)
$^1\Sigma_g^+(II)$	$2\sigma_g^2 1\pi_u^2 1\pi_g^2$ (61), $2\sigma_g^2 1\pi_u^4$ (19)
$^1\Sigma_u^-$	$2\sigma_g^2 1\pi_u^3 1\pi_g^1$ (83)
$^1\Sigma_g^-$	$2\sigma_g^2 1\pi_u^4 1\pi_g^2$ (80), $2\sigma_g^1 1\pi_u^2 1\pi_g^3$ (9)
$^3\Sigma_g^-$	$2\sigma_g^2 1\pi_u^2 1\pi_g^2$ (87)
$^1\Sigma_g^+(III)$	$2\sigma_g^2 1\pi_u^2 1\pi_g^2$ (80)
$^1\Delta_g$	$2\sigma_g^2 1\pi_u^2 1\pi_g^2$ (92)
$^3\Pi_u(II)$	$2\sigma_g^1 1\pi_u^3 1\pi_g^2$ (87)
$^1\Sigma_u^+$	$2\sigma_g^2 1\pi_u^3 1\pi_g^1$ (45), $2\sigma_g^1 1\pi_u^4 2\sigma_u^1$ (24), $2\sigma_g^2 1\pi_u^1 1\pi_g^3$ (20)
$^1\Pi_u$	$2\sigma_g^1 1\pi_u^3 1\pi_g^2$ (83), $2\sigma_g^1 1\pi_u^1 1\pi_g^4$ (2)
$^1\Sigma_g^-$	$2\sigma_g^2 1\pi_u^2 1\pi_g^2$ (61), $1\pi_u^4 1\pi_g^2$ (7), $2\sigma_g^1 1\pi_u^3 1\pi_g^1 2\sigma_u^1$ (14)
$^1\Pi_u(II)$	$2\sigma_g^1 1\pi_u^3 1\pi_g^2$ (77), $2\sigma_g^2 1\pi_u^2 1\pi_g^1 2\sigma_u^1$ (3)
$^1\Pi_g(II)$	$2\sigma_g^1 1\pi_u^3 2\sigma_u^1$ (68), $2\sigma_g^2 1\pi_u^1 1\pi_g^2 2\sigma_u^1$ (14)
$^3\Sigma_u^+(II)$	$2\sigma_g^1 1\pi_u^4 2\sigma_u^1$ (68), $2\sigma_g^1 1\pi_u^2 1\pi_g^2 2\sigma_u^1$ (8), $2\sigma_g^1 1\pi_u^4 3\sigma_u^1$ (4)
$^3\Pi_u$	$2\sigma_g^1 1\pi_u^3 1\pi_g^2$ (87)

[a] From ref 219. Complete $1\sigma_g$ and $1\sigma_u$ shells are not shown.

since decrease in D_e is brought about by the bonding–antibonding mixing as a result of contamination with the $^3\Pi_g$ state. The stabilization of the 1_u component of the $^3\Sigma_u^+$ state is primarily due to the mixing of $^3\Sigma_u^+(1_u)$ with $^3\Delta_u(1_u)$. Similarly, the $^3\Delta_u(2_u)$ is stabilized by mixing with $^1\Delta_u(2_u)$ (about 5%). Thus, the conventional

Hund's ordering of $^3\Delta_u$ spin–orbit states $(1_u, 2_u, 3_u)$ is violated since 2_u is lowered by contamination with $^1\Delta_u$.

Table 36 shows the gross and overlap Mulliken populations of 22 electronic states of Sb_2 obtained from the FOCI natural orbitals. As seen from Table 36, the gross s populations of most of the electronic states are <2.0 while the gross p populations for most of the states are >3.0. The small increases in the d populations were primarily a consequence of the contribution from the d polarization functions. Also reported in Table 36 is the population analysis for $^1\Sigma_g^+$ at a long distance (6.5 Å) to comprehend the effect of atomic correlation in the population. The effect of relativistic mass–velocity contraction on the stabilization of the 5s shell is of interest. For the next row, it is known that the $6s^2$ shell is so stabilized by the relativistic mass–velocity effects that it does not participate in chemical bonding (the "inert-pair" effect). The gross s populations of most of the states are smaller than 2.0, indicating the participation of the 5s shell in the bond. The ground state has the largest overlap population (0.88) since the Sb–Sb bond is composed of a triple bond. It is interesting to note that the overlap population of the comparable In_2 molecule[194] in its ground state is 0.335, implying that the Sb_2 bond is much stronger than the In_2. The ratio of the two overlaps could approximately be taken as the ratio of the bond orders (2.62). The negative overlap population in the $^1\Sigma_u^+$ state appears to be primarily due to mixing of the $2\sigma_g 2\sigma_u$ configuration in this state, in which the $2\sigma_u$ orbital is antibonding.

I. Te₂

The electronic spectra of Te_2 have been the topics of many studies[170,220–235] for several years. The electronic spectra of Te_2 are of considerable interest since they serve as possible wavelength standards. Further, the Te_2 molecule has been considered as a candidate for optically pumped lasers. Theoretically, the Te_2 molecule is considered interesting as a result of relativistic effects and the complexity of electronic states due to large spin–orbit coupling.

The strongest observed transitions of Te_2 are the B ↔ X and A ↔ X systems. These transitions were observed in both absorption and emission spectra as well as laser-induced fluorescence and chemiluminescence spectra. Yee and Barrow[170] observed a weak fluorescence serive originating from the perturbed $B(0_u^+)$ terminating to a state X_2 <2230 cm⁻¹ above the X ground state. Laser-induced fluorescence investigations by a number of authors[231,232,234] later revealed that the X_2 state is 1975–1977 cm⁻¹ above the X ground state.

Bondybey and English[231] have investigated laser-induced fluorescence spectra of Te_2 in Ar and Ne matrices. These authors observed a fluorescence series in the 16 400-cm⁻¹ region. The lower state involved in this fluorescence was assigned to the $X_2(1_g)$ state, since excitation to the emitting state from the ground state X could not be achieved. The emitting state (A′) was tentatively assigned to $^3\Pi_u(2_u)$. Later, Ahmed and Nixon[232] reassigned the A′ state to a 1_u state since they observed another, weaker, fluorescence series in the 14 091-cm⁻¹ region. Ahmed and Nixon[232] suggested that the upper state in this fluorescence series is a 2_u state. Verges et al.[235] argued that the A′ state is most likely $^3\Sigma_u^+(1_u)$ based on the intensities of the observed bands

TABLE 36. Mulliken Population Analysis of Sb_2[a]

state		Sb	Sb(s)	gross Sb(p)	Sb(d)	overlap Sb–Sb
$^1\Sigma_g^+$	2.5Å	15.000	1.871	3.048	10.081	0.878
	6.5Å	15.000	1.994	3.005	10.001	0.005
$^3\Sigma_u^+$		15.000	1.899	3.023	10.077	0.327
$^3\Delta_u$		15.000	1.899	3.024	10.078	0.404
$^3\Pi_g$		15.000	1.884	3.066	10.050	0.464
$^3\Sigma_u^-$		15.000	1.885	3.038	10.077	0.429
$^1\Delta_u$		15.000	1.899	3.022	10.079	0.438
$^3\Sigma_g^+$		15.000	1.926	3.012	10.062	0.120
$^3\Delta_g$		15.000	1.926	3.012	10.062	0.123
$^1\Sigma_g^+(II)$		15.000	1.926	3.018	10.056	0.225
$^1\Sigma_u^-$		15.000	1.888	3.033	10.078	0.442
$^1\Pi_g$		15.000	1.883	3.069	10.048	0.484
$^3\Sigma_g^-$		15.000	1.909	3.032	10.059	0.125
$^1\Sigma_g^+(III)$		15.000	1.931	3.012	10.058	0.158
$^1\Delta_g$		15.000	1.927	3.011	10.062	0.158
$^3\Pi_u(II)$		15.000	1.916	3.045	10.039	0.192
$^1\Sigma_u^+$		15.000	1.905	3.027	10.068	-0.394
$^1\Pi_u$		15.000	1.905	3.056	10.039	0.180
$^1\Sigma_g^-$		15.000	1.939	3.016	10.045	0.028
$^1\Pi_g(II)$		15.000	1.945	3.023	10.032	0.055
$^1\Pi_g(II)$		15.000	1.946	3.019	10.036	-0.337
$^3\Sigma_u^+(II)^*$		15.000	1.829	3.065	10.107	-3.043
$^3\Pi_u^*$		15.000	1.809	3.078	10.080	-0.035

[a] The population analyses were carried out at $R = 2.50$ Å; for other bound states the analyses were carried out at R_e. From ref 219.

and a comparison to the analogous O_2 bands for which $^3\Sigma_u^+-^3\Sigma_g^-$ system is well characterized.

Effantin et al.[230] have observed a b state, which they assigned to $^1\Sigma_g^+$, in the new $B(0_u^+)–b(^1\Sigma_g^+)$ system using Fourier transform spectroscopy. The spectroscopic properties of the lower state have been characterized. However, no transitions to a lower $^1\Delta_g$ state have been observed to date, although Verges et al.[235] predicted that such a state should be about 6500 cm⁻¹ above the ground state. Verges et al.[229] have also observed an electronic state which they designated $B(1_u)$ which is very close to the $B(0_u^+)$ state.

Balasubramanian and Ravimohan[236] carried out CASSCF/FOCI/RCI calculations on 22 low-lying electronic states of Te_2. These authors employed relativistic effective core potentials with the outer $4d^{10}5s^25p^4$ shells of the Te atom retained explicitly in the valence space. A (3s3p4d/3s3p2d) valence Gaussian basis set was employed. Extensive RCI calculations that included all possible reference configurations to yield the desired Ω states were made employing a double-ζ STO basis set.

Table 37 depicts the spectroscopic constants for 22 low-lying states of Te_2 obtained by Balasubramanian

TABLE 37. Spectroscopic Constants for Te$_2$

State	R_e (Å)		T_e (cm^{-1})		ω_e (cm^{-1})	
	Theory[g]	Expt.	Theory	Expt.	Theory	Expt.
X $^3\Sigma_g^-(0_g^+)$	2.68	2.56[a]	0	0	210	247[a]
$^3\Sigma_g^-(1_g)$	2.66	2.55[a]	2229	1975[a] 1977[b]	216	250[a]
$^1\Delta_g(2_g)$	2.70		6383	[6500][c]	199	[235][c]
$^3\Delta_u(3_u)$	2.92		9142		158	
$^1\Sigma_g^+(0_g^+(II))$	2.73		10 446	9600[d] 9591[b]	182	229[d]
$^3\Delta_u(2_u)$	2.97		11 193		127	
A' $^3\Sigma_u^+(1_u)$	3.00		14 369	14 091[b]	127	
A'' $^3\Delta_u(1_u)$	3.00	2.8±0.05[e]	17 759	17 789[b]	128	120[b]
A $^3\Pi_u(0_u^+)$	3.25	2.88[a]	17 032	19 451[e] 19 399[b]	142	144[e]
B $^3\Sigma_u^-(0_u^+(II))$	3.03[f]	2.32[a]	21 606	22 207[e] 22 155[b]	131	162[e]
B $^3\Sigma_u^-(1_u)$			22 414	22 222[d]		150[d]
$^3\Sigma_g^-$	2.63		3218		222	
$^1\Delta_g$	2.68		6900		203	
$^1\Sigma_g^+$	2.73		9318		187	
$^3\Delta$	2.97		13 900		137	
$^3\Sigma_u^-$	2.98		14 342		133	
$^3\Pi_u$			19 629			
$^3\Sigma_u^-$	3.03[f]		22 413		132	
$^3\Sigma_g^-(II)$	3.57[f]		25 722		92	
$^3\Pi_g(II)$	3.17[f]		27 233		53	
$^3\Pi_g(III)$	3.42[f]		27 647		81	
$^1\Pi_g(II)$	3.05[f]		34 043		147	
$^1\Pi_g(III)$	3.42[f]		37 189		84	

[a] Reference 37. [b] Reference 232. [c] Predicted value as in ref 234. This state is yet to be observed. [d] Reference 230. [e] Reference 231. [f] Calculated R_e and ω_e values for these states may not be accurate due to basis set limitations. [g] All theoretical constants are from ref 236.

and Ravimohan[236] together with available experimental values. The potential energy curves for several of these states are given in Figure 15 (without spin–orbit coupling) and Figure 16 (RCI, including spin–orbit coupling).

As seen from Table 37, the ground state of Te$_2$ is an X(0_g^+) state. The 1_g state, which is the other Ω component of the $^3\Sigma_g^-$ λ–s state, is 2229 cm^{-1} above the 0_g^+ state. The theoretical T_e of the 1_g state was found to be in very good agreement with the value of 1975 cm^{-1} reported in ref. 13 and 14. The calculated R_e, T_e, and ω_e values were found to be in very good agreement with available experimental data for the electronic states below 10 000 cm^{-1}. The theoretical R_e values of excited states above 10 000 cm^{-1} are much longer than the experimental values. This difference was attributed mainly to the basis set limitations in the theoretical calculations by Balasubramanian and Ravimohan.[236] For the excited states the basis sets must be extended

further with more diffuse functions and polarization functions.

As seen from Table 37, theoretical calculations confirmed the earlier assignments of the A(0_u^+)–X(0_g^+) and B(0_u^+)–X(0_g^+) systems. The A(0_u^+) state was found to be $^3\Pi_u(0_u^+)$ while the B(0_u^+) state was found to be $^3\Sigma_u^-(0_u^+)$. The A'' state observed by Bondybey and English[231] in the weak fluorescence, which was assigned to $^3\Pi_u(2_u)$ by these authors,[231] is most consistent with $^3\Delta_u(1_u)$ (Table 37). The theoretical T_e value of 17 759 cm^{-1} was found to be in very good agreement with the experimental state. The notation A' was also used for another electronic state with a T_e value of 14 091 cm^{-1} by other authors, and thus caution must be exercised in talking about this state. The state that Bondybey and English[231] designate A' is observed in the A' $\rightarrow$ X$_2$(1_g) fluorescence. The lower state is assigned to 1_g since excitation to the A' state could not be achieved from the X(0_g^+) ground state. Balasubramanian and Ravi-
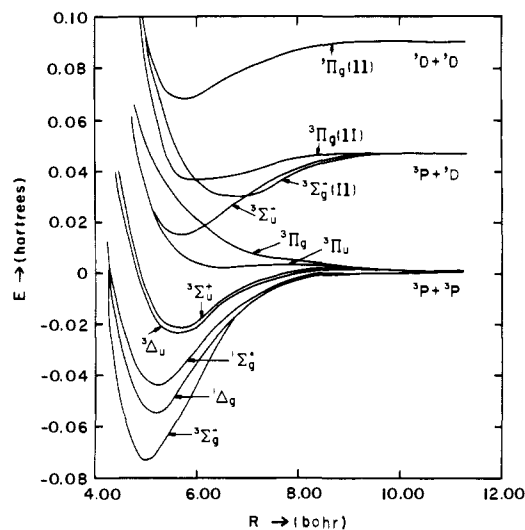
Figure 15. Potential energy curves of some low-lying electronic states of Te_2 (reprinted from ref 236; copyright 1987 Academic Press, Inc.). See Table 37 for spectroscopic labels of known states.
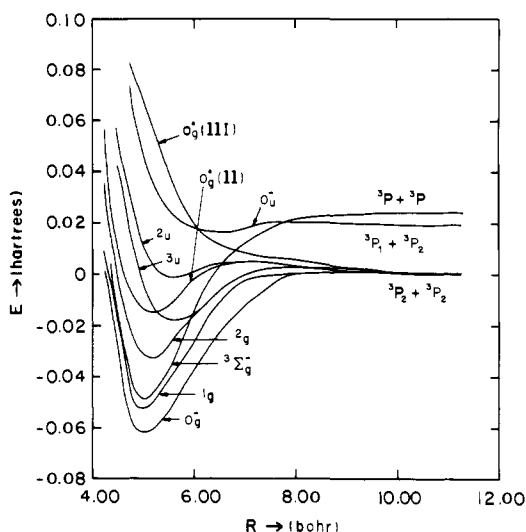

Figure 16. Potential energy curves of low-lying $\omega-\omega$ states of Te_2 obtained with the RCI method including spin–orbit interaction (reprinted from ref 236; copyright 1987 Academic Press, Inc.). See Table 37 for spectroscopic labels of known states.

mohan[236] suggested the notation A'' for the $^3\Delta_u(1_u)$ state to avoid confusion with the A' state participating in the 14 091-cm^{-1} bands.

Ahmed and Nixon[232] observed another weaker fluorescence series in the 14 000-cm^{-1} region, which they assigned to the forbidden $A'(2_u)-X(0_g^+)$ transition. However, Verges et al.[235] correctly argued that the A' state should most probably be $^3\Sigma_u^+(1_u)$. As seen from Table 37, the theoretical T_e value of the $^3\Sigma_u^+(1_u)$ state (14 369 cm^{-1}) is in remarkable agreement with the experimental T_e value of the A' state (14 091 cm^{-1}). Further, the theoretical and experimental ω_e values agree well if the A' state is assigned to $^3\Sigma_u^+(1_u)$. Consequently, the theoretical calculations of Balasubramanian and Ravimohan[236] supported Verges et al.'s[235] tentative assignment.

Verges et al.[229] and Effantin et al.[230] observed a $B(1_u)$ state which was found to be close to $B(0_u^+)$. Balasubramanian and Ravimohan[236] estimated the separation of this state at the R_e of $^3\Sigma_u^-$ (22 414 cm^{-1}). Although this may not be very accurate, it is close to the experimental T_e of 22 222 cm^{-1}.

TABLE 38. Leading Electron Configurations Contributing to Some Low-Lying λ-s States of Te_2 near Equilibrium Geometry^a

State	Configurations
$^3\Sigma_g^-$	$2\sigma_g^2 1\pi_u^4 1\pi_g^2$(90%), $2\sigma_g^2 1\pi_u^2 \pi_g^4$(3%)
$^1\Delta_g$	$2\sigma_g^2 1\pi_u^4 1\pi_g^2$(83%), $2\sigma_g^2 1\pi_u^2 \pi_g^4$(5%)
$^1\Sigma_g^+$	$2\sigma_g^2 1\pi_u^4 1\pi_g^2$(78%), $2\sigma_g^2 1\pi_u^2 1\pi_g^4$(14%)
$^3\Delta_u$	$2\sigma_g^2 1\pi_u^3 1\pi_g^3$(94%)
$^3\Sigma_u^+$	$2\sigma_g^2 1\pi_u^3 1\pi_g^3$(90%)
$^3\Sigma_u^-$	$2\sigma_g^2 1\pi_u^3 1\pi_g^3$(79%), $2\sigma_g 2\sigma_u 1\pi_u^4 1\pi_g^2$(10%)
$^3\Sigma_g^-$(II)	$2\sigma_g^2 1\pi_u^2 1\pi_g^4$(80%), $2\sigma_g^2 1\pi_u^4 1\pi_g^2$(10%)
$^3\Pi_g$(II)	$2\sigma_g 1\pi_u^4 1\pi_g^3$(68%), $2\sigma_g^2 2\sigma_u 1\pi_u^3 \pi_g^2$(18%)
$^3\Pi_g$(III)	$2\sigma_g^2 2\sigma_u 1\pi_u^3 1\pi_g^2$(82%), $2\sigma_g 2\sigma_u^2 1\pi_u^2 \pi_g^3$(4%)
$^3\Pi_u$(I)	$2\sigma_g^2 2\sigma_u 1\pi_u^4 1\pi_g$(46%), $2\sigma_g^2 2\sigma_u 1\pi_u^2 1\pi_g^3$(32%)
$^1\Pi_g$(II)	$2\sigma_g 1\pi_u^4 1\pi_g^3$(87%)
$^1\Pi_g$(III)	$2\sigma_g^2 2\sigma_u 1\pi_u^3 1\pi_g^2$(92%)

^{a} From ref 236.

Verges et al.[229] identified a singlet state (b) with a T_e value of 9600 cm^{-1}. These authors tentatively assigned the b state to $^1\Sigma_g^+$. As seen from Table 37 the calculations of Balasubramanian and Ravimohan are in agreement with this assignment. Verges et al.[235] in another investigation predicted that there should be a $^1\Delta_g$ state with an approximate T_e value of 6500 cm^{-1}, although this state is yet to be observed. The theoretical separation of the $^1\Delta_g$ state (6383 cm^{-1}) was found to be in remarkable agreement with this prediction.

Table 37 also lists the properties of many electronic states without spin–orbit coupling with T_e values 25 700 cm^{-1}, none of which, so far, have been observed experimentally. The theoretical R_e, T_e, and ω_e values for these states, however, should not be considered to be very accurate since the basis set and level of theory employed by Balasubramanian and Ravimohan[236] were not adequate to calculate these properties with reliable accuracy.

The theoretical dissociation energy[236] (D_e) obtained with the CASSCF/FOCI/RCI method for the $X(0_g^+)$ state of Te_2 was found to be 1.69 eV. The spin–orbit interaction decreased the D_e value, since the separated atoms are more stabilized by the spin–orbit interaction compared to the molecule. Huber and Herzberg[37] listed a D_0^0 value of 2.68 eV based on a weighted mean of a number of values obtained from spectroscopic and thermochemical methods. The difference between this value and the theoretical value is primarily due to limitations of theoretical calculations. As pointed out by Saxon and Liu,[173] although D_es of group IV dimers such as O_2 are not obtained accurately by (modest level) theoretical calculations, the spectroscopic properties near the well should be reasonable.

Table 38 shows the leading configurations in the CI

TABLE 39. Experimental and Theoretical Spectroscopic Constants of I_2[a]

State	ijkl	$T(cm^{-1})$ Theory	$T(cm^{-1})$ Expt	Assignment	R_e (Å) Theory	R_e (Å) Expt	ω_e (cm^{-1}) Theory	ω_e (cm^{-1}) Expt
$^1\Sigma_g^+(0_g^+)$	2440	0	0	X	2.70	2.67	210	214.5
$^3\Pi_u(2_u)$	2431	11500	10042	A'	3.30	3.08	93	109
$^3\Pi_u(1_u)$	2431	12522	11888	A	3.30		90	93
$^3\Pi_u(0_u^+)$	2431	16560	15725	B	3.25	3.02	110	126
$^3\Pi_u(0_u^-)$	2431	21000 (repulsive)		B'				
$^1\Pi_u(1_u)$	2431	25700 (repulsive)	21000 (max)	B"				
$^3\Pi_g(1_g)$	2341	27900 (repulsive)		a				
$^3\Pi_g(2_g)$	2341	30763 (repulsive)						
$^3\Sigma_g^-(0_g^+)$	2422	31700 (repulsive)		a'				
$^3\Sigma_u^+(1_u)$	1441	32500 (repulsive)	37000 (max)	c				
$^3\Sigma_g^-(1_g)$	2422	34700 (repulsive)						
$^3\Pi_g(0_g^+)$	2341	35800 (repulsive)						
$^3\Pi_g(0_g^-)$	2341	35869						
$^1\Pi_g(1_g)$	2341	36200						
$^1\Pi_u(^3\Delta,^3\Sigma^+)_u$	2332	36750						
$^1\Delta_g(2_g)$	2422	37340						
$^3\Sigma_u^-(0_u^+)$	2332	41800	41029	D	3.74	3.58	90	95
$^3\Delta_u$	2332	41940	41621	$\gamma\ 1_u$		3.67		95
			41789	$\delta\ 2_u$		(4.0)		100
$^3\Sigma_g^-(II)$	2242	42500						
$^3\Pi_g(II)$	1432	42711	40386	D'(2_g)	3.85	3.61	90	105
$^3\Pi_g(II)0_g^+$	1432		41412	E(0_g^+)	-	3.67	-	101
$^3\Pi_u(II)$	1342	46014	45230	F'?	4.02		94	93
$^1\Sigma_u^+(0_u^+)$	1441	47500	47217	F	3.596	3.61	102	96
$^1\Sigma_g^+(II)$	0442	51200	47026	f	-	3.574	103	104
$^1\Delta_u(2_u)$	2332	53145		H?	3.69		101	
$^1\Sigma_g^+(III)$	2422	54350 (repulsive)						
$^3\Pi_g(II)1_g$	1432	55000	47559	G	3.528		89	
$^3\Pi_g(II)1_g$	1432	56000	52000	?	3.84		92	107
$^3\Pi_u(II)$	1342	57200			3.94		95	
$^1\Sigma_u^+(II)$	2332	65200	51706	F"0_u^+	3.63	3.48	102	131

[a] Theoretical $D_e(I_2)$ = 1.45 eV including spin–orbit effects. Experimental $D_e(I_2)$ = 1.54 eV. The notation $ijkl$ is used to designate the electronic configuration $2\sigma_g^i 1\pi_u^j 1\pi_g^k 2\sigma_u^l$ following Mulliken.[180] Theoretical values are from ref 251 while experimental values are from ref 38. For repulsive states the reported T values are vertical energy separations. For bound states these are T_e.

wave functions of the bound electronic states of Te_2. The nature of electronic states listed in Table 37 could be best understood by using Table 38. Spin–orbit coupling makes significant contributions to the electronic states of Te_2. The $X(0_g^+)$ ground state was found to be actually 71% $^3\Sigma_g^-(0_g^+)$ and 19% $^1\Sigma_g^+(0_g^+)$ at its

equilibrium geometry. The $0_g^+(II)$ state was found to be 73% $^1\Sigma_g^+(0_g^+)$ and 18% $^3\Sigma_g^-(0_g^+)$ at its equilibrium geometry. The spin–orbit contamination for other states such as $^1\Delta_g(2_g)$, $^3\Sigma_g^-(1_g)$, $^3\Delta_u(3_u)$, $^3\Delta_u(2_u)$, $^3\Sigma_u^+(1_u)$, etc. were not particularly significant at their equilibrium geometries, although at longer distances, the spin–orbit contaminations became significant for all electronic states.

J. I_2 and I_2^+

The spectroscopic properties of I_2 and I_2^+ have been studied for many years; a summary of the investigations up to 1977 can be found in Huber and Herzberg.[37] A more recent review of the spectroscopic properties of I_2 can be found in Brand and Hoy.[38] Some of the earlier assignments of I_2 were found to be incorrect, and thus the review of Brand and Hoy[38] should be consulted for revised constants and assignments. From empirical evidence and known experimental data at the time, Mulliken and other authors[237-239] obtained potential curves of I_2, together with conclusions and assignments.

The electronic spectra of I_2 in the region below 55 000 cm^{-1} indicate the existence of X, A', A, B, B', B'', C, D, D', E, G', F', F, G, H, and I states. The A', A, B, and B' states are the 2_u, 1_u, 0_u^+, and 0_u^- spin–orbit components of the $^3\Pi_u$ state.[237-244] The B'' state is assigned to the $^1\Pi_u(1_u)$ state.[37,243] The G, G', E, and F states are assigned to the 2_g, 1_g, and 0_g^+ components of the $^3\Pi_g$ state and $^1\Sigma_u^+$, respectively.[245] Among these states, the transitions A ← X, B ↔ X, B'' ↔ X, C ← X, G ← A', D ↔ X, E → B, G' ← A, F' → X, F ↔ X, H → B, I → B, and D' → A' are observed.

The absorption spectra of I_2 in CCl_4 and n-heptane are analyzed in terms of transitions from the ground state to the three electronically excited states ($^3\Pi(1_u)$, $^1\Pi(1_u)$, $^3\Pi_u(0_u^+)$).[239] King and McLean[247] have recorded the three-photon absorption spectrum of I_2 at 16 400–18 300 cm^{-1} and confirmed the presence of the $F'(0_u^+)$ state by rotational analysis of the 3P2C spectrum. Venkateswarlu et al.[245,248] have studied the photoacoustic spectroscopy of I_2 and found that the structure observed at 20 200–20 750 cm^{-1} is beyond the convergence limit of $X^1\Sigma^+(0_g^+) \rightarrow B^3\Pi(0_u^+)$; this transition was attributed to a two-photon absorption. They have also studied the E → B transition of I_2 at 4400–4000 Å and discussed the origin of the upper state, $E(0_g^+)$, of this transition. Many weakly bound electronic states and ion-pair states of I_2 have also been detected. Experimental investigations[238] on diffuse and predissociation spectra of I_2 have led to the characterization of electronic states labeled a and another state labeled D', which was earlier called G.[37]

The I_2^+ halogen positive ion has also been the topic of many investigations in recent years.[249,250] In the most recent investigation, Leach[249] has reviewed the various experimental investigations on I_2^+, Br_2^+, and Cl_2^+.

Li and Balasubramanian[251] carried out CASSCF/ FOCI/SOCI/RCI calculations on many electronic states of I_2 and I_2^+. They found 30 low-lying electronic states of I_2 and 13 electronic states of I_2^+. These authors employed RECPs that retained the $4d^{10}5s^25p^5$ outer shells of the iodine atom in the calculations while the rest of the core electrons were replaced by RECPs. A flexible (4s4p2d) valence Gaussian basis set was employed for the iodine atom. The final SOCI calculations

TABLE 40. Spectroscopic Properties of I_2^+ Calculated by the FOCI (SOCI)/RCI Method[a]

State	T (cm^{-1}) calculated	T (cm^{-1}) assignment	r_e (Å)	ω_e (cm^{-1})	D_e (eV)
$^2\Pi_g(\frac{3}{2}g)$	0	X	2.70	213	1.92
	SOCI: 0		2.69	217	2.06
$^2\Pi_g(\frac{1}{2}g)$	5979	X	2.70	204	1.16
	SOCI: 5979		2.69	208	1.30
$^4\Sigma_u^-(\frac{1}{2}u)$	7948		3.17	126	0.92
$^4\Sigma_u^-(\frac{3}{2}u)$	8258		3.19	125	0.88
$^2\Delta_u$	12215		3.48	99	0.74
$^2\Pi_u(\frac{3}{2}u)$	9961	A	3.12	128	
	SOCI: 10068	(vert:12687)	3.09	132	
$^2\Pi_u(\frac{1}{2}u)$	15010	A	3.14	108	
	SOCI: 15117	(vert:17736)	3.11	112	
$^2\Sigma_u^+$	14470		3.52	102	
$^2\Delta_g$	17739		3.61	71	
$^2\Sigma_g^+$	19361	B	3.52	72	
$^2\Pi_g(II)$	40358 (repulsive)				
$^2\Pi_u(II)$	44162 (repulsive)				
$^4\Sigma_u^-(II)$	44462 (repulsive)				

[a] All values are from ref 251. Reported T values are adiabatic for bound states. Otherwise they are vertical separations.

included up to 105 004 configurations for I_2 and up to 230 000 configurations for I_2^+. Spin–orbit effects were taken into account by using relativistic configuration interaction calculations.

Table 39 shows the calculated spectroscopic properties (R_e, T_e, ω_e) of 29 electronic states of I_2. Table 40 shows the spectroscopic constants of 13 electronic states of I_2^+. In Table 39, the experimental spectroscopic constants are shown for comparison. The spectroscopic properties in Tables 39 and 40 were obtained by using the (4s4p2d) basis set and a combination of FOCI/ SOCI/RCI methods. For many of the excited states with energy separations >30 000 cm^{-1}, only the FOCI method was used. The Ts in these tables are T_es for the bound states and are the vertical transition energies for the repulsive states.

Figure 17 shows the potential energy curves of the low-lying electronic states of I_2 including the spin–orbit effects obtained by using the FOCI/RCI method. Figure 18 shows the potential energy curves of many low-lying and high-lying states of I_2 constructed from the FOCI calculations, while Figure 19 shows the potential energy curves of I_2^+. Tables 41 and 42 depict the contributions of important configurations to the FOCI/RCI wave functions of I_2 and I_2^+, respectively.

In Table 39, the principal components of the electronic states are shown in Mulliken's $ijkl$ notation, where the set of integers i, j, k, and l designate the electronic configuration $2\sigma_g^i 1\pi_u^j 1\pi_g^k 2\sigma_u^l$. The labels for the various experimentally observed states are as per the recent review by Brand and Hoy.[38] It must be pointed out that some of these labels have changed during the years. For example, the electronic state labeled D' in Table 39 was denoted G earlier as seen
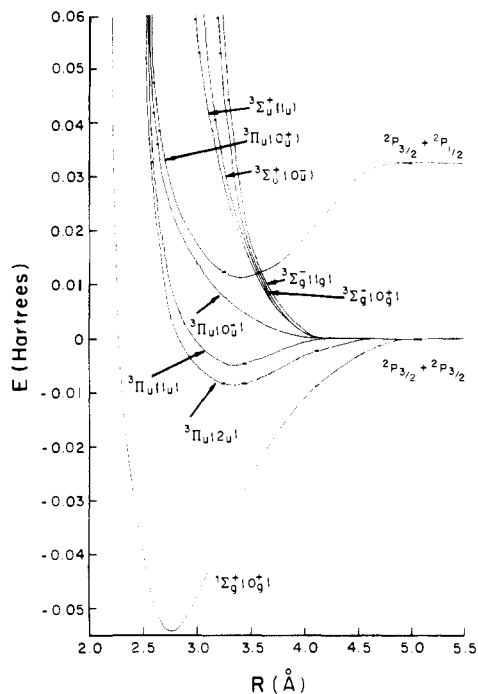
Figure 17. Potential energy curves of the low-lying electronic states of I_2 including spin–orbit effects (reprinted from ref 251; copyright 1989 Academic Press, Inc.). See Table 39 for spectroscopic labels of known states.
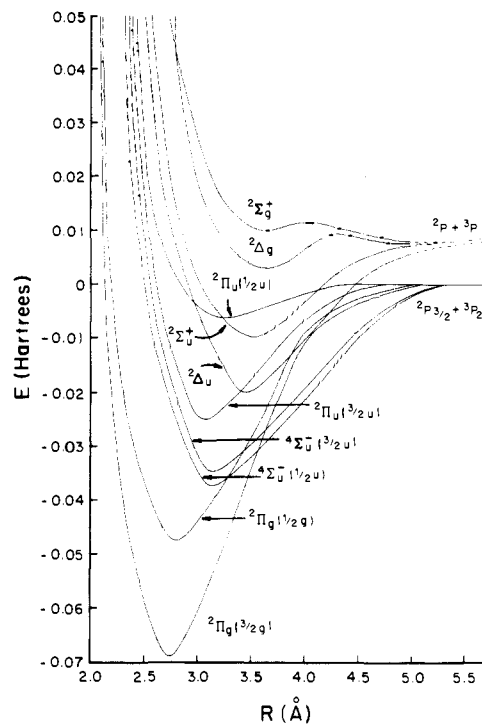

Figure 18. Potential energy curves of the electronic states of I_2 without spin–orbit effects (reprinted from ref 251; copyright 1989 Academic Press, Inc.). See Table 39 for spectroscopic labels of known states.

in ref 37. The labels with question marks are tentative assignments. The ensuing discussion should be consulted for the possibilities.

The theoretical ground-state spectroscopic constants[251] are R_e = 2.70 (SOCI/RCI) and 2.77 Å

Figure 19. Potential energy curves of the electronic states of I_2^+ (reprinted from ref 251; copyright 1989 Academic Press, Inc.). See Table 40 for spectroscopic labels of known states.
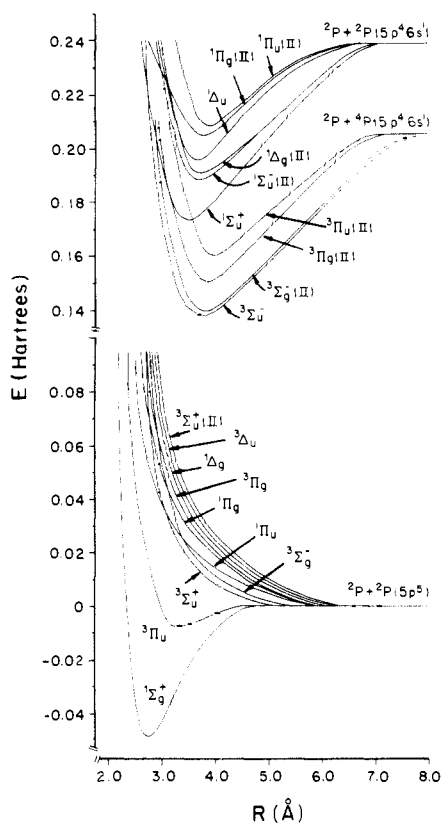
(FOCI/RCI), ω_e = 210 cm^{-1} (FOCI/RCI), and D_e = 1.45 eV, which includes the spin–orbit effects. From Table 41 it is seen that the main configuration contributing to the ground state is $2\sigma_g^2$ (95%) at R_e; at longer distance (R = 4.0 Å) the contributions from $2\sigma_u^2$ (28%) and $1\pi_u^3 2\sigma_u^1$ (5%) become significant. The I–I bond in the $^1\Sigma_g^+(0_g^+)$ state is weakened due to the spin–orbit interaction. The experimental spectroscopic data[37] are R_e = 2.67 Å, ω_e = 214.5 cm^{-1}, and D_0^0 = 1.54 eV, which are in excellent agreement with the Li–Balasubramanian calculational results.

Skorko[252] found a strong continuous absorption region at higher temperatures and pressures in the spectrum of I_2 at λ 3427 Å and a similar but weaker region with a long-wavelength edge at λ 3263 Å. Mulliken[237] assumed that the λ 3427 Å and λ 3263 Å regions can be identified with absorptions from the $^3\Pi_u(2_u)$ and $^3\Pi_u(1_u)$ states terminating to $^3\Pi_g(2_g)$ and $^3\Pi_g(1_g)$, respectively, and estimated a T_e value of 10 100 cm^{-1} for $^3\Pi(2_u)$ and 11 888 cm^{-1} for $^3\Pi_u(1_u)$. Ashby et al.[241] have photographed the $A^3\Pi_u(1_u) - X^1\Sigma_g^+$ system of I_2 at 8000–13 400 Å in absorption which facilitated calculation of constants for the $A^3\Pi_u(1_u)$ state: T_e = 10 906 cm^{-1}, D_e = 1641 cm^{-1}, and ω_e = 92.5 cm^{-1}. Gerstenkorn et al.[242] have determined the IR absorption spectrum of the $A^3\Pi_u(1_u)$ state at 7000–12 500 cm^{-1} using Fourier spectroscopy and found the separation between the $X^1\Sigma_g^+$ and $A^3\Pi_u(1_u)$ states to be 10 846 cm^{-1}; the D_e of the A state was calculated as 1639.77 cm^{-1}. Gerstenkorn et al.[253] obtained some visible absorption bands of I_2 by the same technique. The separation between the $X^1\Sigma_g^+$ and $B^3\Pi_u(0_u^+)$ states deduced by these authors is $T_{0,0}$ = 15724.586 cm^{-1}.

The spin–orbit components of the $^3\Pi_u$ state of I_2 are not as strongly bound as the ground state. The basis sets and levels of electron correlation treatments employed by Li and Balasubramanian[251] are not likely to

be as accurate for less bound excited states compared to the ground state. Nevertheless, a full SOCI treatment that included up to 105 000 configurations in the D_{2h} symmetry cannot be regarded as a poor approximation. Thus, the theoretical R_e and ω_e values of the

B(0_u^+) state are not in as good agreement with the experimental values as the ground state is.

The $B'^3\Pi_u(0_u^-)$ and $B''^1\Pi_u(1_u)$ states were both assigned as repulsive states[37] from the $^2P_{3/2} + ^2P_{3/2}$ atomic states at long distance; the B'' state is also the state

TABLE 41. Contributions of Important Configurations to the FOCI/RCI Wave Functions of I_2^a

State	r(Å)	Percentage of Contributions	State	r(Å)	Percentage of contributions
$^1\Sigma_g^+(0_g^+)$	2.75	$2\sigma_g^2 1\pi_u^4 1\pi_g^4(^1\Sigma_g^+)$ (95), $1\pi_u^4 1\pi_g^4 2\sigma_u^2(1)$ $(^1\Sigma_g^+)$ (4), $2\sigma_g^2 1\pi_u^3 1\pi_g^4 2\sigma_u^1(^3\Pi_g)$ (0.6), $2\sigma_g^2 1\pi_u^4 1\pi_g^2 2\sigma_u^2(^3\Sigma_g^-)$ (0.3)	$^3\Pi_g(1_g)$	2.75	$2\sigma_g^2 1\pi_u^3 1\pi_g^4 2\sigma_u^1(^3\Pi_g)$ (51), $2\sigma_g^1 1\pi_u^4 1\pi_g^3 2\sigma_u^2(^3\Pi_g)$ (47)
	4.00	$2\sigma_g^2 1\pi_u^4 1\pi_g^4(^1\Sigma_g^+)$ (67), $1\pi_u^4 1\pi_g^4 2\sigma_u^2(^1\Sigma_g^+)$ (28), $2\sigma_g^2 1\pi_u^3 1\pi_g^4 2\sigma_u^1(^3\Pi_g)$ (5)	$^3\Sigma_g^-(0_g^+)$	2.75	$2\sigma_g^2 1\pi_u^4 1\pi_g^2 2\sigma_u^2(^3\Sigma_g^-)$ (93), $2\sigma_g^2 1\pi_u^2 1\pi_g^4 2\sigma_u^2(^3\Sigma_g^-)$ (2)
$^3\Pi_u(2_u)$	3.25	$2\sigma_g^2 1\pi_u^4 1\pi_g^3 2\sigma_u^1(^3\Pi_u)$ (97)	$^3\Sigma_g^-(1_g)$	2.75	$2\sigma_g^2 1\pi_u^4 1\pi_g^2 2\sigma_u^2(^3\Sigma_g^-)$ (94)
	3.50	$2\sigma_g^2 1\pi_u^4 1\pi_g^3 2\sigma_u^1(^3\Pi_u)$ (97)	$^1\Delta_g(2_g)$	2.75	$2\sigma_g^2 1\pi_u^4 1\pi_g^2 2\sigma_u^2(^1\Delta_g)$ (92), $2\sigma_g^2 1\pi_u^2 1\pi_g^4 2\sigma_u^2(^1\Delta_g)$ (4)
	4.00	$2\sigma_g^2 1\pi_u^4 1\pi_g^3 2\sigma_u^1(^3\Pi_u)$ (67), $2\sigma_g^1 1\pi_u^3 1\pi_g^4 2\sigma_u^2(^3\Pi_u)$ (30)	$^3\Pi_g(II)(2_g)$	3.75	$2\sigma_g^1 1\pi_u^4 1\pi_g^3 2\sigma_u^2(^3\Pi_g)$ (62), $2\sigma_g^2 1\pi_u^3 1\pi_g^4 2\sigma_u^1(^3\Pi_g)$ (33)
$^3\Pi_u(1_u)$	3.25	$2\sigma_g^2 1\pi_u^4 1\pi_g^3 2\sigma_u^1(^3\Pi_u)$ (57), $2\sigma_g^2 1\pi_u^4 1\pi_g^3 2\sigma_u^1(^1\Pi_u)$ (3), $2\sigma_g^1 1\pi_u^3 1\pi_g^4 2\sigma_u^1(^3\Sigma_u^+)$ (39)	$^3\Pi_g(II)(0_g^+)$	3.75	$2\sigma_g^1 1\pi_u^4 1\pi_g^3 2\sigma_u^2(^3\Pi_g)$ (52), $2\sigma_g^2 1\pi_u^3 1\pi_g^4 2\sigma_u^1(^3\Pi_g)$ (33)
	3.50	$2\sigma_g^2 1\pi_u^4 1\pi_g^2 2\sigma_u^1(^3\Pi_u)$ (11), $2\sigma_g^1 1\pi_u^4 1\pi_g^4 2\sigma_u^1(^3\Sigma_u^+)$ (86), $2\sigma^2 1\pi_u^4 1\pi_g^3 2\sigma_u^1(^1\Pi_u)$ (1)	$^3\Pi_g(II)(0_g^-)$	3.75	$2\sigma_g^1 1\pi_u^4 1\pi_g^3 2\sigma_u^2(^3\Pi_g)$ (62), $2\sigma_g^2 1\pi_u^3 1\pi_g^4 2\sigma_u^1(^3\Pi_g)$ (33)
	4.00	$2\sigma_g^2 1\pi_u^4 1\pi_g^3 2\sigma_u^1(^3\Pi_u)$ (31), $2\sigma_g^1 1\pi_u^4 1\pi_g^4 2\sigma_u^1(^3\Sigma_u^+)$ (47), $2\sigma_g^2 1\pi_u^3 1\pi_g^4 2\sigma_u^1(^3\Pi_u)$ (13), $2\sigma_g^2 1\pi_u^4 1\pi_g^3 2\sigma_u^1(^1\Pi_u)$ (2)	$^3\Pi_g(II)(1_g)$	3.75	$2\sigma_g^1 1\pi_u^4 1\pi_g^3 2\sigma_u^2(^3\Pi_g)$ (58), $2\sigma_g^1 1\pi_u^4 1\pi_g^3 2\sigma_u^2(^1\Pi_g)$ (0.3), $2\sigma_g^2 1\pi_u^3 1\pi_g^4 2\sigma_u^1(^3\Pi_g)$ (38), $2\sigma_g^2 1\pi_u^3 1\pi_g^4 2\sigma_u^1(^1\Pi_g)$ (0.3)
$^3\Pi_u(0_u^+)$	3.25	$2\sigma_g^2 1\pi_u^4 1\pi_g^3 2\sigma_u^1(^3\Pi_u)$ (96), $2\sigma_g^1 1\pi_u^4 1\pi_g^4 2\sigma_u^1(^1\Sigma_u^+)$ (1)	$^1\Sigma_u^-$	2.75	$2\sigma_g^2 1\pi_u^3 1\pi_g^3 2\sigma_u^2(^1\Sigma_u^-)$ (99)
	3.50	$2\sigma_g^2 1\pi_u^4 1\pi_g^3 2\sigma_u^1(^3\Pi_u)$ (96), $2\sigma_g^1 1\pi_u^4 1\pi_g^4 2\sigma_u^1(^1\Sigma_u^+)$ (1)	$^3\Sigma_u^-$	3.75	$2\sigma_g^2 1\pi_u^3 1\pi_g^3 2\sigma_u^2(^3\Sigma_u^-)$ (88)
	4.00	$2\sigma_g^2 1\pi_u^4 1\pi_g^3 2\sigma_u^1(^3\Pi_u)$ (67), $2\sigma_g^1 1\pi_u^3 1\pi_g^4 2\sigma_u^2(^3\Pi_u)$ (31)	$1_u(^3\Delta_u,$ $^3\Sigma_u^+(II))$	2.75	$2\sigma_g^2 1\pi_u^3 1\pi_g^3 2\sigma_u^2(^3\Delta_u)$ (49), $2\sigma_g^2 1\pi_u^3 1\pi_g^3 2\sigma_u^2(^3\Sigma_u^+)$ (48)
$^3\Pi_u(0_u^-)$	2.75	$2\sigma_g^2 1\pi_u^4 1\pi_g^3 2\sigma_u^1(^3\Pi_u)$ (84), $2\sigma_g^1 1\pi_u^4 1\pi_g^4 2\sigma_u^1(^3\Sigma_u^+)$ (10)	$^3\Delta_u$	2.75	$2\sigma_g^2 1\pi_u^3 1\pi_g^3 2\sigma_u^2(^3\Delta_u)$ (98)
	3.25	$2\sigma_g^2 1\pi_u^4 1\pi_g^3 2\sigma_u^1(^3\Pi_u)$ (32), $2\sigma_g^1 1\pi_u^4 1\pi_g^4 2\sigma_u^1(^3\Sigma_u^+)$ (66)	$^3\Sigma_g^-(II)$	3.75	$2\sigma_g^2 1\pi_u^4 1\pi_g^2 2\sigma_u^2(^3\Sigma_g^-)$ (55), $2\sigma_g^1 1\pi_u^4 1\pi_g^2 2\sigma_u^2(^3\Sigma_g^-)$ (34)
	4.00	$2\sigma_g^2 1\pi_u^4 1\pi_g^3 2\sigma_u^1(^3\Pi_u)$ (28), $2\sigma_g^1 1\pi_u^4 1\pi_g^4 2\sigma_u^1(^3\Sigma_u^+)$ (55), $2\sigma_g^1 1\pi_u^3 1\pi_g^4 2\sigma_u^2(^3\Pi_u)$ (15)	$^3\Sigma_u^+(II)$	2.75	$2\sigma_g^2 1\pi_u^3 1\pi_g^3 2\sigma_u^2(^3\Sigma_u^+)$ (97)
$^1\Pi_u(1_u)$	2.75	$2\sigma_g^2 1\pi_u^4 1\pi_g^3 2\sigma_u^1(^1\Pi_u)$ (87), $2\sigma_g^2 1\pi_u^4 1\pi_g^3 2\sigma_u^1(^3\Pi_u)$ (12)	$^3\Pi_u(II)$	4.00	$2\sigma_g^1 1\pi_u^3 1\pi_g^4 2\sigma_u^2(^3\Pi_u)$ (63), $2\sigma_g^2 1\pi_u^4 1\pi_g^3 2\sigma_u^1(^3\Pi_u)$ (25)
$^1\Pi_g(1_g)$	2.75	$2\sigma_g^2 1\pi_u^3 1\pi_g^4 2\sigma_u^1(^1\Pi_g)$ (50), $2\sigma_g^1 1\pi_u^4 1\pi_g^3 2\sigma_u^2(^1\Pi_g)$ (48)	$^1\Sigma_u^+$	3.50	$2\sigma_g^1 1\pi_u^4 1\pi_g^4 2\sigma_u^1(^1\Sigma_u^+)$ (78), $2\sigma_g^2 1\pi_u^3 1\pi_g^3 2\sigma_u^2(^1\Sigma_u^+)$ (14)
$^3\Sigma_u^+(1_u)$	2.75	$2\sigma_g^1 1\pi_u^4 1\pi_g^4 2\sigma_u^1(^3\Sigma_u^+)$ (93)	$^1\Sigma_g^+(II)$	4.00	$1\pi_u^4 1\pi_g^4 2\sigma_u^2(^1\Sigma_g^+)$ (50), $2\sigma_g^2 1\pi_u^4 1\pi_g^4(^1\Sigma_g^+)$ (16), $2\sigma_g^2 1\pi_u^2 1\pi_g^4 2\sigma_u^2(^1\Sigma_g^+)$ (12), $2\sigma_g^2 1\pi_u^4 1\pi_g^2 2\sigma_u^2(^1\Sigma_g^-)$ (10)
$^3\Sigma_u^+(0_u^-)$	2.75	$2\sigma_g^1 1\pi_u^4 1\pi_g^4 2\sigma_u^1(^3\Sigma_u^+)$ (98)	$^1\Sigma_u^-(II)$	3.75	$2\sigma_g^2 1\pi_u^3 1\pi_g^3 2\sigma_u^2(^1\Sigma_u^-)$ (89)
$^3\Pi_g(2_g)$	2.75	$2\sigma_g^2 1\pi_u^3 1\pi_g^4 2\sigma_u^1(^3\Pi_g)$ (51), $2\sigma_g^1 1\pi_u^4 1\pi_g^3 2\sigma_u^2(^3\Pi_g)$ (46)	$^1\Delta_g(II)$	3.75	$2\sigma_g^2 1\pi_u^2 1\pi_g^4 2\sigma_u^2(^1\Delta_g)$ (51), $2\sigma_g^2 1\pi_u^4 1\pi_g^2 2\sigma_u^2(^1\Delta_g)$ (36)
$^3\Pi_g(0_g^+)$	2.75	$2\sigma_g^2 1\pi_u^3 1\pi_g^4 2\sigma_u^1(^3\Pi_g)$ (53), $2\sigma_g^1 1\pi_u^4 1\pi_g^3 2\sigma_u^2(^3\Pi_g)$ (45)	$^1\Sigma_g^+(III)$	2.75	$2\sigma_g^2 1\pi_u^4 1\pi_g^2 2\sigma_u^2(^1\Sigma_g^+)$ (85), $2\sigma_g^2 1\pi_u^2 1\pi_g^4 2\sigma_u^2(^1\Sigma_g^+)$ (4)
$^3\Pi_g(0_g^-)$	2.75	$2\sigma_g^2 1\pi_u^3 1\pi_g^4 2\sigma_u^1(^3\Pi_g)$ (53), $2\sigma_g^1 1\pi_u^4 1\pi_g^3 2\sigma_u^2(^3\Pi_g)$ (45)	$^1\Delta_u$	3.75	$2\sigma_g^2 1\pi_u^3 1\pi_g^3 2\sigma_u^2(^1\Delta_u)$ (88)
			$^1\Pi_g(II)$	3.75	$2\sigma_g^1 1\pi_u^4 1\pi_g^3 2\sigma_u^2(^1\Pi_g)$ (67), $2\sigma_g^2 1\pi_u^3 1\pi_g^3 2\sigma_u^1(^1\Pi_g)$ (23)
			$^1\Pi_u(II)$	4.00	$2\sigma_g^1 1\pi_u^3 1\pi_g^4 2\sigma_u^2(^1\Pi_u)$ (57), $2\sigma_g^2 1\pi_u^4 1\pi_g^3 2\sigma_u^1(^1\Pi_u)$ (31)
			$^3\Pi_g(III)$	3.00	$2\sigma_g^2 1\pi_u^4 1\pi_g^3 3\sigma_g^1(^3\Pi_g)$ (83), $2\sigma_g^1 1\pi_u^3 1\pi_g^4 2\sigma_u^1 3\sigma_g^1(^3\Pi_g)$ (5)

TABLE 41 (Continued)

State	r (Å)	Percentage of Contributions	State	r(Å)	Percentage of Contributions
$^1\Pi_g$	3.00	$2\sigma_g^2 1\pi_u^4 1\pi_g^3 3\sigma_g^1 (^1\Pi_g)$ (84), $2\sigma_g^1 1\pi_u^3 1\pi_g^4 2\sigma_u^1 3\sigma_g^1 (^1\Pi_g)$ (5),	$^1\Pi_u$	3.00	$2\sigma_u^1 1\pi_u^3 1\pi_g^4 2\sigma_g^2 (^1\Pi_u)$ (42), $2\sigma_g^2 1\pi_u^4 1\pi_g^3 3\sigma_u^1 (^1\Pi_u)$ (33)
$^1\Sigma_u^+$	3.75	$2\sigma_g^2 1\pi_u^3 1\pi_g^3 2\sigma_u^2 (^1\Sigma_u^+)$ (73), $2\sigma_g^1 1\pi_u^4 1\pi_g^4 2\sigma_u^1 (^1\Sigma_u^+)$ (15)			$1\sigma_g^2 1\pi_u^3 1\pi_g^3 3\sigma_g^1 (^1\Pi_u)$ (8), $2\sigma_g^2 1\pi_u^4 1\pi_g^3 2\sigma_u^1 (^1\Pi_u)$ (5)
$^3\Sigma_u^-$	3.50	$2\sigma_g^2 1\pi_u^4 1\pi_g^2 2\sigma_u^1 3\sigma_g^1 (^3\Sigma_u^-)$ (50), $2\sigma_g^2 1\pi_u^2 1\pi_g^4 2\sigma_u^1 3\sigma_g^1 (^3\Sigma_u^-)$ (32)	$^1\Sigma_u^+$	3.25	$2\sigma_g^2 1\pi_u^4 1\pi_g^1 2\sigma_u^1 3\sigma_g^1 (^1\Sigma_u^+)$ (60), $2\sigma_g^2 1\pi_u^2 1\pi_g^4 2\sigma_u^1 3\sigma_g^1 (^1\Sigma_u^+)$ (32)
		$2\sigma_g^1 1\pi_u^3 1\pi_g^3 2\sigma_u^2 3\sigma_g^1 (^3\Sigma_u^-)$ (4)			$2\sigma_g^1 1\pi_u^3 1\pi_g^2 2\sigma_u^2 3\sigma_g^1 (^1\Sigma_u^+)$ (4)
$^3\Pi_u$	3.00	$2\sigma_g^1 1\pi_u^4 1\pi_g^3 3\sigma_g^1 (^3\Pi_u)$ (43), $2\sigma_g^2 1\pi_u^3 1\pi_g^4 3\sigma_g^1 (^3\Pi_u)$ (39),	$^3\Sigma_u^-$	3.25	$2\sigma_g^1 1\pi_u^4 1\pi_g^4 3\sigma_g^1 (^3\Sigma_u^-)$ (90)
		$2\sigma_g^1 1\pi_u^3 1\pi_g^4 2\sigma_u^2 (^3\Pi_u)$ (5)	$^3\Sigma_g^-$(II)	3.00	$2\sigma_g^2 1\pi_u^4 1\pi_g^3 2\pi_g^1 (^3\Sigma_g^+)$ (72), $2\sigma_g^1 1\pi_u^4 1\pi_g^4 3\sigma_g^1 (^3\Sigma_g^+)$ (15)

^{a} From ref 251.

TABLE 42. Contributions of Important Configurations to the FOCI/RCI Wave Functions of I_2^{+} ^{a}

State	r(Å)	Percentage of contributions	State	r(Å)	Percentage of contributions
$^2\Pi_g(\frac{3}{2}g)$	2.75	$2\sigma_g^2 1\pi_u^4 1\pi_g^3 (^2\Pi_g)$ (93), $1\pi_u^4 1\pi_g^3 2\sigma_g^2 (^2\Pi_g)$ (3)		3.50	$2\sigma_g^2 1\pi_u^3 1\pi_g^3 2\sigma_u^1 (^2\Delta_g)$ (87), $2\sigma_g^1 1\pi_u^4 1\pi_g^3 2\sigma_u^2 (^2\Delta_g)$ (6)
$^2\Pi_g(\frac{1}{2}g)$	2.75	$2\sigma_g^2 1\pi_u^4 1\pi_g^3 (^2\Pi_g)$ (92), $1\pi_u^4 1\pi_g^3 2\sigma_g^2 (^2\Pi_g)$ (3)		5.00	$2\sigma_g^1 1\pi_u^3 1\pi_g^4 2\sigma_u^2 (^2\Delta_g)$ (32), $2\sigma_u^1 1\pi_u^4 1\pi_g^4 2\sigma_g^2 (^2\Delta_g)$ (30),
$^4\Sigma_u^-(\frac{1}{2}u)$	3.25	$2\sigma_g^2 1\pi_u^4 1\pi_g^2 2\sigma_u^1 (^4\Sigma_u^-)$ (65), $2\sigma_g^2 1\pi_u^3 1\pi_g^4 2\sigma_u^1 (^4\Sigma_u^-)$ (31)			$2\sigma_g^2 1\pi_u^3 1\pi_g^3 2\sigma_u^1 (^2\Delta_g)$ (34)
		$2\sigma_g^1 1\pi_u^4 1\pi_g^4 2\sigma_u^1 (^2\Sigma_u^+)$ (2)	$^2\Sigma_u^-$	2.75	$2\sigma_g^1 1\pi_u^4 1\pi_g^4 (^2\Sigma_u^+)$ (87), $2\sigma_g^2 1\pi_u^3 1\pi_g^3 2\sigma_u^1 (^2\Sigma_u^-)$ (5)
$^4\Sigma_u^-(\frac{3}{2}u)$	3.25	$2\sigma_g^2 1\pi_u^4 1\pi_g^2 2\sigma_u^1 (^4\Sigma_u^-)$ (64), $2\sigma_g^2 1\pi_u^3 1\pi_g^4 2\sigma_u^1 (^4\Sigma_u^-)$ (33)		3.50	$2\sigma_g^2 1\pi_u^3 1\pi_g^3 2\sigma_u^1 (^2\Sigma_g^+)$ (87), $2\sigma_g^1 1\pi_u^4 1\pi_g^3 2\sigma_u^2 (^2\Sigma_g^+)$ (5)
$^2\Delta_u$	3.50	$2\sigma_g^2 1\pi_u^4 1\pi_g^3 2\sigma_u^1 (^2\Delta_u)$ (58), $2\sigma_g^2 1\pi_u^3 1\pi_g^4 2\sigma_u^1 (^2\Delta_u)$ (35)		5.00	$2\sigma_g^1 1\pi_u^4 1\pi_g^3 2\sigma_u^2 (^2\Sigma_g^+)$ (32), $2\sigma_g^1 1\pi_u^2 1\pi_g^4 2\sigma_u^2 (^2\Sigma_g^+)$ (30),
$^2\Pi_g(\frac{3}{2}u)$	3.00	$2\sigma_g^2 1\pi_u^3 1\pi_g^4 (^2\Pi_u)$ (78), $2\sigma_g^1 1\pi_u^4 1\pi_g^3 2\sigma_u^1 (^2\Pi_u)$ (14)			$2\sigma_g^2 1\pi_u^3 1\pi_g^3 2\sigma_u^1 (^2\Sigma_g^+)$ (32)
$^2\Pi_u(\frac{1}{2}u)$	3.00	$2\sigma_g^1 1\pi_u^3 1\pi_g^4 (^2\Pi_u)$ (57), $2\sigma_g^2 1\pi_u^3 1\pi_g^3 2\sigma_u^1 (^2\Pi_u)$ (19)	$^2\Pi_g(II)$	2.75	$2\sigma_g^2 1\pi_u^4 1\pi_g^1 2\sigma_u^2 (^2\Pi_g)$ (72), $2\sigma_g^2 1\pi_u^2 1\pi_g^3 2\sigma_u^2 (^2\Pi_g)$ (19)
		$2\sigma_g^1 1\pi_u^4 1\pi_g^3 2\sigma_u^1 (^2\Pi_u)$ (9)	$^2\Pi_u(II)$	2.75	$2\sigma_g^1 1\pi_u^4 1\pi_g^3 2\sigma_u^1 (^2\Pi_u)$ (91)
$^2\Sigma_u^-$	3.50	$2\sigma_g^2 1\pi_u^4 1\pi_g^2 2\sigma_u^1 (^2\Sigma_u^-)$ (57), $2\sigma_g^2 1\pi_u^3 1\pi_g^3 2\sigma_u^1 (^2\Sigma_u^-)$ (36)	$^4\Sigma_u^-(II)$	2.75	$2\sigma_g^2 1\pi_u^2 1\pi_g^4 2\sigma_u^1 (^4\Sigma_u^-)$ (78), $2\sigma_g^1 1\pi_u^3 1\pi_g^3 2\sigma_u^2 (^4\Sigma_u^-)$ (13)
$^2\Delta_g$	2.75	$2\sigma_g^2 1\pi_u^3 1\pi_g^3 2\sigma_u^1 (^2\Delta_g)$ (94)			

^{a} From ref 251.

---

responsible for the absorption continuum with a maximum at 20050 cm^{-1} and for the predissociation of B$^3\Pi_u(0_u^+)$. As can be seen from Figure 17 the $^3\Pi_u(0_u^+)$ curve crosses with the $^3\Sigma_u^+(1_u)$, $^3\Sigma_u^+(0_u^-)$, $^3\Sigma_g^-(0_g^+)$, $^3\Sigma_g^-(1_g)$, $^1\Pi_g(1_g)$, and $^1\Pi_u(1_u)$ curves. Hence the $^3\Pi_u(0_u^+)$ state is predissociated. This has been noted before[238] based on experimental findings. There has been some doubt about the B$'^3\Pi_u(0_u^-)$ state being responsible for the magnetic field induced predissociation of the $^3\Pi_u(0_u^+)$ state (see ref 37). The theoretical calculations of Li and Balasubramanian[251] show (Figure 17) that the repulsive state $^3\Pi_u(0_u^-)$ lies below the $^3\Pi_u(0_u^+)$ state and thus may not be responsible for the predissociation. The theoretical B$''^1\Pi_u(1_u)$ state is repulsive, and its vertical energy from the ground state is 22% higher than the data from the absorption spectrum. The vertical energy separations of most of the states were not calculated exactly at the R_e of the ground state. A distance close

to the R_e for which the calculational value existed was used. Part of the difference could be attributed to this, although the basis sets and the levels of electron correlations used by Li and Balasubramanian are not fully adequate for accurate determination of the energy separations of the excited states.

The C state of I_2 has been studied by many authors. Mathieson and Rees[255] assigned the C state to 2332 $^3\Sigma_u^+(II)(0_u^-)$. Mulliken[237] and Clear and Wilson[254] assigned the C state to 1441 $^3\Sigma_u^+(1_u)$. The experimental data indicate that the C state has a weak but broad absorption continuum with a maximum at 2700 Å (37000 cm^{-1}) and dissociates into $^2P_{3/2} + ^2P_{1/2}$ atomic states. The theoretical calculations of Li and Balasubramanian[251] revealed (see Figure 17 and Table 39) that the 1441 $^3\Sigma_u^+(1_u)$ state dissociates into $^2P_{3/2} + ^2P_{3/2}$ at long distance; the theoretical vertical energy of the C state was found to be 32510 cm^{-1}, which is lower than

the experimental value. However, the 1_u state, which is a mixture of the 2332 $^3\Delta_u(1_u)$ and 2332 $^3\Sigma_u^+(II)(1_u)$ states, dissociates into $^2P_{3/2} + ^2P_{1/2}$ and has a vertical energy (36 751 cm^{-1}) near the experimental value. The mixing between $^3\Sigma_u^+(1_u)$ and $^3\Delta_u(1_u)$ could provide the necessary transition moment for the C $\leftarrow$ X transition if the C state is assigned to this state. Thus, the possibility of C being this state should not be ruled out. In both cases, theoretical calculations of Li and Balasubramanian[251] supported Mulliken's argument that C should be a 1_u state.

Chen et al.[246] observed the D $\leftarrow$ X (resonance enhanced) three-photon excitation spectrum of I_2 by a CW intracavity absorption method. The spectroscopic constants for the D state obtained by these authors are ν_{00} = 40 998 cm^{-1}, ω_0' = 113 cm^{-1}, and $\omega_0' x_0$ = 0.045 cm^{-1}. Other authors[37,237] assigned the D state to the $^1\Sigma_u^+$ state with T_e = 40 679 cm^{-1} and ω_e = 104.4 cm^{-1}. On the basis of the strong intensity of the D–X emission system, Mulliken[237] suggested two possible assignments for the D state. He argued that the D–X system could be 2332 $^3\Sigma_u^-(0_u^+)$ $\leftarrow$ X, 1441 $^1\Sigma_u^+$–X, or 1342 $^3\Pi_u(0_u^+)$ $\leftarrow$ X. The last one was excluded based on the low intensity and higher frequency. The 2332 $^3\Sigma_u^-(0_u^+)$–X transition needs excitation of two electrons from the ground state and consequently would be less probable in comparison to the 1441 $^1\Sigma_u^+$ system. However, as Mulliken correctly argued, the spin–orbit mixing between 2332 $^3\Sigma_u^-(0_u^+)$ and 1441 $^1\Sigma_u^+(0_u^+)$ would be significant and thus could provide a considerable transition moment for the 2332 $^3\Sigma_u^-(0_u^+)$–X system. In any event, the $^3\Sigma_u^-(0_u^+)$ state should be observable for I_2 since less intense systems have been characterized for I_2.

The theoretical energy separations[251] in Table 39 tended to substantiate the assignment of the D state to a mixture of $^3\Sigma_u^-(0_u^+)$ and $^1\Sigma_u^+(0_u^+)$. If this assignment is correct, then the intense F state observed in the F–X system (experimental T_e of 41 000 cm^{-1}) could be assigned to 1441 $^1\Sigma_u^+$. Furthermore, theoretical calculations of Li and Balasubramanian[251] placed the 2332 $^1\Sigma_u^+$ state which was thought of as a candidate for the experimental F state ($T_e \sim$ 41 000 cm^{-1}) 65 000 cm^{-1} above the ground state. Theoretical calculations of Li and Balasubramanian[251] were most consistent with the assignment of D to a mixture of $^3\Sigma_u^-(0_u^+)$ and $^1\Sigma_u^+(0_u^+)$ and the assignment of F to 1441 $^1\Sigma_u^+(0_u^+)$. The theoretical energy separation of the F state is higher than the experimental value as expected.

The Li–Balasubramanian[251] theoretical R_e and ω_e values of the 1441 $^1\Sigma_u^+$ state are 3.55 Å and 102 cm^{-1}, in very good agreement with the experimental R_e and ω_e values of the F state (3.61 Å, 96 cm^{-1}); this agreement provides further confidence in the assignment of the F state to 1441 $^1\Sigma_u^+$.

The electronic states labeled a and a′ observed from the diffuse and predissociation spectra[238] were assigned before to 2341 $^3\Pi_g(1_g)$. The a′ state was assigned to a 0_g^+ state, although the exact principal configuration contributing to this state was not known. As seen from Table 39, the theoretical calculations confirm the assignment of a to 2341 $^3\Pi_g(1_g)$ and suggest that the a′ state would be 2422 $^3\Sigma_g^-(0_g^+)$. The a state is responsible for the predissociation of B–X systems. As seen from Figure 17, both the $^3\Sigma_g^-(1_g)$ and $^3\Sigma_g^-(0_g^+)$ curves cross the 0_u^+ curve near the well of the 0_u^+ state. However, $^3\Pi_g(1_g)$ is lower than $^3\Sigma_g^-(0_g^+)$ (Table 39) and thus would cross

with the B(0_u^+) state at a shorter distance in comparison to $^3\Sigma_g^-(0_g^+)$. Thus, the earlier assignment of the state causing predissociation to a(1_g) rather than a′(0_g^+) is in agreement with the results of the theoretical calculations of Li and Balasubramanian.[251]

The presence of the F′(0_u^+) state has been confirmed by King et al.[247] with the three-photon absorption spectrum of I_2. Spectroscopic constants reported in ref 37 for this state are T_e = 45 230 cm^{-1} and ω_e = 93.4 cm^{-1}. The calculated data in Table 39 are most consistent with the assignment of the F′ state to $^3\Pi_u(II)(0_u^+)$. The theoretical ω_e value is in excellent agreement with the experimental results.

Brand et al.[256] have studied the resonant two-photon E(0_g^+) $\leftarrow$ B(0_u^+) $\leftarrow$ X(0_g^+) transition of I_2 vapor by polarization spectroscopy. Huber and Herzberg[37] assigned the E state to the $^3\Pi_g(0_g^+)$ state with T_e = 41 411.4 cm^{-1}, ω_e = 101.59 cm^{-1}, and R_e = 3.65 Å. Theoretical calculations[251] confirmed this assignment. The E(0_g^+) state is thus a 1432 $^3\Pi_g(0_g^+)$ state. Viswanathan et al.[257] examined an emission system of I_2 in Ar at 2830–2890 Å and interpreted this system as a charge-transfer transition originating from an ion-pair state near T_e = 47 000 cm^{-1} and ω_e = 105.7 cm^{-1} and terminating in a weakly bound state that dissociates into two ground-state atoms. The transition is tentatively assigned to the 0_g^- $\rightarrow$ 2431 $0_u^-(^3\Pi)$ transition. Table 39 shows that the 0_g^- state should be the 1432 $^3\Pi_g$ state of the theoretical calculations. The theoretical calculations predicted that the 2431 $0_u^-(^3\Pi_u)$ state is a repulsive state.[251] This prediction is consistent with a somewhat repulsive $^3\Pi_u(0_u^-)$ constructed from experimental results with a weak vibrational structure in the long-range part of the well.

Kawasaki et al.[258] studied the two- and three-photon absorption spectra of I_2 in the gas phase. The emission band at $\approx$340 nm is attributed to the 1432 $^3\Pi_g(2_g)$ $\rightarrow$ 2431 $^3\Pi_u(2_u)$ transition, and the 385-nm band is attributed to the $^3\Pi_g(1_g)$ $\rightarrow$ $^3\Pi_u(1_u)$ transition. Huber and Herzberg[37] assigned the G state to the $^3\Pi_g(2_g)$ state with T_e = 42 300 cm^{-1}, although later the label D′ was given instead of G. Theoretical calculations of Li and Balasubramanian[251] supported these assignments. Tellinghuisen and co-workers[238,259] have studied the emission spectrum D′(2_g) $\rightarrow$ 2332 $^3\Delta_u(2_u)$ and the detailed vibrational system for the D′(2_g) $\rightarrow$ A′($^3\Pi_u(2_u)$) transition. The experimental spectroscopic constants of the D′ state are T_e = 40 388.24 cm^{-1}, D_e = 31 794 cm^{-1}, R_e = 3.61 Å, and ω_e = 103.953 cm^{-1}. As seen from Table 39, theoretical calculations confirm the assignment of the D′ (called G earlier) state.

The emission bands in the 3460–3015-Å region in the presence of foreign gases were assigned to the H $\rightarrow$ B transition.[37] The H state, later denoted as f′, has the constants T_e = 46 063 cm^{-1} and ω_e = 103.7 cm^{-1}. The weak emission bands (2785–2731 Å) were found and attributed to the I $\rightarrow$ B transition.[37] The spectroscopic constants of the I state are T_e = 51 973 cm^{-1} and ω_e = 112.4 cm^{-1}. These assignments are both based on the assumption that the lower state is the B state, but it is not entirely certain that the lower state has been correctly identified as the B state.[37] As seen from Table 39, there are two bound states, $^1\Sigma_g^+(II)$ and $^1\Pi_g(II)$, whose T_es are both around 50 000 cm^{-1}. Thus, the assignments of the f′ state as the $^1\Sigma_g^+(I)$ state and the I state as the $^1\Pi_g(II)$ state seem reasonable.

The spectroscopic properties of the low-lying states

of I_2^+ can be discussed in terms of ionization of the highest occupied orbitals of the $^1\Sigma_g^+$ ground state of I_2. Upon ionizing the $1\pi_g$ orbital, one would obtain the lowest state of I_2^+ as the $^2\Pi_g$ state arising from the $1\sigma_g^2 1\sigma_u^2 2\sigma_g^2 1\pi_u^4 1\pi_g^3$ configuration. There are other possible low-lying states arising from the configurations $1\sigma_g^2 1\sigma_u^2 2\sigma_g^2 1\pi_u^4 1\pi_g^2 2\sigma_u^1$, $1\sigma_g^2 1\sigma_u^2 2\sigma_g^2 1\pi_u^3 1\pi_g^4$, and $1\sigma_g^2 1\sigma_u^2 2\sigma_g^1 1\pi_u^4 1\pi_g^4$.

Li and Balasubramanian[251] carried out CASSCF/FOCI/(SOCI)/RCI calculations on 13 electronic states (Table 40) of I_2^+. It can be seen from Table 40 that the ground state of I_2^+ is the $^2\Pi_g(3/2_g)$ state arising primarily from the $1\sigma_g^2 1\sigma_u^2 2\sigma_g^2 1\pi_u^4 1\pi_g^3$ configuration. The first excited state is $^2\Pi_g(1/2_g)$ from the same configuration.

The photoelectron spectrum of $I_2^{260,261}$ reveals the IP of I_2 is 9.311 eV for the $^1\Sigma_g^+(I_2) \rightarrow {}^2\Pi_g(3/2_g)(I_2^+)$ ionization, and IP = 9.953 eV for the $^1\Sigma_g^+(I_2) \rightarrow {}^2\Pi_g(1/2_g)(I_2^+)$. The theoretical adiabatic ionization potentials by the SOCI/RCI methods are IP = 8.62 eV (to $^2\Pi_g(3/2_g)$) and IP = 9.38 eV (to $^2\Pi_g(1/2_g)$).

The experimental spectroscopic constants[37,260] are D_0^0 = 2.683 eV and ω_e = 240 cm^{-1} for the $^2\Pi_g(3/2_g)$ state and T_e = 5180 cm^{-1} and ω_e = 220 cm^{-1} for the $^2\Pi_g(1/2_g)$ state. For the $^2\Pi_g(3/2_g)$ state, the theoretical constants obtained by SOCI/RCI are D_e = 2.06 eV and ω_e = 217 cm^{-1}, and for the $^2\Pi_g(1/2_g)$ state, T_e = 5979 cm^{-1} and ω_e = 208 cm^{-1}. As seen from Table 40, the $^2\Pi_g(3/2_g)$ and $^2\Pi_g(1/2_g)$ states are quite pure. Hund's rule should apply in this case; i.e., the energy level of the $^2\Pi_g(3/2_g)$ state should be lower than that of the $^2\Pi_g(1/2_g)$ state. There are no experimental R_e values reported for the electronic states of I_2^+. Since the (4s4p2d) basis set yields an R_e value about 0.06 Å longer, Li and Balasubramanian[251] predicted that the experimental R_e values of the $^2\Pi_g(3/2, 1/2)$ states should both be around 2.63 Å.

The A state of I_2^+ has been assigned to the $^2\Pi_u(1/2, 3/2)$ states by photoelectron spectra[37,261,262] with T_e = 12 420 cm^{-1} ($^2\Pi_u(3/2_u)$) and T_e = 18 950 cm^{-1} ($^2\Pi_u(1/2_u)$). The calculated T_es and the vertical transition energies from the ground state to the $^2\Pi_u(3/2_u)$ and $^2\Pi_u(1/2_u)$ states are listed in Table 40. Table 42 shows that the $^2\Pi_u(3/2_u)$ component is relatively pure while the $^2\Pi_u(1/2_u)$ state exhibits considerable contamination with the $^4\Sigma_u^-(1/2_u)$ component due to the spin–orbit coupling, which raises the energy level of the $^2\Pi_u(1/2_u)$ state.

The photoelectron spectra of Br_2 revealed substantially different vibrational frequencies for the two components of the $^2\Pi_u$ state (see section III.E).[37] Specifically, the experimental ω_e values of the $^2\Pi_u(3/2)$ and $^2\Pi_u(1/2)$ states are 190 and 152 cm^{-1}. The theoretical calculations on Br_2^+ by Balasubramanian[181] confirmed these experimental findings. The theoretical ω_e values of the $^2\Pi_u(3/2)$ and $^2\Pi_u(1/2)$ states of Br_2^+ were found to be 194 and 137 cm^{-1}, respectively.[181] This anomaly was attributed to the fact that the $^2\Pi_u(3/2)$ state of Br_2 is pure while the $^2\Pi_u(1/2)$ state mixes strongly with $^4\Sigma_u^-(1/2)$ and $^2\Sigma_u^+(1/2)$ near the equilibrium geometry.[181]

The $^2\Pi_u(1/2)$ state of I_2^+ also behaves qualitatively similar to Br_2^+ in that it also mixes with $^4\Sigma_u^-(1/2)$, which results in a lower ω_e for the $^2\Pi_u(1/2)$ component. The actual amount of mixing is smaller for I_2^+ compared to Br_2^+. Actually, for Br_2^+ there is an avoided crossing of

$^2\Pi_u(1/2)$ and $^4\Sigma_u^-(1/2)$.[181] The $^2\Pi_u(1/2)$ state of Br_2^+ is designated as the A state and was observed by Hamilton[190] recently in a laser spectroscopic investigation. Direct laser spectroscopic investigation of the electronic states of I_2^+ is yet to be undertaken.

An electronic state labeled the B state and assigned to a $^2\Sigma_g^+$ state[37,249,250,261,262] was observed with T = 27 900 cm^{-1}. Éland[261] suggested that the $B^2\Sigma_g^+$ state of I_2^+ is fully dissociated to the ground state $I^+ + I$. The calculated $^2\Sigma_g^+$ state is a weakly bound state with T_e = 19 361 cm^{-1}, R_e = 3.62 Å, and ω_e = 72 cm^{-1}. Figure 18 shows that the $B^2\Sigma_g^+$ state is dissociated to the ground state $I^+ + I$. Leach[249] and McLoughlin et al.[250] have predicted that the $B^2\Sigma_g^+$ state curve should have a maximum at a long distance. The theoretical potential curve of the B state obtained by Li and Balasubramanian (Figure 18) confirmed this prediction of a maximum near 4 Å. This maximum is due to an avoided crossing of configurations contributing to the CI wave functions (Table 42). This state is dominated by mainly $1\sigma_g^2 1\sigma_u^2 2\sigma_g^2 1\pi_u^3 1\pi_g^3 2\sigma_u^1$ at 3.5 Å; at long distances (>4 Å), the state is a heavy mixture of $1\sigma_g^2 1\sigma_u^2 2\sigma_g^1 1\pi_u^4 1\pi_g^4 2\sigma_u^2$ and $1\sigma_g^2 1\sigma_u^2 2\sigma_g^1 1\pi_u^3 1\pi_g^4 2\sigma_u^2$ configurations (see Table 42). This avoided crossing resulted in the maximum in the potential curve of the $B^2\Sigma_g^+$ state. At very short distance there is another avoided crossing.

Table 42 shows the weights of the various configurations contributing to the RCI wave functions of the electronic states of I_2^+. As seen from Table 42, most of the electronic states are relatively pure. The contribution of $^4\Sigma_u^-(1/2)$ to $^2\Pi_u(1/2)$ is noticeable (9%) as seen from Table 42. The $^4\Sigma_u^-(3/2)$ state is somewhat purer at its equilibrium geometry.

K. Tl_2 and Tl_2^+

The thallium dimer (Tl_2) is much more weakly bound compared to In_2 due to the inert-pair effect. For the same reason, most of the sixth-row p-block dimers are much less bound compared to the fifth-row dimers. This will be discussed in section VII. Early experimental investigations on Tl_2 were focused on the determination of the dissociation energies. Drowart and Honig[263] suggested an upper limit of 0.9 eV for D_0^0 of Tl_2 based on failure to observe Tl_2 in Tl vapor above 900 K.[264] Ginter et al.[122] observed emission bands in the 15 300–16 000-cm^{-1} region and absorption bands in the 23 000-cm^{-1} region. It is not evident if these bands arise from Tl_2 or another cluster of thallium atoms. The related Tl_2^+ ion has been observed by Berkowitz and Walter,[265] but no experimental spectroscopic constants have been reported for Tl_2. Balducci et al.[266] have carried out a more recent mass spectrometric investigation of Tl_2 and obtained a D_0^0 value of 0.63 eV using ω_e = 136 cm^{-1} for Tl_2.

Christiansen and Pitzer[195] made small MCSCF–spinor calculations for the electronic states of Tl_2 which dissociated into the $^2P_{1/2} + {}^2P_{1/2}$ ground-state Tl atoms. For the 0_g^+ state, a two-configuration MCSCF treatment was used while for the 0_u^- and 1_u states, only one configuration was included. A double-ζ STO basis set was employed. This is one of the earliest relativistic molecular calculations and thus electron correlation effects could not be included to high order. In a later study, Christiansen[196] carried out GVB/RCI calculations on the low-lying electronic states of Tl_2. This study,
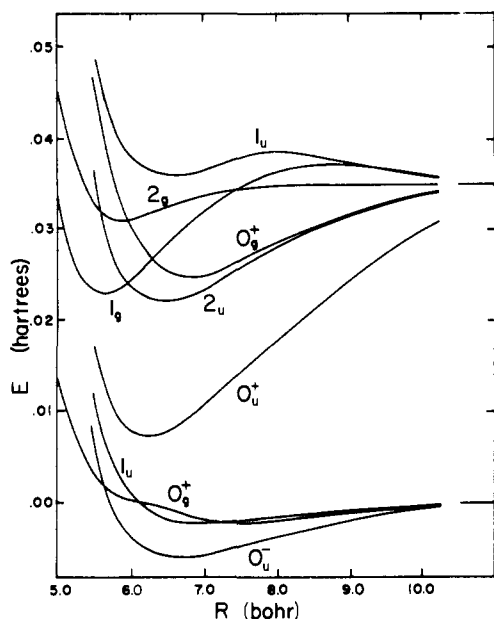
Figure 20. Potential energy curves of nine low-lying states of Tl_2 including spin–orbit effects (reprinted from ref 196; copyright 1983 American Institute of Physics).

TABLE 43. Spectroscopic Constants for the Low-Lying States of Tl_2[a]

State	T_e (cm^{-1})	R_e (Å)	ω_e (cm^{-1})
$X0_u^-$	0	3.54	39
$1_u(I)$	814	3.71	30
$0_g^+(I)$	860	3.97	25
0_u^+	2900	3.30	85
2_u	6200	3.41	54
1_g	6370	3.00	87
$0_g^+(II)$	6780	3.51	54
2_g	8130	3.14	61
$1_u(II)$	9280	3.49	39

[a] All values are theoretical constants from ref 196.

however, yielded only a weakly bound ground state for Tl_2. In the earlier investigation, Christiansen and Pitzer[195] also considered the potential energy curves of the $1/2_g$ and $1/2_u$ states of Tl_2^+.

Potential energy curves of nine low-lying electronic states of Tl_2 obtained by Christiansen[196] dissociating to the ground-state atoms and the excited $^2P_{1/2} + {}^2P_{3/2}$ limits including spin–orbit coupling are shown in Figure 20. The theoretical spectroscopic constants are shown in Table 43. The potential energy curves of the $1/2_g$ and $1/2_u$ states of Tl_2^+ are shown in Figure 21. As seen from Figure 20, the ground state of Tl_2 is a 0_u^- state and is only weakly bound. The Tl_2^+ ion in fact is a bit more bound ($D_e = 0.58$ eV) compared to Tl_2 (Figure 20).[195]

Christiansen's[196] intermediate-coupling RCI calculations gave only a weakly bound 0_u^- state ($D_e = 0.16$ eV), in conflict with an experimental mass spectral value
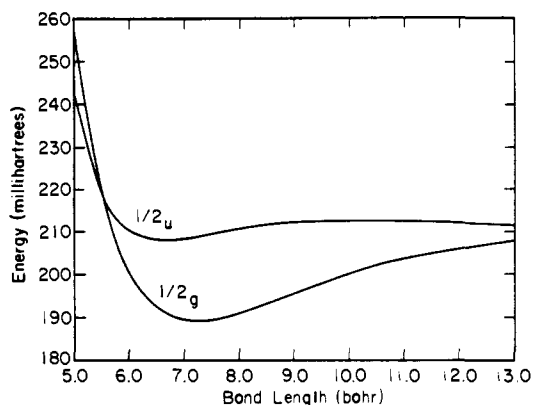

Figure 21. Potential energy curves of two low-lying states of Tl_2^+ (reprinted from ref 195; copyright 1981 American Institute of Physics).

TABLE 44. Molecular States of Pb_2 Related to Atoms in Several Low-Energy States and Their Energies[a]

dissociation limit		molecular states
$^3P_0 + {}^3P_0$	0.0	0_g^+
$^3P_0 + {}^3P_1$	7 819.4	0_g^-, 0_u^-, 1_g, 1_u
$^3P_0 + {}^3P_2$	10 650.5	0_g^+, 0_u^+, 1_g, 1_u, 2_g, 2_u
$^3P_1 + {}^3P_1$	15 638.7	$0_g^+(2)$, 0_u^-, 1_g, 1_u, 2_g
$^3P_1 + {}^3P_2$	18469.8	0_g^+, 0_u^+, $0_g^-(2)$, $0_u^-(2)$, $1_g(3)$, $1_u(3)$, $2_g(2)$, $2_u(2)$, 3_g, 3_u
$^3P_2 + {}^3P_2$	21 300.9	$0_g^+(3)$, $0_u^-(2)$, $1_g(2)$, $1_u(2)$, $2_g(2)$, 2_u, 3_g, 3_u, 4_g
$^3P_0 + {}^1D_2$	21 457.9	0_g^+, 0_u^+, 1_g, 1_u, 2_g, 2_u

[a] In parentheses is the number of states of a given symmetry. The energies of the dissociated atoms are in cm^{-1} and are from ref 134.

obtained by Balducci and Piacente[266] (0.6 ± 0.15 eV). However, Christiansen recalculated the D_0^0 value by using a more accurate partition function derived from his molecular calculations as 0.37 eV. This value is in more reasonable agreement with the RCI value of 0.16 eV. Electron correlation effects are expected to be large, and thus more accurate calculations that include electron correlation effects to a higher order may bring the D_0^0 value of Tl_2 closer to the revised experimental value of 0.37 eV. In any event, Tl_2 is much more weakly bound compared to In_2.

Presently, there are no theoretical calculations on more excited electronic states of Tl_2 that would aid in the assignment of the observed spectra. Thus, such calculations are warranted to aid in the interpretation of experimental data and they are in progress.[267]

L. Pb_2

Shawhan[268] in 1935 carried out the first vibrational analysis of the observed spectrum of Pb_2. Subse-

TABLE 45. Spectroscopic Parameters for Pb₂[a]

term	T_e (cm⁻¹) Theo.	Expt.	ω_e (cm⁻¹) Theo.	Expt.	R_e (Å) Theo.	Expt.
X σ_g^+	0	0	103	110	2.97	2.93
A 1_g	4150	a≈3500	124	122	2.96	
2_u	5670		119		2.70	
1_u	7370		119		2.71	
2_g	10130		105		3.03	
B 0_u^-	12920	12 437	106		2.75	
$1_g(II)$	13320		100		3.07	
$0_u^+(II)$	13640		~4		3.18	
C 0_u^-	14130	13 314	113	129	2.74	
D		a+13 433				
E		a+14 500				
$1_g(II)$	15620		111		2.73	
F 0_u^-		13 800		157		

[a] The X, A, B, and C labels are those of Bondybey and English.[87,197] The theoretical constants are from ref 277.

quently, many others have studied the electronic spectra of Pb₂ in both the gas phase and rare-gas matrices.[87,197,269-273,275,278,279] There are many mass spectrometric studies of Pb₂ also.[263,274,276] Johnson et al.[272] using the laser-induced fluorescence technique obtained superior spectra and showed that the early analysis of Shawhan cannot be correct. Bondybey and English[87,197] have studied the lead dimer LIF spectra extensively in rare-gas matrices.

The spectroscopic investigations of the lead dimer summarized above have revealed the presence of at least seven low-energy electronic states. Pitzer and Balasubramanian[277] carried out SCF/RCI calculations of ten electronic states of Pb₂ and their potential energy curves.

Table 44 gives the molecular states of Pb₂ that dissociate to atoms with total energies up to 22 000 cm⁻¹ above the lowest states $^3P_0 + {}^3P_0$. Pitzer and Balasubramanian[277] have limited their calculations to those terms expected to be relatively low in energy (within about 15 000 cm⁻¹ of the lowest 0_g^+ state).

Table 45 shows the theoretical spectroscopic constants of Pb₂ obtained by Pitzer and Balasubramanian[277] together with available experimental data. The potential energy curves are shown in Figure 22 for the g terms and in Figure 23 for the u terms, with the lowest 0_g^+ state shown in both figures. These potential energy curves were obtained by Pitzer and Balasubramanian.[207]

As seen from Figure 22, the spin–orbit (SO) effect greatly lowers the 0_g^+ component state of $^3\Sigma_g^-(\sigma_g^2\pi_u^2)$ near the potential minimum. At shorter distances this 0_g^+ state undergoes an avoided crossing with the $^1\Sigma_g^+(\pi_u^4)$
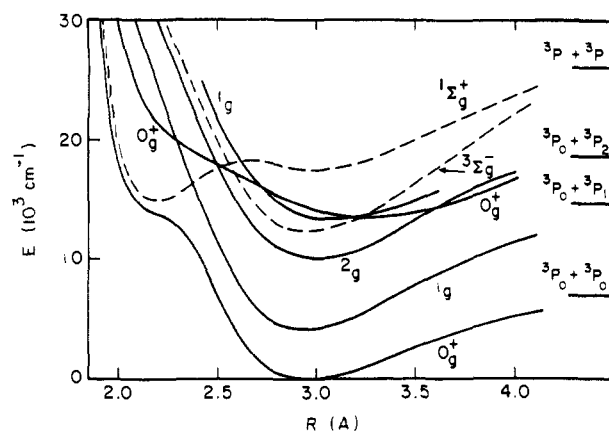

Figure 22. Potential energy curves of the g states of Pb₂ (reprinted from ref 277; copyright 1982 American Chemical Society). See Table 45 for spectroscopic labels of known states.
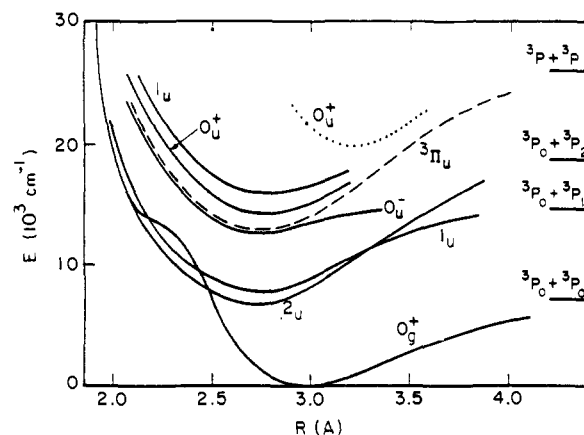

Figure 23. Potential energy curves for the u states of Pb₂ (reprinted from ref 277; copyright 1982 American Chemical Society). See Table 45 for spectroscopic labels of known states.

state (also 0_g^+), yielding a marked shoulder in the repulsive side of the curve. The other component of $^3\Sigma_g^-$, the 1_g term, is lowered less by the SO effect and has a normal curve shape. Likewise the 2_g curve ($^1\Delta_g$ in type a) is quite normal. The $^1\Sigma_g^+$ state (without SO) has a second minimum at longer distances; in this region it is primarily $\sigma_g^2\pi_u^2$ rather than π_u^4.

The $^3\Pi_u$ state splits into 2_u, 1_u, 0_u^-, and 0_u^+ components in increasing energy near their minima. But the 2_u term dissociates to higher energy atoms than 1_u and thus the curves cross near 3.3 Å. The energy differences in these u terms can be understood best by considering first the π_u^3 component, which yields a lower $^2\Pi_{3/2}$ term if a high-energy $\pi_{3/2}$ spinor is vacant. If a lower energy $\pi_{1/2}$ spinor is vacant, a higher energy $^2\Pi_{1/2}$ term results. Then when the spin of the σ_g electron is coupled to the π_u^3 group, there is a smaller splitting of $^2\Pi_{3/2}$ to 2_u and 1_u, with 2_u lowest, in agreement with Hund's third rule. From the $^2\Pi_{1/2}$ term for π_u^3 there arises the 0_u^- and 0_u^+ terms and the second 1_u term, which is $^1\Pi_u$ in type a coupling.

The spin–orbit effect induces large changes in dissociation energies. The ground 0_g^+ state is only about half as strongly bound as the $^3\Sigma_g^-$ state without SO. Among the states arising from $^3\Pi_u$ on introduction of the SO term, the dissociation energy of 2_u is almost unchanged whereas that for 0_u^- is considerably reduced. Some of these differences are due to different dissociation limits.

The strongest absorption (near $19\,800$ cm^{-1}) is from $X(0_g^+)$ to the second 0_u^+ or F state denoted by $F \leftarrow X$.[275] An energy curve for this state was added by Pitzer and Balasubramanian[277] to Figure 23 at the experimental energy. Since this state arises primarily from the configuration $\sigma_g^2 \pi_u \pi_g$, it is expected to have a larger R_e than that for $\sigma_g^2 \pi_u^2$; this was found to be in agreement with the red shading of the experimental bands. The transition probability from 0_g^+ to the lower 0_u^+ state was found to be experimentally much smaller, in agreement with the nature of these states. Theoretical spectroscopic properties obtained by Pitzer and Balasubramanian for this state agreed reasonably well with those measured, in particular the large anharmonicity and low dissociation energy. Also the theoretical R_e value for the lowest 0_u^+ is smaller than that for 0_g^+, in agreement with the blue shading of the observed bands.[87,197]

Bondybey and English[87,197] interpreted a set of emission bands for Pb$_2$ in an inert matrix as arising by internal conversion from the F state to the long-lived B state at $12\,457$ cm^{-1}. Although this state is not connected to the ground state by a dipole-allowed transition, it was found to radiate slowly as a result of matrix distortion or higher order effects. Bondybey and English[197] suggested the 2_u state, but its energy is much too low as seen from Table 45. However, theoretical calculations of Pitzer and Balasubramanian[277] indicated this to be the 0_u^- state.

Matrix spectra exhibited emission bands near $13\,400$ cm^{-1} connecting two new states. Since the upper D state arises by internal conversion from the F state, the lower or A state cannot be more than 6540 cm^{-1} above the ground state. Pitzer and Balasubramanian argued that the most probable assignment for the A state is 1_g. The theoretical T_e of the 1_g state was found to be 4150 cm^{-1}. The 2_u state cannot be completely eliminated from consideration since the Pitzer–Balasubramanian[217] theoretical energy of 6670 cm^{-1} might be in error by several hundred cm^{-1}. The theoretical ω_e of the 1_g term was found to agree quite well with the experimental value. The D state at an energy of $17\,500$ cm^{-1} (or $19\,800$ cm^{-1} if the A state is 2_u) could not be calculated with reliable accuracy.[277]

The theoretical D_e for the 0_g^+ ground state of Pb$_2$ of 0.88 eV[277] was almost in exact agreement with an experimental value of 0.86 ± 0.01 eV obtained by Gingerich et al.[276] Although this agreement was considered fortuitous by Pitzer and Balasubramanian,[277] the agreement of such magnitude on a very heavy dimer such as Pb$_2$, for which both spin–orbit effects and relativistic effects are large, must be considered impressive.

Sontag and Weber[278] obtained the R_e value of the ground state of Pb$_2$ from experimental spectra after the publication of the theoretical calculations on Pb$_2$ by Pitzer and Balasubramanian.[277] The experimental R_e of 2.930 Å agrees very well with the earlier theoretical value of 2.97 Å.[277] In general, R_e values obtained by RECP/RCI calculations tend to be a bit longer, and thus this agreement should be considered excellent.

The blue-green system that Bondybey and English[87] called the $F \leftarrow X$ system was studied further by Berg et al.[279] in laser-induced fluorescence. From these spectra the spectroscopic constants of the X and F (Berg et al.[279] call the F state B) states were obtained by these authors.[279] The constants thus obtained were

close to the values obtained by Bondybev and English.

Pitzer[203] corrected the D_0^0 value of Pb$_2$ obtained from mass spectrometric measurements. This correction was obtained by recalculating the partition function of Pb$_2$. The corrected D_0^0 value of Pb$_2$ was found to be in excellent agreement with the direct theoretical D_e value.

Pacchioni[202] completed calculations on the low-lying states of Sn$_2$ and Pb$_2$ after the appearance of the paper by Pitzer and Balasubramanian.[277] Pacchioni[202] used the Hafner–Schwarz model potentials[63] compared to the ab initio RECPs derived from DHF calculations which were used by Balasubramanian and Pitzer.[277] Pacchioni ignored spin–orbit effects in his computation of the potential energy curves (PEC) of Pb$_2$ and Sn$_2$. As demonstrated by the calculations of Pitzer and Balasubramanian,[277] the PEC obtained for Pb$_2$ without spin–orbit effects have little resemblence to the actual PEC which included spin–orbit effects. Consequently, Pacchioni obtained a D_e approximately twice the experimental value, which he subsequently corrected using a semiempirical procedure to arrive at a D_e close to the value obtained by Balasubramanian and Pitzer.[277] For dimers of the sixth-row atoms, spin–orbit effects are so large that calculations without inclusion of spin–orbit terms have very little to do with the real molecule.

Figure 24 shows the weights of various λ–s configurations in the Ω states of Pb$_2$. As seen from this figure, for Pb$_2$ the λ–s populations change dramatically as a function of internuclear distances. At short distances, there is an avoided crossing of $\pi_u^4(^1\Sigma_g^+)$ with $\sigma_g^2\pi_g^2(^3\Sigma_g^-)$. This results in the shoulder of the $X(0_g^+)$ curve of Pb$_2$. At long distances many configurations contribute, leading to dissociation into $^3P_0 + {}^3P_0$ atoms instead of $^3P + {}^3P$.

M. Bi$_2$

There are many experimental spectroscopic investigations[280–291] on Bi$_2$ and Bi$_4$ clusters. In fact, for sometime a band that was actually due to Bi$_4$ was incorrectly attributed to Bi$_2$. This interpretation led to another new ground state for Bi$_2$. This confusion has now been resolved, and since then the ground state of Bi$_2$ has been unambiguously established as a 0_g^+ state.

Christiansen[292] carried out generalized valence bond calculations followed by RCI calculations. A double-ζ STO basis set was employed in the GVB calculations. Figure 25 gives the potential energy curves of Bi$_2$ under various approximations. The spectroscopic constants of two well-characterized states of Bi$_2$ are shown in Table 46. Among the curves in Figure 25, the curve labeled FV7R (limited full valence + seven reference singles + doubles CI) is the best at this level of approximation. These calculations yielded $R_e = 2.79$ Å, $\omega_e = 170$ cm^{-1}, $\omega_e x_e = 0.3$ cm^{-1}, and $D_e = 2.3$ eV.[292] The corresponding experimental values for the $X(0_g^+)$ state are $R_e = 2.66$ Å, $\omega_e = 173$ cm^{-1}, $\omega_e x_e = 0.34$ cm^{-1}, and $D_e = 2.04$ eV.[37] The theoretical R_e is expected to be a bit longer at this level of approximation, and thus the 0.13 Å longer bond length for Bi$_2$ is not surprising. However, as seen in section III.H, for Sb$_2$ a more sophisticated and accurate CASSCF/MRSDCI/RCI calculation yielded $R_e = 2.59$ Å compared to an experimental value for the $X(0_g^+)$ ground state of 2.48 ± 0.02 Å. Consequently, even calculations that included
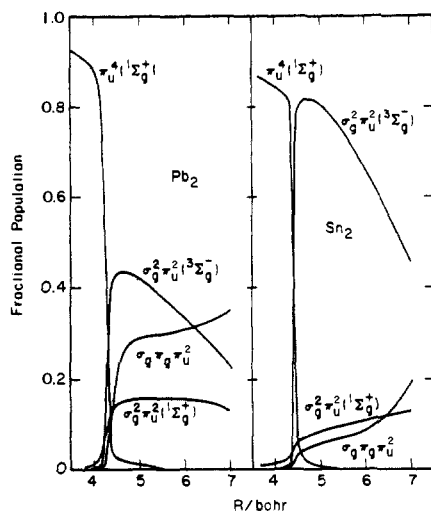
Figure 24. Fractional Λ–S populations with low-lying states of Pb_2 and Sn_2 (reprinted from ref 201; copyright 1983 American Institute of Physics).
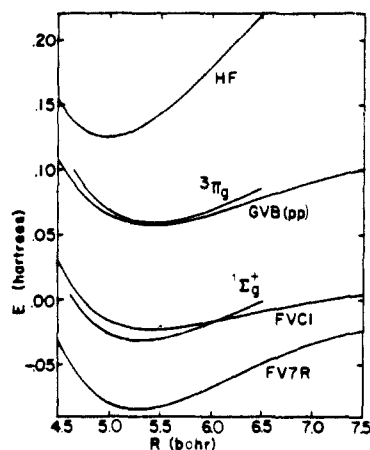

Figure 25. Potential energy curves for the ground state of Bi_2 using various methods (reprinted from ref 292; copyright 1984 Elsevier Science Publishers B.V.).

TABLE 46. Experimental Spectroscopic Constants for Bi_2[a]

State	R_e (Å)	T_e (cm^{-1})	ω_e (cm^{-1})
$X0_g^+$	2.66 (2.79)	0	173 (170)
B $^3\Sigma_u^- 0_u^+$	2.863	17 739	132.4

[a] Experimental $D_e(Bi_2)$ = 2.04 eV compared to a GVB/RCI value of 2.3 eV.[292] The state labeled B' was also called A by Ehret and Gerber.[281] These authors obtained the transition moment of the A–X system as 1.4 ± 0.4 D. The lifetimes of the vibrational levels ($v' = 1$–34) ranged between 50 and 600 ns. Theoretical values are in parentheses and are from ref 292.

effects and to a smaller extent due to the inert-pair effect.

CASSCF/FOCI/RCI calculations on both the ground state and excited states of Bi_2 are being made in the present author's group. Such calculations should especially be of use in comprehending the electronic spectra of Bi_2 and the nature of the excited electronic states of Bi_2.

IV. Spectroscopic Properties and Potential Energy Curves of Heteronuclear Dimers

A. GaAs and GaAs⁺

GaAs semiconductors are of immense technological value since they are useful in constructing fast devices among other applications. As a result, a number of investigators have studied the properties of GaAs surfaces.[293-300] Smalley and co-workers[97] have generated supersonic beams of semiconductor clusters of formula Ga_xAs_y by laser vaporization of pure GaAs. Cluster beams were characterized by laser spectrometry. Mass analysis of the large clusters revealed a binomial distribution while the abundance of smaller clusters deviated considerably from the binomial distribution. In particular, the diatomic clusters were found to be mostly GaAs and As_2 with very little Ga_2. Further, photoionization with an ArF excimer laser revealed even–odd alternation in the photoionization cross sections.

Balasubramanian[301] made complete active space MCSCF calculations followed by first-order CI calculations of potential energy curves and spectroscopic properties of the low-lying electronic states of GaAs and GaAs⁺. He considered 12 electronic states of GaAs and 4 electronic states of GaAs⁺. Valence Gaussian (3s3p1d) basis sets for Ga and As atoms in conjunction with RECPs that retained the outer $4s^24p^1$ and $4s^24p^3$ shells of Ga and As, respectively, were used in these calculations. After these calculations were published, M. Morse and co-workers at Utah completed their experimental spectroscopic study on GaAs. The bond lengths calculated by Balasubramanian were longer than the experimental values of Morse. This motivated Balasubramanian to reinvestigate GaAs. An error was found in one of the ECP parameters, which was subsequently corrected. The corrected spectroscopic constants for GaAs were, however, found to be in good agreement with both experiment and all-electron calculations.

Following the theoretical calculations of Balasubramanian,[301] Knight and Petty[302] observed the ESR spectrum of GaAs⁺ by laser-evaporated GaAs followed

electron correlation effects to a much higher order yielded slightly longer bond lengths within the RECP approximation.

The theoretical RCI D_e value of Bi_2 (2.3 eV) obtained by Christiansen[292] was surprisingly larger than the corresponding experimental value of 2.04 eV. This primarily appears to be due to size inconsistency in the treatment of spin–orbit coupling in small-scale RCI calculations. Analogous to Pb_2, the D_e of Bi_2 should be much larger when the spin–orbit coupling is omitted. For Pb_2, note that the D_e without spin–orbit coupling is twice the true value (see section III.L). Spin–orbit coupling thus stabilizes the atoms more than the molecule destabilizing the bond. Consequently, the higher D_e obtained by Christiansen[292] should be attributed to size inconsistency at long distance in the treatment of the spin–orbit term.

The spin–orbit contamination of the $^1\Sigma_g^+(0_g^+)$ state with the $^3\Pi_g(0_g^+)$ state is of interest since this contamination destabilizes the bond. The $X(0_g^+)$ state of Bi_2 was found to have 25% $^3\Pi_g$ character. Since the $^3\Pi_g$ state arises from occupying the antibonding π_g orbital, this would lead to a bond order lower than 3.0 for Bi_2. Christiansen[292] approximately calculated the bond order from predominant configurations as 2.17. Evidently, the bonding is much weaker both due to spin–orbit

by photoionization. The experimental spectrum confirmed the $^4\Sigma^-$ ground state for GaAs$^+$ predicted by Balasubramanian.

Lemire et al.[303] have recently studied the optical spectra of jet-cooled GaAs generated by laser vaporization of a GaAs crystal. These authors observed bands in the 23000–24000-cm^{-1} region. All the bands except the $^3\Pi(0^+)$–$X^3\Sigma^-(0^+)$ bands were found to be predissociated above the $v = 1$ level. Basically, the results of these calculations confirmed Balasubramanian's prediction[301] of a $^3\Sigma^-$ ground state for GaAs.

The possible low-lying electronic states of GaAs and GaAs$^+$ are shown in Tables 47 and 48, respectively. Three possible candidates for the ground state of GaAs are $^3\Sigma^-$, $^3\Pi$, and $^1\Sigma^+$, while the corresponding candidates for the ground state of GaAs$^+$ are $^4\Sigma^-$ and $^2\Pi$. The CASSCF/FOCI calculations of Balasubramanian[301] included up to 592 configurations at the CASSCF level and 26 200 configurations at the FOCI level.

Tables 49, 49A, and 50 show the spectroscopic properties of GaAs and GaAs$^+$, respectively. The theoretical potential energy curves of some of the electronic states of GaAs and GaAs$^+$ are shown in Figures 26 and 27, respectively. The ground states of GaAs and GaAs$^+$ are $^3\Sigma^-$ and $^4\Sigma^-$, respectively. As seen from Table 49, there are six bound states for GaAs below 18000 cm^{-1}. None of these states except the X ground state and $^3\Pi(III)$ state appear to have been characterized experimentally. Some of the allowed electric dipole transitions among the states in Table 49 are $^3\Pi \leftrightarrow {}^3\Sigma^-$, $^1\Sigma^+(II) \leftrightarrow {}^1\Sigma^+$, and $^1\Sigma^+ \leftrightarrow {}^1\Pi$. These transitions are observable in the neighborhood of 1500–1600, 8200, and 1315 cm^{-1}, respectively.

Table 51 shows the vertical and adiabatic transition energies of several allowed electric dipole transitions. As seen from that table and Figure 26, the $^3\Sigma^-(II)$ and $^3\Sigma^-(III)$ states are not bound electronic states. Thus, transitions from the ground state to those excited electronic states could be observed only as broad absorption bands. These transitions occur (Table 51) in the region of 20000–30000 and 35000 cm^{-1}, respectively. Hence Balasubramanian[301] predicted two broad absorption bands in this region.

The $^4\Sigma^-(II) \leftrightarrow {}^4\Sigma^-$ transition of GaAs$^+$ was predicted to lie in the region of 40000–42000 cm^{-1}. The $^2\Pi(II) \leftrightarrow {}^2\Pi$ transition was predicted to be observable in the 9186-cm^{-1} region. The vertical ionization energy of GaAs was calculated as 6.85 eV. The ionization potential of the As atom was calculated from asymptotic splittings as 9.76 eV. The corresponding experimental value[134] is 9.81 eV. Consequently, the agreement is good.

The theoretical FOCI dissociation energy of GaAs is 1.25 eV. The GaAs$^+$ ion is much less stable compared to neutral GaAs, since its D_e was found to be only 0.36 eV. The theoretical dissociation energies of Ga$_2$ and As$_2$ were found to be 1.2 and 2.71 eV, respectively (see sections III.A,C). The calculated D_es of these species were found to be consistent with the observation of O'Brien et al.[97] that the diatomic species detected upon laser vaporization of the GaAs crystal were mostly As$_2$ and GaAs with very little Ga$_2$. The CASSCF/FOCI calculations in general yield a D_e in the range of 75–85% of the experimental values. Thus, the D_e of GaAs should be higher than the theoretical value.

After publication of Balasubramanian's theoretical

TABLE 47. A Few Low-Lying Molecular States of GaAs Arising from Atomic States of Ga and As

Molecular states	Atomic states	Energy of the separated atoms[a] (cm^{-1})
	Ga + As	
$^3\Sigma^-$, $^3\Pi$, $^5\Sigma^-$, $^5\Pi$	$^2P + {}^4S$	0
$^1\Sigma^+$, $^1\Sigma^-(2)$, $^1\Pi(3)$, $^1\Delta(2)$, $^1\Phi$	$^2P + {}^2D$	10 790
$^3\Sigma^+$, $^3\Sigma^-(2)$, $^3\Pi(3)$, $^3\Delta(2)$, $^3\Phi$		
$^1\Sigma^+(2)$, $^1\Sigma^-$, $^1\Pi(2)$, $^1\Delta$, $^3\Sigma^+(2)$, $^3\Sigma^-$, $^3\Pi(2)$, $^3\Delta$	$^2P + {}^2P$	18 530

[a] From ref 134.

TABLE 48. A Few Low-Lying States of GaAs$^+$ and Their Dissociation Limits

Molecular states	Atomic states	Energy of the separated atoms[a] (cm^{-1})
$^4\Sigma^-$	Ga$^+(^1S)$ + As(^4S)	0.0
$^2\Delta$, $^2\Pi$, $^2\Sigma^-$	Ga$^+(^1S)$ + As(^2D)	10 790
$^2\Pi$, $^2\Sigma^+$	Ga$^+(^1S)$ + As(^2P)	18 530
$^2\Sigma^+$, $^2\Sigma^-(2)$, $^2\Pi(2)$, $^2\Delta$,	Ga(^2P) + As$^+(^3P)$	[30 729]
$^4\Sigma^+$, $^4\Sigma^-(2)$, $^4\Pi(2)$, $^4\Delta$		
$^4\Sigma^-$, $^4\Pi$	Ga$^+(^1S)$ + As(^4P)	52 100

[a] From ref 134.

calculations,[301] there were two experimental studies on GaAs and GaAs$^+$ as mentioned before. Knight and Petty[302] recorded the ESR spectra of GaAs$^+$ generated by laser evaporation of a GaAs crystal followed by photoionization. The ESR spectra revealed a quartet structure, confirming Balasubramanian's prediction of a $^4\Sigma^-$ ground state of GaAs$^+$.

Lemire et al.[303] studied the rotationally resolved electronic spectra of jet-cooled GaAs diatomic. These authors obtained a $^3\Sigma^-$ ground state for GaAs, confirming Balasubramanian's[301] prediction of a $^3\Sigma^-$ ground state. The experimental spectroscopic constants obtained from the analyses of the observed bands by Lemire et al.[303] are shown in Table 49A together with Balasubramanian's theoretical constants.[301] As seen from Table 49A, theoretical constants obtained by Balasubramanian are in very good agreement with experimental values.

The ground state of GaAs ($^3\Sigma^-$) was found to be predominantly (89%) $1\sigma^2 2\sigma^2 3\sigma^2 1\pi^2 (^3\Sigma^-)$ at its equilib-

TABLE 49. FOCI Spectroscopic Constants for GaAs[a]

State	R_e (Å)	T_e (cm^{-1})	ω_e (cm^{-1})	D_e (eV)
$X^3\Sigma^-$	2.645	0	197	1.24
$^3\Pi$	2.370	996	241	1.12
$^1\Pi$	2.336	5 943	280	
$^1\Sigma^-$	2.237	7 192	291	
$^1\Delta$	2.582	8 232	213	
$^1\Sigma^+(II)$	2.475	15 930	-	
$^3\Pi(II)$	3.053	19 900	142	
$^3\Sigma^+$	2.421	22 503	210	
$^3\Pi(III)$	2.687	22 564	187	
$^1\Pi(II)$	2.693	24 679	148	
$^3\Sigma^+(II)$	2.421	31 106	201	
$^5\Pi(II)$	2.818	40 352	168	
$^5\Delta$	2.449	45 431	237	
$^5\Pi(III)$	2.794	51 174	187	

[a] All constants are from ref 301 and 404.

TABLE 49A. SOCI Spectroscopic Constants and Known Experimental Constants for GaAs[a]

State	R_e (Å) Theory	R_e (Å) Expt.	T_e (cm^{-1}) Theory	T_e (cm^{-1}) Expt.	ω_e (cm^{-1}) Theory	ω_e (cm^{-1}) Expt.
$X^3\Sigma^-$	2.60[b]	2.516	0	0	215	214
$^3\Pi$	2.38		1830		236	
$^1\Sigma^+$	2.23		7768		279	
$^1\Delta$	2.58		7874		214	
$^1\Sigma^+(II)$	2.47		14383		321	
$^3\Pi(II)$	3.10		18590		133	
$^3\Pi(III)$	2.68	2.66	24600	23800	160	152

[a] Experimental values are from ref 303; theoretical values are from ref 404. [b] An R_e value of $\sim$2.55 Å is estimated if d correlation effects are included.

rium geometry. The $^3\Sigma^-$ state arising from $1\sigma^2 2\sigma^2 1\pi^2 2\pi^2$ makes a small contribution (2.4%). At long distances the contributions from $1\sigma^2 2\sigma^2 3\sigma^2 2\pi^2$ as well as $1\sigma^2 2\sigma^2 3\sigma 4\sigma 1\pi^2$ increase.

The $^1\Sigma^+$ state of GaAs exhibited an avoided crossing reminiscent of the corresponding state of the isoelectronic Ge$_2$. This state is predominantly $1\sigma^2 2\sigma^2 1\pi^4(^1\Sigma^+)$ at short distances and near equilibrium geometries. At its equilibrium geometry, the $^1\Sigma^+$ state is 73% $1\sigma^2 2\sigma^2 1\pi^4(^1\Sigma^+)$ and 12% $1\sigma^2 2\sigma^2 3\sigma^2 1\pi^2(^1\Sigma^+)$. The $1\sigma^2 2\sigma^2 3\sigma^2 1\pi^2$ configuration dominates at longer distances. Thus, this state resembles the $^1\Sigma^+$ state of many group IV dimers such as Ge$_2$,[139] Sn$_2$,[201] and Pb$_2$.[277]

The $^3\Pi$ and $^1\Pi$ states of GaAs are predominantly $1\sigma^2 2\sigma^2 3\sigma 1\pi^3$ (87%). As seen from Figure 26, the $^3\Sigma^-(II)$ and $^3\Sigma^-(III)$ curves are repulsive. A number of configurations such as $1\sigma^2 2\sigma^2 3\sigma^2 1\pi 2\pi$, $1\sigma^2 2\sigma 3\sigma 1\pi^3 2\pi$, and $1\sigma^2 2\sigma^2 1\pi^3 2\pi$ contribute to these states. The $^1\Sigma^+(II)$ state is 52% $1\sigma^2 2\sigma^2 3\sigma^2 1\pi^2$, 16% $1\sigma^2 2\sigma^2 1\pi^4$, and 10% $1\sigma^2 2\sigma 3\sigma 1\pi^4$ at its equilibrium geometry. The $^1\Delta$ state

TABLE 50. Spectroscopic Constants for GaAs$^+$[a]

State	R_e (Å) FOCI	R_e (Å) SOCI	T_e (cm^{-1}) FOCI	T_e (cm^{-1}) SOCI	ω_e (cm^{-1}) FOCI	ω_e (cm^{-1}) SOCI
$^4\Sigma^-$	2.877	2.944	0	0	103	89
$^2\Sigma^-$	2.519		9 707		250	
$^2\Pi$	2.968		11 604		134	
$^2\Delta$	2.632	2.719	13 034	12 148	141	125
$^2\Pi(II)$	2.560		18 600		293	
$^2\Sigma^+$	2.530	2.653	20 551	18 155	177	138
$^4\Pi$	2.624		30 024		168	
$^2\Pi(III)$	2.907		33 854		100	
$^4\Sigma^-(II)$	2.566	2.592	34 070	33 279	218	210
$^4\Delta$	2.938		36 237		126	
$^4\Pi(II)$	2.346		39 982		362	
$^4\Pi(III)$	2.909		46 290		402	

[a] All constants are from ref 301 and 404.

was found to arise dominantly from the $1\sigma^2 2\sigma^2 3\sigma^2 1\pi^2$ configuration.

The $^4\Sigma^-$ ground state of GaAs$^+$ is primarily composed of the $1\sigma^2 2\sigma^2 3\sigma 1\pi^2$ (92%) configuration at its equilibrium geometry. The contribution of this configuration does not change much as a function of internuclear distance. The $^4\Sigma^-(II)$ state of GaAs$^+$ exhibits an interesting behavior as a function of internuclear distance. The contributions of various configurations to the $^4\Sigma^-(II)$ state for a few distances are shown in Table 52. As seen from Table 52, this state is predominantly $1\sigma^2 2\sigma^1 3\sigma^2 1\pi^2$ at short distances, although other configurations such as $1\sigma^2 2\sigma^2 3\sigma 1\pi 2\pi$ make a significant contribution. As the distance increases, the contribution of $1\sigma^2 2\sigma^2 3\sigma 1\pi 2\pi$ increases accompanied by a decrease in the contribution of $1\sigma^2 2\sigma^1 3\sigma^2 1\pi^2$ configuration. At distances >2.75 Å these two configurations make equal contributions, indicating an avoided crossing. At 3.00 Å, the contribution from $1\sigma^2 2\sigma^2 3\sigma 1\pi 2\pi$ (49%) dominates. The contribution from this configuration decreases as R increases further and the contribution from $1\sigma^2 2\sigma^2 4\sigma 1\pi^2$ configuration increases. At longer distances the $1\sigma^2 2\sigma^2 4\sigma 1\pi^2$ configuration dominates. The two avoided crossings in this state explain the shape of the $^4\Sigma^-(II)$ curve (Figure 27). At long distances the 1σ, 2σ, 3σ, and 4σ orbitals are dominantly As(s), Ga(s), As(p), and Ga(p), respectively, whereas the 1π orbital was found to be predominantly As(p). Thus, the $1\sigma^2 2\sigma^2 4\sigma 1\pi^2$ configuration corresponds to Ga(s^{2}p^1) and As$^+$(s^{2}p^2) or Ga(^{2}P) + As$^+$(^{3}P). This explains the domination of the $1\sigma^2 2\sigma^2 4\sigma 1\pi^2$ configuration at long distances since the $^4\Sigma^-(II)$ state dissociates into Ga(^{2}P) + As$^+$(^{3}P).

At short distances the $^2\Pi$ state was found to be primarily composed of the $1\sigma^2 2\sigma^2 1\pi^3$ configuration (82%).[301] However, at 2.50 Å, it is made up of $1\sigma^2 2\sigma^2 1\pi^3$ (54%) and $1\sigma^2 2\sigma^2 3\sigma^2 1\pi$ (32%). For R > 2.50 Å, this state was found to be a mixture of $1\sigma^2 2\sigma^2 1\pi^3$ and
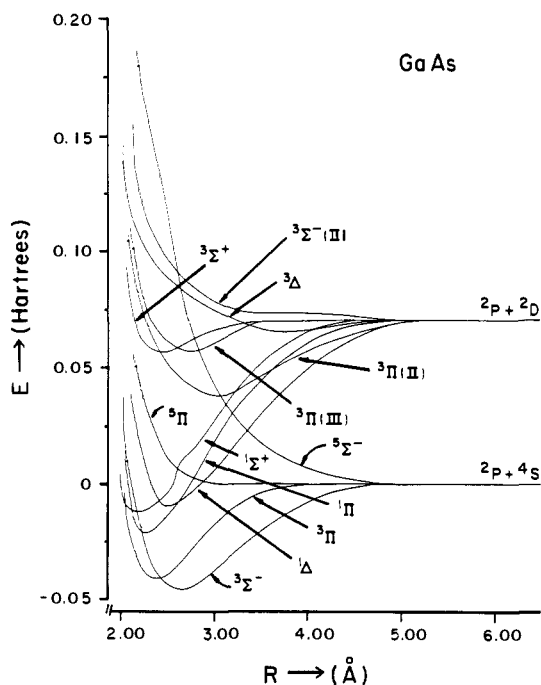
Figure 26. Potential energy curves of some low-lying states of GaAs (reprinted from ref 404; copyright 1990 Academic Press, Inc.).
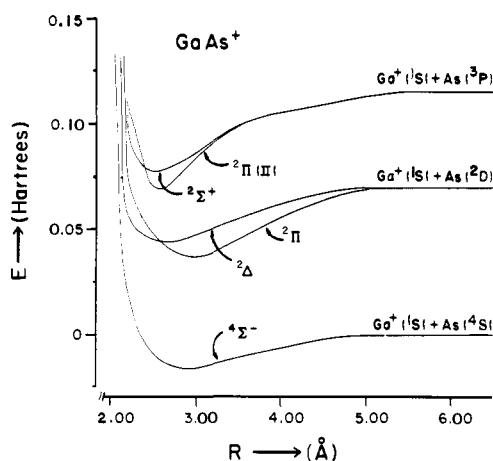

Figure 27. Potential energy curves of four electronic states of GaAs⁺ (reprinted from ref 301; copyright 1987 American Institute of Physics).

$1\sigma^2 2\sigma^2 3\sigma^2 1\pi$ configurations. The $^2\Pi(\text{II})$ state was found to be predominantly $1\sigma^2 2\sigma^2 3\sigma^2 1\pi$ (87%) at short distances. At 2.50 Å, it was found to be a mixture of $1\sigma^2 2\sigma^2 3\sigma^2 1\pi$ (57%), $1\sigma^2 2\sigma^2 1\pi^3$ (26%), and $1\sigma^2 2\sigma^2 1\pi^2 2\pi$ (4%) configurations. At 2.74 Å, the $^2\Pi(\text{II})$ state is composed of $1\sigma^2 2\sigma^2 1\pi^3$ (60%), $1\sigma^2 2\sigma^2 3\sigma^2 1\pi$ (13%), and $1\sigma^2 2\sigma^2 1\pi^2 2\pi$ (5%) configurations. Thus, in this region this state exhibited an avoided crossing. At longer distances the $1\sigma^2 2\sigma^2 1\pi^3$ configuration dominated so that this state would dissociate into $Ga^+(^1S) + As(^2P)$.

After the appearance of Balasubramanian's paper, Meier et al.[403] published an all-electron study of the electronic states of GaAs. They also found a $^3\Sigma^-$ ground state for GaAs and a very low lying $^3\Pi$ state $(T_e \sim 0.17-0.24 \text{ eV})$ above the ground state using the Hartree–Fock/MRDCI method. Most of the discrepancies between Balasubramanian's earlier results[301] and Meier et al.'s all-electron results[403] are due to an error in one of the ECP parameters mentioned before. The bond

TABLE 51. Vertical and Adiabatic Energies of the Allowed Electric Dipole Transitions of GaAs[a]

Transition	T_e	T_{vert} (cm^{-1})
$^3\Sigma^- \to {}^3\Pi$	1 830	--
$^3\Sigma^- \to {}^3\Sigma^-(\text{II})$	--	29 780
$^3\Sigma^- \to {}^3\Sigma^-(\text{III})$	--	34 548
$^3\Pi \to {}^3\Delta$	-	30 220
$^3\Pi \to {}^3\Sigma^-(\text{II})$	--	32 046
$^1\Pi \to {}^1\Sigma^+$	1 249	1 371
$^1\Pi \to {}^1\Sigma^+(\text{II})$	10 007	9 989
$^1\Sigma^+ \to {}^1\Sigma^+(\text{II})$	8 758	10 298

[a] From ref 301.

TABLE 52. Contributions of Leading Configurations to the $^4\Sigma^-(\text{II})$ State of GaAs⁺[a]

R(Å)	Contribution
2.50	$1\sigma^2 2\sigma^1 3\sigma^2 1\pi^2$ (52), $1\sigma^2 2\sigma^2 3\sigma 1\pi 2\pi$ (20), $1\sigma^2 2\sigma 3\sigma^2 1\pi 2\pi$ (6), $1\sigma^2 2\sigma^2 4\sigma 1\pi^2$ (5), $1\sigma^1 2\sigma^2 3\sigma^2 1\pi^2$ (3)
2.75	$1\sigma^2 2\sigma 3\sigma^2 1\pi^2$ (34), $1\sigma^2 2\sigma^2 3\sigma 1\pi 2\pi$ (26), $1\sigma^2 2\sigma 3\sigma^2 1\pi 2\pi$ (10), $1\sigma^2 2\sigma^2 4\sigma 1\pi^2$ (6)
3.00	$1\sigma^2 2\sigma^2 3\sigma 1\pi 2\pi$ (49), $1\sigma^2 2\sigma 3\sigma^2 1\pi^2$ (11), $1\sigma^2 2\sigma 3\sigma^2 1\pi 2\pi$ (11), $1\sigma^2 2\sigma^2 3\sigma 1\pi\pi_{Ry}$ (10)
3.50	$1\sigma^2 2\sigma^2 3\sigma 1\pi 2\pi$ (39), $1\sigma^2 2\sigma^2 4\sigma 1\pi^2$ (26), $1\sigma^2 2\sigma^2 3\sigma 1\pi\pi_{Ry}$ (10), $1\sigma^2 2\sigma^2 \sigma_{Ry} 1\pi^2$ (5)
3.75	$1\sigma^2 2\sigma^2 4\sigma^1 1\pi^2$ (56), $1\sigma^2 2\sigma^2 \sigma_{Ry} 1\pi^2$ (13), $1\sigma^2 2\sigma^2 3\sigma \ 1\pi 2\pi$ (10)
4.00	$1\sigma^2 2\sigma^2 4\sigma 1\pi^2$ (66), $1\sigma^2 2\sigma^2 \sigma_{Ry} 1\pi^2$ (16), $1\sigma^2 2\sigma 3\sigma 4\sigma 1\pi^2$ (2)

[a] Ry suffix indicates that the orbital is a Rydberg orbital from ref 301. Numbers in parentheses are contributions in percentage.

lengths in Table 49 are within 0.04–0.05 Å of the all-electron results for these states. The revised ω_es are also in much better agreement with the all-electron results. It is, however, worth noting that the $^1\Delta$ state has a larger ω_e if $^1A_1$ CASSCF orbitals are used in the calculations while the $^1A_2$ orbitals yield a more reasonable ω_e. Hence the larger ω_e for the $^1\Delta$ state obtained before[301] is due to the change of $^1A_1$ orbitals due to avoided crossing of the $1\sigma^2 2\sigma^2 1\pi^4$ and $1\sigma^2 2\sigma^2 3\sigma^2 \pi^2$ configurations in the CASSCF calculations.

Meier et al.[403] obtained $R_e = 2.60$ Å and $\omega_e = 202$ cm^{-1} for the $X^3\Sigma^-$ ground state of GaAs using the all-electron MRDCI method. Balasubramanian's calculations included electron correlations to a much higher order compared to a restricted configuration space of less than 10 000 configurations in the MRDCI. Although the FOCI method includes most of the significant electron correlations, a full SOCI method is much superior to
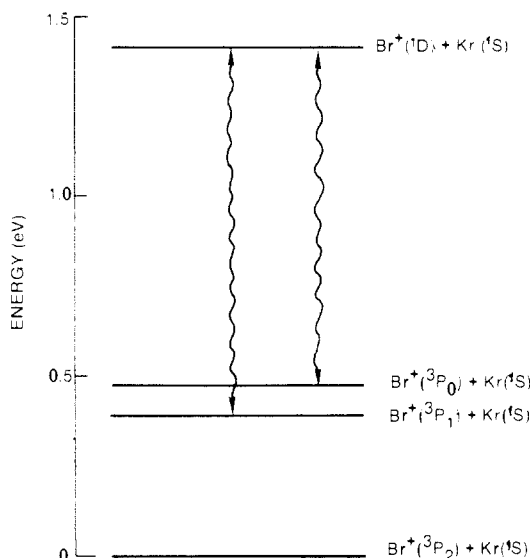
Figure 28. Energy level diagram of the Br⁺-Kr system at infinite interatomic separation. The observed transitions are indicated (reprinted from ref 326; copyright 1986 Elsevier Science Publishers B.V.).
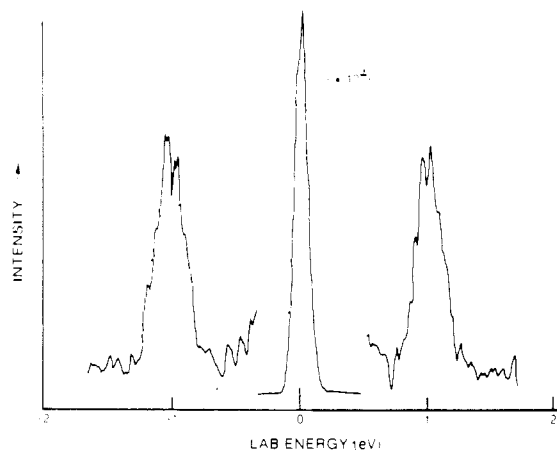

Figure 29. Energy spectrum of subelastic and superelastic collisions of Br⁺ with Kr at a relative kinetic energy of 4 eV (reprinted from ref 326; copyright 1986 Elsevier Science Publishers B.V.).

both the MRDCI and FOCI methods. Even at the FOCI level R_e = 2.645 Å and ω_e = 187 cm⁻¹ of the $^3\Sigma^-$ state are in good agreement with the all-electron MRDCI calculations. It is worth noting that although Meier et al. employ an all-electron method, they do not include relativistic effects while Balasubramanian's calculations took into account relativistic effects. Meier et al. obtained R_e = 2.38 Å and ω_e = 260 cm⁻¹ for the $^3\Pi$ state while Balasubramanian obtained R_e = 2.37 Å and ω_e = 241 cm⁻¹ at the FOCI level. Similarly, good agreement was found for the other states listed in Table 49 with the exception of the $^1\Sigma^+$(II) state, for which FOCI calculations starting from a CASSCF orbital set of $^1A_1$ symmetry yield a larger ω_e of 420 cm⁻¹. However, when SOCI calculations are made using FOCI natural orbitals, this discrepancy vanishes and thus the higher ω_e of the $^1\Sigma^+$(II) state at the FOCI level must be concluded as due to the strong variation of the composition of the CASSCF orbitals due to the avoided crossing of the $1\sigma^2 2\sigma^2 1\pi^4$ and $1\sigma^2 2\sigma^2 3\sigma^2 1\pi^2$ configurations. The D_e(GaAs) obtained at the FOCI level is 1.24 eV compared to a MRDCI value of 1.40 eV. However, SOCI calculations when corrected for d correlation effects yield a much better D_e of 1.9 eV in closer agreement with the value predicted by Lemire et al.

For GaAs⁺, the D_e obtained by Meier et al.[403] is only 0.11 eV compared to Balasubramanian's D_e of 0.36 eV obtained with the full SOCI method. Thus, the MRDCI method yields much poorer D_es compared to a full second-order CI method due to truncation of configurations in the MRDCI method. However, R_e and ω_e values obtained by the MRDCI method were found to be in good agreement with Balasubramanian's SOCI results, which he obtained in a more recent ambitious CASSCF/SOCI study[404] on GaAs, GaAs⁻, and GaAs⁺ that included up to 700 000 configurations.

Balasubramanian[305] has recently completed CASSCF/FOCI/MRSDCI calculations on many low-lying electronic states of the iso-valence-electronic diatomic InSb. Fifteen low-lying bound electronic states (T_e < 26 000 cm⁻¹) were found for InSb without spin–orbit effects. When spin–orbit coupling was in-

cluded, more electronic states resulted. Analogous to the diatomic GaAs, the ground state of InSb dimer was found to be a $^3\Sigma^-$ state. The $^3\Pi$ state of InSb was considerably higher ($T_e \sim$ 2300 cm⁻¹). The R_e and ω_e values of the $X^3\Sigma^-_{0^+}$ ground state of InSb were found to be 3.0 Å and 121 cm⁻¹, respectively. The adiabatic IP and electron affinity of InSb were calculated as 6.33 and 1.41 eV compared to 6.85 and 1.3 eV for GaAs.

B. KrBr⁺ and Energy Transfer in Br⁺-Kr Collisions

The interest in rare gas–halogen neutral and ionic compounds arises partly because these are potential candidates for chemical lasers.[306-331] The generation and deexcitation of neutral RgX species have also been extensively studied. Rare-gas oxides have also been the topics of many investigations since they are potential candidates for optical pumping reactions.

In the collision of halogen positive ions with rare-gas atoms there is an efficient transfer of electronic energy to translational energy and vice versa.[325-330] An energy level diagram of the Kr–Br⁺ system at infinite interatomic separation is shown in Figure 28. Since the excitation experiments by Koski and co-workers[329] were carried out at relative energies of <5 eV,[326] no states other than the ones shown in Figure 28 were found to be energetically accessible. The experiments on KrBr⁺ made by Koski and co-workers[329] dealt mainly with the excitation and deexcitation as represented by the process

$$Br^+(^3P) + Kr(^1S) \rightleftharpoons Br^+(^1D) + Kr(^1S)$$
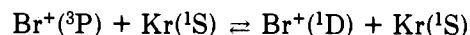
and the observed transitions are indicated in Figure 28. Whereas Br⁺($^3P_0$) transitions have been observed, this is not so for Br⁺($^1D_2$).

The energy transfers in the Kr + Br⁺ collisions seem to be governed by a Landau–Zener process, which suggests that efficient energy transfers are observed at the intersections of the potential energy curves of the intermediate complex, which in this case is KrBr⁺.

Balasubramanian et al.[326] carried out SCF/RCI calculations on nine low-lying Ω states of KrBr⁺ including spin–orbit effects. Some λ–s electronic states without spin–orbit effects were also studied by the same method. A valence double-ζ + d polarization STO basis

TABLE 53. Dissociation Limits of a Few Low-Lying ω–ω States

Molecular states	Dissociation limit	Energy of the separated atoms (cm^{-1})	
		Expt.[a]	Theory[b]
	Kr + Br$^+$		
$2,1,0^+(I)$	$^1S_0 + {}^3P_2$	0.0	0
$1(II),0^-$	$^1S_0 + {}^3P_1$	3139	3182
$0^+(II)$	$^1S_0 + {}^3P_0$	3840	4675
$2(II),1(III),0^+(III)$	$^1S_0 + {}^1D_2$	11409	14639
	Kr$^+$ + Br		
$3,2(III),2,(IV),1(IV)$ $1(V),1(VI),0^-(II),$ $0^-(III),0^+(IV),0^+(V)$	$^2P_{3/2} + {}^2P_{3/2}$	17389	
$2(V),1(VII),1(VIII),$ $0^-(IV),\ 0^+(VI)$	$^2S_{3/2} + {}^2P_{1/2}$	21074	
$2(VI),1(IX),1(X),0^-(V),$ $0^+(VII)$	$^2P_{1/2} + {}^2P_{3/2}$	22760	
$1(XI),0^+(VIII),0^-(VI)$	$^2P_{1/2} + {}^2P_{1/2}$	27075	
	Kr + Br$^+$		
$0^+(IX)$	$^1S_0 + {}^1S_0$	27867	

[a] From ref 134. [b] From ref 326.

set was employed together with RECPs for Kr and Br atoms. These authors[326] also carried out experimental investigations of energy transfers in Kr–Br$^+$ collisions. Related ArCl$^+$ species have also been investigated recently.[328]

Experimental studies were carried out by colliding Br$^+$ and Kr using a tandem mass spectrometer.[324] It consists of an ion source, an electrostatic analyzer, and a quadrupole mass filter as an input section. The ions were prepared by electron bombardment of CH$_3$Br. The beam composition so produced was found to have approximately equal amounts of Br$^+$(^{3}P) and Br$^+$(^{1}D) as determined by attenuation measurements. The Br$^+$ beam from this section was passed through a shallow reaction chamber containing the Kr target gas. The ions scattered at 0° to the beam direction were then detected with a second quadrupole mass spectrometer followed by an electrostatic analyzer and an electron multiplier.

The Br$^+$ experimental spectrum obtained in ref 326 is shown in Figure 29. The central peak was interpreted as due to the unperturbed primary ion beam. Two unresolved doublets appear on each side of the primary beam and are separated from it by an energy of $\sim$1 eV. Balasubramanian et al.[326] interpreted these peaks as arising from the transitions Br$^+$(^{3}P$_{0,1}$) $\rightleftarrows$ Br$^+$(^{1}D$_2$). The "subelastic" peak on the right of the spectrum corresponds to the Br$^+$(^{1}D$_2$) $\rightarrow$ Br$^+$(^{3}P$_{0,1}$) transition while the "superelastic" satellite on the left is due to the transition Br$^+$(^{3}P$_{0,1}$) $\rightarrow$ Br$^+$(^{1}D$_2$). The peaks due to the transitions Br$^+$(^{3}P$_2$) $\rightleftarrows$ Br$^+$(^{1}D$_2$) were
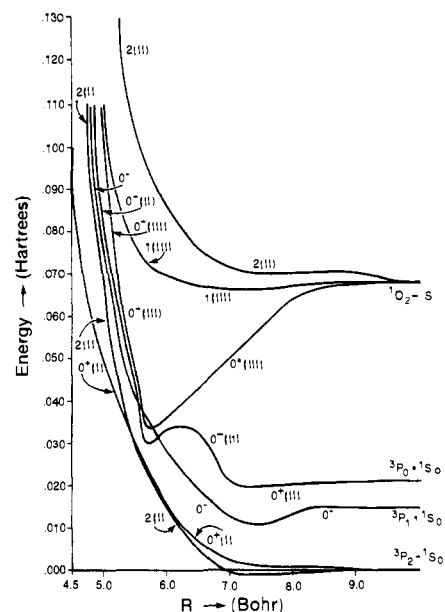

Figure 30. Potential energy curves of the low-lying states of KrBr$^+$ in the presence of spin–orbit interaction (reprinted from ref 326; copyright 1986 Elsevier Science Publishers B.V.). The potential energies of the 1(I) and 1(II) states are shown in Table 54.
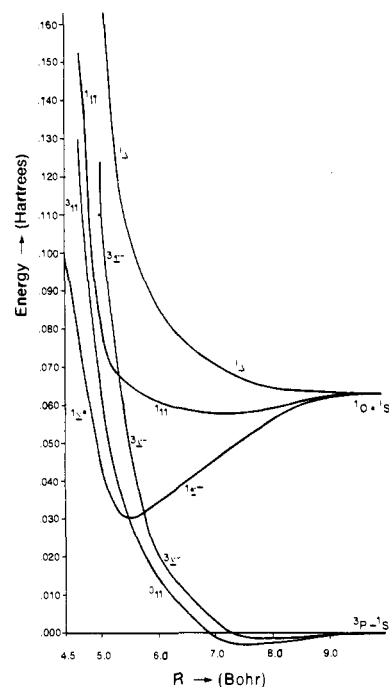

Figure 31. Potential energy curves of KrBr$^+$ in the absence of spin–orbit interaction (reprinted from ref 326; copyright 1986 Elsevier Science Publishers B.V.).

absent (see Figure 29). The peaks due to these transitions should have appeared at about 1.4 eV on each side of the peak due to the projectile ions. However, all attempts to observe these peaks failed.[326]

Table 53 shows the molecular states arising from the low-lying states of Kr and Br$^+$. Balasubramanian et al.[326] investigated all low-lying states dissociating below 11 500 cm^{-1}.

Figures 30 and 31 show the SCF/RCI potential energy curves of seven of the low-lying ω–ω and λ–s states of KrBr$^+$, respectively. Table 54 shows the energies of nine low-lying ω–ω states (arising from the $^3\Pi$, $^3\Sigma^-$, $^1\Sigma^+$, $^1\Pi$, and $^1\Delta$ λ–s states) of KrBr$^+$. As seen from Figure

TABLE 54. Potential Energy Curves of KrBr+ [a]

R	2(I)	1(I)	0+(I)	I(II)	0-	0+(II)	0+(III)	1(III)	2(II)
4.5	-0.1599	0.1639	0.1044	0.1987	0.1705	0.1720	0.2016	0.1999	0.3186
5.0	0.0634	0.0073	0.0492	0.0990	0.0801	0.0814	0.1110	0.1090	0.1899
5.25	0.0431	0.0478	0.0395	0.0725	0.0556	0.0585	0.0677	0.1038	0.1285
5.5	0.0289	0.0334	0.0289	0.0502	0.0419	0.0454	0.0468	0.0771	0.1036
5.75	0.0213	0.0242	0.0227	0.0344	0.0350	0.0301	0.0341	0.0713	0.0963
6.0	0.0169	0.0146	0.0163	0.0224	0.0287	0.0331	0.0381	0.0696	0.0846
7.0	-0.0010	-0.0001	0.0021	0.0119	0.0129	0.0205	0.0497	0.0662	0.0711
9.0	-0.0008	-0.0007	0.0015	0.0135	0.0137	0.0206	0.0635	0.0671	0.0690
11.0	0.0	0.0	0.0	0.0145	0.0145	0.0213	0.0677	0.0667	0.0667

[a] From ref 326. Energies in hartrees.

30, KrBr+ has a few low-lying bound states but the ground state (2(I)) is mostly repulsive.

In the Landau–Zener model the energy transfer between several states induced by collision takes place at the points where the potential energy curves of the appropriate electronic states of the rare gas–halogen ion complex cross. As seen from Table 53, the 2, 1, and 0+(I) states of KrBr+ correspond to $Kr(^1S_0) + Br^+(^3P_2)$ atoms. Similarly, the 1(II) and 0- states correlate to $Kr(^1S_0) + Br^+(^3P_1)$, and 2(II), 1(III), and 0+(III) correspond to $Kr(^1S_0) + Br^+(^1D_2)$ atoms. In the Landau–Zener model, for example, the transition between $Br^+(^1D_2)$ and $Br^+(^3P_1)$ is allowed if one of the curves that dissociate into $Kr(^1S_0) + Br^+(^1D_2)$, namely, 2(II), 1(III), or 0+(III), crosses with one of the curves that dissociate into $Kr(^1S_0) + Br^+(^3P_1)$ (1(II), 0-(I)). There are two restrictions imposed by symmetry: (i) two curves of the same (ω–ω) symmetry cannot cross; (ii) the selection rule for predissociation should be applicable. The selection rule for predissociation is $\Delta\Omega = 0, \pm 1, + \leftarrow/\rightarrow -$. Thus, for example, if the 0+(III) curve crosses with 1(II), then the transition $^1D_2 \leftrightarrow {}^3P_1$ of Br+ is allowed. From Table 54, it can be seen that the 0+(III) and 1(II) curves cross at 5.75 bohr, which explained the experimental observation of the $^1D_2 \rightarrow {}^3P_1$ transition.

The 0+(II) curve does not cross with the 0+(III), 1(III), or 2(II) curves; however, it crosses with the 1(II) curve (between 5.75 and 6.0 bohr). Since the 1(II) curve is a channel for the $^1D_2 \rightarrow {}^3P_1$ transition, a complex formed by $Br^+(^1D_2)$ which goes through this channel could meet the bound 0+(II) state. Consequently, through this process Br+ ion which starts as $^1D_2$ could be converted into the 0+(II) state of KrBr+ and subsequently dissociate into $Kr(^1S_0) + Br^+(^3P_0)$ atoms. Consequently, the transition $^1D_2 \rightarrow {}^3P_0$ becomes allowed and was observed experimentally.[326]

The curves that dissociate into the ground-state atoms (2, 0+, 1) do not intersect with the curves that dissociate into $Kr(^1S_0) + Br^+(^1D_2)$. Moreover, the 2, 0+, and 1 curves do not cross with the curves dissociating into $Kr(^1S_0) + Br^+(^3P_0)$ or $Kr(^1S_0) + Br^+(^3P_1)$. Hence there are no channels for $^1D_2(Br^+)$ to go into $^3P_2(Br^+)$. All experimental attempts to observe this transition

failed. Theoretical calculations offered an explanation for this failure.

Among the 0+ states calculated by Balasubramanian et al.,[326] the 0+(II) and 0+(III) states are bound (see Figure 30). The 0+(II) state could be converted into 0+(III) by the 1(II) channel, which crosses with both these states. The experimentally measured dissociation energy of KrBr+ is 1.5 eV.[320] The theoretical separation between the 0+(III) state and its dissociation limit was found to be 0.91 eV, while the separation of the 0+(II) state with respect to $Kr(^1S_0) + Br^+(^1D_2)$ atoms was found to be 1.05 eV.[326] Since KrBr+ in the 0+(II) state could go to the 0+(III) state through the 1(II) channel, this possibility was not ruled out. This would mean a dissociation energy of 1.05 eV. The theoretical dissociation energy should not be regarded as very accurate since only a small number of configurations were included in the CI calculations. Theoretical calculations of these levels on similar systems yielded only 70% of the experimental D_e values. Consequently, the experimental value of 1.5 eV was regarded as more accurate.[326]

The theoretical vibrational frequencies of the 0+(II) and 0+(III) states were found to be 526 and 446 cm⁻¹, respectively. Their R_e values are 3.1 and 3.09 Å, respectively.

The nature of the electronic states of KrBr+ as a function of the internuclear distance is quite interesting. At 5.5 bohr the σ orbital is a slightly bonding MO to which the Br $4p_z$ orbital makes the predominant contribution. The σ^* orbital was found to be predominantly on Kr but was found to be slightly antibonding. The π orbital was found to be a nonbonding Kr 4p orbital, while the π^* orbital was found to be predominantly the Br 4p orbital and also nonbonding.

At short distances the 0+(I) state was found to be predominantly $^1\Sigma^+_{0^+}$. At 5.5 bohr the 0+(I) state was found to be composed of 13% ($\sigma^2\pi^{*4}$, $^1\Sigma^+$), 26% ($\sigma\sigma^*\pi^{*4}$, $^1\Sigma^+_{0^+}$), 34% ($\sigma^2\sigma\pi^{*3}$, $^3\Pi_{0^+}$), 17% ($\sigma\sigma^2\pi^{*3}$, $^3\Pi_{0^+}$), and 2% ($\sigma^2\sigma^{*2}\pi^{*2}$, $^3\Sigma^-_{0^+}$). At 6.2 bohr the composition of the 0+(I) state was found to be 0.1% ($\sigma^2\pi^{*4}$, $^1\Sigma^+_{0^+}$), 17% ($\sigma^2\sigma^*\pi^{*3}$, $^3\Pi_{0^+}$), 22% ($\sigma\sigma^{*2}\pi^{*3}$, $^3\Pi_{0^+}$), 1% ($\sigma\sigma^*\pi^{*4}$, $^1\Sigma^+_{0^+}$), and 56% ($\sigma^2\sigma^{*2}\pi^{*2}$, $^3\Sigma^-_{0^+}$). Thus, the 0+(I) state was found to exhibit avoided crossings.

TABLE 55. A Few Low-Lying MO Configurations of ICl and the Related States in Both λ-s and ω-ω Couplings[a]

Configuration	λ-s states	ω-ω states
$\sigma^2\pi^4\pi^{*4}$	$^1\Sigma^+$	0^+
$\sigma^2\sigma^*\pi^4\pi^{*3}$	$^3\Pi$	$2,1,0^-,0^+$
	$^1\Pi$	1
$\sigma^2\sigma^{*2}\pi^4\pi^{*2}$	$^3\Sigma^-$	$0^+,1$
	$^1\Delta$	2
	$^1\Sigma^+$	0^+
$\sigma\sigma^*\pi^4\pi^{*4}$	$^3\Sigma^+$	$0^-,1$
	$^1\Sigma^+$	0^+
$\sigma^{*2}\pi^4\pi^{*4}$	$^1\Sigma^+$	0^+
$\sigma\sigma^{*2}\pi^4\pi^{*3}$	$^3\Pi$	$2,1,0^-,0^+$
	$^1\Pi$	1
$\sigma^2\sigma^{*2}\pi^3\pi^{*3}$	$^3\Sigma^-$	$0^+,1$
	$^3\Delta$	3,2,1
	$^3\Sigma^+$	$0^-,1$
	$^1\Sigma^-$	0^-
	$^1\Delta$	2
	$^1\Sigma^+$	0^+

[a] Only the p electrons of I and Cl are shown.

TABLE 56. A Few MO Configurations of ICl+ and the Related Terms in the λ-s and ω-ω Coupling Schemes[a]

Configurations	λ-s states	ω-ω states
$\sigma^2\pi^4\pi^{*3}$	$^2\Pi$	3/2,1/2
$\sigma^2\pi^3\pi^{*4}$	$^2\Pi$	3/2,1/2
$\sigma\pi^4\pi^{*4}$	$^2\Sigma^+$	1/2
$\sigma\sigma^*\pi^4\pi^{*3}$	$^4\Pi$	5/2,3/2,1/2
	$^2\Pi$	3/2,1/2
$\sigma^2\sigma^*\pi^4\pi^{*2}$	$^4\Sigma^-$	3/2,1/2
	$^2\Sigma^-$	1/2
	$^2\Sigma^+$	1/2
	$^2\Delta$	5/2,3/2

[a] Only the p electrons of I and Cl are shown.

At short distances 0^+(II) was found to be predominantly made of $^3\Pi_{0^+}$. At 5.5 bohr this state became 1% ($\sigma^2\pi^{*4}$, $^1\Sigma^+_{0^+}$), 2.6% ($\sigma\sigma^*\pi\pi^{*4}$, $^1\Sigma^+_{0^+}$), 12% ($\sigma^2\sigma^*\pi^{*3}$, $^3\Pi_{0^+}$), 10% ($\sigma\sigma^2\pi^{*3}$, $^3\Pi_{0^+}$), and 70% ($\sigma^2\sigma^{*2}\pi^{*2}$, $^3\Sigma^-_{0^+}$). At long distances the $^3\Pi_{0^+}$ arising from $\sigma\sigma^{*2}\pi^{*3}$ and $\sigma^2\sigma^*\pi^{*3}$ dominated. At short distances the 0^+(III) state was found to be 43% ($\sigma^2\sigma^{*2}\pi^{*2}$, $^3\Sigma^-_{0^+}$), 27% ($\sigma^2\sigma^*\pi^{*3}$, $^3\Pi_{0^+}$), 15% ($\sigma\sigma^*\pi^{*3}$, $^3\Pi_{0^+}$), 4% ($\sigma^2\pi^{*4}$, $^1\Sigma^+_{0^+}$), and 6% ($\sigma\sigma^*\pi^{*4}$, $^1\Sigma^+_{0^+}$). However, at 5.5 bohr the composition of this state changed to 14.4% ($\sigma^2\pi^{*4}$), 26% ($\sigma\sigma^*\pi^{*4}$), 33% ($\sigma^2\sigma^*\pi^{*3}$), 17% ($\sigma\sigma^*\pi^{*3}$), and 5% ($^3\Sigma^-_{0^+}$). At long distances it was found to be predominantly $^1\Sigma^+_{0^+}$.

The variations of the compositions of the RCI wave functions of the 0^+, 0^+(II), and 0^+(III) states resulted in several avoided crossings in these states. These crossings are the results of the crossings of the $^3\Pi$, $^3\Sigma^-$, and $^1\Sigma^+$ curves in the absence of spin–orbit interaction (see Figure 31).

Experimental and theoretical investigations of Ar–Cl+ collisions[328,329] as well as Ne–F+ energy transfers[327] have also been carried out. Theoretical calculations on KrF+ have also been done by Liu and Schaefer.[323] More recently, the transition moments for energy transfers in Ar–Cl+ collisions were obtained.[329] Theoretical calculations and experimental work are also in progress on Xe–I+ collisions.[331]

C. ICl and ICl+

Interhalogen diatomics have been the topics of numerous studies for many years.[332–354] The IF, ICl and IBr species have been some of the most studied species in this group. Brand and Hoy[38] have reviewed the spectroscopic properties and ion-pair states of homonuclear and heteronuclear halogens. The present review

is restricted to a comparison of theory and experiment on the ICl and ICl+ species.

The spectroscopic properties of the ICl diatomic have been obtained by a number of techniques such as absorption spectra,[332,333] emission spectra,[345,349] vacuum-UV spectra,[341] time-resolved fluorescence,[337] chemiluminescence of the I + Cl reaction,[336] two-step excited fluorescence,[340] and three-photon resonance.[348] The photoelectron spectra of ICl have been recorded and reveal the existence of four low-lying states of ICl+.[350] Balasubramanian[353] carried out RCI calculations of the spectroscopic properties of five low-lying states of ICl [0^+(I), 2, 1, 0^-, 0^+(II)], and spectral assignments of various transitions among these states were accomplished or confirmed. The continuous absorption spectra as well as diffuse emission spectra of ICl in the region below 45 000 cm^{-1} were interpreted and assigned to appropriate electronic transitions.

In a subsequent paper Balasubramanian[354] extended his calculations on ICl to the 0^-(II), 0^+(III), and 1(II) states as well as the corresponding states without spin–orbit interaction. He also carried out RCI calculations on the 3/2, 1/2, 3/2(II), 1/2(II), 5/2, $^2\Pi$, $^2\Sigma^+$, and $^4\Pi$ states of ICl+.[354]

Balasubramanian[353,354] employed relativistic effective potentials for the iodine atom that retained the outer $d^{10}s^2p^5$ shells explicitly in the valence shell. He included the seven valence electrons arising from the s^2p^5 configuration of the Cl atom in these calculations.

Balasubramanian[354] employed a double-ζ STO basis set optimized for the ground states of the two atoms. He then carried out SCF/RCI calculations that included up to 3000 configurations for ICl and ICl+.

Tables 55 and 56 show a few low-lying configurations of ICl and ICl+, respectively, and the corresponding λ-s and ω-ω states arising from them. Since the ionization potential of the iodine atom is much smaller than that of Cl, the ICl+ states are expected to dissociate into I+ and Cl. Tables 57 and 58 show the dissociation relationship of the ω-ω molecular states of ICl and ICl+, respectively. Since the π^* orbital is expected to be predominantly on the iodine atom and the electronic states of ICl+ are open-shell states, the spin–orbit splitting of the ground state of ICl+ is likely to be large.

Table 59 shows the spectroscopic constants for the low-lying electronic states of ICl. Figures 32 and 33

TABLE 57. Dissociation Limits of Several Low-Lying Electronic States of ICl and the Experimental Energies of the Separated Atoms

Molecular states	Dissociation limit I + Cl	Energy[a] (cm^{-1})
3,2,2(II),1(I), 1(II),1(III),0$^+$(I) 0$^+$(II),0$^-$(I),0$^-$(II)	$^2P_{3/2} + ^2P_{3/2}$	0.0
2(III),1(IV),1(V), 0$^+$(III),1^9(V),1(V), 0$^+$(III),0$^+$(IV),0$^-$(III), 0$^-$(V)	$^2P_{3/2} + ^2P_{1/2}$	881
2(IV),1(VI),1(VII), 0$^+$(V),0$^+$(VI),0$^-$(V), 0$^-$(VI)	$^2P_{1/2} + ^2P_{3/2}$	7603
1(VIII),0$^+$(VII),0$^-$(VIII)	$^2P_{1/2} + ^2P_{1/2}$	8484

[a] From ref 134.

TABLE 58. Dissociation Limits of $\omega-\omega$ Electronic States of ICl$^+$

| $\omega-\omega$ states	Dissociation limit I$^+$ + Cl	Energy (cm^{-1})[a]
7/2,5/2,5/2(II), 3/2,3/2(II)	$^3P_2 + ^2P_{3/2}$	0.0
3/2(III),1/2,1/2(II), 1/2(III),1/2(IV)		
5/2(III),3/2(IV),3/2(V), 1/2(V),1/2(VI)	$^3P_2 + ^2P_{1/2}$	881

[a] From ref 134.

show the potential energy curves for the low-lying electronic states of ICl. As seen from Table 59, the theoretical spectroscopic constants are in reasonable agreement with those obtained from experiments. In general, the bond lengths are longer compared to experimental values, a trend we see at a modest RECP-SCF/RCI level of theory.

The theoretical calculations of Balasubramanian[353] on ICl facilitated confirmation of the assignment of the experimentally observed X(0$^+$), A'(2), A(1), B(0$^+$), and B'(0$^+$(II)) states of ICl. The second minimum in the 0$^+$(II) curve is now well characterized both experimentally and theoretically and is due to an avoided crossing of $^3\Pi_{0^+}$ with $^3\Sigma^-_{0^+}$ at long distances. Balasubramanian[353] also assigned continuous and diffuse spectra below 45 000 cm^{-1}. The continuous absorption with a maximum at 21 000 cm^{-1} was assigned to the X(0$^+$) → B(0$^+$) absorption. Another absorption system with a maximum at 25 200 cm^{-1} was assigned to the A(1) ← X(0$^+$) system. The continuous absorption with a maximum at 41 600 cm^{-1} was assigned to the X(0$^+$) → 0$^+$(III) transition. The diffuse emission bands in the 18 700–27 000-cm^{-1} region were assigned to emissions from the D(1) → 1(II) states, where D(1) is the ion-pair state observed by Brand et al.[347] However, this appears to be a tentative assignment.

TABLE 59. Spectroscopic Properties of the Low-Lying Bound States of ICl[a]

State	R_e (Å)		T_e (cm^{-1})		ω_e (cm^{-1})	
	theory	expt.	theory	expt.	theory	expt.
X 0$^+$(I)	2.53	2.32	0	0	327	384
A' 2(I)	2.93	2.65	13261	12680	171	226
A 1(I)	3.07	2.69	13870	13742	146	212
0$^-$(I)	3.05	-	16665	-	155	-
B 0$^+$(II)	2.96	2.66	17935	17363	174	221
B'0$^+$(II)	3.46	-	17652	18157	-	-
$^1\Sigma^+$	2.52	-	316	-	327	-
$^3\Pi$	2.90	-	16245	-	188	-

[a] Theoretical constants are from ref 353 and 354. Experimental values are from ref 37.
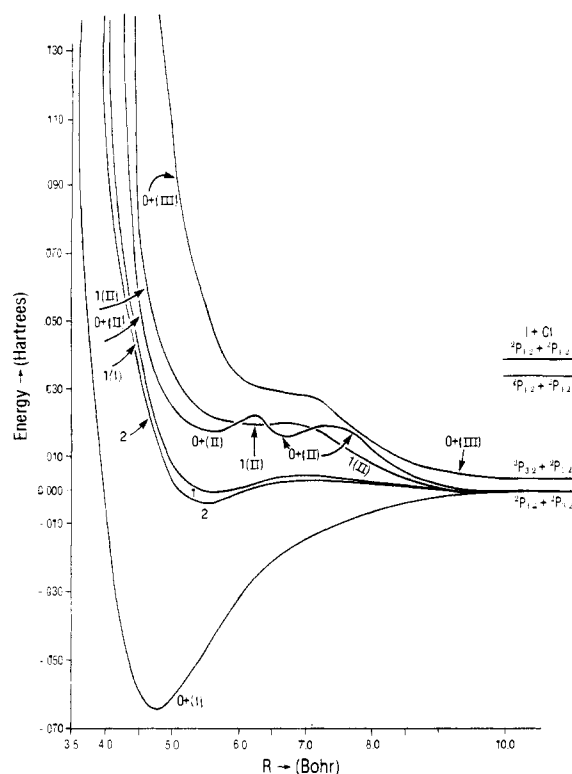
Figure 32. Potential energy curves of the low-lying states of ICl (reprinted from ref 353; copyright 1985 Academic Press, Inc.). See Table 59 for spectroscopic labels of known states.

As seen in Figure 33, there is a barrier in the 0$^-$(I) state. This state has not yet been characterized experimentally but could be characterized through multiphoton techniques as suggested by Balasubramanian.[353]

Table 60 shows the spectroscopic constants of the 3/2, 1/2, 3/2(II), 1/2(II), and 1/2(III) states of ICl$^+$. Table 60 also shows the results obtained by Potts and Price[350] from the photoelectron spectra of ICl. The experimental photoelectron spectrum of ICl contained four peaks.[350] The first two peaks were assigned to the 3/2 and 1/2 states. The experimental splitting of these two peaks ($\approx$4680 cm^{-1}) was found to be in reasonable agreement with the theoretical value of 5424 cm^{-1}. The ω_e value calculated from the photoelectron spectra (390

TABLE 60. Spectroscopic Properties of ICl⁺ [a]

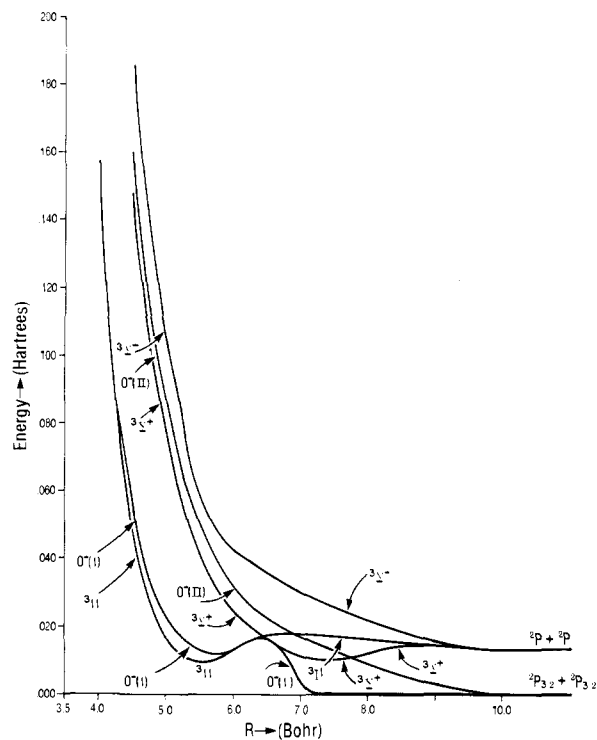| State	R_e (Å) theory	T_e (cm⁻¹) theory	expt.	ω_e (cm⁻¹) theory	expt.	Theoretical vertical excitation energy at 4.65 bohr	Separation of the photoelectron spectral peaks from the 3/2 peak (350)
X 3/2	2.47	0	0	311	390		0
1/2	2.46	5424	4680	314	-		4680
A ²Π(II)	2.78	14352		207	-	17140	22420
B ²Σ⁺₁/₂	3.44	22835		168	-	30950	33550

[a] Theoretical constants are from ref 354.

Figure 33. Potential energy curves of more electronic states of ICl (reprinted from ref 354; copyright 1985 Elsevier Science Publishers B.V.). See Table 59 for spectroscopic labels of known states.

Figure 34. Potential energy curves of ICl⁺ (reprinted from ref 354; copyright 1985 Elsevier Science Publishers B.V.). See Table 60 for spectroscopic labels of known states.

cm⁻¹) for the ground state of ICl⁺ is also in reasonable agreement with the theoretical value of 310 cm⁻¹.

As seen from Table 60, the minima of the excited states 3/2(II), 1/2(II), and 1/2(III) are at longer distances than the corresponding minimum of the ground state. Further, the T_e values of the excited states are much smaller than the separations of the corresponding peaks in the photoelectron spectra of ICl. Thus, it was suggested by Balasubramanian[354] that the peaks observed in the photoelectron spectra should be attributable to Franck–Condon-type vertical excitations. Since the 3/2(II), 5/2, and 1/2(III) states are quite repulsiver near the equilibrium bond distance of the ground state of ICl⁺, the vertical excitation energies reported in Table 60 are only estimates, although these are in good agreement with the experimental splittings. Further, since Franck–Condon-type excitation occurs at a slightly shorter distance, the theoretical splittings at the equilibrium bond distance of the ground state are somewhat lower than the corresponding experimental values.
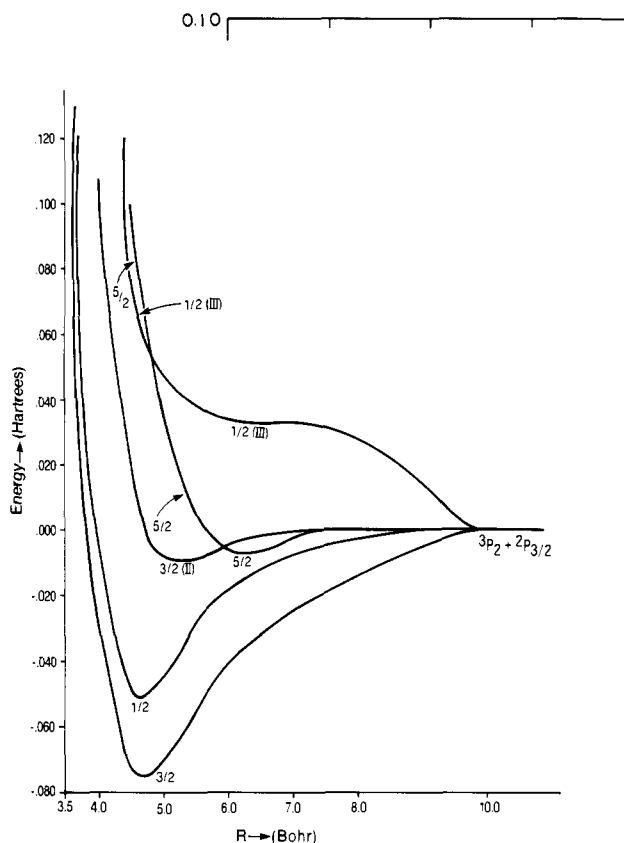
Table 61 shows the vertical ionization energies of ICl as obtained by SCF, SOCI, and Koopmans' theorem. The SOCI values are the best and are in good agreement with the values reported by Potts and Price[350] from the photoelectron spectra of ICl. Although Koopmans' theorem predicts the correct ordering of the various low-lying states of ICl, the IP values are rather high. The errors in these values arise from several sources such as lowering of the ²Π₃/₂ state by the spin–orbit term, correlation, and orbital relaxation effects. The SCF ionization energy of the ²Π state is in remarkably good agreement with the experimental results.

Venkateswarlu[341] studied the vacuum-UV spectra of ICl. The convergence of Rydberg series attributable to $(\sigma^2\pi^4\pi^{*3}, {}^2\Pi_{3/2})$ $ns\sigma$ and $(\sigma^2\pi^4\pi^{*3}, {}^2\Pi_{3/2})$ $np\sigma$ was estimated to be 81362 cm⁻¹. These Rydberg series were fit

TABLE 61. Vertical Ionization Energies of ICl by Various Methods[a]

Method	State	Ionization energy (eV)	Method	State	Ionization energy (eV)
SCF[b]	$^2\Pi$	10.19	CI[d]	$^2\Pi$	10.45
Koopmans' theorem	$^2\Pi(I)$	11.02		$^2\Pi(II)$	12.07
	$^2\Pi(II)$	13.43		$^2\Sigma^+$	13.78
	$^2\Sigma^+$	13.57		$^4\Pi$	14.20
RCI[c]	3/2	10.16	photoelectron spectroscopy (350)	3/2	10.10
	1/2	10.84		1/2	10.68
	3/2(II)	12.15		A($^2\Pi$)	12.88
	1/2(II)	12.18		$^2\Sigma^+_{1/2}$	14.26
	$^2\Sigma^+_{1/2}$, 1/2(III)	13.78	Rydberg series (341)	3/2	10.10
	5/2	13.87		1/2	10.60

[a] Theoretical values are from ref 354. [b] This is the difference of the SCF energy of the $^1\Sigma^+$ state of ICl and the $^2\Pi$ state of ICl$^+$ at 4.75 bohr. [c] This is the RCI energy separation of the relevant state of ICl$^+$ with respect to the 0$^+$(I) state of ICl at 4.75 bohr. [d] This is the CI energy separation without spin–orbit coupling.

into the formula of the type

$$\nu_{00} = 81362 - R/(n-s)^2$$

where s is a screening constant. This suggested that the ionization energy of the 3/2(I) state with respect to the ground state of the neutral ICl should be 81 362 cm^{-1} or 10.09 eV. This value was found to be in very good agreement with the theoretical value of 10.16 eV.[355]

The Rydberg series arising from the $(\sigma^2\pi^4\pi^{*3}, {}^2\Pi_{1/2})$ core were represented by the formula

$$\nu_{00} = 85996 - R/(n-s)^2$$

Thus, the separation of the 1/2 state from the 0$^+$(I) state is 85 996 cm^{-1} or 10.66 eV. This was also found to be in reasonable agreement with the theoretical value of 10.84 eV.

Conford[352] obtained the $^2\Pi_{3/2}$–$^2\Pi_{1/2}$ separation as 4650 cm^{-1} by photoelectron spectroscopy, which was found to be in reasonable agreement with the theoretical value of 5424 cm^{-1} (see Table 10). Conford reported a separation of ≈2.49 eV between the $\sigma^2\pi^4\pi^{*3}({}^2\Pi_{3/2})$ and the $\sigma^2\pi^3\pi^{*4}({}^2\Pi_{3/2})$ states of ICl$^+$. The theoretical separation at 4.75 bohr is around 1.99 eV. Theoretical ionization energies thus confirmed the earlier assignments of various Rydberg series.

The nature of the electronic states of ICl and ICl$^+$ can be understood in terms of the highest occupied orbitals and the composition of the RCI wave functions. The highest occupied σ orbital of ICl is quite bonding, while the highest occupied π orbital is predominantly on iodine but it is slightly antibonding. The highest occupied σ orbital of ICl$^+$ has an increased iodine p-orbital coefficient compared to the corresponding orbital of ICl. This is compensated by a decrease in the coefficient of the Cl p orbital. The highest occupied π orbital of ICl$^+$ is also more localized on the iodine atom compared to the corresponding orbital of ICl.

The 0$^+$(I) state of ICl was found to be 90% ($^1\Sigma^+_{0^+}$) and 1.5% ($^3\Pi_{0^+}$) at 4.75 bohr. Consequently, at equilibrium bond distances the spin–orbit contamination from $^3\Pi_{0^+}$ was found to be rather small. The $\sigma^{*2}\pi^4\pi^{*4}$

(doubly excited) configuration makes a nonnegligible contribution at 4.75 bohr (3.1%). At longer distances contributions from both $^3\Pi_{0^+}$ and $\sigma^{*2}\pi^4\pi^{*4}$ increased to a considerable extent. The $^3\Pi_{0^+}$, $^3\Pi_{0^-}$, $^3\Pi_2$, and $^3\Pi_1$ states were found to be predominantly $\sigma^2\sigma^*\pi^4\pi^{*3}$ states at 5.5 bohr, but $\sigma\sigma^{*2}\pi^4\pi^{*3}$ as well as $\sigma\sigma^{*2}\pi^3\pi^{*4}$ made significant contributions at the minimum of the $^3\Pi$ states. There is significant mixing of the $^3\Pi_1$ and $^1\Pi_1$ states in the 1(I) state at 5.5 bohr. The 1(I) state was found to be 69% ($\sigma^*\pi^{*3}$, $^3\Pi_1$), 12.6% ($\sigma^*\pi^{*3}$, $^1\Pi_1$), 4.7% ($\sigma\sigma^{*2}\pi^4\pi^{*3}$), 1.3% ($^3\Sigma^-_1$), 4.5% ($^3\Pi_1$, $\sigma\sigma^{*2}\pi^3\pi^{*4}$), and 1.6% ($^1\Pi_1$, $\sigma\sigma^{*2}\pi^4\pi^{*3}$).

The 0$^+$(II) state of ICl exhibited an interesting behavior as a function of distance resulting in the double minima in the PEC. It was found to be predominantly $^3\Pi_{0^+}$ arising from $(\sigma^2\sigma^*\pi^4\pi^{*3})_{0^+}$ at 5.5 bohr, although appreciable contamination comes from other references. However, near 6.5 bohr an avoided crossing of $^3\Sigma^-_{0^+}$ arising from $\sigma^2\sigma^*\pi^3\pi^{*3}$ with $^3\Pi_{0^+}$ led to a second minimum. This is a consequence of the fact that $(\sigma^2\sigma^{*2}\pi^3\pi^{*3})_{0^+}$ dissociates into I($^2P_{3/2}$) + Cl($^2P_{3/2}$) atoms, while $^3\Pi_{0^+}$ dissociates into I($^2P_{3/2}$) + Cl($^2P_{1/2}$) atoms. Mixing of $^3\Pi_{0^+}$ and $^3\Sigma^-_{0^+}$ was found to be significant in the 6–7.0-bohr region.

The 0$^+$(III) state exhibited opposite behavior compared to 0$^+$(II); it is predominantly $^3\Sigma^-_{0^+}$ below 5.5 bohr. It became predominantly $^3\Pi_{0^+}$ at longer distances as a result of the above-mentioned avoided crossing. The 0$^-$(II) state is predominantly $^3\Sigma^+_{0^-}$ at near-equilibrium distances. The 1(II) state is a mixture of $^1\Pi_1$ and $^3\Pi_1$, with $^1\Pi_1$ making dominant contributions in the region 4.5–6.0 bohr.

The electronic states of ICl$^+$ exhibited larger spin-orbit splitting than spin–orbit contamination. The 3/2 state of ICl$^+$ was found to be 89.4% ($^2\Pi_{3/2}$, $\sigma^2\pi^4\pi^{*3}$) and 4% ($^2\Pi_{3/2}$, $\sigma^{*2}\pi^4\pi^{*3}$). At very long distances the $(\sigma\sigma^*\pi^4\pi^{*3})_{3/2}$ states make dominant contributions so that the 3/2 state would dissociate into I$^+$($^3P_2$) + Cl-($^2P_{3/2}$) atoms. The 1/2(I) state was found to be 84% ($^2\Pi_{1/2}$) and 1.1% $^2\Sigma^+_{1/2}$ at 4.75 bohr. At longer distances $(\sigma\sigma^*\pi^4\pi^{*3})_{1/2}$ states made significant contributions.

TABLE 62. Geometries of Energies of the Electronic States of Ga$_3$[a]

		CASSCF			POLCI		
Species	State	θ (°)	r (Å)[b]	E^c (eV)	θ (°)	r (Å)	E^c (eV)
Ga$_3$	$^2A_1$	62.4	2.51	0.0	61.2	2.58	0.0
Ga$_3$	$^4A_2$	76.4	2.62	0.24	72.6	2.57	0.24
Ga$_3$	$^2B_1$	50.6	2.92	0.27	61.2	2.60	0.28
Ga$_3$	$^4B_1$	54.5	2.88	0.29	56.5	2.74	0.32
Ga$_3$	$^2B_2$	68.8	2.54	0.67	65.5	2.58	0.69
Ga$_3$	$^4B_2$	58.3	3.05	0.78	61.8	2.93	1.27
Ga$_3$	$^4A_1$	180	2.80	1.18	180	2.79	1.38
Ga$_3^+$	$^1A_1$	180	3.07	4.92	180	3.00	5.99
Ga$_3^+$	$^3B_2$	180	2.90	5.57	180	2.78	6.36

[a] All constants are from theoretical calculations in ref 355. [b] The two equal sides of the isosceles triangle; θ = apex angle. [c] Zero energy for CASSCF is −6.086778 hartrees; zero energy for POLCI is −6.159135 hartrees.
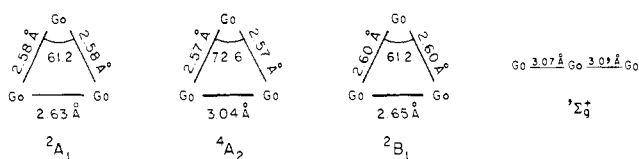
Figure 35. Equilibrium geometries of the low-lying states of Ga$_3$ (reprinted from ref 355; copyright 1988 Elsevier Science Publishers B.V.).

The 3/2(II) and 1/2(II) states of ICl$^+$ were found to be predominantly $^2\Pi$ arising from the $\sigma^2\pi^3\pi^{*4}$ configuration. Since the π orbital was found to be predominantly on the Cl atom, the splitting between the 3/2(II) and 1/2(II) states was small. This is also consistent with unresolved peaks in the photoelectron spectra of ICl which corresponded to these states. The 1/2(III) state was found to be predominantly $^2\Sigma^+_{1/2}(\sigma\pi^4\pi^{*4})$ at near-equilibrium bond distances while the 5/2 state was found to be $^4\pi_{5/2}$.

V. Spectroscopic Properties and Potential Energy Surfaces of Trimers

A. Ga$_3$

There are no experimental spectroscopic studies on Ga$_3$ except the one done by Smalley and co-workers,[97] who detected Ga$_3$ in a laser-evaporated GaAs supersonic jet beam of composition Ga$_x$As$_y$. Balasubramanian and Feng[355] carried out complete active space MCSCF followed by CI calculations that included up to 32 000 configurations. They employed the same RECPs and basis sets used in the earlier calculations on Ga$_2$.[133] Those calculations were carried out on seven low-lying electronic states of Ga$_3$ and the linear $^1A_1$ closed-shell state of Ga$_3^+$.

Isoelectronic Al$_3$ was investigated by Basch[356] theoretically and by Howard et al.[359] experimentally using the ESR spectroscopic method and subsequently by Fu et al.[358] using optical spectroscopy of jet-cooled Al$_3$. Basch[356] found a $^2A_1$ ground state (near-equilateral-triangle geometry) with a low-lying $^4A_2$ state only 5 kcal/mol above $^2A_1$. The ESR spectra of Al$_3$ in a

TABLE 63. Dipole Moments of the Isosceles Triangular Electronic States of Ga$_3$[a]

State	μ (D)	State	μ (D)
$^2A_1$	0.02	$^4B_1$	0.60
$^4A_2$	0.17	$^2B_2$	0.17
$^2B_1$	0.04	$^4B_2$	0.26

[a] From ref 355.

rare-gas matrix favored a quartet ground state. Fu et al.[358] obtained the spectra of jet-cooled Al$_3$. A discrete band system in the 5200–6100-Å region was observed together with an absorption continuum that exhibited a lifetime of 24–35 μs. These authors[358] deduced D_0-(Al$_2$–Al) $\le$ 2.40 eV from the predissociation of the continuous absorption bands. Morse and co-workers are also considering high-resolution spectroscopic studies of Al$_3$, which would facilitate determination of the ground-state symmetry and geometry. Until such studies are done, it seems that the ground state of both Al$_3$ and Ga$_3$ would remain uncertain.

Table 62 shows the optimized equilibrium geometries of seven electronic states of Ga$_3$ and two electronic states of Ga$_3^+$ using both the CASSCF and POLCI methods.[355] Figure 35 shows the POLCI geometries of the three lowest lying electronic states of Ga$_3$. As seen from Table 62, the ground state of Ga$_3$ is a $^2A_1$ state with an equilibrium geometry of a near-equilateral triangle. The apex angle reduces by 1° upon inclusion of high-order correlations in the POLCI calculations. The bond length of the base of the triangle is about 2.63 Å at the POLCI level while the equal sides are a bit shorter (2.58 Å). It is expected that the Ga–Ga bond lengths should be slightly longer than the actual bond lengths since for Ga$_2$ and GaAs, the 3e-RECPs of Ga gave slightly longer bond lengths. The $^2A_1$ state was found to be predominantly made of the $1a_1^2 2a_1^2 3a_1 1b_2^2 1b_1^2$ configuration.

Two very low lying excited electronic states, namely, $^4A_2$ and $^2B_1$, were found by Balasubramanian and Feng.[355] The $^4A_2$ state was found to be 5.5 kcal/mol above the $^2A_1$ state while the T_e of the $^2B_1$ state was 6.5 kcal/mol. The $^4A_2$ state arises from the $1a_1^2 2a_1^2 3a_1 1b_2^2 2b_2 1b_1$ electronic configuration while the $^2B_1$ state arises from the $1a_1^2 2a_1^2 3a_1^2 1b_2^2 1b_1$. The equilibrium geometries of the $^4A_2$ and $^2B_1$ states are isosceles triangles.

The $^4B_1$ state ($1a_1^2 2a_1^2 3a_1 4a_1 1b_2^2 1b_1$) has a very acute triangular equilibrium geometry. The two equal sides of the isosceles triangle have longer bond lengths (2.74 Å). The base of the triangle has a shorter bond length (2.59 Å), which suggests enhanced bonding along the base of the triangle. The other three electronic states, namely, $^2B_2$, $^4B_2$, and $^4A_1$, are considerably well separated from the ground states. The $^2B_2$ and $^4B_2$ states have isosceles triangular geometries while the $^4A_1$ state has a linear equilibrium geometry.

The effect of higher order electron correlations on the geometries is not substantial as seen from Table 62 by comparing the CASSCF and POLCI geometries for most of the states except the $^2B_1$ state for which CASSCF calculations yield a very acute triangle

TABLE 64. CASSCF-CI Wave Functions of the Electronic States of Ga₃ and Ga₃⁺ [a]

Coefficient	Configuration	Coefficient	Configuration

Ga₃
²A₁

	1a₁	2a₁	3a₁	4a₂	1b₂	2b₂	3b₂	1b₁	2b₁	1a₂
-0.918	2	2	1	0	2	0	0	2	0	0
0.106	2	2	1	0	2	0	0	0	2	0
-0.104	2	2	1	0	1	1	0	2	0	0
0.100	2	2	1	1	2	0	0	0	0	2

⁴A₂

	1a₁	2a₁	3a₁	4a₂	1b₂	2b₂	3b₂	1b₁	2b₁	1a₂
0.947	2	2	1	0	2	1	0	1	0	0

²B₁

	1a₁	2a₁	3a₁	4a₂	1b₂	2b₂	3b₂	1b₁	2b₁	1a₂
-0.919	2	2	2	0	2	0	0	1	1	0
0.173	2	2	0	0	2	2	0	1	1	0
0.131	0	2	0	2	2	1	0	1	1	0

⁴B₁

	1a₁	2a₁	3a₁	4a₁	1b₂	2b₂	1b₁	3b₂	2b₁	1a₂
-0.955	2	2	1	1	2	0	1	0	1	0

²B₂

	1a₁	2a₁	3a₁	4a₁	1b₂	2b₂	3b₂	1b₁	2b₁	1a₂
0.914	2	2	0	0	2	1	0	2	0	0
-0.176	2	2	0	0	2	0	0	2	1	0
-0.115	2	2	0	0	2	0	0	2	1	0

Ga₃
⁴B₂

	1a₁	2a₁	3a₁	4a₁	1b₂	2b₂	3b₂	1b₁	2b₁	1a₂
-0.962	2	2	1	1	2	1	0	0	0	0

⁴A₁

	1a₁	2a₁	3a₁	4a₁	1b₂	2b₂	3b₂	1b₁	2b₁	1a₂
-0.951	2	2	0	0	2	1	0	1	0	1
0.113	2	1	0	0	2	2	0	1	1	0

Ga₂⁺
¹A₁

	1a₁	2a₁	3a₁	4a₁	1b₂	2b₂	3b₂	1b₁	2b₁	1a₂
-0.940	2	2	0	0	2	2	0	0	0	0
-0.127	2	1	0	0	2	1	0	0	1	1
-0.114	2	1	0	1	2	1	1	1	0	0
0.102	2	2	2	0	1	1	0	0	0	0

²B₂

	1a₁	2a₁	3a₁	4a₁	1b₂	2b₂	3b₂	1b₁	2b₁	1a₂
0.957	2	2	1	0	2	1	0	0	0	0

[a] From ref 355.

structure which is corrected to a near-equilateral triangle structure by POLCI. The energy separations are, in general, more sensitive to electron correlation effects.

The CASSCF atomization energy was calculated by carrying out a long-distance CASSCF calculation for the linear ²A₁ geometry (R = 8.0 Å). The atomization energy calculated in this way was found to be 2.32 eV.[355] Higher order correlation effects not included in the CASSCF can certainly increase the atomization energy. The corresponding CASSCF D_e of the Ga₂ dimer calculated earlier by Balasubramanian[133] is 0.92 eV. Consequently, Ga₃ is at least 1.4 eV more stable than the dimer. The corresponding calculations on Al₃ by Basch[357] revealed that the aluminum trimer is about 1.93 eV more stable than the dimer while the experimental results of Fu et al.[358] imply D_0(Al₂-Al) < 2.4 eV.

Table 63 depicts the dipole moments of the isosceles triangular states of Ga₃ calculated from the POLCI natural orbitals. As seen from Table 63, the ground state (²A₁) and ²B₁ excited states have nearly vanishing dipole moments while the other electronic states have nonnegligible dipole moments. The positive charge is on the apex atom of the isosceles triangle. The ⁴A₂, ⁴B₁, ²B₂, and ⁴B₂ states of Ga₃ are slightly ionic while the ²A₁ and ²B₁ states are essentially nonionic.

As seen from Table 62, there are two low-lying electronic states for the Ga₃⁺ positive ion. The ground state is a closed-shell ¹A₁ state with a linear geometry. The adiabatic ionization energy of Ga₃ is 5.99 eV. The ¹A₁–³B₂ splitting of the Ga₃⁺ positive ion is 0.65 and 0.37 eV at the CASSCF and POLCI levels of theory, respectively. Consequently, this energy separation is influenced to a large extent by higher order correlations. Most of the ionization occurs at the base atoms of the

triangle than the apex atom as evidenced from the Mulliken population analysis. The adiabatic ionization potential of the Ga₃ cluster (5.99 eV) is quite comparable to the experimental ionization potential of the Ga atom,[134] which is 6.0 eV. It is interesting to note that both the Ga atom and Ga₃ clusters form a stable closed-shell singlet electronic state upon ionization leading to lower adiabatic ionization energies compared to even clusters. Hence odd–even alternations are anticipated in ionization energies.

The nature of the electronic states of Ga₃ is discussed next. The lowest 1a₁ orbital is the totally symmetric bonding combination of the 4s orbitals of the three Ga atoms. The 2a₁ orbital is also predominantly composed of the 4s orbitals on the three Ga atoms with the combination −4s(1) + 4s(2) + 4s(3), where the label 1 is given for the central apex atom. Consequently, the 2a₁ orbital is antibonding along the sides and bonding along the base of the triangle. The 1b₂ orbital was predominantly found to be the 4p_y(1) + 4s(2) − 4s(3) orbital. Hence this orbital is antibonding along the base and bonding along the sides. Consequently, the 1b₂ orbital is stabilized if the sides are shorter than the base of the triangle. Conversely, the 2a₁ orbital is stabilized if the sides are longer than the base of the triangle. The 1b₁ orbital is a symmetric combination of the 4p_x orbitals on the three Ga atoms perpendicular to the plane of the cluster and thus is "π-like" in character. The 3a₁ orbital is a bonding orbital resulting from the mixing of the 4p_z orbital of the central atom with the 4p_y and 4p_z orbitals of the base of the triangle. The 4s orbitals on the three atoms also participate in this orbital. Similarly, the 2b₂ orbital is a bonding orbital resulting from the interaction of the 4p_y orbital of the central atom with the

TABLE 65. Mulliken Population Analysis for Ga₃ and Ga₃⁺ᵃ

States	Net								Gross								Overlapᵇ
	M_1	M_2	$M_1(s)$	$M_2(s)$	$M_1(p)$	$M_2(p)$	$M_1(d)$	$M_2(d)$	M_1	M_2	$M_1(s)$	$M_2(s)$	$M_1(p)$	$M_2(p)$	$M_1(d)$	$M_2(d)$	
Ga₃																	
$^2A_1$	2.51	6.52	1.657	3.291	0.782	1.980	0.026	0.067	2.993	6.007	1.647	3.299	1.232	2.479	0.114	0.230	0.959
$^4A_2$	2.634	5.435	1.667	3.515	0.919	1.717	0.027	0.065	3.100	5.900	1.629	3.429	1.361	2.232	0.109	0.238	0.931
$^2B_1$	2.609	5.612	1.780	3.662	0.814	2.002	0.037	0.097	2.998	6.002	1.703	3.416	1.184	2.353	0.111	0.233	0.778
$^2B_2$	2.550	5.442	1.547	3.166	0.892	1.728	0.024	0.052	3.054	5.946	1.588	3.311	1.353	2.393	0.113	0.242	1.008
$^4B_1$	2.602	5.842	1.793	3.392	0.726	2.220	0.024	0.072	2.880	6.120	1.738	3.351	1.024	2.529	0.117	0.240	0.556
$^4B_2$	2.774	5.813	1.888	3.623	0.847	1.989	0.020	0.066	2.981	6.019	1.799	3.533	1.096	2.263	0.085	0.223	0.413
$^4A_1$	2.665	5.831	1.695	3.906	0.849	1.861	0.023	0.051	2.917	6.083	1.691	3.619	1.097	2.320	0.129	0.144	0.504
Ga₃⁺																	
$^1A_1$	2.819	4.990	1.673	3.931	0.999	0.829	0.021	0.065	2.915	5.085	1.708	3.555	1.073	1.262	0.134	0.268	0.190
$^3B_2$	2.857	4.736	1.555	3.801	1.127	0.675	0.024	0.048	3.060	4.940	1.624	3.560	1.300	1.122	0.137	0.258	0.406

ᵃM₂ refers to the two equivalent atoms of the cluster. From ref 355. ᵇTotal overlap of the central atom with the two side atoms.

antisymmetric combination of the $4p_y$ and $4p_z$ orbitals of the base atoms with appropriate signs. The $2b_1$, $4a_1$, and $1a_2$ orbitals are antibonding orbitals.

Table 64 contains the important configurationws contributing to the CASSCF-CI wave functions of the electronic states of Ga₃ and Ga₃⁺. As seen from Table 64, the leading configurations have coefficients ≥0.9 for all the electronic states. The second and third leading configurations have coefficients >0.1 for the doublet states. The second leading configuration is less important for the quartet states with the exception of the $^4A_1$ state. In summary, the $^4B_2$ and $^3B_2$ states of Ga₃ and Ga₃⁺ ion are described well by a single-configuration treatment. The other electron states seem to require a multiconfiguration treatment. The $^1A_1$ state of the Ga₃⁺ ion is predominantly $1a_1^2 2a_1^2 1b_2^2 2b_2^2$, suggesting that this state is formed by removal of the $3a_1$ electron from the $^2A_1$ ground state of the neutral cluster. This is anticipated since the single electron resides in the $3a_1$ orbital of the $^2A_1$ state of Ga₃.

Table 65 depicts the Mulliken populations of the POLCI natural orbitals of the various electronic states of Ga₃ and Ga₃⁺. The total s populations of the three metal atoms in all the electronic states are between 4.90 and 5.33. The $^2B_2$ and $^2A_1$ states have the smallest s populations while the $^4B_2$ and $^4A_1$ states have the largest s populations. The corresponding p populations are between 3.36 and 3.75. The $^2A_1$ and $^2B_2$ states have the largest p populations while the $^4B_2$ and $^4A_1$ states have the smallest p populations. Hence there is considerable 4s to 4p electron transfer in the electronic states of Ga₃. The d populations are about 0.3–0.35 for all the electronic states of Ga₃. Consequently, the participation of the d polarization functions is quite important for all the electronic states of Ga₃. A comparison of the total gross populations of the central and side atoms

of Ga₃ and Ga₃⁺ ($^2A_1$, $^1A_1$) revealed that most of the electron removed in the ionization process comes from the base atoms than the central atom. Of course, there is considerable rearrangement of this geometry from a near-equilateral-triangular to a linear structure upon ionization. Comparison of the total s, p, and d populations of the ground states of Ga₃ and Ga₃⁺ shows that the electron is removed from the 4p orbital and that there is considerable 4p → 4s electron transfer upon ionization.

The electronic states of Al₃ show considerable similarities to the corresponding states of Ga₃. Basch[356] found the ground state of Al₃ to be a $^2A_1$ state with an isosceles triangular geometry (apex angle = 56.2°). The $^2B_1$ and $^4A_2$ states were found to be 0.22 and 0.23 eV above the ground state. The energy separations for Al₃ are thus comparable to the corresponding electronic states of Ga₃. The geometries are, however, somewhat different as expected. The Al₃⁺ ion has a $^1A_1$ closed-shell ground state. The $^1A_1$–$^3B_2$ splitting for Al₃⁺ was found to be 0.42 and 0.39 eV at restricted and full levels of CASSCF calculations, respectively. The POLCI $^1A_1$–$^3B_2$ splitting for Ga₃⁺ obtained by Balasubramanian and Feng[355] (0.37 eV) is quite comparable to the corresponding splitting for Al₃⁺.

B. GaAs₂

Presently, there are no experimental spectroscopic parameters of GaAs₂, although it has been observed among trimers by Smalley and co-workers[97] in a laser-evaporated jet beam of general composition Ga$_x$As$_y$. Balasubramanian[359] carried out CASSCF/multireference singles + doubles CI calculations on the low-lying electronic states of GaAs₂. Three lowest lying states were found for GaAs₂. All these calculations were done

TABLE 66. Geometries and Energy Separations of $GaAs_2$[a]

State	R_e (Å)	θ_e (°)	E (eV)
$^2B_2$	2.76	47	0
$^2A_1$	2.37	58.5	0.67
$^2B_1$	2.75	51	1.7

[a] MRSDCI geometries and energies for the $^2B_2$ and $^2A_1$ states. CASSCF geometry for the $^2B_1$ state. Energy of the $^2B_1$ state based on the CASSCF $^2B_1$–$^2A_1$ separation. R_e refers to the Ga–As equal bond lengths while θ_e is the As–Ga–As bond angle. From ref 359.
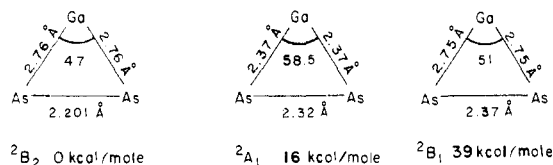
Figure 36. Equilibrium geometries and energy separations of the low-lying electronic states of $GaAs_2$.

TABLE 67. CI Wave Functions of the $^2B_2$ and $^2A_1$ States of $GaAs_2$ at Their Equilibrium Geometries[a]

	$^2B_2$								
coefficient	configuration								
	$1a_1$	$2a_1$	$3a_1$	$4a_1$	$5a_1$	$1b_2$	$2b_2$	$1b_1$	$1a_2$
0.919	2	2	2	2	0	2	1	2	0
-.106	2	2	2	2	0	2	1	0	2

	$^2A_1$								
coefficient	configuration								
	$1a_1$	$2a_1$	$3a_1$	$4a_1$	$5a_1$	$1b_2$	$2b_2$	$1b_1$	$1a_2$
0.916	2	2	2	1	0	2	2	2	0
-.107	2	2	2	1	0	2	2	0	2

[a] From ref 359.

by using RECPs for the various atoms together with valence (3s3p1d) basis sets for Ga and As. The CASSCF calculations included up to 3600 configurations while the MRSDCI calculations included up to 93 000 configurations.

In all the theoretical calculations, the $GaAs_2$ molecule was oriented on the yz plane, and the z axis bisected the As–Ga–As angle. The x axis was perpendicular to the $GaAs_2$ molecular plane. If one assumes the $GaAs_2$ structure to be triangular, a few possible low-lying doublet states arising from the outer s^2p^1 and s^2p^3 shells of Ga and As in the C_{2v} group in this orientation are $1a_1^2 2a_1^2 1b_2^2 3a_1^2 1b_1^2 4a_1^2 2b_2^1$ ($^2B_2$), $1a_1^2 2a_1^2 1b_2^2 3a_1^2 1b_1^2 2a_2^2 4a_1^1$ ($^2A_1$), $1a_1^2 2a_1^2 1b_2^2 3a_1^2 4a_1^2 2b_2^1 1b_1^1$ ($^2B_1$), and $1a_1^2 2a_1^2 1b_2^2 3a_1^2 1b_1^2 4a_1^2 1a_2^1$ ($^2A_2$). While quartet states could be generated by promoting one of the closed-shell electrons into an unoccupied orbital, they would be much higher since the two electrons of the As atoms tend to pair up to form a stable configuration similar to the ground state of As_2. If the ground state of As_2 were to bind to the Ga ground state (^2P) it would form doublet states. Further, attempts by Balasubramanian[359] to find an equilibrium structure for the $^4B_2$ state failed. The $^2A_2$ state is also expected to be higher in energy since this state results from occupying the antibonding combination of the p_x orbitals of the As atoms. The states resulting from correlating the ground states of Ga (^2P) and As_2 ($^1\Sigma_g^+$) to the C_{2v} group are $^2B_2$, $^2A_1$, and $^2B_1$. Consequently, Balasubramanian[359] argued that the probable candidates for the ground state of $GaAs_2$ are $^2B_2$, $^2A_1$, and $^2B_1$.

Table 66 and Figure 36 show the equilibrium geometries and energies of the three electronic states ($^2B_2$, $^2A_1$, and $^2B_1$).[359] The geometries in ref 359 were in slight error due to the ECP parameter mentioned in GaAs work. Corrected geometries are reported here. As seen from Table 66, all three states have isosceles triangular geometries. The $^2B_2$ state is the ground state of $GaAs_2$. The apex angle of the $^2B_2$ state ($\sim 47°$) is the smallest of the apex angles of the three states, implying enhanced As–As bonding over Ga–As bonding, since the Ga–As bonds are the equal sides of the isosceles triangle and the As–As bond corresponds to the base of the isosceles triangle. The As–As bond length for the $^2B_2$ state (MRSDCI) was found to be 2.201 Å. The apex

angle of the $^2A_1$ state ($\sim 58.5°$) is the largest while that of the $^2B_2$ state is the smallest (47°).

The MRSDCI calculations for the $^2B_2$ and $^2A_1$ states change the Ga–As bond length by only 0.03–0.04 Å with respect to the 5320-CASSCF. The apex angle of the isosceles triangle decreased at most by 0.5–0.7° (<1%). The T_e value of the $^2A_1$ state obtained by the MRSDCI method is 0.67 eV. Consequently, the theoretical geometries using the 5320-CASSCF were found to be within 1.5% of the MRSDCI results while the energy differences were within 7%. Consequently, Balasubramanian[359] believed that the 5320-CASSCF method is a more attractive method since it is computationally less intensive. For this reason, Balasubramanian[359] did not carry out MRDCI calculations for the excited $^2B_1$ state. Nevertheless, the 5320-CASSCF geometry for the $^2B_1$ state should be within 2% of the MRSDCI values, and it is believed that the Ga–As bond length would become longer accompanied by a decrease in the As–As bond lengths.

As seen from Table 66, the $GaAs_2$ trimer is found to be more stable than $Ga(^2P)$ + $As_2(^1\Sigma_g^+)$. The dissociation energy for separating the Ga atom from $GaAs_2$ was calculated as 1.32 eV at the CI level and 1.11 eV at the MCSCF level.[359] It is anticipated that the experimental $D_e \geq 1.5$ eV for removing Ga from $GaAs_2$. Note that the theoretical $D_e(Ga_2$–Ga) is 1.4 eV (cf. section V.A). Consequently, $D_e(As_2$–Ga) and $D_e(Ga_2$–Ga) are comparable.

The Ga–As bond length (MRSDCI) of 2.76 Å in the $^2B_2$ state is comparable to the CASSCF/FOCI bond length of 2.64 Å for the $^3\Sigma^-$ ground state of GaAs obtained by Balasubramanian.[359] However, considering that this bond length is 0.09 Å longer than the experimental value, a corresponding correction should be applied for $GaAs_2$ (see section IV.A). The As–As bond length of the $^2B_2$ state (2.20 Å) is comparable to the As–As bond length of 2.16 Å for the $^1\Sigma_g^+$ ground state of As_2 obtained earlier.[159] The As–As bond length of the $^2A_1$ state is 2.32 Å, which is much larger, implying weakening of the As–As bond in the $^2A_1$ state. The $^2B_2$ state exhibits enhanced As–As bonding and is more stable than the $^2A_1$ state, which shows greater Ga–As bonding. This is consistent with earlier theoretical

TABLE 68. Mulliken Population Analysis of the Natural Orbitals of the MRSDCI Wave Functions of the $^2B_2$ and $^2A_1$ States of GaAs$_2$[a]

| State | Net Population | | | | | | Gross Population | | | | | | Overlap[c] |
| | Total | | | | | | Total | | | | | | |
	Ga	As[b]	Ga(s)	Ga(p)	As(s)	As(p)	Ga	As[b]	Ga(s)	Ga(p)	As(s)	As(p)	
$^2B_2$	2.43	10.23	2.01	0.33	4.11	6.24	2.60	10.40	1.84	0.64	3.76	6.40	0.34
$^2A_1$	2.22	9.92	1.53	0.56	4.06	5.92	2.64	10.35	1.52	0.99	3.73	6.33	0.86

[a] From ref 395. [b] As population refers to the populations of both As atoms. [c] Overlap population between Ga and both As atoms.

calculations (see section III) that have shown that D_e-(As$_2$) > D_e(GaAs) > D_e(Ga$_2$). Consequently, among the smaller clusters, the states that exhibit greater As–As bonding appear to be more stable. It was predicted[359] that the order of stabilities for the trimers of formula Ga$_x$As$_y$ ($x + y = 3$) should be AE(As$_3$) > AE(GaAs$_2$) > AE(Ga$_2$As) > AE(Ga$_3$), where AE represents the atomization energy. Balasubramanian's theoretical results on those species and diatomics containing Ga and As were used by Reents[360] in the interpretation of chemical etching of GaAs.

Table 67 shows the leading configurations in the MRSDCI wave function of the $^2B_2$ and $^2A_1$ states of GaAs$_2$.[359] As seen from Table 67, the leading configurations of these two states are $1a_1^2 2a_1^2 3a_1^2 4a_1^2 1b_2^2 2b_2^1 1b_1^2$ and $1a_1^2 2a_1^2 3a_1^2 4a_1^1 1b_2^2 2b_2^2 1b_1^2$, respectively.

The $1a_1$ natural orbital of the MRSDCI wave function of the $^2B_2$ state at its equilibrium geometry was found to be predominantly composed of As 4s while the $2a_1$ orbital is mainly Ga 4s but mixes more with As 4s, 4p, and d compared to the Ga–As mixing in the $1a_1$ orbital. The $3a_1$ orbital is a mixture of bonding As(s$_1$) + As(s$_2$), As$_1$(p$_y$) – As$_2$(p$_y$) and small amounts of Ga s and Ga p$_z$. The $4a_1$ orbital was found to be a mixture of Ga(s), Ga(p$_z$), As(s) (small amount), and As$_1$(p$_z$) + As$_2$(p$_z$). The $1b_2$ orbital is predominantly As$_1$(s)–As$_2$(s) while the $2b_2$ orbital is a mixture of Ga(p$_y$) and As$_1$(p$_y$) + As$_2$(p$_y$) (p$_{y_1}$ + p$_{y_2}$) linear combination. The $1b_1$ orbital was mainly As (p$_{x_1}$ + p$_{x_2}$) a bonding orbital perpendicular to the plane while the $2b_1$ orbital is mixture of Ga(p$_x$) and As (p$_{x_1}$ + p$_{x_2}$). The coefficients of the d functions were found to be nonnegligible for the $2b_2$, $4a_1$, and $2b_1$ orbitals.

Table 68 depicts the net, gross, and overlap Mulliken populations of the MRSDCI natural orbitals of the $^2B_2$ and $^2A_1$ states of GaAs$_2$. As seen from Table 68, the $^2B_2$ state exhibits a greater total net population and less overlap population (between Ga and the two As atoms) than the $^2A_1$ state. Thus, the $^2A_1$ state shows enhanced Ga–As bonding compared to the $^2B_2$ state. This is consistent with the earlier qualitative analysis of the natural orbitals of the two states. Further, the $^2B_2$ and $^2A_1$ states are ionic (see Table 68).

C. Ge$_3$ and Si$_3$

Pacchioni and Koutecky[361] have investigated the low-lying states of Ge$_n$ (n = 3–7) using a simple Hartree–Fock single-configuration SCF followed by single-reference CI calculations. Related Si$_n$ clusters have also been studied theoretically by many authors.[362–368] Calculations at the HF/MP4 level were made by Raghavachari on Si$_n$ (n = 3–10).[363,364] Balasubramanian[367] made high-level CASSCF/MRSDCI calculations em-

TABLE 69. Geometries and Energy Separations of the Low-Lying States of Ge$_3$[a]

state	r_e (Å)	θ_e (°)	E (kcal/mole)
$^1A_1$	2.39		0
$^1\Sigma_g^+$	2.40	180.0	1.8
$^3A_2'$	2.64	60°	7.5

[a] Theoretical constants are from ref 361. Bond distances are assumed to be the same in these SCF/CI calculations, although for the $^1A_1$ state, the base must have different bond lengths compared to the sides. Thus, the geometries are not fully optimized.

ploying a large McLean–Chandler all-electron Gaussian basis sets for Si$_3$ and Si$_3^+$. Comparable calculations were also made by Balasubramanian[368] on Si$_4$ using RECPs.

Pacchioni and Koutecky[361] found basically two very low lying electronic states for Ge$_3$ of $^1A_1$ and $^3A_2'$ symmetry analogous to Si$_3$.[367] The geometries and energy separation for the electronic states of Ge$_3$ are shown in Table 69. Balasubramanian's CASSCF/MRSDCI results for Si$_3$ and Si$_3^+$ are shown in Table 70.[367] Potential energy curves for the two lowest electronic states of Si$_3$ obtained by Balasubramanian[367] are shown in Figure 37.

As seen from the two tables, both Si$_3$ and Ge$_3$ form a $^1A_1$ ground state with an equilibrium geometry of an isosceles triangle. The $^3B_2$ state forms an equilateral triangular structure with a longer Ge–Ge bond length. The $^1A_1$–$^1\Sigma_g^+$ separation calculated by Pacchioni and Koutecky[361] (1.8 kcal/mol) appears to be a bit too low compared to the corresponding separation of 18 kcal/mol for Si$_3$ calculated by Balasubramanian using the CASSCF/FOCI method.[367]

Table 71 shows the absolute energies in hartrees for the $^1A_1$ and $^3B_2$ states using two sets of d-type polarization functions. The ground state at this level is a $^1A_1$ state. The final $^1A_1$–$^3A_2'$ separation of Si$_3$ is 4.6 kcal/mol. The earlier calculations by Grev and Schaefer[365] had shown how sensitive this separation is to the basis set and electron correlation effects. A SCF/SDCI with double-ζ + 1d set gave a $^3A_2'$ as the ground state of Si$_3$, which led Grev and Schaefer[365] to predict that there are two nearly degenerate isomers for Si$_3$.

D. In$_3$

Feng and Balasubramanian[369] carried out complete active space MCSCF followed by multireference singles + doubles CI calculations which included up to 177 000 configurations on seven low-lying electronic states of

TABLE 70. Properties of the Low-Lying States of Si_3[a]

State	Method	$r(Å)$[b]	θ	E (Hartrees)
$^1A_1$	4410-CAS[a]	2.17	79.6	-866.71138
$^1A_1$	5410-CAS	2.19	79.6	-866.72846
$^1A_1$	RFOCI	2.19	79.6	-866.78532
$^1A_1$	MRSOCI	2.19	79.6	-866.903244
$(^3A_2)\ ^3B_2$	4410-CAS	2.29	60.0	-866.70253
$(^3A_2)\ ^3B_2$	5410-CAS	2.30	60.0	-866.72333
$(^3A_2)\ ^3B_2$	RFOCI	2.30	60.0	-866.77734
$(^3A_2)\ ^3B_2$	MRSOCI	2.30	60.0	-866.897436
$^1B_2$	4410-CAS	2.28	60.0	-866.68631
$^1B_2$	RFOCI	2.28	60.0	-866.77008
$^3A_2$	4410-CAS	2.41	60.0	-866.67245
$^3A_2$	RFOCI	2.41	60.0	-866.75448
$^3B_1$	4410-CAS	2.41	60.0	-866.67010
$^3B_1$	RFOCI	2.41	60.0	-866.75196
$^1A_2$	4410-CAS	2.42	60.0	-866.65581
$^1A_2$	RFOCI	2.42	60.0	-866.73914
$^1B_1$	4410-CAS	2.41	60.0	-866.65417
$^1B_1$	RFOCI	2.41	60.0	-866.73603
$^3B_2$	4410-CAS	2.24	160.5	-866.65614
$^3B_2$	RFOCI	2.24	160.5	-866.72596
$^1A_1$	4410-CAS	2.17	180.0	-866.68027
$^1A_1$	RFOCI	2.17	180.0	-866.75638
$^3B_2$	4410-CAS	2.24	180.0	-866.65506
$^3B_2$	RFOCI	2.24	180.0	-866.52533

[a] $ijkl$-CAS stands for a CASSCF calculation in which i a_1 orbitals, j b_2 orbitals, k b_1 orbitals, and l a_2 orbitals were included in the active space. From ref 367. [b] R refers to the two equal distances of the isosceles triangle.

TABLE 71. Properties of the $^1A_1$ and $^3B_2$ ($^3A_2'$) States of Si_3 Calculated with Two Sets of d-Type Functions[a]

State	Method	$r(Å)$[b]	θ	E (Hartrees)
$^1A_1$	5410-CAS	2.19	79.6	-866.75067
$^1A_1$	RFOCI	2.19	79.6	-866.82526
$^3B_2$	5410-CAS	2.30	60.0	-866.74408
$^3B_2$	RFOCI	2.30	60.0	-866.81959

[a] From ref 367. [b] R refers to the two equal distances of the isosceles triangle.

TABLE 72. Geometries of Energies of the Bent Electronic States of In_3[a]

	CASSCF				MRSDCI		
state	θ (deg)	r[b] (Å)	E[c] (eV)	state	θ (deg)	r[b] (Å)	E[c] (eV)
$^4A_2$	75.2	2.97	0.0	$^4A_2$	71.04	2.95	0.0
$^4B_1$	54.8	3.25	0.03	$^4B_1$	55.2	3.12	0.01
$^2B_1$	47.6	3.37	0.07	$^2B_1$	48.9	3.31	0.11
$^2A_1$	49.6	3.60	0.28	$^4B_2$	60.0	3.29	0.35
$^4B_2$	58.4	3.39	0.35	$^2A_1$	51.0	3.49	0.45
$^2B_2$	74.3	3.17	0.37	$^2B_2$	74.4	3.04	0.45

[a] From ref 369. [b] The two equal sides of the isosceles triangle; θ = apex angle. [c] Zero energy for CASSCF is -5.513007 hartrees; zero energy for MRSDCI is -5.609780 hartrees. The zero energy is for the $^4A_2$ ground state at the reported geometry.

Figure 37. Potential energy curves for the $^1A_1$ and $^3B_2$ states of Si_3 (reprinted from ref 367; copyright 1986 Elsevier Science Publishers B.V.).

In_3.[194] They employed a valence (3s3p1d) basis set used earlier for In_2 together with 3e-RECPs for the In atom. In addition, spin–orbit effects for the low-lying states of In_3 were obtained. Complete bending potential energy surfaces as a function of bending angle were also obtained.[369]

Table 72 shows the equilibrium geometries of the bent states of In_3 and their energy separations at both the CASSCF and MRSDCI levels of theory. Figure 38 shows the optimized MRSDCI equilibrium geometries of the electronic states of In_3. Figure 39 shows the actual bending potential energy surfaces for several electronic states obtained with the CASSCF method. As seen from Table 72, the equilibrium geometries predicted by CASSCF calculations are not substantially different from the MRSDCI geometries. The bond lengths changed at most by 0.13 Å. The bond angles changed at most by 4° at the MRSDCI level of theory compared to the zeroth-order CASSCF level. Table 73 shows the equilibrium geometries and the energy separations of the linear electronic states of In_3.

MRSDCI calculations predicted two nearly degenerate states of $^4A_2$ and $^4B_1$ symmetry as candidates for the ground state. The equilibrium geometries of both $^4A_2$ and $^4B_1$ are isosceles triangles, although $^4B_1$ is very acute. Note that the linear limit of the $^4A_2$ ($^4\Sigma_u^-$) state is only 0.07 eV above the ground state.
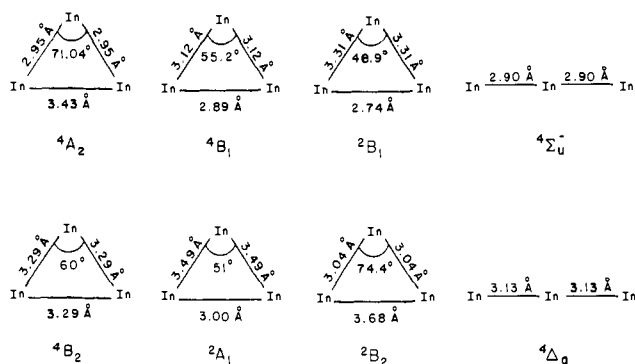
Figure 38. Equilibrium geometries of the low-lying states of In_3 (reprinted from ref 369; copyright 1989 Elsevier Science Publishers, B.V.).
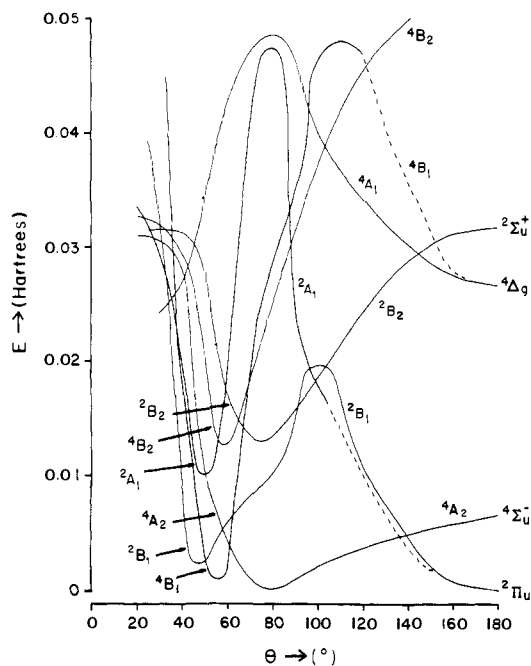

Figure 39. Bending potential energy curves for the low-lying states of In_3 (reprinted from ref 369; copyright 1989 Elsevier Science Publishers, B.V.).

The geometry of the $^2B_1$ state is acute and thus the In–In bond lengths for the two sides of the isosceles triangle are large. As seen from Figure 38, both $^4B_1$ and $^2B_1$ have short In–In bond lengths at the base of the isosceles triangle. Hence, the $^4B_1$, $^2B_1$, and $^2A_1$ electronic states exhibited enhanced bonding at the base while for the other states, bond strengths at the equal sides of the isosceles triangles are greater.

Table 74 shows the effect of $4d^{10}$ shells on the geometries of the low-lying states of In_3. As seen from Table 74, the effect of the $4d^{10}$ shell on the bond lengths is <1.3% and that on the bond angles is <0.5° for the three electronic states that were compared by Feng and Balasubramanian.[369]

The energy separations of the various electronic states are quite sensitive to higher order correlations. As seen from Table 72, the $^2A_1$ and $^4B_2$ states switch order between CASSCF and MRSDCI calculations. The energy separations of most of the excited states increase at the MRSDCI level of theory, implying stabilization of the ground state.

The atomization energy, i.e., the energy for the process $In_3 \rightarrow 3In$, was calculated through a long-distance

TABLE 73. Properties of the Linear Electronic States of In_3[a]

| | CASSCF | | | MRSDCI | |
State	R (Å)	E (eV)	State	R (Å)	E (eV)
$^2\Pi_u$	3.07	-0.02	$^4\Sigma_u^-$	2.90	0.07
$^4\Sigma_u^-$	2.90	0.18	$^2\Pi_u$	3.05	0.37
$^4\Delta_g$	3.14	0.73	$^4\Delta_g$	3.13	0.77
$^2\Sigma_u^+$	2.95	0.87	$^2\Sigma_u^+$	2.92	0.85
$^4\Pi_g$	2.85	1.29	$^4\Pi_g$	2.90	1.13

[a] From ref 369.

TABLE 74. Effect of Including the $4d^{10}$ Core in the CASSCF Calculations of the Electronic States of In_3[a]

| | with $4d^{10}$ | | without $4d^{10}$ | |
state	R_e (Å)	θ_e (deg)	R_e (Å)	θ_e (deg)
$^4A_2$	3.01	75.3	2.97	75.2
$^2B_1$	3.36	49.1	3.37	47.6
$^2A_1$	3.62	49.7	3.60	49.6

[a] From ref 369.

TABLE 75. Dipole Moments of the Electronic States of In_3 with Isosceles Triangular Geometry[a]

state	μ (0)[b]
$^4A_2$	-0.48
$^4B_1$	0.51
$^2B_1$	0.95
$^2A_1$	0.80
$^2B_2$	-0.65

[a] From ref 369. [b] Positive polarity means the positive charge is on the apex atom of the isosceles triangle.

calculation ($R = 8.0$ Å) for the linear $^4A_2$ state. The MRSDCI calculations yielded an atomization energy of 48 kcal/mol for the ground state of In_3.[369]

Table 75 shows the MRSDCI dipole moments for the electronic states of In_3 at their equilibrium geometries. As seen from Table 75, all the isosceles triangular structures have large dipole moments. The $^4A_2$ and $^2B_2$ states have positive charges at the base atoms while all other isosceles triangular states have positive charges on the apex atom of the triangle.

Figure 39 shows the bending potential energy surfaces for the various electronic states of In_3 obtained with the CASSCF method. The $^4A_2$ surface contains a bent minimum which correlated into the $^4\Sigma_u^-$ linear state. The $^4B_1$ surface is very narrow near θ_e, goes through a barrier, and correlates with the $^4\Delta_g$ linear state.

Table 76 shows the coefficients of the important configurations in the CASSCF wave functions of the

Error

An error occurred while processing this page. See the system log for more details.

TABLE 77. Mulliken Population Analyses for the Electronic States of In$_3$[a]

state	Gross								Overlap[d]
	M_1[b]	M_2[c]	$M_1(s)$	$M_2(s)$	$M_1(p)$	$M_2(p)$	$M_1(d)$	$M_2(d)$	
$^4A_2$	3.105	5.896	1.728	3.616	1.326	2.192	0.052	0.086	0.686
$^4B_1$	2.899	6.100	1.821	3.524	1.034	2.484	0.044	0.094	0.402
$^2B_1$	2.906	6.094	1.860	3.478	0.995	2.526	0.051	0.090	0.310
$^4B_2$	3.001	5.998	1.839	3.686	1.122	2.238	0.040	0.076	0.312
$^2A_1$	2.914	6.086	1.877	3.654	0.997	2.344	0.040	0.086	0.212
$^2B_2$	3.058	5.942	1.786	3.704	1.217	2.146	0.054	0.092	0.398
$^4A_1$	2.937	6.064	1.770	3.688	1.125	2.310	0.041	0.066	0.474
$^4\Sigma_u^-$	3.293	5.707	1.498	3.448	1.638	1.973	0.156	0.286	0.959

[a] From ref 369. [b] Apex atom. [c] The two base atoms. [d] Overlap between the apex atom and the two base atoms.

in the properties of Ga$_3$ and In$_3$ seems to arise from both relativistic effects and the fact that the atomic energy separations are lower for In compared to Ga.[134] The ^4P state arising from $4s4p^2$ is 38000 cm^{-1} above for Ga while the corresponding state ($5s5p^2$) is 35000 cm^{-1} above the ground state for In.[134]

A major difference between the electronic states of Ga$_3$ and In$_3$ is in the ionicity of the metal–metal bonding. The dipole moments of the electronic states of In$_3$ were found to be considerably larger compared to the corresponding states of Ga$_3$. For example, the dipole moment of the $^2A_1$ state of Ga$_3$ was found to be 0.02 D while the corresponding state of In$_3$ has a dipole moment of 0.80 D. Similarly, the dipole moment of the $^4A_2$ state of Ga$_3$ is 0.17 D, while the corresponding state of In$_3$ has a dipole moment of –0.48 eV. This trend is consistent with the greater metallic character of the (more electropositive) In atom compared to the gallium atom.

E. Sn$_3$

The electronic structure of tin clusters is a topic of considerable importance from both fundamental and applied standpoints.[370] At room temperature in the solid state Sn is metallic, but at low temperature it exhibits a semiconducting crystallographic modification with Ge structure.[370] The mass spectra of Sn$_n$ clusters have been recorded by Martin and Schaber.[370] The mass spectrum of Sn$_x^+$ exhibited a gradual decrease in intensity for x = 1–13, and the x = 14 peak was almost absent; however, for x = 15 and 16, the intensity increases. For the Ge$_x^+$ clusters, the peak with x = 13 is the low-intensity peak. All the clusters exhibited enhanced stabilities for x = 6, 10. Further, Martin and Schaber[370] showed that Ge$_{14}^+$ is quite stable while Sn$_{14}^+$ is unstable.

Balasubramanian[371] studied the low-lying electronic states of equilateral triangular, isosceles triangular, and

TABLE 78. Properties of the Low-Lying Electronic States of Sn$_3$[a]

State	Method	r_e (Å)[b]	θ	E[c]
$^1A_1$	5410-CAS	2.757	85°	-204.080 192
$^1A_1$	4310-CAS	2.728	85°	-204.038 657
$^1A_1$	MRSDCI	2.757	85°	-204.158 123
$^1A_1$	POLCI	2.757	85°	-204.124 953
$^3A_2'$ ($^3B_2$)	5410-CAS	2.96	60°	-204.074 416
$^3A_2'$ ($^3B_2$)	4310-CAS	2.944	60°	-204.035 962
$^3A_2'$ ($^3B_2$)	MRSDCI	2.96	60°	-204.148 786
$^3A_2$	4310-CAS	3.077	60°	-204.029 980
$^1B_2$	4310-CAS	2.927	60°	-204.022 106
$^1A_2$	4310-CAS	3.088	60°	-204.014 320
$^3B_1$	4310-CAS	3.073	60°	-204.028 423
$^1B_1$	4310-CAS	3.084	60°	-204.012 746
$^1\Sigma_g^+$ ($^1A_1$)	5410-CAS	2.714	180°	-204.067 007
$^3B_2$	5410-CAS	2.792	180°	-204.048 230
3 Sn (^3P)	SCF			-203.986 119
3 Sn (^3P)	SOCI			-204.045 293
$^1A_1$	5410-CAS	7.500	130°	-203.991 671
$^1A_1$	POLCI	7.500	130°	-204.000 095

[a] From ref 371. [b] Refers to the two equal distances of the isosceles triangle for the triangular structure. For the linear structure this refers to the Sn–Sn bond length. MRSDCI calculations for the $^1A_1$ and $^3B_2$ states were carried out at the 5410-CAS-optimized geometries. [c] Energies are in hartrees. 1 hartree = 27.21 eV.

linear configurations of Sn$_3$ employing a complete active space MCSCF followed by multireference singles and
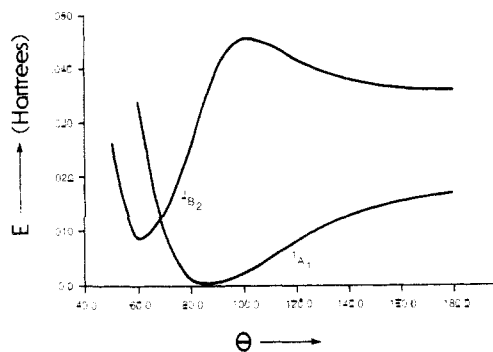
Figure 40. Potential energy surfaces of Sn_3 (reprinted from ref 371; copyright 1986 American Institute of Physics).
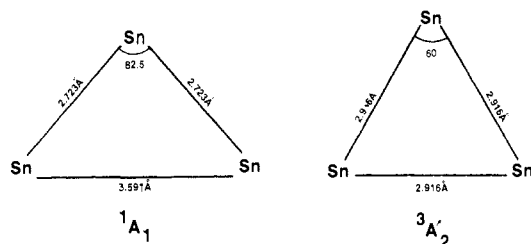

Figure 41. Equilibrium geometries of the low-lying states of Sn_3 (reprinted from ref 371; copyright 1986 American Institute of Physics).

TABLE 79. Properties of Sn_3 Obtained with a 2d Basis[a]

Method	State	r_e (Å)	θ_e	E
5410-CAS	$^1A_1$	2.723	82.5	-204.091 872
5410-CAS	$^3A_2'$	2.916	60°	-204.088 241
MRSOCI	$^1A_1$	2.723	82.5	-204.213 709
MRSOCI	$^3A_2'$	2.916	60°	-204.207 492

[a] From ref 371.

doubles CI calculations that included up to 228 250 configurations. He employed relativistic effective potentials for the tin atom with the $d^{10}s^2p^2$ outer shell as the valence shell. A valence + polarization Gaussian (3s3p2d) basis set was employed for the tin atom.

Table 78 depicts the properties of several electronic states of Sn_3 obtained with many methods employing a (3s3p1d) basis set.[371] As seen from Table 78, two nearly degenerate structures exist for Sn_3. The first structure is an isosceles triangle with an apex angle of 85° and is the minimum of the $^1A_1$ state. The other structure is an equilateral triangular structure which is a minimum of the $^3B_2$ state. The splitting of these two states was calculated as 3.6 kcal/mol at the 5410-CAS level and 5.9 kcal/mol at the MRSDCI level.[371]

The energy separation between the bent $^1A_1$ structure and the $^1\Sigma_g^+$ linear structure was found to be about 8.3 kcal/mol.[371] Consequently, Sn_3 resembles Si_3 in possessing two nearly degenerate equilibrium geometries (see section V.C).

The bending potential energy surfaces of the two nearly degenerate states, viz., $^1A_1$ and $^3B_2$, are shown in Figure 40. As seen from Figure 40, the $^3B_2$ state has a barrier at about $\theta = 100°$ and a weakly bound second minimum at near-linear geometry. This was attributed to an avoided crossing by Balasubramanian.[371] This is reminescent of the potential energy surfaces of Si_3 (see Figure 37).

The properties of the $^1A_1$ and $^3B_2$ states were also calculated with a (3s3p2d) basis (Table 79). As seen from Table 79, the uncontraction of the most diffuse d function shrinks the bond length for the $^1A_1$ and $^3B_2$ states by about 0.04 Å. The actual geometries of these two states calculated this way are shown in Figure 41. The $^1A_1-^3A_2'$ splitting was calculated as 2.3 kcal/mol at the CASSCF and 3.9 kcal/mol at the MRSDCI levels. Consequently, this splitting was found to decrease in the larger basis set.

The atomization energy of Sn_3, i.e., the energy for $Sn_3 \rightarrow 3Sn$, was calculated by the MRSDCI method in the absence of spin–orbit interaction as 3.07 eV or 71 kcal/mol. A POLCI calculation carried out by setting the Sn–Sn bond lengths to 7.5 Å gave an atomization energy of 3.4 eV. The POLCI value should be considered more accurate since in the MRSDCI method, the energy of the individual atoms (SDCI) was compared with the MRSDCI energy of the molecule. Thus, the value of 71 kcal/mol is not correlation consistent and is only a lower bound. The spin–orbit interaction should decrease the atomization energy of Sn_3. This is because the contribution of spin–orbit interaction for the closed-shell $^1A_1$ state is small. However, the spin–orbit splitting of the ^3P state of the Sn atom is somewhat larger. The RCI calculations by Balasubramanian and Pitzer[201] indicated that the Sn $^3P_0$ state was lowered by 0.33 eV with respect to the ^3P state. Thus, the overall lowering of the three $^3P_0$ states of the Sn atom is 0.99 eV. It was assumed by Balasubramanian that the contribution of spin–orbit interaction for the closed-shell $^1A_1$ isosceles triangular structure is zero. Thus, applying a correction of 0.99 eV to the atomization energy, Balasubramanian[371] obtained a lower bound of 2.4 eV or 55.3 kcal/mol. The dissociation energy of Sn_2 was calculated[201] as 1.86 eV in the presence of spin–orbit interaction. It is thus evident that Sn_3 is at least 0.5 eV more stable than the dimer.

The effect of spin–orbit interaction should be interesting on the PES of Sn_3. It would split the $^3B_2$ state into A_1, B_1, and A_2 components in the C_{2v}^2 double group. For the equilateral triangle, $^3A_2'$ is split into A_1' and E'' representations in the D_{3h}^2 double group. The $^1A_1$ isosceles structure correlates into the A_1 representation in the double group. As seen from Figure 40, the bending potential energy surfaces of the $^1A_1$ and $^3B_2$ states cross at $\theta = 70°$. Thus, the corresponding A_1 components in the presence of spin–orbit interaction would undergo avoided crossing. In the presence of spin–orbit interaction, the PES of the A_1 component may thus contain shoulder and minimum or double minima (one at $\theta = 60°$ and the other at $\theta = 85°$) separated by a small barrier.

The electronic structure of Sn_3 resembles that of Si_3 and Ge_3 in many ways. For Si_3 (see section V.C) also there are two nearly degenerate structures ($^1A_1$ and $^3A_2'$). The splitting between these two states was found to be about 3.6 kcal/mol. The atomization energy of Si_3 is larger as expected. Relativistic effects are, however, negligible for Si_3.

Table 80 shows the coefficients of the leading configurations in the CASSCF of the various electronic

TABLE 80. CASSCF/CI Wave Functions of the Low-Lying States of Sn₃ᵃ

Coefficient	Configuration

$^1A_1$ (θ = 95°)

Coefficient	$1a_1$	$2a_1$	$3a_1$	$4a_1$	$5a_1$	$1b_2$	$2b_2$	$3b_2$	$4b_2$	$1b_1$
0.921	2	2	2	0	0	2	2	0	0	2
-0.149	2	2	2	2	0	2	0	0	0	2
+0.137	1	2	2	1	0	2	1	0	1	2
-0.128	0	2	2	0	0	2	2	0	2	2
-0.121	0	2	2	2	0	2	2	0	0	2

$^1A_1$ (θ = 180°)

Coefficient	$1a_1$	$2a_1$	$3a_1$	$4a_1$	$5a_1$	$1b_2$	$2b_2$	$3b_2$	$4b_2$	$1b_1$
0.903	2	2	2	0	0	2	2	0	0	2
-0.353	2	2	0	0	0	2	2	2	0	2
-0.144	2	2	1	1	0	2	1	1	0	2
-0.104	2	2	2	2	0	2	0	0	0	2

$^3B_2$ (θ = 60°)

Coefficient	$1a_1$	$2a_1$	$3a_1$	$4a_1$	$5a_1$	$1b_2$	$2b_2$	$3b_2$	$4b_2$	$1b_1$
0.949	2	2	2	1	0	2	1	0	0	2

$^3B_2$ (θ = 130°)

Coefficient	$1a_1$	$2a_1$	$3a_1$	$4a_1$	$5a_1$	$1b_2$	$2b_2$	$3b_2$	$4b_2$	$1b_1$
0.953	2	2	1	0	0	2	2	1	0	2
-0.156	2	2	1	2	0	2	0	1	0	2
+0.096	2	2	1	1	1	2	1	0	0	2

$^1B_2$ (θ = 60°)

Coefficient	$1a_1$	$2a_1$	$3a_1$	$4a_1$	$1b_2$	$2b_2$	$3b_2$	$1b_1$
0.982	2	2	2	1	2	1	0	2
0.117	2	2	2	1	1	1	1	2

$^3A_2$ (θ = 60°)

Coefficient	$1a_1$	$2a_1$	$3a_1$	$4a_1$	$1b_2$	$2b_2$	$3b_2$	$1b_1$
0.972	2	2	2	2	2	1	0	1
-0.171	2	0	2	2	2	1	2	1

$^3B_1$ (θ = 60°)

Coefficient	$1a_1$	$2a_1$	$3a_1$	$4a_1$	$1b_2$	$2b_2$	$3b_2$	$1b_1$
0.975	2	2	2	1	2	2	0	1
-0.146	2	2	2	1	2	0	2	1
+0.113	2	2	2	1	2	1	1	1

$^1B_1$ (θ = 60°)

Coefficient	$1a_1$	$2a_1$	$3a_1$	$4a_1$	$1b_2$	$2b_2$	$3b_2$	$1b_1$
0.969	2	2	2	1	2	2	0	1
0.155	2	2	2	1	2	1	1	1
-0.153	2	2	2	1	2	0	2	1

$^1A_2$ (θ = 60°)

Coefficient	$1a_1$	$2a_1$	$3a_1$	$4a_1$	$1b_2$	$2b_2$	$3b_2$	$1b_1$
0.974	2	2	2	2	2	1	0	1
-0.176	2	2	2	0	2	1	2	1

ᵃFrom ref 371.

states of Sn₃. As seen from Table 80, the CASSCF wave function of the $^1A_1$ state contains eight configurations with coefficients ≥0.07, although all of these are not shown in Table 80. The leading configuration has a coefficient of 0.921. For the linear $^1A_1$ state ($^1\Sigma_g^+$), a number of configurations contribute to the CASSCF. The CASSCF wave function of the $^3B_2$ state contains four configurations with coefficients ≥0.07. The leading configuration has a coefficient of 0.949. Thus, corre-
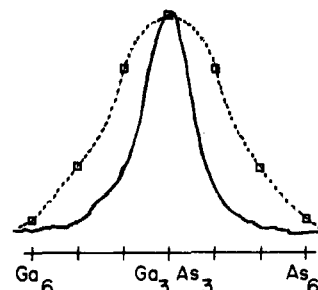
Figure 42. Experimental distribution of six-atom clusters of GaAs (reprinted from ref 97; copyright 1986 American Institute of Physics). The dotted line represents a binomial distribution while the solid line is the observed distribution.

lation effects appeared to be more important for the $^1A_1$ state than the $^3B_2$ state.

The bond lengths of the two equal sides of the isosceles triangle (2.723 Å) are shorter than the bond lengths for the $^3A_2'$ structure (see Figure 40). This implies double bonds along the sides of the isosceles triangle. The linear ($^1\Sigma_g^+$) structure was found to exhibit multiple bonding. The $^3A_2'$ structure can be regarded as a resonance hybrid of three equivalent structures, each having one double bond. Thus, the bond lengths for the $^3A_2'$ equilateral structure are a bit longer than the two equal sides of the isosceles triangle. The bond lengths obtained with the 2-d basis set are about 0.03 Å shorter than the corresponding values obtained using a 1-d basis set. This was attributed by Balasubramanian[371] primarily to a polarization effect resulting from the uncontraction of the most diffuse d function.

VI. Enumeration of the Isomers of Gallium Arsenide Clusters (Ga$_m$As$_n$)

As mentioned in section IV.A, Smalley and co-workers[97] generated clusters of GaAs of general formula Ga$_m$As$_n$ by laser evaporation of a GaAs crystal. The mass analysis of the larger clusters revealed a binomial distribution while the smaller clusters deviated from binomial distributions to a large extent. For example, the observed distribution of six-atom clusters is shown in Figure 42.

Balasubramanian[372] enumerated the isomers of Ga$_m$As$_n$ containing up to ten atoms and icosahedral clusters using Pólya's theorem[378] and partition generation techniques. The use of Pólya's theorem and its ramifications to many chemical applications can be found in Balasubramanian's papers.[373-377] Generating functions obtained in this way for various polyhedra together with bond strength criterion facilitated interpretation of the experimentally observed distribution of Ga$_m$As$_n$ clusters. In this section, we outline the formalism to enumerate isomers of Ga$_m$As$_n$ and review the results obtained by Balasubramanian[372] for the distribution of these clusters.

Balasubramanian[372] constructed the most interesting polyhedra with fewer than 10 vertices using the partition counting method. The construction of polyhedra of various types can be simplified by considering the possible equivalence classes of the vertices of polyhedra. For example, all 5 vertices are equivalent for a pentagon while for a square pyramid the apex vertex is not equivalent to the base vertices. Similarly, the trigonal

bipyramid has two equivalence classes of vertices (the axial and equatorial vertices).

The possible equivalence classes of n objects correspond to the possible partitions of an integer n. For example, the possible partitions of the integer 5 are 5, $4 + 1, 3 + 2, 3 + 1 + 1, 2 + 2 + 1, 2 + 1 + 1 + 1$, and $1 + 1 + 1 + 1 + 1$. The number of partitions of an integer n into p parts (P_n^p) is generated by the coefficient of x^n in the following expression:

$$F(x) = x^p(1 - x)^{-1}(1 - x^2)^{-1}...(1 - x^p)^{-1}$$

The P_n^ms are also given by the following recursive relation:

$$P_{n+m}^m = P_n^1 + P_n^2 + P_n^3 + ... + P_n^m$$

If each partition of n is conceived as a partitioning of the vertices of a polyhedron, then possible polyhedra for that partition of vertices could be constructed by intuitive arguments. To illustrate, possible polyhedra for the partition 4 of four vertices are the tetrahedron and rhombus. Note that the square is a special case of the rhombus. For the partition $2 + 2$, one could assign linear or trapezoidal structures. The 1^n partition corresponds to a totally distorted structure. It may not be possible to find the structure for some partitions or the structure would not be of sufficient interest. The concept of ligand partition to construct chirality polynomials has been used by King.[379,380] King and Rouvray[381] also used Pólya's[378] theorem for the enumeration isomers of polyhedral boron clusters.

The cycle index of a group G is defined as

$$P_G = \frac{1}{|G|} \sum_{g \in G} x_1^{b_1} x_2^{b_2}...x_n^{b_n}$$

where $x_1^{b_1} x_2^{b_2}...x_n^{b_n}$ is said to be a cycle representation for an element g in the group G, if g generates b_1 cycles of length 1, b_2 cycles of length 2, ... b_n cycles of length n upon application of g on the set of vertices of the polyhedron under consideration and where $|G|$ is the number of all elements in the group. Pólya's theorem[378] has been applied before for regular polyhedra such as the tetrahedron, octahedron, etc. and for enumerating isomers of inorganic complexes (see ref 373 for a review).

Pólya's theorem[378] yields a generating function for the various possible isomers. If w_1 and w_2 denote the weights for gallium and arsenic atoms, respectively, then a generating function for enumeration that is a polynomial in w_1 and w_2 can be obtained by the following substitution in the cycle index:

$$GF = P_G(x_k \rightarrow w_1^k + w_2^k)$$

where the arrow stands for replacing every x_k in P_G by $w_1^k + w_2^k$.

The group G is the rotational subgroup of the point group of the polyhedron if enantiomers need to be enumerated. Pólya's theorem can be illustrated with a cube. The cycle index of the rotational subgroup of the cube is as follows:

$$P_G = \frac{1}{24}[x_1^8 + 6x_4^2 + 9x_2^4 + 8x_1^2 x_3^2]$$

Substituting for every x_k in the above expression by $w_1^k + w_2^k$, one obtains

$$GF = \frac{1}{24}[(w_1 + w_2)^8 + 6(w_1^4 + w_2^4)^2 + 9(w_1^2 + w_2^2)^4 + 8(w_1 + w_2)^2(w_1^3 + w_2^3)^2]$$
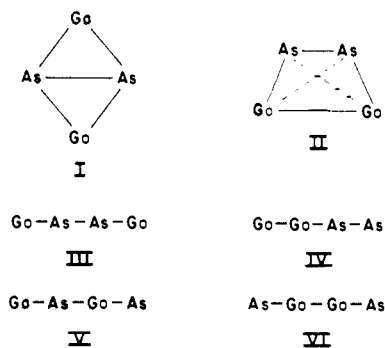
Figure 43. Possible isomers of Ga_2As_2 (reprinted from ref 372; copyright 1988 Elsevier Science Publishers B.V.).

which upon simplification yields

$$w_1^8 + w_1^7 w_2 + 3w_1^6 w_2 + 3w_1^5 w_2^3 + 7w_1^4 w_2^4 + 3w_1^3 w_2^5 + 3w_1^2 w_2^6 + w_1 w_2^7 + w_2^8$$

The coefficient of $w_1^m w_2^n$ in the above expression enumerates the number of isomers of $Ga_m As_n$ that have cubic polyhedral structure. Thus, there would be one Ga_8 isomer, one Ga_7As isomer, three Ga_6As_2 isomers, etc., if it had a cubic structure. Balasubramanian[372] constructed such polynomials for different polyhedral forms containing up to 10 vertices.

Table 81 shows the vertex partitions, the polyhedral forms, the point group of the polyhedron, and the corresponding generating functions obtained by Balasubramanian.[372] All possible vertex partitions are not shown in Table 81. The reason is that vertex partitions such as 1^n correspond to a totally distorted unsymmetrical form or for some vertex partitions there are no interesting polyhedra. The only polyhedron with 12 vertices considered by Balasubramanian[372] was an icosahedron. The actual probable polyhedral form for a given isomer would be determined by many factors such as electron counts, stability criterion, bond lengths vibronic (Jahn–Teller) distortions, imaginary vibrational frequencies, etc. The weight w_1 in Table 81 corresponds to the gallium atom while the weight w_2 stands for the arsenic atom. The coefficient of $w_1^m w_2^n$ enumerates the number of isomers of the GaAs cluster with the formula $Ga_m As_n$.

As seen from Table 78, there are no isomers for the tetrahedral clusters as expected. The rhombus, trapezoidal, and linear forms of four-atom clusters exhibit isomerism to the contrary. There exist two possible isomers for Ga_2As_2 with a rhombus structure while there are four isomers for the trapezoidal form. However, the actual bond length considerations predict that the rhombus structure is favored if the Ga atoms are diagonally across each other and a trapezoidal structure is preferred if the gallium atoms are next to each other. The two isomers of Ga_2As_2 together with the isomers for the linear Ga_2As_2 are shown in Figure 43. Since the As–As bond length is much shorter than the Ga–Ga bond length, the shorter side of the trapezium is occupied by the arsenic atoms while the longer side is occupied by the gallium atoms. In the rhombus structure, the As–As diagonal would be considerably shorter than the Ga–Ga diagonal.

The Ga–Ga bonding is the most favored in the trapezoidal form. Thus, both structures are probable candidates, although the actual geometry for a given electronic state would depend on spin, spatial symme-

TABLE 81. Generating Functions for the Isomers of GaAs Clusters in Various Polyhedral Forms[a]

n	P_n	G	Polyhedron	GF
4	4	T_d	Tetrahedron	$w_1^4 + w_1^3 w_2 + w_1^2 w_2^2 + w_1 w_2^3 + w_2^4$
4	4	D_{4h}	Rhombus	$w_1^4 + w_1^3 w_2 + 2w_1^2 w_2^2 + w_1 w_2^3 + w_2^4$
4	3+1	C_{3v}	Triangular pyramid	$w_1^4 + 2w_1^3 w_2 + 2w_1^2 w_2^2 + 2w_1 w_2^3 + w_2^4$
4	2+2	C_{2v}	Linear	$w_1^4 + 2w_1^3 w_2 + 4w_1^2 w_2^2 + 2w_1 w_2^3 + w_2^4$
4	2+2	C_{2v}	Trapezoid	$w_1^4 + 2w_1^3 w_2 + 4w_1^2 w_2^2 + 2w_1 w_2^3 + w_2^4$
5	5	D_{5h}	Pentagon	$w_1^5 + w_1^4 w_2 + 2w_1^3 w_2^2 + 2w_1^2 w_2^3 + w_1 w_2^4 + w_2^5$
5	4+1	C_{4v}	Square pyramid	$w_1^5 + 2w_1^4 w_2 + 3w_1^3 w_2^2 + 3w_1^2 w_2^3 + 2w_1 w_2^4 + w_2^5$
5	4+1	T_d	Tetrahedron with central atom	$w_1^5 + 2w_1^4 w_2 + 2w_1^3 w_2^2 + 2w_1^2 w_2^3 + 2w_1 w_2^4 + w_2^5$
5	3+2	D_{3h}	tbp	$w_1^5 + 2w_1^4 w_2 + 3w_1^3 w_2^2 + 3w_1^2 w_2^3 + 2w_1 w_2^4 + w_2^5$
5	3+1+1	C_{3v}	Distorted tbp	$w_1^5 + 3w_1^4 w_2 + 4w_1^3 w_2^2 + 4w_1^2 w_2^3 + 3w_1 w_2^4 + w_2^5$
5	2+2+1	C_{2v}	Polarized tbp	$w_1^5 + 3w_1^4 w_2 + 6w_1^3 w_2^2 + 6w_1^2 w_2^3 + 3w_1 w_2^4 + w_2^5$
5	2+2+1	C_{2v}	Linear	$w_1^5 + 3w_1^4 w_2 + 6w_1^3 w_2^2 + 6w_1^2 w_2^3 + 3w_1 w_2^4 + w_2^5$
5	3+1+1	C_{3v}	Capped tetrahedron	$w_1^5 + 3w_1^4 w_2 + 4w_1^3 w_2^2 + 4w_1^2 w_2^3 + 3w_1 w_2^4 + w_2^5$
6	6	D_{6h}	Hexagon	$w_1^6 + w_1^5 w_2 + 3w_1^4 w_2^2 + 3w_1^3 w_2^3 + 3w_1^2 w_2^4 + w_1 w_2^5 + w_2^6$
6	6	D_{3h}	Trigonal prism	$w_1^6 + w_1^5 w_2 + 4w_1^4 w_2^2 + 4w_1^3 w_2^3 + 4w_1^2 w_2^4 + w_1 w_2^5 + w_2^6$
6	6	D_{3d}	Trigonal antiprism	$w_1^6 + w_1^5 w_2 + 4w_1^4 w_2^2 + 4w_1^3 w_2^3 + 4w_1^2 w_2^4 + w_1 w_2^5 + w_2^6$
6	6	O_h	Octahedron	$w_1^6 + w_1^5 w_2 + 2w_1^4 w_2^2 + 2w_1^3 w_2^3 + 2w_1^2 w_2^4 + w_1 w_2^5 + w_2^6$
6	5+1	C_{5v}	Pentagonal pyramid	$w_1^6 + 2w_1^5 w_2 + 3w_1^4 w_2^2 + 4w_1^3 w_2^3 + 3w_1^2 w_2^4 + 2w_1 w_2^5 + w_2^6$
6	4+2	D_{4h}	Square bP	$w_1^6 + 2w_1^5 w_2 + 4w_1^4 w_2^2 + 4w_1^3 w_2^3 + 4w_1^2 w_2^4 + 2w_1 w_2^5 + w_2^6$
6	2+2+2	C_{2v}	Bicapped tetrahedron	$w_1^6 + 3w_1^5 w_2 + 9w_1^4 w_2^2 + 10w_1^3 w_2^3 + 9w_1^2 w_2^4 + 3w_1 w_2^5 + w_2^6$
6	2+2+2	C_{2v}	Tri-distorted octahedron	$w_1^6 + 3w_1^5 w_2 + 9w_1^4 w_2^2 + 10w_1^3 w_2^3 + 9w_1^2 w_2^4 + 3w_1 w_2^5 + w_2^6$
6	2+2+2	C_{2v}	Bicapped tetrahedron	$w_1^6 + 3w_1^5 w_2 + 9w_1^4 w_2^2 + 10w_1^3 w_2^3 + 9w_1^2 w_2^4 + 3w_1 w_2^5 + w_2^6$
6	2+2+1+1	C_{2v}	Edge-capped TbP	$w_1^6 + 4w_1^5 w_2 + 9w_1^4 w_2^2 + 12w_1^3 w_2^3 + 9w_1^2 w_2^4 + 4w_1 w_2^5 + w_2^6$
7	7	D_{7h}	Regular heptagon	$w_1^7 + w_1^6 w_2 + 3w_1^5 w_2^2 + 4w_1^4 w_2^3 + 4w_1^3 w_2^4 + 3w_1^2 w_2^5 + 3w_1 w_2^6 + w_2^7$
7	6+1	C_{6v}	Hexagonal pyramid	$w_1^7 + 2w_1^6 w_2 + 4w_1^5 w_2^2 + 7w_1^4 w_2^3 + 7w_1^3 w_2^4 + 4w_1^2 w_2^5 + 2w_1 w_2^6 + w_2^7$
7	5+2	D_{5h}	Pentagonal bipyramid	$w_1^7 + 2w_1^6 w_2 + 4w_1^5 w_2^2 + 5w_1^4 w_2^3 + 5w_1^3 w_2^4 + 4w_1^2 w_2^5 + 2w_1 w_2^6 + w_2^7$
7	3+3+1	C_{3v}	Capped octahedron	$w_1^7 + 3w_1^6 w_2 + 7w_1^5 w_2^2 + 13w_1^4 w_2^3 + 13w_1^3 w_2^4 + 7w_1^2 w_2^5 + 3w_1 w_2^6 + w_2^7$
7	3+3+1	C_{3v}	Capped triangular prism	$w_1^7 + 3w_1^6 w_2 + 7w_1^5 w_2^2 + 13w_1^4 w_2^3 + 13w_1^3 w_2^4 + 7w_1^2 w_2^5 + 3w_1 w_2^6 + w_2^7$
7	3+3+1	C_{3v}	Tri-capped tetrahedron	$w_1^7 + 3w_1^6 w_2 + 7w_1^5 w_2^2 + 13w_1^4 w_2^3 + 13w_1^3 w_2^4 + 7w_1^2 w_2^5 + 3w_1 w_2^6 + w_2^7$
7	2+2+2+1	C_{2v}	4-Capped elongated triangular prism	$w_1^7 + 4w_1^6 w_2 + 12w_1^5 w_2^2 + 19w_1^4 w_2^3 + 19w_1^3 w_2^4 + 12w_1^2 w_2^5 + 4w_1 w_2^6 + w_2^7$

TABLE 81 (Continued)

8	8	D_{8h}	Octagon	$w_1^8 + w_1^7 w_2 + 4w_1^6 w_2^2 + 5w_1^5 w_2^3 + 8w_1^4 w_2^4 + 5w_1^3 w_2^5 + 4w_1^2 w_2^6 + w_1 w_2^7 + w_2^8$
8	8	O_h	Cube	$w_1^8 + w_1^7 w_2 + 3w_1^6 w_2^2 + 3w_1^5 w_2^3 + 7w_1^4 w_2^4 + 3w_1^3 w_2^5 + 3w_1^2 w_2^6 + w_1 w_2^7 + w_2^8$
8	8	D_{4d}	Square antiprism	$w_1^8 + w_1^7 w_2 + 6w_1^6 w_2^2 + 7w_1^5 w_2^3 + 13w_1^4 w_2^4 + 7w_1^3 w_2^5 + 6w_1^2 w_2^6 + w_1 w_2^7 + w_2^8$
8	7+1	C_{7v}	heptogonal pyramid	$w_1^8 + 2w_1^7 w_2 + 4w_1^6 w_2^2 + 8w_1^5 w_2^3 + 10w_1^4 w_2^4 + 8w_1^3 w_2^5 + 4w_1^2 w_2^6 + 2w_1 w_2^7 + w_2^8$
8	6+2	D_{6h}	hexagonal bipyramid	$w_1^8 + 2w_1^7 w_2 + 5w_1^6 w_2^2 + 7w_1^5 w_2^3 + 10w_1^4 w_2^4 + 7w_1^3 w_2^5 + 5w_1^2 w_2^6 + 2w_1 w_2^7 + w_2^8$
8	6+2	D_{3h}	Bicapped triangular prism	$w_1^8 + 2w_1^7 w_2 + 7w_1^6 w_2^2 + 10w_1^5 w_2^3 + 16w_1^4 w_2^4 + 10w_1^3 w_2^5 + 7w_1^2 w_2^6 + 2w_1 w_2^7 + w_2^8$
8	6+2	D_{3h}	Bicapped octahedron	$w_1^8 + 2w_1^7 w_2 + 7w_1^6 w_2^2 + 10w_1^5 w_2^3 + 16w_1^4 w_2^4 + 10w_1^3 w_2^5 + 7w_1^2 w_2^6 + 2w_1 w_2^7 + w_2^8$
8	4+4	D_{2h}	Parallelopiped	$w_1^8 + 2w_1^7 w_2 + 10w_1^6 w_2^2 + 14w_1^5 w_2^3 + 22w_1^4 w_2^4 + 14w_1^3 w_2^5 + 10w_1^2 w_2^6 + 2w_1 w_2^7 + w_2^8$
8	4+4	D_{2d}	Bidisphenoid	$w_1^8 + 2w_1^7 w_2 + 10w_1^6 w_2^2 + 14w_1^5 w_2^3 + 22w_1^4 w_2^4 + 14w_1^3 w_2^5 + 10w_1^2 w_2^6 + 2w_1 w_2^7 + w_2^8$
9	9	D_{9h}	Nonagon	$w_1^9 + w_1^8 w_2 + 4w_1^7 w_2^2 + 7w_1^6 w_2^3 + 10w_1^5 w_2^4 + 10w_1^4 w_2^5 + 7w_1^3 w_2^6 + 4w_1^2 w_2^7 + w_1 w_2^8 + w_2^9$
9	8+1	C_{8v}	Octagonal pyramid	$w_1^9 + 2w_1^8 w_2 + 5w_1^7 w_2^2 + 11w_1^6 w_2^3 + 17w_1^5 w_2^4 + 17w_1^4 w_2^5 + 11w_1^3 w_2^6 + 5w_1^2 w_2^7 + 2w_1 w_2^8 + w_2^9$
9	7+2	D_{7h}	hept bp	$w_1^9 + 2w_1^8 w_2 + 5w_1^7 w_2^2 + 8w_1^6 w_2^3 + 12w_1^5 w_2^4 + 12w_1^4 w_2^5 + 8w_1^3 w_2^6 + 5w_1^2 w_2^7 + 2w_1 w_2^8 + w_2^9$
9	3+3+3	C_{3v}	Tricapped octahedron	$w_1^9 + 3w_1^8 w_2 + 12w_1^7 w_2^2 + 30w_1^6 w_2^3 + 42w_1^5 w_2^4 + 42w_1^4 w_2^5 + 30w_1^3 w_2^6 + 12w_1^2 w_2^7 + 3w_1 w_2^8 + w_2^9$
9	4+4+1	C_{4v}	Capped cube	$w_1^9 + 3w_1^8 w_2 + 10w_1^7 w_2^2 + 22w_1^6 w_2^3 + 34w_1^5 w_2^4 + 34w_1^4 w_2^5 + 22w_1^3 w_2^6 + 10w_1^2 w_2^7 + 3w_1 w_2^8 + w_2^9$
9	4+4+1	C_{4v}	Capped square antiprism	$w_1^9 + 3w_1^8 w_2 + 10w_1^7 w_2^2 + 22w_1^6 w_2^3 + 34w_1^5 w_2^4 + 34w_1^4 w_2^5 + 22w_1^3 w_2^6 + 10w_1^2 w_2^7 + 3w_1 w_2^8 + w_2^9$
9	6+3	D_{3h}	Three-layer triangular prism	$w_1^9 + 2w_1^8 w_2 + 8w_1^7 w_2^2 + 17w_1^6 w_2^3 + 24w_1^5 w_2^4 + 24w_1^4 w_2^5 + 17w_1^3 w_2^6 + 8w_1^2 w_2^7 + 2w_1 w_2^8 + w_2^9$
10	10	D_{10h}	Decagon	$w_1^{10} + w_1^9 w_2 + 5w_1^8 w_2^2 + 8w_1^7 w_2^3 + 16w_1^6 w_2^4 + 16w_1^5 w_2^5 + 16w_1^4 w_2^6 + 8w_1^3 w_2^7 + 5w_1^2 w_2^8 + w_1 w_2^9 + w_2^{10}$
10	10	D_{5d}	Bipunctured icosahedron	$w_1^{10} + w_1^9 w_2 + 7w_1^8 w_2^2 + 12w_1^7 w_2^3 + 26w_1^6 w_2^4 + 26w_1^5 w_2^5 + 26w_1^4 w_2^6 + 12w_1^3 w_2^7 + 7w_1^2 w_2^8 + w_1 w_2^9 + w_2^{10}$
10	9+1	C_{9v}	Nonagonal pyramid	$w_1^{10} + 2w_1^9 w_2 + 5w_1^8 w_2^2 + 14w_1^7 w_2^3 + 24w_1^6 w_2^4 + 28w_1^5 w_2^5 + 24w_1^4 w_2^6 + 14w_1^3 w_2^7 + 5w_1^2 w_2^8 + 2w_1 w_2^9 + w_2^{10}$
10	8+2	D_{4h}	Bicapped cube	$w_1^{10} + 2w_1^9 w_2 + 9w_1^8 w_2^2 + 16w_1^7 w_2^3 + 33w_1^6 w_2^4 + 34w_1^5 w_2^5 + 33w_1^4 w_2^6 + 16w_1^3 w_2^7 + 9w_1^2 w_2^8 + 2w_1 w_2^9 + w_2^{10}$
10	8+2	D_{4d}	Bicapped square antiprism	$w_1^{10} + 2w_1^9 w_2 + 9w_1^8 w_2^2 + 16w_1^7 w_2^3 + 33w_1^6 w_2^4 + 34w_1^5 w_2^5 + 33w_1^4 w_2^6 + 16w_1^3 w_2^7 + 9w_1^2 w_2^8 + 2w_1 w_2^9 + w_2^{10}$
10	8+2	D_{8h}	Octagonal bipyramid	$w_1^{10} + 2w_1^9 w_2 + 6w_1^8 w_2^2 + 10w_1^7 w_2^3 + 19w_1^6 w_2^4 + 20w_1^5 w_2^5 + 19w_1^4 w_2^6 + 10w_1^3 w_2^7 + 6w_1^2 w_2^8 + 2w_1 w_2^9 + w_2^{10}$
10	6+4	T_d	Tetracapped octahedron	$w_1^{10} + 2w_1^9 w_2 + 5w_1^8 w_2^2 + 14w_1^7 w_2^3 + 22w_1^6 w_2^4 + 24w_1^5 w_2^5 + 22w_1^4 w_2^6 + 14w_1^3 w_2^7 + 5w_1^2 w_2^8 + 2w_1 w_2^9 + w_2^{10}$
10	6+4	T_d	Adamantane	$w_1^{10} + 2w_1^9 w_2 + 5w_1^8 w_2^2 + 14w_1^7 w_2^3 + 22w_1^6 w_2^4 + 24w_1^5 w_2^5 + 22w_1^4 w_2^6 + 14w_1^3 w_2^7 + 5w_1^2 w_2^8 + 2w_1 w_2^9 + w_2^{10}$
12	12	I_h	Icosahedron	$w_1^{12} + w_1^{11} w_2 + 3w_1^{10} w_2^2 + 5w_1^9 w_2^3 + 12w_1^8 w_2^4 + 14w_1^7 w_2^5 + 24w_1^6 w_2^6 + 14w_1^5 w_2^7 + 12w_1^4 w_2^8 + 5w_1^3 w_2^9 + 3w_1^2 w_2^{10} + w_1 w_2^{11} + w_2^{12}$

^{a} From ref 372. n is the number of vertices, P_n is the vertex partition of the polyhedron, and G is the point group.

tries, and levels of electron correlation. In the $^1A_1$ ground state, it seems that the rhombus structure shown in Figure 43 would be lower. Preliminary CASSCF calculations on Ga_2As_2 by Balasubramanian revealed that the ground state has a rhombus structure. The trapezoidal form is much higher in energy.

Among the four possible linear isomers of Ga_2As_2 enumerated by the generating function method (see Figure 43), it seems that structures III and IV should be more stable than structures V and VI since the relative strength of bonding is $D(As-As) > D(Ga-As) > D(Ga-Ga)$. The comparison of III and IV in Figure 43 seems to suggest that III would be more stable in the lowest state.

Through mass analysis of the laser-evaporated GaAs cluster beams O'Brien et al.[97] observed that smaller clusters deviated from binomial distributions while larger clusters followed approximately a binomial dis-
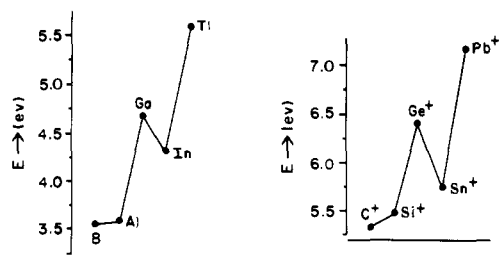
Figure 44. $^2P-^4P$ energy separations of B to Al and C^+ to Pb^+ (reprinted from ref 52; copyright 1989 American Chemical Society).
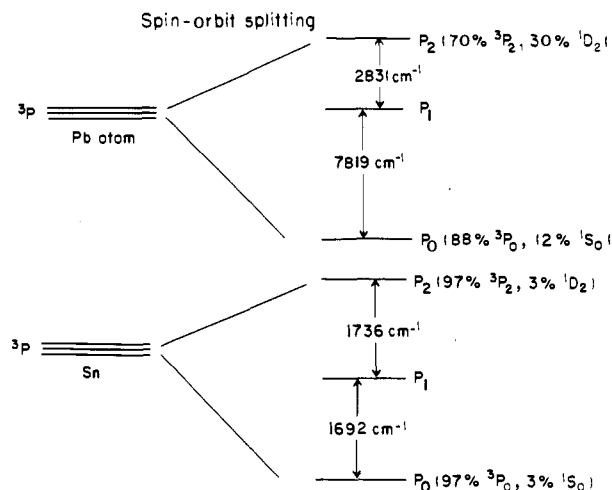

Figure 45. Spin–orbit splittings of Sn and Pb atoms (reprinted from ref 52; copyright 1989 American Chemical Society).

tribution. The dimeric species were predominantly found to be As_2 and GaAs with only traces of Ga_2. The MCSCF/CI calculations of Balasubramanian (see sections III and IV.A) on the three dimers predicted that the dissociation energies of the three species are 1.4 (Ga_2), 1.9 (GaAs), and 2.71 eV (As_2). The theoretical D_es of GaAs and As_2 should be lower than their true value since the electron correlation correction for As_2 is particularly large. Since As_2 and Ga–As are considerably more stable than Ga_2, there is strong deviation from the binomial distribution.

The experimental abundance of the trimers was found to be 50% As_3 and 30% $GaAs_2$. The generating function obtained with Pólya's theorem for trimers is given by the following expression:

$$w_1^3 + 2w_1^2 w_2 + 2w_1 w_2^2 + w_2^3$$

As seen from the above expression there are two isomers for $GaAs_2$ and Ga_2As. Of course, $GaAs_2$ would be more stable than Ga_2As. The generating function obtained above implies that the probability of forming $GaAs_2$ should be twice that of forming As_3 should the relative strengths of the As–As and Ga–As bonding be the same. However, $GaAs_2$ contains two Ga–As bonds and one As–As bond while As_3 contains three As–As bonds. If the probability is multiplied with the approximate ratios of the D_es of the two species (As_2, GaAs), then the ratio of the probability for forming As_3 and $GaAs_2$ is obtained as 1.4, which is not far from the observed distribution[97] of As_3 (50%) and $GaAs_2$ (30%). A weighted distribution obtained from the above generating function and using approximate bond strengths was found to be As_3 (51%), $GaAs_2$ (37%), Ga_2As (9%), and Ga_3 (3%). This distribution was very close to the experimental distribution of trimers.[97] Again, the tetramers are overrepresented by Ga_2As_2 and $GaAs_3$.

As seen from Table 81, the coefficient of the $w_1^3 w_2^3$ term is the largest for six-atom clusters in various forms. On the basis of simple electron count arguments, it can be concluded that only a few forms in Table 78 are stable. However, all forms in that table exhibit larger coefficients for the $w_1^3 w_2^3$ term. The HF/MP4 calculations of Raghavachari[364] indicated that the edge-capped trigonal bipyramid (tbp) is the preferred form of Si_6. Since Ga_3As_3 is isoelectronic with Si_6, the edge-capped tbp form is a probable candidate for Ga_3As_3. Further Si_4 and Si_6 exhibit extra stability for silicon clusters (magic number). Nevertheless, since two types of atoms exist, other forms are certainly possible. Even with the larger coefficient of the $w_1^3 w_2^3$ term, the observed distribution of Ga_3As_3 (70%) seems somewhat larger. It seems that there are more polyhedral forms or isomers for Ga_3As_3 compared to the other six-atom

clusters. This combined with the fact that there could be three As–As bonds and several Ga–As bonds seems to suggest that the probability of forming Ga_3As_3 should certainly be larger than forming Ga_2As_2. Thus, the only explanation for a dramatically larger abundance of Ga_3As_3 (see Figure 42) is the possibility of the existence of more forms and thus more isomers for Ga_3As_3, in addition to six being a magic number for these clusters.

As the number of atoms becomes large, the existence of larger numbers of Ga–As bonds and only a very few As–As bonds should offset the difference in the strengths of the As–As and Ga–As bonds leading to a binomial distribution. Thus, the abundance of $Ga_{n/2}As_{n/2}$ would be largest for even n while the abundance of $Ga_{(n-1)/2}As_{(n+1)/2}$ would be largest for odd n.

The other applications of combinatorics and graph theory to clusters involve electron count arguments to predict the stabilities of main-group clusters,[379-387] generation of characteristic polynomials, and spectra of polyhedral clusters which included C_{60} and C_{120}.[398,399] The dynamics of polyhedral isomerizations could also be represented by reaction isomerization graphs or floppy graphs.[385-397,400,401] There are numerous such applications of graph theory, but these are beyond the scope of the present review.

VII. Comparison of the Properties and Periodic Trends among Dimers

In this section we compare the spectroscopic properties of the low-lying electronic states of dimers of some of the groups for which complete sets of data are available. Before comparison of the properties of dimers is made, it is relevant to compare a few atomic properties within some of the main-group elements considered here. Figure 44 shows the $^2P(ns^2np^1)$– $^4P(ns^1np^2)$ energy separations of B–Tl and C^+–Pb^+ as obtained from experimental atomic spectral data. This comparison reveals an interesting trend. In going from In to Tl as well as Sn^+ to Pb^+, we see a dramatic rise in this energy separation. This increase is primarily due to a phenomenon referred to as the relativistic inert-pair effect. The relativistic mass–velocity contraction stabilizes the 6s orbital of the atoms Au to At. As a result, the $6s^2$ shell is quite stabilized and does not participate in bonding. Consequently, the 6s–6p promotion energy
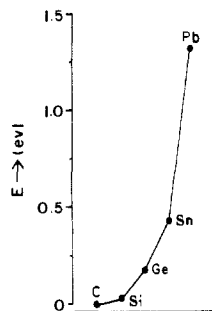
Figure 46. The relative trend of $^3P_0$–$^3P_2$ separations of C to Pb (reprinted from ref 52; copyright 1989 American Chemical Society).

Figure 48. Comparison of the dissociation energies of Ga_2 to Bi_2. The dashed line below the solid line (experimental values) is the theoretical curve.
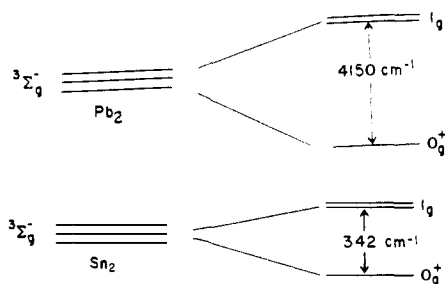

Figure 47. Spin–orbit splittings of the $^3\Sigma_g^-$ states of Sn_2 and Pb_2 (reprinted from ref 52; copyright 1989 American Chemical Society).

Figure 49. Comparison of the R_e values of the ground states of Ga_2 to Bi_2.

dramatically increases compared to the corresponding 5s–5p promotion energy as evidenced from Figure 44.

The other important relativistic effect that has substantial impact on the binding energies and spectroscopic properties of very heavy dimers is the spin–orbit effect, which is also a relativistic effect. This is illustrated in Figure 45 for the Pb and Sn atoms. Figure 46 shows the periodic trend for $^3P_0$–$^3P_2$ splittings of atoms C to Pb of group(IV) elements. As seen from these figures, the spin–orbit splitting is significantly larger for Pb compared to Sn. This changes the coupling of the Pb atom to intermediate in that the ground state of the Pb atom is 88% $^3P_0$ and 12% $^1S_0$. Similarly, the $J = 2$ state of Pb is 70% $^3P_2$ and 30% $^1P_2$.

The spectroscopic properties of heavier dimers within a group appear to be governed primarily by the relativistic effects mentioned above. For example, Figure 47 compares the spin–orbit splitting of the $X^3\Sigma_g^-$ state of Sn_2 and Pb_2, respectively. As seen from this figure, the splitting is dramatically larger for Pb_2 compared to Sn_2. This also enhances coupling of the $^3\Sigma_g^-(0_g^+)$ state with the $^1\Sigma_g^+(0_g^+)$ state, resulting in a pronounced shoulder in the 0_g^+ ground state curve of Pb_2 (see Figure 23).

Figure 48 compares the dissociation energies of the heavy dimers of three of the groups considered in this investigation. The dashed line below the solid line is the theoretical curve. As seen from Figure 48, the theoretical trend mimics the experimental trend closely. With the exception of Pb_2, the theoretical D_e is always lower than the corresponding experimental value. As seen from Figure 48, as one goes down a column of the periodic table, the D_e decreases. The decreases in the D_e are especially larger in comparing In_2 to Tl_2 or Sn_2 to Pb_2. The As_2–Bi_2 curve is almost collinear. The experimental D_e[266] of Tl_2 is a bit uncertain, although it has been corrected recently.[267] The sharp drop in the
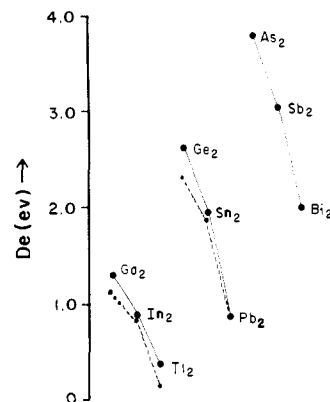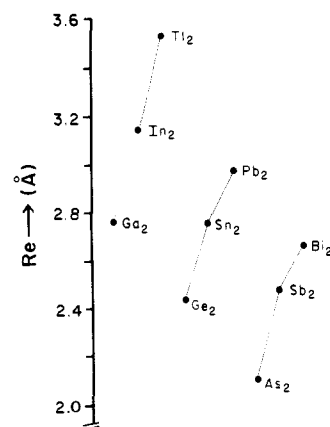
D_e in moving down from In to Tl is primarily a consequence of the inert-pair effect and the spin–orbit effect. As mentioned above, the $6s^2$ shell of Tl is inert. The spin–orbit effects further weaken the bonding since the atoms are more stabilized compared to the dimer. The destabilization of the bond in Pb_2 compared to Sn_2 is primarily due to the spin–orbit coupling since the D_e obtained without the spin–orbit integrals is approximately twice the corresponding value with the spin–orbit term.

Figure 49 compares the equilibrim bond lengths (R_es) of Ga_2 to Bi_2. As seen from Figure 49, the bond length increases as one goes down the periodic table within a column. The increase is especially large in moving from In to Tl due to both the inert-pair effect and the spin–orbit effect. The bond length decreases as one moves toward the right of the periodic table (i.e., from Ga_2 to As_2 and from In_2 to Sb_2). This is primarily because of increases in the bond order as one moves to the right until one reaches group V. The dimers of As and Sb form almost a triple bond while the bond order of Bi_2 decreases to 2.2 mainly due to spin–orbit coupling of $^1\Sigma_g^+(0_g^+)$ with $^3\Pi_g(0_g^+)$. Thus, Ga_2, Ge_2, and As_2 form approximately single, double, and triple bonds, respectively, while the bond orders for Tl_2, Pb_2, and Bi_2 are much smaller. The ratio of bond orders as obtained from the ratio of Mulliken overlap populations for In_2 and Sb_2 is 2.62.

Next we compare the energy separations of some spectroscopically interesting states of the various dimers. Figure 50 compares the experimental transition
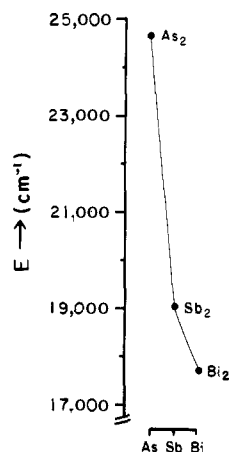
Figure 50. Comparison of $^3\Sigma_u^-(0_u^+)$-$X^1\Sigma_g^+(0_g^+)$ energy separations of As_2, Sb_2, and Bi_2.

energy for the $^3\Sigma_u^-(0_u^+)$-$X^1\Sigma_g^+(0_g^+)$ transition of As_2 to Bi_2. As seen from Figure 50, this transition energy decreases as one goes down the periodic table. This is the usual trend except that the decrease is smaller for Bi_2 primarily due to spin–orbit coupling.

Figure 51 compares the $^3\Pi_u(0_u^+)$-$X^3\Sigma_g^-(0_g^+)$ energy separations of Ge_2 to Pb_2. Note that this has an opposite trend compared to Figure 50. The spin–orbit effects are substantially larger for both the states of group IV dimers. Note the dramatic increase in the energy separation for Pb_2. This is primarily a consequence of the large spin–orbit splitting of the Pb atom. For both Ge_2 and Si_2 the $^3\Pi_u$ state is very low lying and has a very small spin–orbit splitting. For Si_2, it is, in fact, speculated that $^3\Pi_u$ could be the ground state.[37]

Figure 52 shows the periodic trend for the $^3\Sigma_u^-(0_u^+)$-$X^3\Sigma_g^-(0_g^+)$ separation of Ge_2, Sn_2, and Pb_2. This exhibits a very interesting trend as seen from Figure 52. The tin dimer follows the trend of decrease in the energy separation as one goes down the periodic table. However, this energy separation increases in comparing Sn_2 with Pb_2 primarily because of spin–orbit effects. Consequently, relativistic effects seem to play an important role in the spectroscopic properties of the sixth-row dimers.

VIII. Conclusion

In this review, I have catalogued and compared the known theoretical and experimental spectroscopic properties of heavy dimers (Ga_2 to Bi_2), heteronuclear dimers ($GaAs$, $GaAs^+$, $KrBr^+$, ICl, and ICl^+), and heavy trimers. The potential energy curves and spectroscopic constants obtained through relativistic CASSCF/CI theoretical methods were presented for these species. The spectroscopic constants of the dimers were compared, and periodic trends were critically examined for each group. In all cases the sixth-row dimers exhibited considerable deviations from the expected trends due to large relativistic mass–velocity and spin–orbit effects.

While the spectroscopic properties and potential energy curves of many of the dimers have now been obtained, our knowledge on the electronic properties and geometries of many larger clusters is far from complete. The only exception to the p-block elements appears to be the silicon and germanium clusters, for which calculations have been made for larger clusters.[361,364]
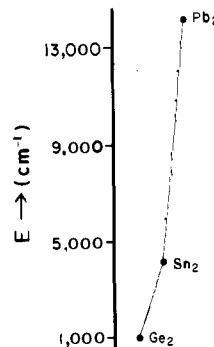
Figure 51. Comparison of $^3\Pi_u(0_u^+)$-$X^3\Sigma_g^-(0_g^+)$ energy separations of Ge_2, Sn_2, and Pb_2.
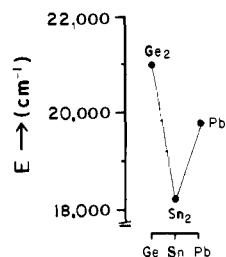

Figure 52. Comparison of $^3\Sigma_u^-(0_u^+)$-$X^3\Sigma_g^-(0_g^+)$ energy separations of Ge_2, Sn_2, and Pb_2.

Whereas the experimental investigations of many of these compounds have provided a wealth of information on these species, a complete understanding of all of the available information has not been accomplished. With the advent of supercomputers and more powerful theoretical tools available today, theoretical calculations are on the increase. The strong interaction between the theoretical calculations and experiments could provide a more comprehensive understanding of many of the larger clusters.

Many of the experimentally observed fragmentation patterns of clusters and other colorful patterns of odd–even alternations have not been fully understood. The relative abundance of clusters as a function of size is very intriguing. It is hoped that this review will stimulate such theoretical calculations which will eventually provide sound explanations for these baffling experimental phenomena.

IX. Acknowledgments

References

(1) Mandich, M. L.; Reents, W. D.; Bondybey, V. E. Main Group Clusters: A Review. In *Atomic and Molecular Clusters*; Bernstein, E., Ed.; Elsevier, in press.
(2) Morse, M. D. *Chem. Rev.* 1986, *86*, 1049.
(3) Koutecky, J.; Fantucci, P. *Chem. Rev.* 1986, *86*, 539.
(4) Jarrold, M. F. In *Modern Inorganic Chemistry: Gas Phase Inorganic Chemistry*; Russell, D. H., Ed., in press.
(5) Corbett, J. D. *Chem. Rev.* 1985, *85*, 383.
(6) Corbett, J. D. *Prog. Inorg. Chem.* 1976, *21*, 129.
(7) Grätzel, M. *Acc. Chem. Res.* 1981, *14*, 376.
(8) Baetzold, R. C.; Hamilton, J. F. *Prog. Solid State Chem.* 1983, *15*, 1.
(9) Smalley, R. E. Supersonic Carbon Cluster Beams. In *Cluster Spectroscopy*; Bernstein, E. R., Ed.; Elsevier, in press.
(10) King, R. B. In *Physics and Chemistry in Small Clusters*; Jena, P., Rao, B. K., Khanna, S. N., Eds.; Plenum: New York, 1987.
(11) Kappe, M. *Chem. Rev.* 1988, *88*, 369.
(12) Sagano, S.; Nishina, Y.; Ohinishi, S., Eds.; *Microclusters*; Springer-Verlag: Berlin, 1987.
(13) Moskovits, M., Ed. *Metal Clusters*; Wiley: New York, 1986.
(14) Beuhler, R.; Friedman, L. *Chem. Rev.* 1986, *86*, 521.
(15) Phillips, J. C. *Chem. Rev.* 1986, *86*, 619.
(16) Alford, J. M.; Williams, P. E.; Trevor, D. J.; Smalley, R. E. *Int. J. Mass Spectrom. Ion Phys.* 1986, *72*, 33.
(17) Comisarow, M. *Advances in Mass Spectrometry*; Daly, N. R., Ed.; Heyden: London, 1978.
(18) Martin, T. P., Ed. *Elemental and Molecular Clusters*; Springer: New York, 1987.
(19) Margrave, J. L., Ed. *The Characterization of High-Temperature Vapors*; Wiley: New York, 1967.
(20) Honig, R. E. *Advances in Mass Spectrometry*; Elliott, R. M., Ed.; Pergamon: London, 1963.
(21) Beauchamp, J. L. *Annu. Rev. Phys. Chem.* 1971, *22*, 571.
(22) Gingerich, K. A. *Mass Spectroscopy in Inorganic Chemistry*; Gould, R. F., Ed.; Advances in Chemistry Series 72; American Chemical Society: Washington, DC, 1968; pp 291–300.
(23) Henglein, A. *Pure Appl. Chem.* 1984, *56*, 1215.
(24) Brus, L. *J. Phys. Chem.* 1986, *90*, 2555.
(25) Robbins, E. S.; Leckenby, R. E.; Willis, P. *Adv. Phys.* 1967, *16*, 739.
(26) Bowers, M. T., Ed. *Gas Phase Ion Chemistry*; Academic: New York, 1979.
(27) Steudel, R. *Top. Curr. Chem.* 1982, *102*, 149.
(28) Steudel, R. *Studies in Inorganic Chemistry*; Müller, A., Kerbs, B., Eds.; Elsevier: Amsterdam, 1984.
(29) Ozin, G. A. *Cata. Rev.* 1977, *16*, 191.
(30) Muetterties, E. L. *Science* 1977, *196*, 839.
(31) Smalley, R. E. In *Comparison of Ab Initio Quantum Chemistry with Experiment*; Bartlett, R. J., Ed.; Reidel: Dordrecht, 1985.
(32) Bares, A. J.; Muller, A.; Orville-Thomas, W. J.; Gaufreys, R. *Matrix-Isolation Spectroscopy*; Reidel: Dordrecht, 1981.
(33) Geusic, M. F.; Morse, M. D.; O'Brien, S. C.; Smalley, R. E. *Rev. Sci. Instrum.* 1985, *56*, 2123.
(34) Cheshnovsky, O.; Yang, S. H.; Pettiette, C. L.; Craycraft, M. J.; Smalley, R. E. *Rev. Sci. Instrum.* 1987, *58*, 2131.
(35) Weltner, W., Jr.; Van Zee, R. J. *Annu. Rev. Phys. Chem.* 1984, *35*, 291.
(36) Cheshnovsky, O.; Pettiette, C. L.; Smalley, R. E. In *Ion and Cluster Ion Spectroscopy*; Maier, P., Ed.; Elsevier: Amsterdam, 1988.
(37) Huber, K. P.; Herzberg, G. *Molecular Spectra and Molecular Structure. IV. Constants of Diatomic Molecules*; Van Nostrand Reinhold: New York, 1979.
(38) Brand, J. C. D.; Hoy, A. R. *Appl. Spectrosc. Rev.* 1987, *23*, 285.
(39) Brau, Ch. A. *Excimer Lasers*, 2nd ed.; Rhodes, Ch. K., Ed.; Springer: Berlin, 1984.
(40) Tellinghuisen, J. *Applied Atomic Collision Physics*; Academic: New York, 1982; Vol. 3.
(41) Pitzer, K. S. *Acc. Chem. Res.* 1979, *12*, 271.
(42) Pyykkö, P.; Desclaux, J. P. *Acc. Chem. Res.* 1979, *12*, 276.
(43) Pitzer, K. S. *Int. J. Quantum Chem.* 1984, *25*, 131.
(44) Krauss, M.; Stevens, W. J. *Annu. Rev. Phys. Chem.* 1984, *35*, 357.
(45) Pyykkö, P. *Adv. Quantum Chem.* 1978, *11*, 353.
(46) Pyykkö, P., Ed. Proceedings of the Symposium on Relativistic Effects in Quantum Chemistry. *Int. J. Quantum Chem.* 1984, *25*.
(47) Balasubramanian, K.; Pitzer, K. S. *Adv. Chem. Phys.* 1987, *67*, 287.
(48) Pyykkö, P. *Chem. Rev.* 1988, *88*, 563.
(49) Schwarz, W. H. E. In *Theoretical Models of Chemical Bonding*; Maksič, Z., Ed., in press.
(50) Malli, G. *Stud. Phys. Theor. Chem.* 1982, *21*, 199.
(51) Pyykkö, P. *Relativistic Theory of Atoms and Molecules*; Springer-Verlag: Berlin, New York, 1986.

(52) Balasubramanian, K. Feature Article, *J. Phys. Chem.*, in press.
(53) Balasubramanian, K. *J. Mol. Struct.*, special issue, in press.
(54) Balasubramanian, K. *Chem. Rev.*, in press.
(55) Lee, Y. S.; Ermler, W. C.; Pitzer, K. S. *J. Chem. Phys.* 1977, *67*, 5961.
(56) Lee, Y. S.; Ermler, W. C.; Pitzer, K. S. *J. Chem. Phys.* 1980, *73*, 360.
(57) Christiansen, P. A.; Lee, Y. S.; Pitzer, K. S. *J. Chem. Phys.* 1979, *71*, 4445.
(58) Lee, Y. S.; Ermler, W. C.; Pitzer, K. S.; McLean, A. D. *J. Chem. Phys.* 1979, *70*, 288.
(59) Kahn, L.; Baybutt, P.; Truhlar, D. G. *J. Chem. Phys.* 1976, *65*, 3826.
(60) Ermler, W. C.; Lee, Y. S.; Christiansen, P. A.; Pitzer, K. S. *Chem. Phys. Lett.* 1981, *71*, 70.
(61) Hurley, M. M.; Pacios, L. F.; Christiansen, P. A.; Ross, R. B.; Ermler, W. C. *J. Chem. Phys.* 1986, *84*, 6840.
(62) LaJohn, L. A.; Christiansen, P. A.; Ross, R. B.; Atashroo, T.; Ermler, W. C. *J. Chem. Phys.* 1987, *87*, 2812.
(63) Hafner, P.; Schwarz, W. H. E. *Chem. Phys. Lett.* 1979, *65*, 537.
(64) Hay, P. J.; Wadt, W. R. *J. Chem. Phys.* 1985, *82*, 270.
(65) Wadt, W. R.; Hay, P. J. *J. Chem. Phys.* 1985, *82*, 284.
(66) Hay, P. J.; Wadt, W. R. *J. Chem. Phys.* 1985, *82*, 299.
(67) Christiansen, P. A.; Balasubramanian, K.; Pitzer, K. S. *J. Chem. Phys.* 1982, *76*, 5087.
(68) Balasubramanian, K. *J. Chem. Phys.* 1988, *89*, 5731.
(69) Pitzer, R. M.; Winter, N. W. *J. Phys. Chem.* 1988, *92*, 3061.
(70) The major authors of ALCHEMY II are B. Liu, B. Lengsfield, and M. Yoshimine.
(71) Gibson, G. E.; MacFarlane, A. *Phys. Rev.* 1934, *46*, 1059.
(72) Herzberg, G. *Ann. Phys.* 1932, *15*, 677.
(73) Almy, G. M.; Sparks, F. M. *Phys. Rev.* 1933, *44*, 365.
(74) Naude, S. M. *Phys. Rev.* 1934, *45*, 280.
(75) Chupka, W. A.; Ingram, M. G. *J. Chem. Phys.* 1953, *21*, 1313.
(76) Drowart, J.; Burns, R. P.; DeMaria, G.; Ingram, M. G. *J. Chem. Phys.* 1959, *31*, 1131.
(77) Martin, T. P. *J. Chem. Phys.* 1985, *83*, 78.
(78) Dietz, T. G.; Duncan, M. A.; Powers, D. E.; Smalley, R. E. *J. Chem. Phys.* 1981, *74*, 6511.
(79) Powers, D. E.; Hansen, S. G.; Geusic, M. E.; Michalopoulos, D. L.; Smalley, R. E. *J. Chem. Phys.* 1983, *78*, 2866.
(80) Powers, D. E.; Hansen, S. G.; Geusic, M. E.; Puiu, A. C.; Hopkins, J. B.; Dietz, T. G.; Duncan, M. A.; Langridge-Smith, P. R. R.; Smalley, R. E. *J. Phys. Chem.* 1982, *86*, 2556.
(81) Heath, J. R.; Liu, Y.; O'Brien, S. C.; Zhang, Q.-L.; Curl, R. F.; Tittel, F. K.; Smalley, R. E. *J. Chem. Phys.* 1985, *83*, 5520.
(82) Wheeler, R. G.; LaiHing, K.; Wilson, L. L.; Duncan, M. A. *Chem. Phys. Lett.* 1986, *131*, 8.
(83) LaiHing, K.; Wheeler, R. G.; Wilson, W. L.; Duncan, M. A. *J. Chem. Phys.* 1987, *87*, 3401.
(84) Wheeler, R. G.; LaiHing, K.; Wilson, W. L.; Allen, J. D.; King, R. B.; Duncan, M. A. *J. Am. Chem. Soc.* 1986, *108*, 8101.
(85) Bloomfield, L. A.; Freeman, R. R.; Brown, W. L. *Phys. Rev. Lett.* 1985, *54*, 2246.
(86) Rohlfing, E. A.; Cox, D. M.; Kaldor, A. *J. Chem. Phys.* 1984, *81*, 3322.
(87) Bondybey, V. E.; English, J. H. *J. Chem. Phys.* 1977, *67*, 3405.
(88) Bondybey, V. E. *J. Chem. Phys.* 1977, *66*, 995.
(89) Bondybey, V. E.; English, J. H. *J. Chem. Phys.* 1983, *79*, 4746.
(90) Rosenstock, H. M.; Draxl, K.; Steiner, B. W.; Herron, J. T. *J. Phys. Chem. Ref. Data* 1977, *6*, Supplement 1.
(91) Jacobson, D. B.; Freiser, B. S. *J. Am. Chem. Soc.* 1986, *108*, 27.
(92) Jarrold, M. F.; Illies, A. J.; Bowers, M. T. *J. Am. Chem. Soc.* 1985, *107*, 7339.
(93) Montano, P. A.; Shenoy, G. K.; Alp, E. E.; Schulze, W.; Urban, J. *Phys. Rev. Lett.* 1986, *56*, 2076.
(94) Hamilton, J. F.; Longel, P. C. *Thin Solid Films* 1973, *16*, 49.
(95) Yacaman, M. J.; Heinemann, K.; Yang, C. Y.; Poppa, H. *J. Cryst. Growth* 1979, *47*, 182.
(96) Apai, G.; Hamilton, J. F.; Stohr, J.; Thomson, A. *Phys. Rev. Lett.* 1979, *43*, 165.
(97) O'Brien, S. C.; Liu, Y.; Zhang, Q.; Heath, J. R.; Tittel, F. K.; Curl, R. F.; Smalley, R. E. *J. Chem. Phys.* 1986, *84*, 4074.
(98) Heath, J. R.; Liu, Y.; O'Brien, S. C.; Zhang, Q.; Curl, R. F.; Tittel, F. K.; Smalley, R. E. *J. Chem. Phys.* 1985, *83*, 5520.
(99) Liu, Y.; Zhang, Q.; Tittel, F. K.; Curl, R. F.; Smalley, R. E. *J. Chem. Phys.* 1986, *85*, 7434.
(100) Zhang, Q.; Liu, Y.; Curl, R. F.; Tittel, F. K.; Smalley, R. E. *J. Chem. Phys.* 1988, *88*, 1670.
(101) Cheshnovsky, O.; Yang, S. H.; Pettiette, C. L.; Craycraft, M. J.; Liu, Y.; Smalley, R. E. *Chem. Phys. Lett.* 1987, *138*, 119.
(102) Trevor, D. J.; Cox, D. M.; Reichmann, K. C.; Brickman, R. O.; Kaldor, A. *J. Phys. Chem.* 1987, *91*, 2598.
(103) Bloomfield, L. A.; Geusic, M. E.; Freeman, R.; Brown, W. L. *Chem. Phys. Lett.* 1985, *121*, 33.

(104) Bondybey, V. E.; Reents, W. D.; Mandich, M. L., unpublished results.
(105) Elkind, J. L.; Alford, J. M.; Weiss, F. D.; Laaksonen, R. T.; Smalley, R. E. *J. Chem. Phys.* **1987**, *84*, 2397.
(106) Rasanen, M.; Heimbrook, L. A.; Schwartz, G. P.; Bondybey, V. E. *J. Chem. Phys.* **1986**, *85*, 86.
(107) Phillips, J. C. *J. Chem. Phys.* **1987**, *87*, 1712.
(108) Beck, S. *J. Chem. Phys.* **1987**, *87*, 4233.
(109) Steigerwald, M. L.; Alivisatos, A. P.; Gibson, J. M.; Harris, T. D.; Kortan, K.; Mullar, A. J.; Thayer, A. M.; Duncan, T. M.; Douglass, D. C.; Brus, L. E. *J. Am. Chem. Soc.* **1988**, *110*, 3046.
(110) Laitling, K.; Cheng, P. Y.; Duncan, M. A. *J. Phys. Chem.* **1987**, *91*, 6521.
(111) Wheeler, R. G.; Laitling, K.; Wilson, W. L.; Duncan, M. A. *J. Chem. Phys.* **1988**, *88*, 2831.
(112) Geusic, M. E.; Freeman, R. R.; Duncan, M. A. *J. Chem. Phys.*, in press.
(113) Geusic, M. E.; Freeman, R. R.; Duncan, M. A. *J. Chem. Phys.* **1988**, *88*, 163.
(114) Taylor, S.; Lemire, G. W.; Hamrick, Y.; Fu, Z.; Morse, M. D. *J. Chem. Phys.* **1988**, *89*, 5517.
(115) Dörenburg, E.; Hintenberger, H. *Z. Naturforsch.* **1959**, *14A*, 765.
(116) Richter, C. E.; Trapp, M. *Int. J. Mass Spectrom. Ion Phys.* **1981**, *38*, 21.
(117) Mandich, M. L.; Desantolo, A. M.; Keating, K. A., unpublished results.
(118) Ervin, K. M.; Ho, J.; Lineberger, W. C. *J. Chem. Phys.* **1988**, *89*, 4514.
(119) Leopold, D. G.; Almlöf, J.; Lineberger, W. C.; Taylor, P. R. *J. Chem. Phys.* **1988**, *86*, 3780.
(120) Leopold, D. G.; Ho, J.; Lineberger, W. C. *J. Chem. Phys.* **1987**, *86*, 1715.
(121) Pettiette, C. L.; Yang, S. H.; Craycraft, M. J.; Conceicao, J.; Laaksonen, R. T.; Cheshnovsky, O.; Smalley, R. E. *J. Chem. Phys.* **1988**, *88*, 5377.
(122) Ginter, D. S.; Ginter, M. L.; Innes, K. K. *J. Chem. Phys.* **1965**, *69*, 480.
(123) Douglas, M. A.; Hauge, R.; Margrave, J. L. *J. Phys. Chem.* **1983**, *87*, 2945.
(124) Basch, H.; Stevens, W. J.; Krauss, M. *Chem. Phys. Lett.* **1984**, *109*, 212.
(125) Mohlmann, G. R. *Laser Chem.* **1984**, *5*, 1.
(126) Bauschlicher, C. W.; Langhoff, S. R. *J. Chem. Phys.* **1989**, *90*, 4627.
(127) Douglas, A. E.; Herzberg, G. *Phys. Rev.* **1940**, *57*, 742.
(128) Graham, W. R. M.; Weltner, W., Jr. *J. Chem. Phys.* **1976**, *65*, 1516.
(129) DuPuis, M.; Liu, B. *J. Chem. Phys.* **1973**, *68*, 2092.
(130) Ginter, D. S.; Ginter, M. L.; Innes, K. K. *Astrophys. J.* **1963**, *139*, 365.
(131) Chupka, W. A.; Berkowitz, J.; Giese, C. F.; Inghram, M. G. *J. Phys. Chem.* **1958**, *62*, 611.
(132) Drowart, J.; Honig, R. E. *J. Phys. Chem.* **1957**, *61*, 980.
(133) Balasubramanian, K. *J. Phys. Chem.* **1986**, *90*, 6786; Erratum, *J. Phys. Chem.* **1989**, *93*, 8388.
(134) Moore, C. E. *Atomic Energy Levels*; National Bureau of Standards: Washington, DC, 1971.
(135) Froben, F. W.; Schulze, W. *Surf. Sci.* **1983**, *156*, 765.
(136) Kingcade, J. E., Jr. Choudary, U. V.; Gingerich, K. A. *Inorg. Chem.* **1979**, *18*, 3094.
(137) Shim, I.; Nagarathna-Naik, H. M.; Gingerich, K. A. *Int. J. Quantum Chem.* **1986**, *29*, 975.
(138) Pacchioni, G. *Mol. Phys.* **1983**, *49*, 727.
(139) Balasubramanian, K. *J. Mol. Spectrosc.* **1987**, *123*, 228.
(140) Bondybey, V. E.; Heaven, M.; Miller, T. A. *J. Chem. Phys.* **1983**, *78*, 3593.
(141) Almy, G. M.; Kinzer, G. D. *Phys. Rev.* **1935**, *47*, 721.
(142) Kinzer, G. D.; Almy, G. M. *Phys. Rev.* **1937**, *52*, 814.
(143) Almy, G. M. *J. Phys. Chem.* **1937**, *41*, 47.
(144) Mrozowski, S.; Santaram, C. *J. Opt. Soc. Am.* **1967**, *57*, 522.
(145) Perdigon, P.; Martin, F.; D'Incan, J. *J. Mol. Spectrosc.* **1970**, *36*, 341.
(146) Perdigon, P.; D'Incan, J. *Can. J. Phys.* **1970**, *48*, 1140.
(147) Donovan, R. J.; Strachan, P. *Trans. Faraday Soc.* **1971**, *67*, 3407.
(148) Bennett, S. L.; Margrave, J. L.; Franklin, J. L.; Hudson, J. C. *J. Chem. Phys.* **1973**, *59*, 5814.
(149) Martin, F.; Perdigon, P.; D'Incan, J. *J. Mol. Spectrosc.* **1974**, *50*, 45.
(150) Sibai, A. M.; Perdigon, P.; Topouzkhanian, A. *Z. Naturforsch.* **1974**, *29A*, 429.
(151) Martin, F.; Figuet, J.; Perdigon, P. *J. Mol. Spectrosc.* **1975**, *57*, 319.
(152) Perdigon, P.; Martin, F. *J. Mol. Spectrosc.* **1980**, *83*, 40.
(153) Ebel, S.; Dieck, H. T.; Walthner, H. *Inorg. Chim. Acta* **1981**, *53*, L101.
(154) Wannous, G.; Effantin, C.; Martin, F.; D'Incan, J. *J. Mol. Spectrosc.* **1982**, *91*, 1.
(155) Kok, R. A.; Hall, M. B. *Inorg. Chem.* **1983**, *22*, 728.

(156) Heimbrook, L. A.; Chestnoy, N.; Rasanen, M.; Schwartz, G.; Bondybey, V. E. *J. Chem. Phys.* **1985**, *83*, 6091.
(157) Watanabe, Y.; Sakai, Y.; Kashiwagi, H. *Chem. Phys. Lett.* **1985**, *120*, 363.
(158) Topouzkhanian, A.; Sibai, A. M. *Spectrochim. Acta* **1972**, *28A*, 2197.
(159) Balasubramanian, K. *J. Mol. Spectrosc.* **1987**, *121*, 465.
(160) Barrow, R. F.; Chandler, G. C.; Meyer, C. B. *Philos. Trans. R. Soc. A* **1966**, *260*, 395.
(161) Gouedard, G.; Lehmann, J. C. *J. Phys. B* **1976**, *9*, 2113.
(162) Ibbs, K. G.; McCaffery, A. J. *J. Chem. Soc., Faraday Trans. 2* **1981**, *77*, 631, 637.
(163) Bondybey, V. E.; English, J. H. *J. Chem. Phys.* **1980**, *72*, 6479.
(164) Prosser, S. J.; Barrow, R. F.; Verges, J.; Effantin, C.; D'Incan, J. *J. Phys. B* **1980**, *13*, L547.
(165) Jenouvrier, A. *Can. J. Phys.* **1983**, *61*, 1531.
(166) Ahmed, F.; Nixon, E. R. *J. Mol. Spectrosc.* **1980**, *83*, 64.
(167) Krishnamachari, S. L. N. G.; Venkatachalam, T. V. *Chem. Phys. Lett.* **1979**, *67*, 69.
(168) Winter, R.; Barnes, I.; Fink, E. H.; Wildt, J.; Zabel, F. *Chem. Phys. Lett.* **1980**, *73*, 297.
(169) Heaven, M.; Miller, T. A.; English, J. H.; Bondybey, V. E. *Chem. Phys. Lett.* **1982**, *91*, 251.
(170) Yee, K. K.; Barrow, R. F. *J. Chem. Soc., Faraday Trans. 2* **1972**, *68*, 1181.
(171) Drowart, J.; Smones, S. *J. Chem. Soc., Faraday Trans. 2* **1977**, *73*, 1755.
(172) Balasubramanian, K. *J. Phys. Chem.* **1987**, *91*, 5166.
(173) Saxon, R. P.; Liu, B. *J. Chem. Phys.* **1977**, *67*, 5432.
(174) Bondybey, V. E.; English, J. H. *J. Chem. Phys.* **1978**, *68*, 1865.
(175) Bondybey, V. E.; English, J. H. *J. Chem. Phys.* **1980**, *72*, 3113.
(176) Ricks, J. M.; Barrow, R. F. *Can. J. Phys.* **1969**, *47*, 2423.
(177) Heaven, M. C.; Miller, T. A.; Bondybey, V. E. *J. Phys. Chem.* **1983**, *87*, 2072.
(178) Barrow, R. F.; Clark, T. C.; Coxan, J. A.; Yee, K. K. *J. Mol. Spectrosc.* **1974**, *51*, 428.
(179) Ishiwata, T.; Ohtoshi, M.; Tanaka, I. *J. Chem. Phys.* **1984**, *81*, 2300.
(180) Mulliken, R. S. *Phys. Rev.* **1940**, *57*, 500.
(181) Balasubramanian, K. *Chem. Phys.* **1988**, *119*, 41.
(182) Schwerdtfeger, P.; Szentpaly, L. V.; Vogel, K.; Silberbach, H.; Stoll, H.; Preuss, H. *J. Chem. Phys.* **1986**, *84*, 1606.
(183) Andzelm, J.; Klobukowski, M.; Radzio-Andzelm, E. *J. Comput. Chem.* **1984**, *5*, 146.
(184) Boerrighter, P. M.; Buijse, M. A.; Snijders, J. G. *Chem. Phys.* **1987**, *111*, 47.
(185) Cornford, A. B.; Frost, D. C.; McDowell, C. A.; Ragle, J. L.; Stenhouse, J. A. *J. Chem. Phys.* **1971**, *54*, 2651.
(186) Potts, A. W.; Price, W. C. *Trans. Faraday Soc.* **1971**, *67*, 1242.
(187) Dibeler, V. R.; Walker, J. A.; McCulloh, K. E. *J. Chem. Phys.* **1970**, *53*, 4715.
(188) Venkateswarlu, P. *Can. J. Phys.* **1970**, *48*, 1055.
(189) Balasubramanian, K.; Kaufman, J. J.; Hariharan, P. C.; Koski, W. S. *Chem. Phys. Lett.* **1986**, *129*, 169.
(190) Hamilton, P. A. *Chem. Phys. Lett.* **1987**, *140*, 591.
(191) Wajnkrac, R. *Z. Phys.* **1937**, *104*, 122.
(192) Froben, F. W.; Schulze, W.; Kloss, U. *Chem. Phys. Lett.* **1983**, *99*, 500.
(193) De Maria, G.; Drowart, J.; Ingram, M. G. *J. Chem. Phys.* **1959**, *31*, 1076.
(194) Balasubramanian, K.; Li, J. Q. *J. Chem. Phys.* **1988**, *88*, 4979.
(195) Christiansen, P. A.; Pitzer, K. S. *J. Chem. Phys.* **1981**, *74*, 1162.
(196) Christiansen, P. A. *J. Chem. Phys.* **1983**, *79*, 2928.
(197) Bondybey, V. E.; English, J. H. *J. Chem. Phys.* **1982**, *76*, 2165.
(198) Epting, M. A.; McKenzie, M. T., Jr.; Nixon, E. R. *J. Chem. Phys.* **1980**, *73*, 134.
(199) Bondybey, V. E.; English, J. H. *J. Mol. Spectrosc.* **1980**, *84*, 388.
(200) Teichmann, R. A., III; Epting, M.; Nixon, E. R. *J. Chem. Phys.* **1978**, *68*, 336.
(201) Balasubramanian, K.; Pitzer, K. S. *J. Chem. Phys.* **1983**, *78*, 321; Erratum, *J. Chem. Phys.* **1984**, *80*, 592.
(202) Pacchioni, G. *Mol. Phys.* **1985**, *55*, 211.
(203) Pitzer, K. S. *J. Chem. Phys.* **1981**, *74*, 3078.
(204) Ackerman, M.; Drowart, J.; Stafford, F. E.; Verhaegen, G. *J. Chem. Phys.* **1962**, *36*, 1557.
(205) Drowart, J.; Honig, R. E. *J. Phys. Chem.* **1957**, *61*, 980.
(206) Genard, J. *Phys. Rev.* **1933**, *44*, 468.
(207) Naudé, S. M. *Phys. Rev.* **1934**, *45*, 280.
(208) Nakamura, G.; Shidei, T. *Jpn. J. Phys.* **1935**, *10*, 11.
(209) Almy, G. M.; Schultz, H. A. *Phys. Rev.* **1937**, *51*, 62.
(210) Mrozowski, S.; Santaram, C. *J. Opt. Soc. Am.* **1967**, *57*, 522.
(211) Sfeila, J.; Perdigon, P.; Martin, F.; Femelat, B. *J. Mol. Spectrosc.* **1972**, *42*, 239.
(212) Topouzkhanian, A.; Sibai, A. M.; D'Incan, J. *Z. Naturforsch.* **1974**, *29A*, 436.

(213) Sibai, A. M.; Topouzkhanian, A.; Perdigon, P. Z. Naturforsch. 1976, 31A, 145.
(214) Gerber, G.; Kuscher, G. Chem. Phys. 1981, 60, 119.
(215) Bondybey, V. E.; Schwarz, G. P.; Griffiths, J. E. J. Mol. Spectrosc. 1981, 89, 328.
(216) Sontag, H.; Weber, R. J. Mol. Spectrosc. 1982, 91, 72.
(217) Sontag, H.; Weber, R. Chem. Phys. 1982, 70, 23.
(218) Kordis, J.; Gingerich, K. A. J. Chem. Phys. 1973, 55, 5141.
(219) Balasubramanian, K.; Li, J. Q. J. Mol. Spectrosc. 1989, 135, 169.
(220) Rosen, B. Naturwissenschaften 1926, 14, 978.
(221) Barrow, R. F.; Duparq, R. P. Proc. R. Soc. London, A 1972, 237, 279.
(222) Berkowitz, J.; Chupka, W. A. J. Chem. Phys. 1969, 50, 4245.
(223) Degenkolb, E. O.; Mayforth, H.; Steinfeld, J. I. Chem. Phys. Lett. 1971, 8, 288.
(224) Stone, T. J.; Barrow, R. F. Can. J. Phys. 1975, 53, 1976.
(225) Berkowitz, J. J. Chem. Phys. 1975, 62, 4074.
(226) Lee, S. T.; Suzer, S.; Shirley, D. A. Chem. Phys. Lett. 1976, 41, 25.
(227) Lin, K. K.; Balling, L. C.; Wright, J. J. Chem. Phys. Lett. 1986, 123, 37.
(228) Thorpe, W. G.; Carper, W. R.; Davis, S. J. Chem. Phys. Lett. 1976, 123, 493.
(229) Verges, J.; D'Incan, J.; Effantin, C.; Greenwood, D. J.; Barrow, R. F. J. Phys. B 1979, 12, L301.
(230) Effantin, C.; D'Incan, J.; Verges, J.; MacPherson, M. T.; Barrow, R. F. Chem. Phys. Lett. 1980, 70, 560.
(231) Bondybey, V. E.; English, J. H. J. Chem. Phys. 1980, 72, 6478.
(232) Ahmed, F.; Nixon, E. R. J. Mol. Spectrosc. 1981, 87, 101.
(233) Pardo, A.; Poyato, J. M. L.; Basulto, J. J. Mol. Spectrosc. 1982, 93, 245.
(234) Winter, R.; Barnes, I.; Fink, E. H.; Wildt, J.; Zabel, F. Chem. Phys. Lett. 1982, 86, 118.
(235) Verges, J.; Effantin, C.; Babaky, O.; D'Incan, J.; Prosser, S. J.; Barrow, R. F. Phys. Scr. 1982, 25, 338.
(236) Balasubramanian, K.; Ravimohan, Ch. J. Mol. Spectrosc. 1987, 126, 220.
(237) Mulliken, R. S. Phys. Rev. 1934, 46, 549; J. Chem. Phys. 1971, 55, 288.
(238) Tellinghuisen, J. J. Chem. Phys. 1985, 82, 4012; J. Phys. Chem. 1983, 87, 5136; J. Chem. Phys. 1983, 78, 2374.
(239) Geilhaupt, M.; Dorfmüller, Th. Chem. Phys. 1983, 76, 443.
(240) Ashby, R. A. Can. J. Phys. 1979, 57, 698.
(241) Ashby, R. A.; Johnson, C. W. J. Mol. Spectrosc. 1980, 84, 41.
(242) Gerstenkorn, S.; Luc, P.; Verges, J. J. Phys. B 1981, 14, L193.
(243) Beckman, A.; Fietz, H.; Baierl, P.; Kiefer, W. Chem. Phys. Lett. 1982, 86, 140.
(244) Gerstenkorn, S.; Luc, P. J. Phys. (Les Ulis, Fr.) 1985, 46, 867.
(245) Venkateswarlu, P.; Chakrapani, G.; George, M. C.; Rao, Y. V.; Okafor, C. Pramana 1987, 29, 261.
(246) Chen, K. M.; Steenhoek, L. E.; Yeung, E. S. Chem. Phys. Lett. 1978, 59, 222.
(247) King, G. W.; McLean, T. D. Chem. Phys. Lett. 1985, 121, 57.
(248) Venkateswarlu, P.; Putcha, T.; Vankateswara, R. Y. Spectrochim. Acta, Part A 1986, 42A, 285.
(249) Leach, S. J. Phys. Chem. 1988, 92, 5373.
(250) McLoughlin, R. G.; Morrison, J. D.; Smith, D. L. Int. J. Mass Spectrom. Ion Processes 1984, 58, 201.
(251) Li, J. Q.; Balasubramanian, K. J. Mol. Spectrosc. 1989, 138, 162.
(252) Skorko, E. Nature 1933, 131, 366; Acta Phys. Polon. 1934, 3, 191.
(253) Gerstenkorn, S.; Luc, P.; Sinzelle, J. J. Phys. (Orsay, Fr.) 1980, 41, 1419.
(254) Clear, R. D.; Wilson, K. R. J. Mol. Spectrosc. 1973, 47, 39.
(255) Mathieson, L.; Rees, A. L. G. J. Chem. Phys. 1956, 25, 753.
(256) Brand, J. C. D.; Kalukar, A. K.; Yamashita, A. B. Opt. Commun. 1981, 39, 235.
(257) Viswanathan, K. S.; Tellinghuisen, J. J. Mol. Spectrosc. 1983, 101, 285.
(258) Kawasaki, M.; Tsukiyama, K.; Kuwana, M.; Obi, K.; Tanaka, I. Chem. Phys. Lett. 1979, 67, 365.
(259) Guy, A. L.; Viswanathan, K. S.; Sur, A.; Tellinghuisen, J. Chem. Phys. Lett. 1980, 73, 582. Tellinghuisen, J. J. Mol. Spectrosc. 1982, 94, 231.
(260) Higginson, B. R.; Lloyd, D. R.; Roberts, P. L. Chem. Phys. Lett. 1973, 19, 480.
(261) Eland, J. H. D. J. Chem. Phys. 1979, 70, 2926.
(262) Cornford, A. B.; Frost, D. C.; McDowell, C. A.; Ragle, J. L.; Stenhouse, I. A. J. Chem. Phys. 1971, 54, 2651.
(263) Drowart, J.; Honig, R. E. J. Phys. Chem. 1957, 61, 980.
(264) Miller, R. C.; Kush, P. Phys. Rev. 1955, 99, 1314.
(265) Berkowitz, J.; Walter, T. A. J. Chem. Phys. 1968, 49, 1184.
(266) Balducci, G.; Piacente, V. J. Chem. Soc., Chem. Commun. 1980, 1287.
(267) Balasubramanian, K., work in progress.
(268) Shawhan, E. N. Phys. Rev. 1935, 48, 343.
(269) Puri, S. S.; Mohan, H. Indian J. Pure Appl. Phys. 1975, 13, 206.
(270) Natanson, L. Acta Phys. Polon. 1937, 7, 275.
(271) Weniger, S. J. Phys. 1967, 28, 595.
(272) Johnson, S. E.; Cannell, D.; Lunacek, J.; Broida, H. P. J. Chem. Phys. 1972, 56, 5723.
(273) Lochet, J. J. Phys. B 1978, 11, 1735.
(274) Brewer, L.; Chang, C. A. J. Chem. Phys. 1972, 56, 1728.
(275) Teichman, R. A., III; Nixon, E. R. J. Mol. Spectrosc. 1976, 59, 299.
(276) Gingerich, K. A.; Cooke, D. L.; Miller, F. J. Chem. Phys. 1976, 64, 4027.
(277) Pitzer, K. S.; Balasubramanian, K. J. Phys. Chem. 1982, 86, 3068.
(278) Sontag, H.; Weber, R. J. Mol. Spectrosc. 1983, 100, 75.
(279) Berg, L.-E.; Ismail, S.; Klynning, L.; Martin, H.; Pereira, A.; Royen, P. Phys. Scr. 1981, 23, 1047.
(280) Aslund, N.; Barrow, R. F.; Richards, W. G.; Travis, D. N. Ark. Fys. 1965, 30, 171.
(281) Ehret, G.; Gerber, G. Chem. Phys. 1982, 66, 27.
(282) Rovner, L.; Drowart, A.; Drowart, J. Trans. Faraday Soc. 1967, 63, 2906.
(283) Reddy, S. P.; Ali, M. K. J. Mol. Spectrosc. 1970, 35, 285.
(284) Wellegehausen, B.; Friede, D.; Steger, G. Opt. Commun. 1978, 26, 391.
(285) West, W. P.; Broida, H. P. Chem. Phys. Lett. 1978, 56, 283.
(286) Drosch, S.; Gerber, G. J. Chem. Phys. 1982, 77, 123.
(287) Gerber, G.; Sakurai, K.; Broida, H. P. J. Chem. Phys. 1976, 64, 3410.
(288) Gerber, G.; Broida, H. P. J. Chem. Phys. 1976, 64, 3423.
(289) Teichman, R. A.; Nixon, E. R. J. Chem. Phys. 1977, 67, 2470.
(290) Bondybey, V. E.; English, J. H. J. Chem. Phys. 1980, 73, 42.
(291) Farbe, G.; Bacci, J. P.; Athenour, C.; Stringat, R.; Bernath, P. Can. J. Phys. 1982, 60, 73.
(292) Christiansen, P. A. Chem. Phys. Lett. 1984, 109, 145.
(293) Swarts, C. A.; McGill, T. C.; Goddard, W. A., III. Surf. Sci. 1981, 110, 400.
(294) Swarts, C. A.; Goddard, W. A., III; McGill, T. C. J. Vac. Sci. Technol. 1981, 19, 360, 551.
(295) Agarwal, B. K. Phys. Rev. B 1981, 23, 2995.
(296) Nishida, N. Solid State Commun. 1979, 28, 551; Surf. Sci. 1978, 72, 589.
(297) Demeyer, G.; Hoogewijs, R.; Lambrecht, W.; Vennik, J.; Dalma, G. Surf. Sci. 1981, 106, 498.
(298) Hoepful, R. A.; Shah, J.; Block, D.; Gossard, A. C. Appl. Phys. Lett. 1986, 48, 148.
(299) Marsh, A. C.; Inkson, J. C. J. Phys. C 1986, 19, 43.
(300) Wong, K. B.; Jaros, M.; Gell, M. A.; Ninno, D. J. Phys. C 1986, 19, 53.
(301) Balasubramanian, K. J. Chem. Phys. 1987, 86, 3410.
(302) Knight, L. B.; Petty, P. T. J. Chem. Phys. 1988, 88, 481.
(303) Lemire, G. W.; Bishea, G. A.; Heidecke, S.; Morse, M. D. J. Chem. Phys., submitted.
(304) Shim, I., private communications.
(305) Balasubramanian, K. J. Chem. Phys., submitted.
(306) Piper, L. G.; Velazco, J. E.; Setser, D. W. J. Chem. Phys. 1973, 59, 3323.
(307) Velazco, J. E.; Kolts, J. H.; Setser, D. W. J. Chem. Phys. 1973, 65, 3468.
(308) Tellinghuisen, J.; Hays, A. K.; Hoffman, J. M.; Tisome, G. C. J. Chem. Phys. 1976, 65, 4473.
(309) King, D. L.; Piper, L. G.; Setser, D. W. J. Chem. Soc., Faraday Trans. 2 1977, 73, 177.
(310) Rokni, M.; Jacobs, J. H.; Mangano, J. A. Phys. Rev. 1977, A16, 2216.
(311) Olson, R. E.; Liu, B. Phys. Rev. 1978, A17, 1568.
(312) Dunning, T. H., Jr.; Hay, P. J. J. Chem. Phys. 1977, 66, 3767 and references therein.
(313) Cohen, J. S.; Wadt, W.; Hay, P. J. J. Chem. Phys. 1979, 71, 2955 and references therein.
(314) Watkins, H. P.; Sondergaard, N. E.; Koski, W. S. Radiochim. Acta 1981, 29, 87.
(315) Holloway, J. H. Noble Gas Chemistry; Methuen: London, 1968.
(316) Henglein, A.; Muccini, G. A. Angew. Chem. 1960, 72, 630.
(317) Kuen, I.; Howorka, F. J. Chem. Phys. 1979, 70, 595.
(318) Berkowitz, J.; Chupka, W. A. Chem. Phys. Lett. 1970, 7, 447.
(319) Berkowitz, J.; Chupka, W. A.; Guyon, P. W.; Holloway, J. H.; Sphor, R. J. Phys. Chem. 1971, 75, 1461.
(320) Watkins, H. P.; Koski, W. S. Chem. Phys. Lett. 1981, 77, 470.
(321) Gardner, M. A.; Karo, A. M.; Wahl, A. C. J. Chem. Phys. 1976, 65, 1222.
(322) Liskow, D. H.; Schaefer, H. F., III; Bagus, P. S.; Liu, B. J. Am. Chem. Soc. 1973, 95, 4056.
(323) Liu, B.; Schaefer, H. F., III. J. Chem. Phys. 1971, 55, 2369.
(324) Wendell, K.; Jones, C. A.; Kaufman, J. J.; Koski, W. S. J. Chem. Phys. 1975, 63, 750.
(325) Sharma, R. B.; Koski, W. S., unpublished results.
(326) Balasubramanian, K.; Kaufman, J. J.; Hariharan, P. C.; Koski, W. S. Chem. Phys. Lett. 1986, 129, 165.
(327) Hotoka, M.; Roos, B.; Delos, J. B.; Srivastava, R.; Sharma, R. B.; Koski, W. S. Phys. Rev. A 1987, 35, 4515.
(328) Balasubramanian, K.; Feng, P.; Kaufman, J. J.; Hariharan,

P. C.; Koski, W. S. *Phys. Rev. A* **1988**, *37*, 3204.
(329) Chapman, D. A.; Balasubramanian, K.; Lin, S. H.; Kaufman, J. J.; Hariharan, P. C.; Koski, W. S. *Phys. Rev. A* **1989**, *39*, 4428.
(330) Hotoka, M.; Roos, B.; Balasubramanian, K.; Semo, N.; Sharma, R. B.; Koski, W. S. *Advances in Chemical Reaction Dynamics*; Rencsepis, R., Capellos, C., Eds.; Reidel: Dordrecht, 1986; pp 135–143.
(331) Feng, P. Y.; Balasubramanian, K.; Kaufman, J. J.; Hariharan, P. C.; Koski, W. S. *Phys. Rev. A*, submitted.
(332) Brown, W. G.; Gibson, G. E. *Phys. Rev.* **1932**, *40*, 529.
(333) Brown, W. G. *Phys. Rev.* **1932**, *40*, 1040.
(334) Brooks, W. V. F.; Crawford, B. C. *J. Chem. Phys.* **1955**, *23*, 363.
(335) Hulten, E.; Jarlaster, N.; Koffman, L. *Ark. Fys.* **1960**, *18*, 479.
(336) Clyne, M. A. A.; Coxon, J. A. *Proc. R. Soc. London* **1967**, *298*, 424.
(337) Holleman, G. W.; Steinfeld, J. I. *Chem. Phys. Lett.* **1971**, *12*, 431.
(338) Child, M. S.; Bernstein, R. B. *J. Chem. Phys.* **1973**, *59*, 5916.
(339) Cummings, F. E.; Klemperer, W. *J. Chem. Phys.* **1974**, *60*, 2035.
(340) Barnes, R. H.; Moeller, C. E.; Kircher, J. F.; Verber, C. M. *Appl. Phys. Lett.* **1974**, *24*, 610.
(341) Venkateswarlu, P. *Can. J. Phys.* **1975**, *53*, 812.
(342) Olson, C. D.; Innes, K. K. *J. Chem. Phys.* **1976**, *64*, 2405.
(343) King, G. W.; McFadden, R. G. *Chem. Phys. Lett.* **1978**, *58*, 119.
(344) Gordon, R. D.; Innes, K. K. *J. Mol. Spectrosc.* **1979**, *78*, 350.
(345) Coxon, J. A.; Wickramaaratchi, M. A. *J. Mol. Spectrosc.* **1980**, *79*, 380.
(346) Coxon, J. A.; Gordon, R. M.; Wickramaaratchi, M. A. *J. Mol. Spectrosc.* **1980**, *79*, 363.
(347) Brand, J. C. D.; Deshpande, V. D.; Hoy, A. R.; Jaywant, S. M. *J. Mol. Spectrosc.* **1983**, *100*, 416.
(348) Brand, J. C. D.; Bissieres, D.; Hoy, A. R.; Jaywant, S. M. *Chem. Phys. Lett.* **1984**, *109*, 101.
(349) Spivey, J. D.; Ashmore, J. G.; Tellinghuisen, J. *Chem. Phys. Lett.* **1984**, *109*, 456.
(350) Potts, A. W.; Price, W. C. *Trans. Faraday Soc.* **1971**, *67*, 1242.
(351) Brand, J. C. D.; Hoy, A. R.; Jaywant, S. M. *J. Mol. Spectrosc.* **1984**, *106*, 188.
(352) Cornford, A. B. Ph.D. Thesis, University of British Columbia, Vancouver, BC (as referred to in ref 341).
(353) Balasubramanian, K. *J. Mol. Spectrosc.* **1985**, *110*, 339.
(354) Balasubramanian, K. *Chem. Phys.* **1985**, *95*, 225.
(355) Balasubramanian, K.; Feng, P. Y. *Chem. Phys. Lett.* **1988**, *146*, 155.
(356) Basch, H. *Chem. Phys. Lett.* **1987**, *136*, 289.
(357) Howard, J. A.; Sutcliffe, R.; Tse, T. S.; Dahamane, H.; Mile, B. *J. Phys. Chem.* **1985**, *89*, 3595.
(358) Fu, Z.; Lemire, G. W.; Hamrick, Y. M.; Taylor, S.; Shui, J.-C.; Morse, M. D. *J. Chem. Phys.* **1988**, *88*, 3524.
(359) Balasubramanian, K. *J. Chem. Phys.* **1987**, *87*, 3518.
(360) Reents, W. D. *J. Chem. Phys.* **1989**, *90*, 4258.

(361) Pacchioni, G.; Koutecký, J. *J. Chem. Phys.* **1986**, *84*, 3301.
(362) Sabin, J. R.; Oddershede, J.; Diercksen, G. H. F.; Grüner, N. E. *J. Chem. Phys.* **1986**, *84*, 354.
(363) Raghavachari, K. *J. Chem. Phys.* **1985**, *83*, 3525.
(364) Raghavachari, K. *J. Chem. Phys.* **1986**, *84*, 5672.
(365) Grev, R. S.; Schaefer, H. F., III. *Chem. Phys. Lett.* **1985**, *119*, 111.
(366) Diercksen, G. H. F.; Gruner, N. E.; Oddershede, J.; Sabin, J. R. *Chem. Phys. Lett.* **1985**, *117*, 29.
(367) Balasubramanian, K. *Chem. Phys. Lett.* **1986**, *125*, 400.
(368) Balasubramanian, K. *Chem. Phys. Lett.* **1987**, *135*, 288.
(369) Feng, P. Y.; Balasubramanian, K. *Chem. Phys.* **1989**, *138*, 89.
(370) Martin, T. P.; Schaber, H. *J. Chem. Phys.* **1985**, *83*, 855.
(371) Balasubramanian, K. *J. Chem. Phys.* **1986**, *85*, 3401.
(372) Balasubramanian, K. *Chem. Phys. Lett.* **1988**, *150*, 71.
(373) Balasubramanian, K. *Chem. Rev.* **1985**, *85*, 599.
(374) Balasubramanian, K. *Theor. Chim. Acta* **1979**, *51*, 37.
(375) Balasubramanian, K. *Indian J. Chem.* **1978**, *16B*, 1094.
(376) Balasubramanian, K. *Theor. Chim. Acta* **1979**, *53*, 129.
(377) Balasubramanian, K. *Ann. N.Y. Acad. Sci.* **1979**, *319*, 576.
(378) Pólya, G. *Acta Math.* **1937**, *65*, 145.
(379) King, R. B. *J. Math Chem.* **1987**, *1*, 15, 45.
(380) King, R. B. *Stud. Phys. Theor. Chem.* **1983**, *28*, 99.
(381) King, R. B.; Rouvray, D. H. *Theor. Chim. Acta* **1978**, *48*, 207.
(382) King, R. B. *Inorg. Chem.* **1988**, *27*, 1941.
(383) King, R. B. In *Physics and Chemistry of Small Clusters*; Jena, P., Rao, B. K., Khanna, S. N., Eds.; Plenum: New York, 1987.
(384) King, R. B. *Inorg. Chem.* **1985**, *24*, 1716.
(385) Muetterties, E. L. *J. Am. Chem. Soc.* **1969**, *91*, 1636.
(386) Muetterties, E. L. *J. Am. Chem. Soc.* **1968**, *90*, 5097.
(387) Klemperer, W. G. *J. Am. Chem. Soc.* **1972**, *94*, 6940.
(388) Balasubramanian, K. *Int. J. Quantum Chem.* **1982**, *21*, 411.
(389) Balasubramanian, K. *Int. J. Quantum Chem.* **1982**, *22*, 385.
(390) Balasubramanian, K. *Int. J. Quantum Chem.* **1982**, *22*, 1013.
(391) Balasubramanian, K. *J. Phys. Chem.* **1982**, *86*, 4668.
(392) Lipscomb, W. N. *Science* **1966**, *153*, 373.
(393) King, R. B. *Inorg. Chem.* **1986**, *25*, 506.
(394) King, R. B. *Advances in Dynamic Stereochemistry*; Gielen, M., Ed.; Freund Publishing House, in press.
(395) Balasubramanian, K. *Stud. Phys. Theor. Chem.* **1983**, *23*, 149.
(396) Balasubramanian, K. *J. Comput. Chem.* **1983**, *4*, 302.
(397) Balasubramanian, K. *Croat. Chim. Acta* **1984**, *57*, 1465.
(398) Balasubramanian, K.; Liu, X. Y. *J. Comput. Chem.* **1988**, *9*, 406.
(399) Balasubramanian, K.; Liu, X. Y. *Int. J. Quantum Chem.* **1988**, *22*, 319.
(400) Randić, M.; Oakland, D. O.; Klein, D. J. *J. Comput. Chem.* **1986**, *7*, 35.
(401) Randić, M. *Chem. Phys. Lett.* **1976**, *42*, 383.
(402) Balasubramanian, K. *J. Phys. Chem.*, submitted.
(403) Meier, U.; Peyerimhoff, S. D.; Bruna, P. S.; Grein, F. *J. Mol. Spectrosc.* **1989**, *134*, 259.
(404) Balasubramanian, K. *J. Mol. Spectrosc.*, in press.